BRITISH THESIS SERVICE

DX220865

NUMERICAL ANALYSIS AND THREE DIMENSIONAL MODELLING OF WORM GEARING WITH LOCALISED TOOTH CONTACT

FENG YANG

A thesis submitted in partial fulfilment of the
requirements of The Nottingham Trent University
for the degree of Doctor of Philosophy

This research programme was carried out in the
Department of Mechanical and Manufacturing Engineering,
Faculty of Engineering and Computing,
The Nottingham Trent University, Burton Street, Nottingham, UK.

January 2000

ABSTRACT

This research has developed a new approach to the design of worm gear drives with localised tooth contact (LTC). It has significant advantages over conventional ones: less sensitivity to errors, higher transmission quality, low manufacturing costs and less production lead-time. The approach consists of three main parts: developing the mathematical model, 3D modelling and simulation process and finite element analysis for the worm gear drive.

A mathematical model of the localised conjugate worm gear drive has been established based on differential geometry. The completed model is able to determine the position of the localised contact and to achieve better contact quality. Localised tooth contact is achieved by reducing the worm size and modifying the wheel tooth surface. Moreover, it avoids the re-design and manufacture of the hob. The results of numerical simulation show: in spite of the variation in misalignment, the contact areas of the modified worm gearing stay almost at the same position and the size of the contact area almost remains the same as well. It proves that the modified worm gear drive is insensitive to errors.

Three-dimensional simulation of a worm gear transmission has been conducted by applying the advanced CAE package Pro-engineer. The process comprises (1) the establishment of three models: worm model, wheel model and assembly model; (2) simulation of the localised tooth contact; (3) investigation of the contact and refinement of design parameters to further improve the transmission quality. The simulation has shown the contact pattern and its moving direction for worm gear drives, which provides a great visual aid for the designer to investigate the contact. Any interference between the modified tooth surfaces can be detected by the 3D model, and, hence, can be avoided at the design stage. This is a significant achievement in the analysis of localised contact of worm gears, because the previous methods often cause interference and can not detect contact position. The 3D models also lay the foundation for the finite element analysis.

The finite element analysis offers a solution to calculating tooth stress and evaluating the load sharing of worm gear drives, which both remain unknown in existing design standards such as ISO, BS. Finite element analyses were conducted using the software package ANSYS and the results have been validated by published experimental work. The important characteristics such as meshing stiffness and loaded transmission error have been investigated with the aid of FEA. The load share of a worm gear drive at every moment of engagement has been solved. The results obtained are the fundamentals for the design of worm gear drives with high contact ratio and compact size.

ACKNOWLEDGEMENTS

I received tremendous support from colleagues at The Nottingham Trent University, during the course of my research work, for which I am very grateful.

I would like to express sincere thanks to my Director of Studies, Dr. Daizhong Su, for his enthusiasm and his continuous support, encouragement, guidance throughout this project. Sincere thanks are due to my supervisor Professor Richard Gentle, for his advice, comments, backing and interest in my project.

Special thanks to my colleagues; Dr. Xianfa Wang, Mr. Daniel Reith, Mr. Detlef Plantenberg, Mr. Assefa Ayalew, Mr. Waldek Golinski, for their friendship and advice.

I would like to express my thanks to members of my family in China for all their invaluable support.

Finally, my greatest thanks to my wife Changzhou and son Tianxia, for their support and patience during the last three years.

DEDICATION

To Changzhou and Tianxia

PUBLICATIONS ARISING FROM THIS PROJECT

1. F. Yang, D. Su and C. R. Gentle, 2000 (forthcoming), "Finite Element Modelling and Stress Analysis for Involute Worm Gears with Localised Tooth Contact", Proceedings, International Conference on Gearing, Transmissions and Mechanical Systems, Nottingham UK.
2. F. Yang, D. Su and C. R. Gentle, 1999, "A General Approach for Computer Aided Design and Simulation of Worm Gear Transmissions", Proceedings, 15th International Conference on Production Research, 9th-13th, August, Limerick, Ireland.
3. D. Su, F. Yang and Y. Song, 1999, "A CAD Approach for Reducing Worm Gearing's Sensitivity to Manufacturing and Assembly Errors", Proceedings, 15th International Conference on Computer-Aided Production Engineering, 19th-21st, April, Durham, England.
4. D. Su, F. Yang and C. R. Gentle, 1998, "Optimum Design of Worm Gearing with Preferable Localised Tooth Contact", International Journal of Gearing and Transmissions, No. 1, 1998.
5. F.Yang and D.Su, 1999, "Software Review: Mathcad 8 Professional", Published in the website of CTI engineering: http://www.ctieng.qmw.ac.uk/cti-eng/reviews/.
6. F. Yang, X. Wang, D. Su and C. R. Gentle, 1998, "A Numerical Method To Obtain Preferable Localised Tooth Contact For Cylindrical Worm Gearing", proceedings, International Conference on Mechanics in Design, 6th-9th July, Nottingham, UK
7. D. Su, F. Yang, 1999, "Advancement in Design, Modelling and Simulation of Worm Gearing with Less Sensitivity to Errors", Proceedings, Tenth World Congress on the Theory of Machine and Mechanisms, 20th-24th, June, Oulu Finland
8. F. Yang and D. Su, 1997, "An Operation Planning Method Based on Feature State Analysis and a Case Study", Proceedings, 13th International Conference on Computer-Aided Production Engineering, 9-14, June, Warsaw.
9. D. Su, F Yang, C R Gentle and D Reith, 1998, "A new approach combining numerical analysis and three-dimensional simulation for design of worm gearing with preferable localised tooth contact", proceedings, 25th ASME Biennial Mechanisms Conference, 13th-16th September, Georgia, USA.

10. F. Yang, D. Su and C R Gentle, 1998, "Localised Tooth Contact for Worm Gearing: State of the Art", Proceedings, International Conference on the Theory and Practice of Gearing, 17th-19th, November, Izhevsk, Russian.

NOMENCLATURE

A_0 : the centre distance of the worm and wheel. P31

b: cutting tool mounting parameter for manufacturing side B of the worm. P48

i_{12} : transmission ratio. P34

K_δ : meshing stiffness P124

$k_I^{(i)}, k_{II}^{(i)}$: principal curvatures of the contact surfaces. P119

m: tooth module. P61

m_c: contact ratio P140

M_{21}: the matrix of transmission from Σ_1 to Σ_2. P34

M_{20} : the transfer matrixes from Σ_0 to Σ_2. P55

M_{f1} : transform matrix from the worm to the fixed coodinate system. P57

$M_{\beta 1}$: transform matrix from the misaligned worm to the fixed coodinate system. P58

$M_{0\theta}$: transfer matrixes from the reference coordinate system Σ_θ to Σ_0. P55

$M_{\theta 1}$: transfer matrixes from the hob coordinate system Σ_1 to Σ_θ. P55

$\vec{n}$: the normal to the tooth surface. P34

$\vec{n}_1^A$: the normal vector of side A of the worm tooth surface. P46

$\vec{n}_1^B$: the normal vector of side B of the worm tooth surface. P48

$n_f^{(wm)}(u_1, \phi_{u1}, \phi_1)$: the normal vector of worm tooth surface P57

$n_f^{(wl)}(u_1', \phi_{u1}', \phi_1')$: the normal vector of wheel tooth surface P57

p : the screw parameter of worm. P34

$\vec{r}_1$: the vector of the worm tooth surface. P34

$\vec{r}_2$: the vector of the wheel tooth surface. P34

$\vec{r}_1^A$: the vector of the side A of worm tooth surface. P47

$\vec{r}_1^B$: the vector of the side B of worm tooth surface. P48

r_{01} : radius of the base cylinder of the involute worm. P32

$\vec{r}_1^{(2)}$: the vector of the reference point in the coordinate system Σ_2. P36

u : cutting tool parameter.

r_{1x}, r_{1y}, r_{1z} : the coordinate values of the reference point in Σ_2. P36

$r_f^{(wm)}(u_1, \phi_{u1}, \phi_1)$: the position vector of worm tooth surface P57

$r_f^{(wl)}(u_1', \phi_{u1}', \phi_1')$: the position vector of wheel tooth surface P57

$\vec{v}_{ref}$: the relative velocity at the reference point. P37

$\vec{v}_A^{(12)}$: the vectors of relative velocity between worm and wheel. P51

x_1^A, y_1^A, z_1^A the coordinate values of side A of worm tooth. P50

x_1^B, y_1^B, z_1^B the coordinate values of side B of worm tooth. P50

Z_1: number of worm threads. P61, P134

Z_2: number of wheel teeth. P61, P134

α : the pressure angle. P67

δ_1 : the helix lead angle. P34

ϕ_1: worm rotation angle around it axis $\vec{k}_1$. P32

ϕ_2: wheel rotation angle around its axis $\vec{k}_2$. P32

ϕ_u : cutting tool rotation angle with respect to the worm. P34

θ_h : hob mounting angle. P35

$\vec{\omega}^{(1)}$: angular velocity of worm. P37

$\vec{\omega}^{(2)}$: angular velocity of wheel. P37

λ: angular parameter to describe the meshing point of the modified tooth surface. P39

$\sigma^{(12)}$: angle formed by the vectors of principal directions of contact surfaces P119

$\Sigma_0 = [o; \vec{i}, \vec{j}, \vec{k}]$: the global fixed coordinate system. P31

$\Sigma_1 = [o_1; \vec{i}_1, \vec{j}_1, \vec{k}_1]$: the coordinate system connected to worm. P31

$\Sigma_2 = [o_2; \vec{i}_2, \vec{j}_2, \vec{k}_2]$: the coordinate system connected to the wheel. P31

$\Sigma_u = (o_u; \vec{i}_u, \vec{j}_u, \vec{k}_u)$: the coordinate system fixed on the cutting tool. P31

$\vec{\Delta}$: displacement vector of the tooth pairs in simultaneously contact. P136

$\Delta\vec{\theta}$: rotation increment vector of the tooth pairs in simultaneously contact. P136

$\vec{d}$: torque share vector of the tooth pairs in simultaneously contact. P136

$\vec{T}$: load vector. P137

$\vec{\delta}$: vector to depict the elastic deformation of tooth pairs in contact P137

$\Delta\vec{\varphi}$: vector to depict transmission error of tooth pairs in contact. P138

$\vec{\tau}$: vector to depict displacement caused by the transmission error. P138

$[K]$: meshing stiffness matrix P137

$[R]$: radius matrix P136

ABBREVIATIONS

FE	Finite element
FEA	Finite element analysis
LTC	Localised tooth contact
LTCA	Loaded tooth contact analysis
MSFACP	Meshing stiffness function along contact path
PLTC	Preferable localised tooth contact
TCA	Tooth contact analysis

LIST OF FIGURES

CONTENTS

CHAPTER 1 Introduction

1.1 Background

Worm gear drives are widely used in industry for mechanical transmissions. The most important characteristics of worm gear drives are:

- High loading capacity and smooth transmission motion
- Large reduction ratio
- Low noise and vibration
- Compact size
- Self-locking capability

However, conventional worm gear drives are sensitive to manufacturing and assembly errors, due to the fact that they are designed based on the theory that the conjugated worm-gear tooth surfaces are in line contact. In reality, however, the line contact is almost impossible to achieve due to manufacturing and assembly errors and deflection under loading; instead, worse situations such as edge contact occur which severely reduce the loading capacity and, hence, the service life of worm gear drives.

Much research attention has been attracted to improving the tooth contact in worm gearing. At an early stage attempts were made to deliberately introduce manufacturing errors to improve bearing contact (Janninck, 1988; Colbourne, 1989). Recently, localised tooth contact, a technique that substitutes tooth surface line contact with point contact, has been introduced to provide an ideal bearing contact with low sensitivity to errors. Amongst existing achievements, there are two main approaches:

(1) tooth geometry modification of worm gear drives to achieve localised contact for which some methods were developed by Vanula (1994) and Yoshino (1997); and

(2) numerical methods for tooth contact analysis of localised contact for worm gear drives (Seol and Litvin, 1996, Litvin and Kin, 1992).

These developments contribute the theoretical basis for a better understanding of localised contact in worm gear drives. However, although the existing methods may achieve localised contact, they cannot ensure the contact area is placed at an ideal position and so the meshing quality is uncontrollable.

Furthermore, although existing methods may achieve localized tooth contact, interference between the modified tooth surfaces may also occur. In other words, the modified tooth geometry may achieve the localized contact at a location on the tooth surface, but interference may occur in another part of the tooth surface during the engagement of worm and wheel. In practice, the interference is resolved by an experienced worker/engineer using a trial and error method to adjust the hob setting, which is obviously time consuming and laborious, and the optimum performance of the drive is hardly to be achieved. In addition, since the localized contact is affected by the load applied and tooth geometry, but the existing methods do not provide a proper method to evaluate load share, then, they can only roughly estimate the contact.

The analysis of worm gear tooth contacts is usually based on the assumption of rigid teeth. Stresses in the gears are estimated by assuming a uniform load distribution along an ideal contact line. Although these are known to be over simplifications, they are still applied in practice because of the complexity of tooth geometry and lack of an effective methodology. Due to manufacturing errors and various factors such as elastic deformation under load, tooth profile modification, misalignment and wear, the ideal line contact never occurs in practice and the load allotment on the tooth surface is far from the uniform distribution. The contact lines degenerate into contact areas whose size and position vary with load. Therefore, the results of the analysis are only rough estimates and disagree with the real situation.

The loading capacity and transmission quality of worm gearing depend on the behavior of the worm gear tooth contact under load. The current existing analysis methods are mainly empirical ones, which are based on simplified test data and mathematical models that assume ideal tooth loading. Obviously a design based on these methods is hardly

likely to achieve optimum capacity for worm gears. Loaded tooth contact analysis (LTCA), which is based on the application of finite element analysis, determination of load sharing between the teeth, real contact ratio and stresses, is desired for worm gear design. With LTCA, the deformation of teeth, stresses in gears and load distribution between teeth can be estimated more accurately. Considerable work has been done for gear drives (Litvin et al. 1996, Gosselin et al. 1995, Chen and Tsai 1989). However, LTCA for worm-gear drives has not been seen.

1.2 Aims

The aims of this project are to develop:

(1) a new type of cylindrical worm gearing with preferable localized tooth contact (e.g. 'point' contact),

(2) a novel approach for 3D modelling of worm gear drives using advanced CAD/CAE techniques, and

(3) a new method to evaluate the load share of worm gear drives based on finite element analysis.

Within the research, an analytical model of worm gearing is developed which ensures the localized contact is at a preferable location on the tooth surface. 3D geometric modeling and finite element analysis are employed on the worm gearing to achieve better transmission quality and higher loading capacity than conventional cylindrical worm gearing. The tooth contact analysis for the worm gearing is conducted based on numerical analysis and three-dimensional simulation, and any interference between the modified tooth surfaces can be detected and, hence, avoided. By applying finite element methods to the geometric model, the effect of load is considered in the analysis, and so the load share among the simultaneous contact tooth pairs and the stress in the gear will be estimated more accurately.

1.3 Objectives

The following specific objectives are to be met in order to achieve the aim of the project.

- Development of analytical models for the design of a new type of worm gear drive with preferable localised tooth contact. The localised contact is obtained by modifying the worm while using standard or existing hobs, which is more practical and economical than existing methods. The principles to control the modification parameters will also be developed in order to ensure the high loading capacity and transmission quality of the worm gear drives.
- Application of the advanced CAD package Pro-engineer to build three dimensional models of worm gear drive. With the 3D models, three-dimensional simulation is conducted for the engagement of the tooth surfaces, and the tooth contact is further investigated.
- Application of finite element method (FEM) in the Loaded Tooth Contact Analysis for worm gear drive, prediction of the contact stress and deformation of the local contact worm gear drive.
- Investigation of the tooth contact pattern, meshing stiffness and the loaded transmission error for the loaded teeth of the worm gear drive.
- Development of an analytical method to evaluate the load share of worm gear drives. The deformation compatibility condition of the worm gear drives to determine the load share between the simultaneously contacting tooth pairs will be investigated. A general approach comprising the main governing factors such as contact ratio, meshing stiffness and unloaded transmission error will be developed for load share calculation.

1.4 Layout of the Thesis

Chapter 2. Literature Review

State of the art research in worm gear drives has been investigated and reviewed. The review covers the following topics in worm gear research: localised tooth contact, 3D modelling and loaded tooth contact analysis. The concept of localised tooth contact is introduced. Main existing approaches to achieve the localised tooth contact, known as trial and error method, modification of tooth profiles and tooth contact analysis method,

are investigated. The topics of three dimensional modelling and finite element analysis of gear drives are reviewed in order to identify their capabilities with respect to geometrical modelling and their uses in loaded tooth contact analysis.

Chapter 3. Determination of the Modification Parameters for Worm Gear Drives with Localised Tooth Contact

A new approach is proposed to obtain a preferable localised tooth contact (PLTC) for worm gear drives. With this approach, the initial contact can be located at a preferred position, the moving direction of the contact can be predicted in order to achieve better meshing characteristics, and the contact at every instant of tooth engagement can be investigated. Compared with traditional line contact, the PLTC is much less sensitive to errors and can achieve high transmission quality and cut down the time and effort spent in production and assembly.

Chapter 4. Determination of the Modified Tooth Surfaces

The procedure for the calculation of the modified tooth surfaces has been developed based on differential geometry. It allows the determination of the modified tooth surface for both the worm and the wheel. The universal meshing equation derived in this chapter is capable of determining the tooth surfaces generated by the hob with the arbitrary mounting angle θ_h. The modified worm surface is calculated with the parameters obtained from the analytical method in Chapter 3, while the modified tooth surface of the wheel is generated using the universal meshing equation derived. The computer programme to perform the calculation is also described.

Chapter 5 Three-Dimensional Simulation for Worm Gear Drives

The three-dimensional modelling and simulation for worm gear drives are conducted within the environment of an advanced CAE package Pro-Engineer. Modelling methods for worm, wheel and assembly are invented. The 3D solid models of the involute worm gear drive are created. The assembly model of the worm gear drive consists of the worm

and wheel with accurate geometric and motion relationship. With the assembly model, the drive movement and the instantaneous tooth contact are simulated.

Chapter 6 Finite Element Analysis of worm gear drive

The finite element modelling process of worm gear drives is presented in this chapter. The 3D solid models developed in Pro/Engineer are imported into the software package ANSYS for finite element analysis. To generate the proper mesh for 3D worm and wheel models, the details of geometric operation for modelling worm gear drives are discussed. The material properties and the boundary constraints of the models are briefly described as well. Based on the finite element models, the stress and deformation of the teeth of the worm and wheel are analyzed. The result of the numerical analysis is in a good agreement with published experimental work.

Chapter 7 A General Approach to Calculate Load Share of Worm Gear Drives

The tooth deformation compatibility condition of worm gear drives is defined, providing the fundamental for determination of the load share percentage of the tooth pairs in contact. According to the results of TCA calculation, contact ratio and unloaded transmission error are investigated for worm gear drives. The meshing stiffness of worm gear drives is investigated using the results from both TCA calculation and finite element analysis. Combining all these governing factors affecting the load share, a mathematical model is developed to calculate the load share percentage of the tooth pairs in contact. An explicit expression of load share function is given using the mathematical model developed. The concept of loaded transmission error (transmission error under load) is introduced considering the real load share of the tooth pair. The analysis shows that the transmission error under load is affected by both tooth elastic deformation and unloaded transmission error.

Chapter 8 Discussion and Conclusions

A summary of the conclusions drawn throughout the project is presented in this chapter. The major topics covered in this project are discussed, which include the mathematical model of differential geometry for modification of worm gear design parameters, the tooth contact analysis, three dimensional modelling, finite element analysis and load share evaluation for worm gear drives.

CHAPTER 2. Literature Review

2.1 Worm-Gear Transmission

Worm gear drives are used for transmitting motion and power between perpendicular shafts, usually at right angles, that do not lie in a common plane. They consist of a worm, and a wheel. However, sometime they may be also used to connect shafts at other angles. Because of the screw action of worm gear drives, they have the advantages of high reduction ratio, low noise and smooth transmission. Hence they are widely applied in industry.

Worm gear sets can be classified into two types according to the nature of tooth surface generation: single or double enveloping. In a single enveloping set, the wheel has its tooth width cut into a concave surface, thus enveloping the worm when in mesh. The double enveloping set, in addition to having the wheel tooth width cut concave, has the worm length cut concave too. Therefore, it provides higher load capacity than single enveloping worm sets by getting more teeth into contact.

The wheel tooth surface is generated by the hob surface, i.e., it consists of the envelopes to a family of hob tooth surfaces. If the hob is identical to the worm, the contact pattern of worm gearing is then theoretically a line varying in length up to the full face width of the wheel teeth. Consequently the tooth contact of a worm gear is sensitive to errors. Hence, worm gear sets must be mounted carefully in order to achieve proper operation. The double enveloping type is even more difficult to mount than the single enveloping type.

2.2 Research of Contact Localisation for Worm Gear Drives- State of the Art

The concept of localised tooth contact is introduced to improve the tooth contact of worm gear drives. Instead of pursuing a perfect theoretical "line contact", this method concentrates on achieving a practical contact pattern of "localised contact" or "point contact", which is easy to get, much less sensitive to errors, and provides good meshing quality.

2.2.1. Trial and Error Methods for Contact Localisation

Ufert (1961) suggested removing boundary surfaces of the wheel tooth by hobbing in three positions as shown in Figure 2.1, in order to get local contact. Because the worm wheel tooth surface is over hobbed on two sides, it will lose the contact from the worm surface on both sides. So local contact is achieved. Obviously, this method is very rough and mainly based on expertise and experiment. It is very difficult to control the contact quality. Although local contact can be produced, it is hard to achieve the optimum contact zone.

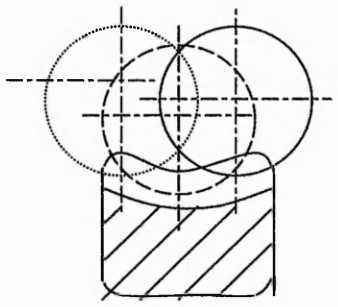

Figure 2.1 Achieving contact localisation by hobbing in three positions

Using a conventional gear hob for manufacturing worm wheels is another way to achieve local contact for worm gears (Zhang XK, 1986). In this method, a conventional involute gear hob is applied to replace the worm hob (especially for an Archimedes' worm). It is applicable if two conditions exist: (1) the normal pitch of the hob equals that of the worm. (2) the engaged surfaces of the hob and wheel must be in tangent contact in the contact point. From the conditions, the parameters of the worm, which is engaged to the gear-hob-made wheel, are derived as follows.

$$\alpha_l = tg^{-1}(tg\alpha_{hn} / \cos\lambda_l)$$

$$m_x = m_{hn} / \cos\lambda_l$$

$$\lambda_l = tg^{-1}(Z_l / q_l)$$

$$d_l = m_x q_l$$

where, m_{hn} is the normal module of the hob, α_{hn} is the normal pressure angle of the hob. The axial pressure angle of the worm is α_l, and the axial module of the worm is m_x. λ_l is the lead angle in the worm pitch. q_l is the diameter quotient of the worm and

d_1 is the pitch diameter of the worm.

Although this method is quite easy and economical, it is mainly applied to Archimedes type worms based on expertise. The tooth contact pattern is difficult to control.

Another idea applied in practice is to use a hob with increased diameter, which is the topic of a series of research works (Wildhaber E, 1954; Janninick WL, 1988; Colbourne JR, 1989). Wildhaber's method locates the contact point M on the shortest centre distance between worm and wheel. When the worm gearing is in line contact, the tangent of the point M in the contact line is expressed as $\vec{\tau}$, and the normal vector is expressed as $\vec{p}$. For a conventional manufacturing method, the worm gearing contact is a line along $\vec{\tau}$ direction. Therefore, if the oversized hob is applied in cutting, it enables a slight increase of the normal curvature of the tooth surface in the wheel along the $\vec{\tau}$ direction. This produces a local contact at the M point.

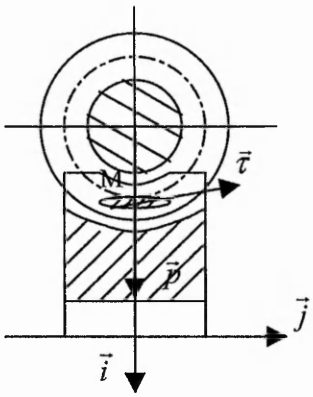

Figure 2.2 Point contact obtained by oversized hob

Research in the early stage was intended to introduce errors deliberately to obtain the mismatch between the tooth surfaces of the worm and wheel. All these works were expertise-based explorations. Although some simple algorithms were developed, the theory for tooth contact analysis was not provided. The localised tooth contact is produced on the basis of a trial and error method. The contact pattern is determined by repeating the experimental test. These methods were not able to avoid the interference caused by the modification introduced.

2.2.2. Modification of Tooth Profiles for Contact Localisation

Modifying the tooth profile is another attempt to achieve localised tooth contact, and intensive research has been done in this area. It is an improvement on the trial and error methods.

Image Rack Method

Yoshino H. and Muta Y. (1997) applied a new tooth surface modification method to cylindrical worm gearing. In their method, the modified hob and the worm both conjugate to an image rack in the axial plane. Tooth surface modifications are made by increasing the pitch circle radius of the hob as well as the number of threads of the hob. The relations of the dimensions of the worm, rack and hob are shown as Figure 2.3 and the equations listed below.

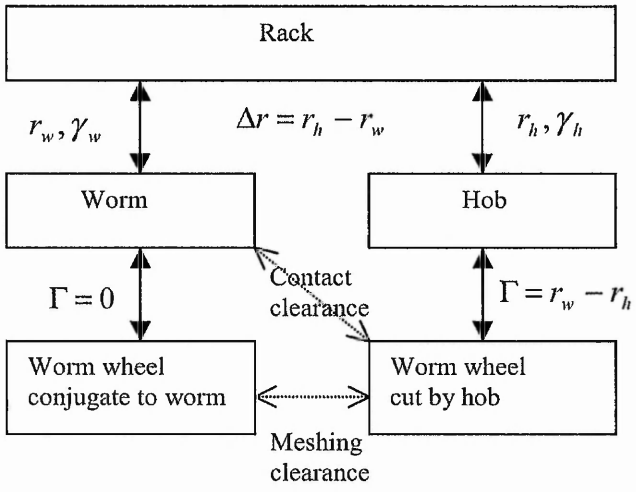

Figure 2.3 Relationship of tooth profiles of worm, rack, Hob, etc. , in the proposed modification methods

The relations among the hob and worm are represented as the following :

$$r_h = r_w + \Delta r$$
$$\gamma_w = \tan^{-1}(p_w N_w / 2\pi r_w)$$
$$p_n = p_w \cos\gamma_w$$
$$\gamma_h = \sin^{-1}(p_n N_h / 2\pi r_h)$$
$$P_h = P_n \cos\gamma_h$$

where, r is the pitch circle radius, Δr is the amount of increasing radius of the hob, p is the axial pitch, N is the number of threads, γ is the lead angle. Subscripts w, h and n are for a worm, hob and rack respectively. Γ is the hob setting angle. The thread numbers of the worm and hob are not necessarily the same. The modifying parameters can be calculated by the equations. However, this method may cause interference and is unable to determine the contact pattern.

Four Parameters Alteration Method

According to Horia Vinula(1994), contact localisation for cylindrical worm gears can be achieved by altering the following four parameters,

-R_A the rolling radius of the wheel (the position of the rolling line is modified by moving towards the interior of the wheel rolling cylinder).

-Z_A the position parameter measuring the distance between the contact point and the median plane of the wheel.

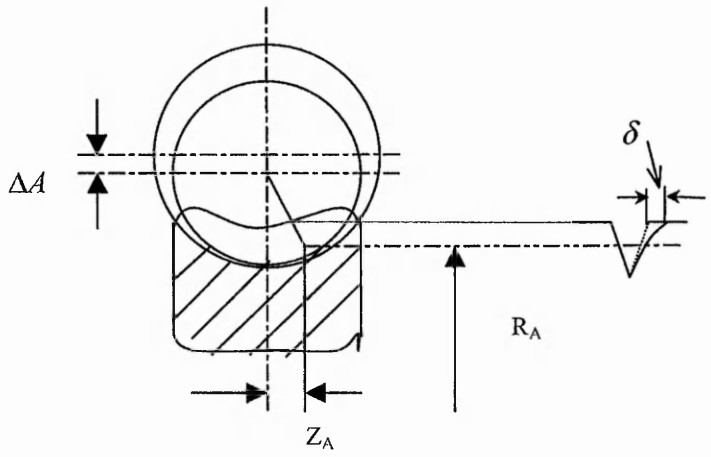

Figure 2.4 Four modification parameters

-Δ_A the correction of the centre distance at the technological gear (basically 50% of

the hob diameter increase).

-δ profile correction (crowning) introduced at the tool.

A computer program for modifying the tooth profile is available. The main procedure consists of the following:

- Generating the functional helicoid and the mating wheel flank
- Establishing the localisation parameters
- Determining the rack interposed to the enveloping worm and to the wheel
- Generating the enveloping worm, disk cutter machining the worm & introduction of crowning.
- Generating the actual wheel flank"Ease-off" topography
- Motion transmission error calculation
- Calculating the contact pattern for no-load worm transmission

The numerical results of this method can give the displacement of the contact pattern and the modification of tooth topography. Vinula's method made progress in analysing local tooth contact by using numerical methods, but the calculation is experience-based and very complicated. It is also difficult to manufacture the modified worm gear in practice.

Controllable Modification for ZC_1 worm gearing

Shuren Wang (1991) presents a method named controllable modification of worm drive for ZC_1 type worm drives. In the method, in order to change the line into a point contact, the worm surface is modified. This is more convenient than other method such as hob modification. The worm flank is modified from the theoretical flank, and the worm is called "match-lost worm". When the "match-lost" worm contacts with the worm wheel, they must be tangent to each other. Thus, the so called "match-lost" can be obtained just to remove a little bit of stock away from the theoretical flank along the common normal of the tangent line Γ at the contact point. The bigger the gap from Γ, the more the amount of modification. The selection of Γ determines the position of local contact, which is the so called controllable modification for worm

drives. As shown in Figure 2.5, the contours of the worm on the axial cross-section before and after modification are EQPF and E'QF' separately, where point p is a point on the reference circle of the theoretical worm.

The modification parameters for the worm are the radius ρ of the circular arch of the grinding wheel, the pressure angle α_n at the calculation point of the grinding wheel, the skew angle γ_u between the axis of the grinding wheel and the axis of the worm. The author provides the calculation procedure of these parameters. Using the parameters, the flank of the match-lost worm can be ground.

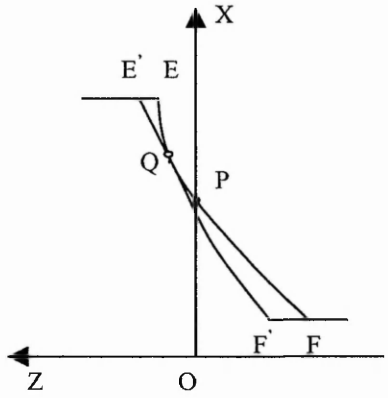

Figure 2.5 Tangential conditions of the worm

This method can determine the parameters for the modification of the worm and ensure the contact point after modification is at the middle of the outlet of the worm. This is advantageous to develop a hydrodynamic oil film and reduces the sensitivity to assembly errors. The limitation of this method is that it is only suitable for ZC_1 worm drives and it cannot predict the contact pattern.

Localised tooth contact for double enveloping worm gearing

Another way to modify the tooth profile has been suggested by D. Qin (1995) and applied for double enveloping worm gears. It depends on changing the manufacturing parameters because a cone tool generates the worm and the wheel is generated by a hob, of which the basic helicoid is formed by a straight generatrix of the cone surface. When the worm is engaged with the worm wheel, the worm could get local

conjugate contact with the worm wheel so long as the straight generatrix of the cone surface, as well as the parameters of the worm gearing, are designed properly.

The principle to get the local tooth contact is shown in Figure 2.6. As the worm is generated by the cone tool, the worm could make contact with the cone surface along the line L_2. If a straight generatrix L_1 of the cone surface is selected as a tool to generate the basic helicoid of the hob, the basic helicoid of the hob could be formed in the movement when the cone tool rotates relatively around the workpiece to generate the worm. As the basic helicoid of the hob is formed by the generatrix L_1 of the cone surface, the hob could make contact with the cone along L_1. Therefore, the worm could contact the hob at the crossing point of lines L_1 and L_2. Line L_1 and the parameters of the wheel, which determine the position and direction of L_2, are selected to make the line L_1 and L_2 intersect at the proper position on the cone surface. The parameters of the cone tool are designed to make the worm tooth surface locate in the substance side of the hob tooth surface, and the worm wheel is generated by the hob with the same geometric and motive relation as that of worm gearing. According to the meshing theory, the contact point on the worm is actually the contact point between the worm and the hob, as mentioned above.

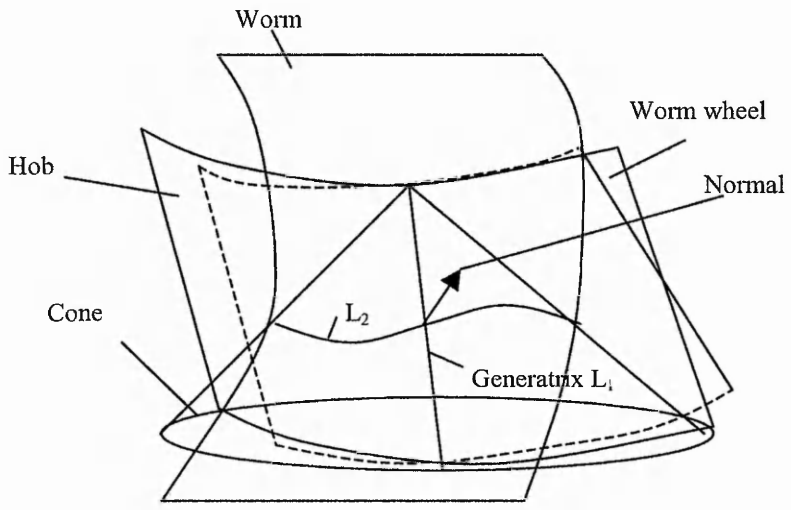

Figure 2.6 Principle of local tooth contact for double enveloping worm gears

From Figure 2.6, it is known that the contact state between the tooth surface of the worm gearing depends on the vertex angle of the cone. In the case that the vertex angle is small, the contact state of the worm gearing is close to that of cone-drive worm gearing, which is in line contact. When the vertex angle is zero, the cone becomes a straight line and the cone-drive worm gearing is achieved. Therefore, the contact state of the proposed local conjugate contact could be designed by changing the vertex angle of the cone tool. However, Qin's method is only applicable to the double enveloping worm gear.

Modification of the tooth profile is also the subject of the research work of Simon (1993, 1990), Gao and Xu (1990). This method may obtain localised tooth contact. However, after modification, the contact pattern of the modified tooth is changed and the conventional meshing theory doesn't fit the modified tooth profile. Most research works were unable to provide an effective analysis for the conjugate of modified tooth surfaces, thus, achieving optimum tooth contact pattern still depends on the experimental results and the interference arising from the tooth profile modification cannot be avoided.

2.2.3 Tooth Contact Analysis for Contact Localisation

The tooth contact analysis (TCA) programs exist to analyse meshing and contact of gear tooth surfaces with localised bearing contact. The main goals of TCA are to determine:

(1) the contact paths on gear tooth surfaces,

(2) the transmission errors caused by gear misalignment, and

(3) the bearing contact as a set of instantaneous contact ellipses.

The idea of TCA was first applied to gear drives. It is reported that spiral bevel gears, hypoid gears and circular arc helical gears with localised tooth contact of surfaces have been developed successfully [Litvin, 1995, Litvin and Zhang (1991b), Litvin and Go-kai, Litvin and Gutman (1980)]. Some new progress on TCA is also reported recently. [Litvin, Chen and SEP, 1995; Litvin Chen, Lu and Handschuh, 1995; Zhang, Litvin and Handschuh, 1995; Litvin, Wang and Handschuh, 1996; Litvin, Seol and Kim etc., 1996]

The application of TCA in worm gearing with localised tooth contact came from Seol and Litvin (1996, 1992). It is recognised as the latest progress in the research of localised tooth contact of worm gears. In their work, the analysis of localised meshing is based on the condition of continuous tangency of worm gear tooth surfaces, which is represented by the following equations

$$\begin{aligned} r_f^{(1)}(u_1,\theta_1,\phi_1,q_j) &= r_f^{(2)}(u_2,\theta_2,\phi_2,q_j) \\ n_f^{(1)}(u_1,\theta_1,\phi_1,q_j) &= n_f^{(2)}(u_2,\theta_2,\phi_2,q_j) \end{aligned} \qquad (2.1)$$

The above equations indicate that at the current point of tangency the contacting surfaces have common position vectors $r_f^{(i)}$ and surface unit normals $n_f^{(i)}$, (i=1,2). The coincidence of directions of the unit normals for both surfaces can be achieved by the proper order of co-factors in the cross products $(\partial r_f^{(i)}/\partial u_i)\times(\partial r_f^{(i)}/\partial \theta_i)$, (i=1,2). The worm gear tooth surfaces Σ_1 and Σ_2 are represented in the fixed coordinate system S_f where axes of gear rotation are located; (u_i,θ_i) $(i=1,2)$ are the surface parameters; ϕ_1 and ϕ_2 are the angles of gear rotation; q_j(j=1,2,...) designate the parameters of assembly.

From the above equations and considering $\left|n_f^{(1)}\right| = \left|n_f^{(2)}\right| = 1$, a system of five independent non-linear equations with six unknowns can be derived, These equations are represented as

$$f_k(u_1,\theta_1,\phi_1,u_2,\theta_2,\phi_2) = 0,\ f_k \in C^1,\ (k=1,5) \qquad (2.2)$$

where, the designation C^1 indicates that vector-function $r_f^{(i)}$ has continuous partial derivatives at least of the first order (Litvin, 1995). One of the unknowns, say ϕ_1, may be chosen as an input. Henceforth, it is assumed that equations (2.2) are satisfied at a point

$$P^0 = (u_1^0,\theta_1^0,\phi_1^0,u_2^0,\theta_2^0,\phi_2^0) \qquad (2.3)$$

and the system Jacobean differs from zero. Thus,

$$\Delta_5 = \frac{D(f_1, f_2, f_3, f_4, f_5)}{D(u_1, \theta_1, u_2, \theta_2, \phi_2)}$$
$$= \begin{vmatrix} \frac{\partial f_1}{\partial u_1} & \frac{\partial f_1}{\partial \theta_1} & \frac{\partial f_1}{\partial u_2} & \frac{\partial f_1}{\partial \theta_2} & \frac{\partial f_1}{\partial \phi_2} \\ \vdots & \vdots & \vdots & \vdots & \vdots \\ \frac{\partial f_5}{\partial u_1} & \frac{\partial f_5}{\partial \theta_1} & \frac{\partial f_5}{\partial u_2} & \frac{\partial f_5}{\partial \theta_2} & \frac{\partial f_5}{\partial \phi_2} \end{vmatrix} \neq 0 \qquad (2.4)$$

It follows from the theorem of existence of implicit function system (Korn, 1968) that equations 2.2 can be solved in the neighbourhood of P^0 by functions

$$[u_1(\phi_1), \theta_1(\phi_1), u_2(\phi_1), \theta_2(\phi_1), \phi_2(\phi_1)] \in C^1 \qquad (2.5)$$

Using equations (2.1) and function (2.5), the paths of contact on surfaces Σ_1 and Σ_2, and the transmission function can be determined. The paths of contact are represented as:

$$r_i(u_i, \theta_i), u_i(\phi_1), \theta_i(\phi_1) \qquad (i = 1,2)$$

and the transmission error is represented as

$$\Delta\phi_2(\phi_1) = \phi_2(\phi_1) - \frac{N_1}{N_2}\phi_1$$

where N_1 and N_2 are the tooth numbers. The contact pattern is determined based on the assumption of instantaneous contact ellipse and uniform load distribution.

Seol and Litvin (1996a) proposed a method to modify the existing geometry of worm gear drives to reduce the sensitivity of worm gear drives to misalignment, and to localise and stabilise the bearing contact as well. It is based on: (1) application of an oversized hob, (2) conjugation of the hob and the worm thread surfaces, and (3) application of a predestined parabolic function of transmission errors.

The worm gear is generated by a hob of an increased diameter in comparison with the worm. The hob and the worm are in internal tangency as shown in Figure 2.7. The axes of the worm and the hob are crossed with angle $\Delta\lambda$; Δr is the shortest distance between the crossed axes. During the generation process the hob and the wheel are in line contact. However the generated wheel tooth surface and the worm are in point contact in the process of their meshing.

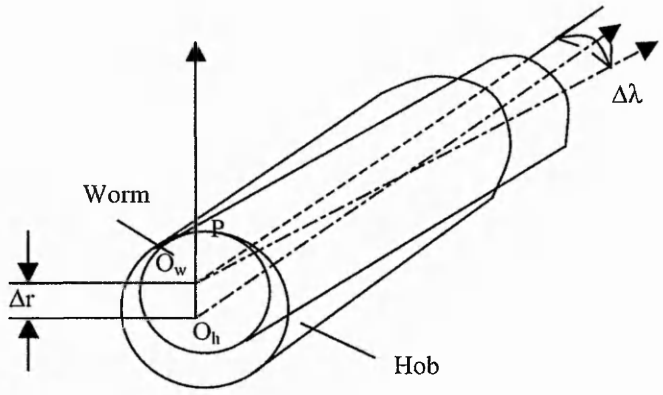

Figure 2.7 Pitch cylinders of the worm and the oversized hob

The bearing contacts for misaligned ZK worm gear drives with the non-modified and modified geometry are obtained by using TCA, shown in Figure 2.8(a) and 2.8(b).

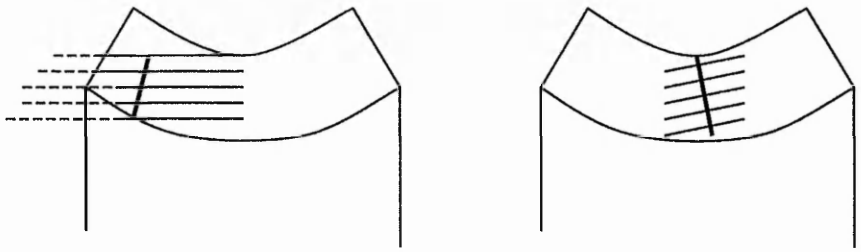

Figure 2.8 Path of contact and bearing contact of a misaligned ZK worm gear drive (a) the non-modified (b) the modified;

It is a considerable achievement to analyse tooth contact and transmission errors using TCA. Unfortunately, the TCA method is not able to solve the following problems:

(1) to define the contact area in a preferred position;

(2) to eliminate the interference arising from tooth profile modification;

(3) to calculate the accurate contact pattern under load.

Another attempt was made by Dudas, Banyal and Varga (1996) to conduct the simulation of meshing of worm gearing. They developed a general mathematical model for meshing simulation based on the differential geometry, which is suitable for cylindrical and bevelled helicoid surfaces. In their research, stochastic values of the different geometrical parameters inside the tolerance zone are given to the model

to simulate the mating of worm drives. The authors indicated that the geometry of worm gear drives is altered by manufacturing errors, assembling errors, elastic strains, thermal load and surface roughness. The following factors affecting the bearing contact are considered in their model:

- The enveloping surfaces swept by the worm and hob are not equal because of the manufacturing errors.
- The tooth surfaces are not perfect, i.e., the points of surfaces have variation.
- The influence of the oil film is considered.

The authors present the effects of the errors on the location of contact lines and the mating nodal points. However, this method is still based on the conventional meshing principle. Only the contact pattern of worm gears with errors within the tolerance zone can be simulated.

2.2.4 The Limit of Current Research in Contact Localisation

The review of the localised tooth contact method indicates that it is a powerful tool for improving existing worm gear sets. This method enables contact localisation to reduce the sensitivity of the worm gear drive due to misalignment, avoids the so-called edge contact and thus achieves better transmission quality. However, the weakness of current research has also been revealed such as:

- Most research is on trial based methods, i.e. the optimum contact pattern of the modified tooth is obtained from trial and error or assessed according to experience.
- The existing research may obtain the localised contact, but does not provide an effective means to avoid tooth surface interference caused by the tooth modification. In other words, although the modified tooth geometry may achieve localised contact at a location on the tooth surface, interference may occur in another part of the tooth surface during the engagement.
- In current research, the load distribution of worm gearing is over simplified and is far away from real situations.

Due to the complexity of tooth surfaces in worm gears, it is difficult for analytical models to solve the problems mentioned above. A three dimensional geometric model would offer a more powerful tool for solutions.

2.3 Three Dimension modelling for Worm Gear Drives

Three dimensional modelling of worm gear drives is highly suitable for industrial and academic purposes. This is due to the fact that three-dimensional models provide the foundation for three-dimensional simulation, finite element analysis and CNC manufacture for worm gear drives. A successful 3D model of a worm gear depends on both an accurate mathematical model and advanced geometric modelling techniques.

The subject has been attracting attention from researchers. Gert Bar (1990) developed a CAD programme to calculate the geometry of worms, threads and similar mechanical elements that can be described by helical or rotatory surfaces and that are to be generated by milling, grinding, or whirling. His work covered:

(a) design of gear or worm profiles by means of curve primitives and their motion and manipulation,
(b) calculation of conjugate gear profiles subjected to trochoidal motion,
(c) calculation of arbitrary plane intersections of helicoids, and
(d) calculation of the rotatory machining tool surface for a given worm and inverse problem, including the solution of the undercut problem.

The programme system developed can generate the important classes of curves like straight line, circle, involute, cycloid, trochoid, and parametrical splines. It also allows motion and manipulation of curves, e.g., to translate, rotate, reflect, or screw a curve, to add or erase parts of curves, to project a spatial curve orthogonally onto a plane, or embed a plane curve into space, and to calculate equidistant curves. The geometric modelling of the workpiece and tool geometry of worms have been done by the author, but the tooth geometry of the wheel is not provided because of the complexity.

Tsay C. B. and Chang S. L. (1994) investigated CAD of the profiles of pencil-type milling cutters that generate one side of the worm surface or cut symmetric worm surfaces. A mathematical model of a worm surface is developed. The generation mechanism is that the worm cylinder performs a screw motion and the pencil-type-milling cutter rotates about an axis perpendicular to the axis of the screw motion. The profile of the pencil-type-milling cutter can be obtained by rotating the instantaneous contact line about the cutter-rotating axis X, as shown in Fig.2.9

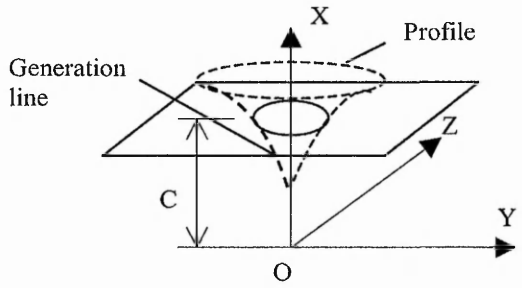

Fig. 2.9 Profile of a pencil milling cutter

The constraints on the dimensions of the cutter are given by limiting the generating line and the cutter radius to avoid cutting the worm surface below the base cylinder. The model can be applied to other types of screw surface generation as well. High precision pencil-type milling cutters can be manufactured with the aid of the proposed mathematical model and CNC machines. This research does not provide the model for a wheel either.

A general method for computing worm gear conjugate mesh is proposed by Zheng C. Q, Lei J. and Savage M.(1989 a, b) The mathematical description of the generating surface was presented for manufacturing worm gears. The method starts with the parametric description of the "dresser" curve (initial curve) from which the generating surface is produced. Four examples of " dresser" curves, i.e., the circle dresser, the involute dresser, the dyad dresser and the four bar linkage dresser are presented. By transforming the description of the initial curve, the expressions for the radial vector, the unit normal vector, the tangent vector and the normal curvature of the generating surface can be obtained.

Any type of worm tooth surface can be manufactured by a generating surface, which is formed by the relative motion of an initial curve. So the expressions developed in the method can offer the general descriptions of the generated worm and wheel teeth. By using the vector algebra method and numerical solution method for the non-linear functions, the authors also developed a general mathematical model of the manufacturing and working process of worm gears. The model can be used for any kind of worm gear sets for calculating their conjugate mesh properties: the contact line, the profile, the normal curvature and relative normal curvature, the angle between the directions of the contact line and the relative velocity vector. This method

provides a general mathematical model for worm gear drives but does not cover geometric modelling.

Developing a mathematical model for CNC hobbing machine is the research subject of Chang S. L., Tsay C. B. and Nagata S (1997). They established a general mathematical model, which is capable of simulating the gear cutting process of CNC hobbing, to facilitate the manufacturer in gear design and manufacturing. They derived the kinematic relationship of the CNC hobbing machines. Based on the cutting theory, generation conception with multi-degrees of freedom and theory of mechanism, a general mathematical model of a 6-axis CNC hobbing machine is developed. Using this model, the equations of the tooth surfaces for different types of existing gears can be obtained and the respective gear tooth surfaces can also be manufactured on the CNC hobbing machine. The developed model can also be applied to noncircular gears and other new types of gears with new manufacturing processes. In their paper, a new type of helipoid gear has been presented to illustrate the design process and the application of the developed model. Although the authors provided a general mathematical model for CNC manufacturing, the three dimensional model is not established.

From the literature, there has been no report of a three dimensional model for a whole worm gear set and geometric modelling has only been achieved for worms, of which the tooth profiles are relatively simple. Due to the complexity of the worm gear tooth profiles, most previous investigations concentrated on mathematical modelling for worm gearing. The literature search found that existing research in geometric modelling has been restricted by the software techniques and packages which are now out of date. For instance, Gert Bar (1990) used a self-developed programme system PC-WORM-TOOL-CAD. Application of current advanced and more powerful software such as ProEngineer is obviously necessary for geometric modelling of worm gears.

2.4 Loaded Tooth Performance Analysis

The gear drives with large power capacity and small size are required more often and development of a method of rational design for such teeth is desired. A recent advance in gear design is an increase of the number of simultaneous contact tooth

pairs as well as the proper modification of tooth flanks, so that the overall mesh stiffness can be increased and the load share can be improved substantially. It is possible under certain conditions to increase the load carrying capacity of a gearset without increasing its weight. Obviously, such a trend of gear design relies on an accurate computation of the loading and stressing distribution over the gearing surfaces at any phase of mesh. Unfortunately, due to the complexity of the tooth geometry, it is very difficult to use the analytical method to estimate its deformation, stress and loading sharing. The existing calculation methods are mainly based on the over-simplified formulas developed from the experimental work, which are not able to fulfil the requirement.

Finite element analysis is well established now as a powerful and reliable tool for engineering mechanic calculation. It is also frequently used as a reference to calibrate other numerical, analytical and experimental results. Hence, it becomes an effective and frequently applied method in loading capacity analysis of gearing design.

2.4.1 Analysis of tooth stress and deformation using finite element models

Early research was aiming at using the finite element method to determine the stresses at the tooth fillet, including the stress distribution and maximum tensile stress in the fillet region of the gear tooth, which are considered as primary causes of gear tooth failures. Due to the limitation of computing technology, the two-dimensional finite element models were widely used at that stage. Wilcox and Coleman (1973) developed 2D finite element models to simulate the shapes of both symmetric and asymmetric teeth. Based on the analysis of the models, the authors presented a simplified semi-empirical formula that gives tensile fillet stress as a function of tooth geometry and general loading conditions. Comparing the formula to other previously accepted formulas for a variety of tooth shapes and loading conditions, the authors also proved the accuracy and wide range of applicability of the stress formula derived from finite element analysis.

Huseyin and Eyercioglu (1995) also evaluated spur gear tooth stresses using 2D finite element method. They analysed the relationship between the tooth stress and the following parameters: module, contact ratio, fillet radius, pressure angle and teeth

numbers. The results show that all these parameters are interdependent variables, therefore, it is not possible to evaluate the effect of each variable on the stress independent from each other.

With the development of computer technology, three-dimensional finite models are widely accepted. Simon(1996a,b) proposed a computer program based on finite element analysis for the calculation of tooth stress and displacements of a cylindrical worm gear drive with concave worm profile. He investigated the influence of the design parameters of the worm gear drive and of the load position on tooth stress and displacements. On the basis of the obtained results, by using regression analysis and interpolation functions, equations for an easy calculation of displacements in the worm thread and in the gear tooth have been derived. Meanwhile, stress analysis of the worm thread and the gear tooth by a finite element method is carried out and the influence of the worm gearing design parameters on tooth stresses have also been investigated. Tooth stress and deformation analysis using finite element method is also the research topic of Bibel et.al(1994) and Moriwaki(1993). However, in all these works, the contact force is simplified as either concentrating force or evenly distributed forces, the results derived are only applicable to the specific type gears within individual circumstances.

2.4.2. Analysis of load distribution on a single tooth

Obviously, the load distribution along the tooth contact zone during the mesh is non-uniform and it will substantially affect the loading capacity and the service life of the gear sets. Since every single tooth is a basic unit for the engagement of gear drives, many researchers concentrate on investigating the load distribution on a single tooth surface.

Li, Wang, et.al (1998a,b) applied finite element analysis to solve load distribution. They proposed a normal stiffness matrix along contact line (NSMACL) method for gears. The method uses the static coagulation technique to coagulate the global stiffness matrix of all contact teeth into a lower-order NSMACL. The authors divide the instantaneous tooth contact line into a series of contact nodes N_1, N_2, …, N_n. They assume that P_i is the normal force acting on the nodes, and $\{f_i\}$ is the deformation of

the corresponding nodes resulting from $\{P_i\}$. If an nth-order square matrix [K] satisfies the following equation:

$$[K]\{f_i\}=\{P_i\}$$

then, [K] is called NSMACL. By adding the concert deformation condition and equilibrium condition, the relation between the torque acting on the driving gear and the load along the contact lines can be established, and the contact stress and gear tooth deformation can also be obtained. Three-dimensional solid models of spur and helical bevel gear teeth have been established in their work, in which the contact range and the whole finite element model can be automatically adjusted with the change of meshing process. In their research, the NSMACL is based on the assumption that the teeth are in line contact.

Zhang, Esat, Shi (1999) introduced a new approach to analyse the loading and stressing distribution on the tooth surface of spur and helical gears. Combining a discrete gear model with finite element analysis (FEA) it has both good computational accuracy and efficiency. The authors use a FEA algorithm to undertake the mechanical analysis. A 2D FEA model is applied to calculate the tooth compliance and mesh stiffness, incorporated to take into account the varying meshing stiffness and geometric modification. The numerical examples presented show acceptable accuracy of this approach.

Additionally, Elkholy, Elsharkawy and Yigit (1998) presented a procedure for calculating transmitted load distribution along face width as well as tooth stresses of straight bevel gears. The procedure assumes that a straight bevel gear, when projected on a plane tangent to the back cone, can be approximated as a spur gear having a pitch radius equal to the back-cone radius and same pitch as the bevel gear. To increase the solution accuracy, the bevel gear is divided into a number of spur gears by a finite number of slicing planes that are parallel to the plane of projection. Each slice is then analyzed as a separate spur gear, and tooth stiffness, load and stresses are determined separately. As a result, the load and stress distributions of the actual bevel gear are obtained. The procedure assumes that the sum of tooth deflection, profile modification and manufacturing errors of the pairs of contacting slices of the pinion and gear are all equal, in order to avoid overlap and tooth interference. It is also assumed that the sum of the normal loads contributed by each pair of contacting slices

is equal to the total normal load on the entire bevel gear, which is obtainable from the transmitted power/torque. Once the normal loads for all slices representing the bevel gear are determined, fillet and Hertzian stresses are calculated from the applied loads and slice geometry. Consequently, the distribution of such stresses for the actual bevel gear is also calculated. An example is presented to explain the procedure. Experimental substantiation, using strain gauge measurements, is also presented to demonstrate the validity of the procedure.

Summarising all the above work, the tooth contact patterns are assumed as line contact, and the solutions obtained are for spur gear or helical gears.

2.4.3 Investigation of loading share of gear drives

Although the loading distribution of a single tooth provides important information for gear design, the most important factors for gear design such as comprehensive load sharing of the simultaneously engaging teeth, real contact ratio as well as the effect of the errors on load sharing still remain unknown.

The evaluation of load sharing among multiple tooth pairs simultaneously in contact is a more complex process but essential for gearing design. Litvin and Chen et.al(1996) developed an approach for Loaded Tooth Contact Analysis (LTCA) of a hypoid gear drive with point tooth contact. In their method, the principal curvatures and directions at a current point of tangency are derived and the point contact is recognised to spread into an ellipse under load. The distributed contact force over the contact area is simplified as an elliptical distribution of contact forces along the major axis of the contact ellipse. Tooth contact analysis (TCA) is applied to determine the contact paths on the tooth surface and the transmission errors caused by misalignment. Then, the authors use finite element models of gear and pinion to conduct the following analyses: (1) determination of the contact force and its distribution; (2) determination of the tooth deflection, the load share, and the real contact ratio; and (3) stress analysis by application of the finite element method. The load share and stress analysis for double circular-arc helical gears is also conducted using this approach (Lu, Litvin, et.al.,1995).

Zhang and Fang (1998) presented an approach for the analysis of tooth contact and load distribution of helical gears with crossed axes. The approach is based on a tooth contact model that accommodates the influence of tooth profile modifications, gear manufacturing errors and tooth surface deformation on gear mesh quality. In their approach, the tooth contact load distribution is assumed as a line distribution along the relative principal direction of the contacting tooth surfaces. As compared with existing tooth contact analysis models that assume rigidity for the contact surfaces, this approach provides a more realistic analysis on gear transmission errors, contact patterns and the distribution of contact load. According to the results of the numerical analysis, it is found that helical gears with small crossed angles have meshing characteristics and load distribution similar to those of parallel-axis gears.

Additionally Bair and Tsay (1998) applied finite element methods to evaluate the actual contact ratio, which is an important gear design parameter for gear bending and contact stresses. The authors calculate the kinematic error of the ZK-type dual-lead worm gear set by applying the tooth contact analysis (TCA) method. Two kinds of contact ratios, the instantaneous contact teeth (ICT) and the average contact ratio (ACR) are investigated and calculated by applying the TCA method. ICT is an important design parameter for a dual-lead worm gear set when the gear set is used in a machine subjected to large impact forces, while ACR is a useful design factor for assessing gear tooth strength and dynamic load. They found that this type of worm gear set with a shorter center distance assembly can increase the value of ACR during gear meshing. The effects of gear parameters on contact teeth, contact ratios, average contact ratios and kinematic errors under various conditions are illustrated by the authors.

Another investigation of the load distribution among the multiple simultaneous contact tooth pairs is provided by Gosselin (1995). He presented a calculation method for load sharing and transmission error of spiral bevel and hypoid gears. The equations presented take into account the tooth displacement under bending and shearing as calculated by FEA, the contact deformation obtained from the classical Hertz theory, and the initial tooth profile separation due to profile mismatch. A simplication of the general case is presented to estimate initial values, as the non-linear system of equations used to find load sharing is solved with a Newton-Raphson

based numerical algorithm. Motion error under load is then calculated from the gear blank rotation produced by bending, shearing and contact deformation of the meshing teeth, and added to the initial kinematical motion error.

The author applied the method to five spiral bevel gear test cases. The results show that low contact ratio gears may experience large motion error under load in the single tooth contact zone; the smaller the unloaded motion error, the larger the loaded motion error is likely to be. However, in this research, edge effects have not been considered in the calculation of the contact deformation.

All the above approaches contribute to a better understanding of load sharing and stress analysis for simultaneously contact tooth pairs for particular gear drives. But these approaches depend on an iterative algorithm and lack an explicit mathematical expression for load share of multiple tooth engagement; meanwhile, the load distribution on the tooth surface is simplified as a line distribution in their method. Moreover, research on the load share of worm gear drives, of which the geometry is much more complex than conventional spur gears, has not been reported yet.

2.5 Conclusions

According to the general review of research in worm gear drives, reducing the sensitivity of worm gearing due to misalignment and stabilising the bearing contact are part of the main goals of current worm gear research. The localised tooth contact enables the designer to reduce the sensitivity. However, although current methods may achieve localised contact, they cannot ensure that the contact area is placed at an ideal position and so the meshing quality is uncontrollable.

With the development of CAD/CAM, a geometric model is necessary for analysis of stress, deformation and load distribution in worm gears. Meanwhile, a three dimensional model of worm gear conducting the virtual tooth engagement is needed to obtain the 3D simulation of assembly and transmission motion of worm gearing. But such a model has never been reported.

The analysis methods for tooth contact in worm gears widely in use now are usually based on the assumption of rigid teeth and a uniform load, while contact stress distribution is considered along an ideal contact line. This is obviously not a true reflection of the reality. However, in spite of the fact that the load can alter the performance of worm gearing substantially, most work reported didn't present an effective method to analyse the tooth behaviour under load.

Therefore, a general method that is capable of optimising the contact area, eliminating any interference of the tooth profile, as well as analysing the tooth behaviour under the real load, is highly overdue. Likewise, evaluation of load share and real contact ratio is a basic requirement for the design of new generation gearing with large loading capacity but compact size.

Hence, this research will contribute a novel approach with an integration of CAD/CAE techniques to develop a new type of worm gearing with preferable localised tooth contact. Further more, this project will develop a general method to evaluate the worm gearing performance under load and determine the comprehensive loading share of the simultaneously engaging teeth, and real contact ratio as well as the effect of errors on load share.

Chapter 3. Determination of the Modification Parameters for Worm Gear Drives with Localised Tooth Contact

The tooth surfaces of conventional worm gear drives are theoretically designed in line contact. However, due to errors of manufacture and assembly, the actual contact may shift to the boundary of the tooth surface and result in so-called "edge contact", which seriously reduces the loading capacity and the service life of worm gear drives.

In this chapter, a new method is proposed to obtain a preferable localised tooth contact (PLTC) for worm gear drives, which means designer can choose the contact position in his preference. With this method, the initial contact can be located at a preferable position, the moving direction of the contact can be predicted in order to achieve better meshing characteristics, and the contact at every instant of tooth contact can be investigated. Compared with traditional line contact, the PLTC is much less sensitive to errors and can achieve high transmission quality and cut down the time and effort spent in production and assembly.

The new method is based on the theory of differential geometry. The mathematical model developed is able to modify the design parameters of the worm gear drive to achieve the preferable localised tooth contact.

3.1 Coordinate Systems

In worm gear research, rotation and transformation of the coordinate system are often applied to calculate the worm gear geometry. The matrix calculator is a proper tool to perform the calculation of coordinate system transforms. To describe the relationships of worm and wheel in a three dimensional space, three coordinate systems are presented as shown in Figure 3.1: the global fixed coordinate system $\Sigma_0 = [o; \vec{i}, \vec{j}, \vec{k}]$; the coordinate system $\Sigma_1 = [o_1; \vec{i}_1, \vec{j}_1, \vec{k}_1]$ which is connected to the worm, rotating around the axis $\vec{k}_1$, and the system $\Sigma_2 = [o_2; \vec{i}_2, \vec{j}_2, \vec{k}_2]$ connected to the wheel and rotating around the axis $\vec{k}_2$. A_0 is the centre distance of the worm and wheel, $\vec{\xi} = \overrightarrow{o_2 o_1} = A_0 \vec{i}$.

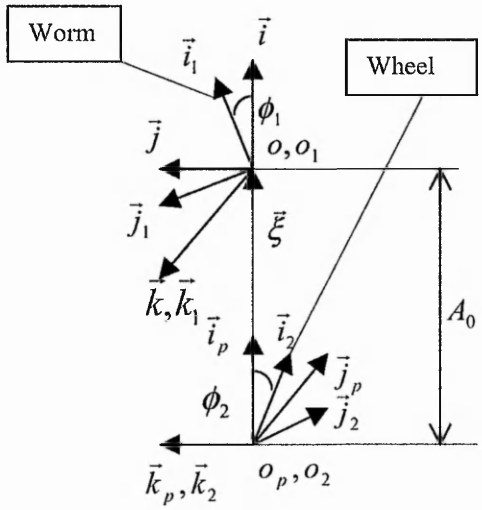

Figure.3.1 Coordinate systems describing worm gear drives

During transmission, the worm rotates with angle ϕ_1 around axis $\vec{k}_1$ while the wheel rotates with angle ϕ_2 around axis $\vec{k}_2$, and the transmission ratio is $i_{12} = \frac{d\phi_1}{dt} / \frac{d\phi_2}{dt} = \frac{\omega^{(1)}}{\omega^{(2)}}$.

3.2 Involute Type Worm Gear

Involute worm gearing (ZI type) is considered as an example in this research. The surface of an involute type worm is generated by a straight line tool that performs a screw motion being tangent to the helix P_0P on the base cylinder as shown in Figure 3.2 where the generation process of the tooth of an involute worm is illustrated. In Figure 3.2, the cutting edge of the tool is tangent to both the base cylinder and the helix curve, the radius of base cylinder is r_{01}, and δ_1 is the angle of the tool cutting edge, which equals the lead angle of the base cylinder of the worm.

The worm cutter is always placed in the tangent plane of the base cylinder. When the cutting tool moves along the screw trajectory, the surface generated by its edge is the tooth profile of the involute worm. The tool parameter u is defined within the coordinate system fixed on the tool $\Sigma_u = \left(o_u; \vec{i}_u, \vec{j}_u, \vec{k}_u\right)$, as shown in Figure 3.3.

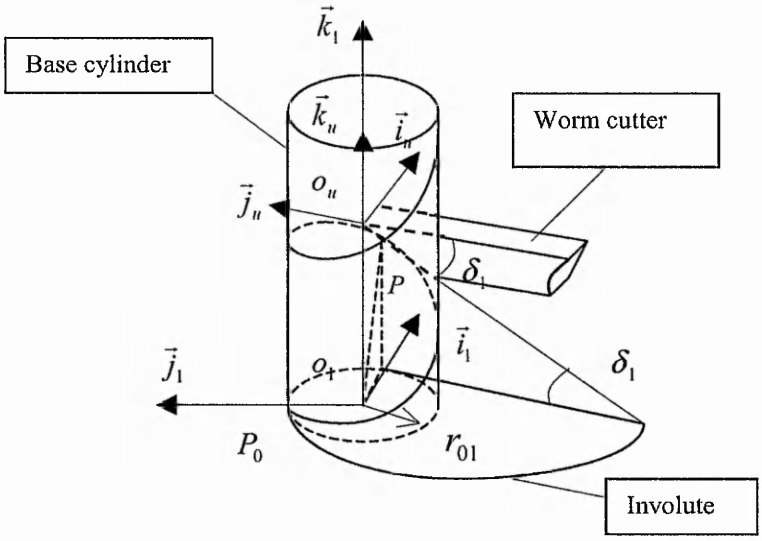

Figure. 3.2 Generation of involute worm surface

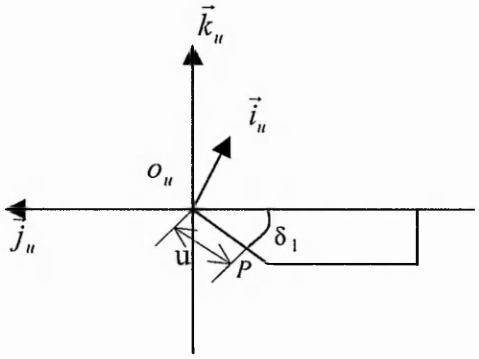

Figure 3.3 Tool parameters

For a conventional worm, it is equivalent to the hob used to produce the wheel, the vector of a point P on the cutting edge is represented in Σ_u as :

$$\vec{r}_u = x_u\vec{i}_u + y_u\vec{j}_u + z_u\vec{k}_u = \begin{pmatrix} x_u \\ y_u \\ z_u \end{pmatrix} = \begin{pmatrix} r_{01} \\ -u\cos\delta_1 \\ -u\sin\delta_1 \end{pmatrix} \qquad (3.1)$$

Hence, using the transform matrix M_{1u}, the tooth surface vector in Σ_1 is given by

$$\vec{r}_1 = \vec{r}_1(u,\phi_u) = M_{1u}\cdot\vec{r}_u = \begin{pmatrix} x_1 \\ y_1 \\ z_1 \end{pmatrix} = \begin{pmatrix} r_{01}\cos\phi_u + u\cos\delta_1\sin\phi_u \\ r_{01}\sin\phi_u - u\cos\delta_1\cos\phi_u \\ -u\sin\delta_1 + p\phi_u \end{pmatrix} \qquad (3.2)$$

$$M_{1u} = \begin{bmatrix} \cos\phi_u & -\sin\phi_u & 0 & 0 \\ \sin\phi_u & \cos\phi_u & 0 & 0 \\ 0 & 0 & 1 & p\phi_u \\ 0 & 0 & 0 & 1 \end{bmatrix}$$

where p is the screw parameter, ϕ_u is the tool rotation angle with respect to the worm , and the normal to the tooth surface is

$$\vec{n}_1 = \frac{\partial\vec{r}_1}{\partial u}\times\frac{\partial\vec{r}_1}{\partial\phi_u} = -\sin\delta_1\sin\phi_u\vec{i}_1 + \sin\delta_1\cos\phi_u\vec{j}_1 - \cos\delta_1\vec{k}_1 \neq 0 \qquad (3.3)$$

The worm wheel tooth surface is the envelope of the family of worm surfaces, and hence

$$\vec{r}_2 = \vec{r}_2(u,\phi_u,\phi_1) = M_{21}\cdot\vec{r}_1(u,\phi_u), \qquad f(u,\phi_u,\phi_1) = 0 \qquad (3.4)$$

$$M_{21} = \begin{bmatrix} \cos\phi_1\cos\phi_2 & -\sin\phi_1\cos\phi_2 & -\sin\phi_2 & A_0\cos\phi_2 \\ -\cos\phi_1\sin\phi_2 & \sin\phi_1\sin\phi_2 & -\cos\phi_2 & -A_0\sin\phi_2 \\ \sin\phi_1 & \cos\phi_1 & 0 & 0 \\ 0 & 0 & 0 & 1 \end{bmatrix}$$

In the above (3.2) ~ (3.4), $f = 0$ is the equation of worm-wheel meshing; $\vec{r}_1, \vec{r}_2$ are the vectors of the worm and wheel surfaces; the subscripts 1 and 2 refer to co-ordinate systems, Σ_1 and Σ_2, which are rigidly connected to the worm and the wheel; M_{21} is the matrix of transmission from Σ_1 to Σ_2; $\vec{n}_1$ is the normal to the worm surface; ϕ_1 and ϕ_2 are the rotation angles of the worm and wheel respectively.

3.3 Modification of the Tooth Geometry

In this research, the basic idea to obtain the localised contact is to modify the worm, while the hob remains unchanged. This enables the use of standard or existing hobs, which is obviously economical. Although the hob is not changed, both the worm surface and the wheel surface are to be modified in order to obtain the preferable localised tooth contact. Considering the requirement of continuous tangency contact, the following are considered for the modifications:

- Reduce the worm diameter and increase the lead angle of the worm.
- Make the modified worm have the same normal pitch at the reference point as the original one.
- Change the hob mounting angle θ_h to modify the wheel tooth surface

As mentioned in section 3.2, involute worm gearing (ZI type) is chosen as an example for the design. To achieve the preferable localised tooth contact, i.e. the contact area is located in a pre-defined position, a new approach has been proposed on the basis of meshing principles. The major steps of the tooth modification are shown in Figure 3.4.

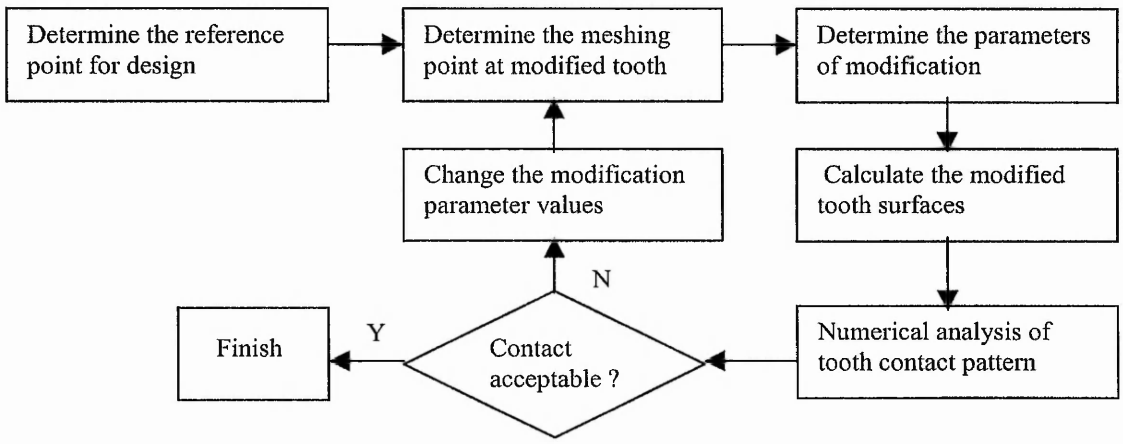

Figure 3.4. Procedure of tooth modification

3.3.1 Determine the Reference Point for Design

It is necessary to determine the reference point for design in order to locate the tooth contact at the position preferred. The point is used as a design reference and can be chosen by the designer for personal preference. However, it is recommended to locate the reference point on the tooth surface where localised contact occurs with the theoretical transmission ratio ($i_{21} = z_1 / z_2$) during tooth meshing. As shown in Figure 3.5, a point P_R on the pitch circle of the worm is chosen as the reference point.

The vector of the reference point can be expressed in the coordinate system Σ_2 as $\vec{r}_1^{(2)} = (r_{1x}, r_{1y}, r_{1z})$, where r_{1x}, r_{1y}, r_{1z} are the coordinate values in Σ_2 representing the position of the reference point. The normal vector at the point is expressed by equation 3.3. Converting the normal vector into the coordinate system Σ_2, we can have the expression below,

$$\vec{n}_1^{(2)} = \begin{pmatrix} n_{1x}^{(2)} \\ n_{1y}^{(2)} \\ n_{1z}^{(2)} \end{pmatrix} = -\sin\delta_1 \cdot \sin\phi_u \vec{i}_2 + \cos\delta_1 \vec{j}_2 + \sin\delta_1 \cdot \cos\phi_u \vec{k}_2 \qquad (3.5)$$

where, the angular parameter ϕ_u at the reference point is determined by its co-ordinate values, δ_1 is the lead angle of the worm.

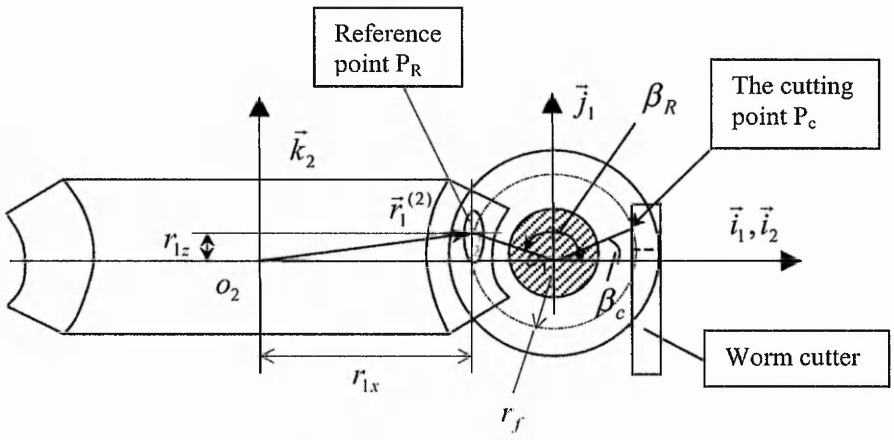

Figure 3.5 Position of the reference point

In the coordinate system $\Sigma_u = \left(o_u; \vec{i}_u, \vec{j}_u, \vec{k}_u\right)$, the radius of the pitch circle is described as $r_f^2 = x_u^2 + y_u^2 = r_{01}^2 + u^2 \cdot \cos^2 \delta_1$. Since the reference point is located at the pitch circle, its tool parameter is expressed as

$$u = \frac{\sqrt{r_f^2 - r_{01}^2}}{\cos \delta_1} \tag{3.6}$$

When the $\Sigma_u = \left(o_u; \vec{i}_u, \vec{j}_u, \vec{k}_u\right)$ of the cutting tool is coincident with $\Sigma_0 = [o; \vec{i}, \vec{j}, \vec{k}]$, the coordinate values of the cutting point P_c are expressed as

$$\begin{cases} x_0 = x_u = r_{01} \\ y_0 = y_u = -u \cos \delta_1 \end{cases} \tag{3.7}$$

$$\beta_c = tg^{-1}\left(\frac{y_0}{x_0}\right)$$

Since r_{1z} is determined as shown in Figure 3.5, the angle of the reference point P_R is written as,

$$\beta_R = \pi - \sin^{-1}\left(\frac{r_{1z}}{r_f}\right)$$

Therefore, the angular parameter ϕ_u at the reference point is determined as

$$\phi_u = \beta_R - \beta_c \tag{3.8}$$

$$r_{1x} = A_0 + r_f \cdot \cos \beta_R \tag{3.9}$$

For the reference point, only coordinate value r_{1y} is unknown, and will be determined later by the meshing equation. The relative velocity at the reference point $\vec{v}_{ref}$ is represented as (Litvin, 1994):

$$\vec{v}_{ref} = \vec{v}(\vec{r}_{ref}, \theta_h) = \vec{\omega}^{(12)} \times \vec{R}_{ref} - \vec{\omega}^{(1)} \times \vec{\xi} \tag{3.10}$$

$$\vec{\omega}^{(1)} = \omega^{(1)}[-\sin \phi_2 \vec{i}_2 - \cos \phi_2 \vec{j}_2] = \omega^{(2)}[-i_{12} \sin \phi_2 \vec{i}_2 - i_{12} \cos \phi_2 \vec{j}_2]$$
$$\vec{\omega}^{(2)} = \omega^{(2)} \vec{k}_2$$
$$\vec{\xi} = A_0 \cos \phi_2 \vec{i}_2 - A_0 \sin \phi_2 \vec{j}_2$$

$$\vec{\omega}^{(12)} = \vec{\omega}^{(1)} - \vec{\omega}^{(2)} = \omega^{(2)}[-i_{12} \sin \phi_2 \vec{i}_2 - i_{12} \cos \phi_2 \vec{j}_2 - \vec{k}_2]$$

$$\vec{\omega}^{(1)} \times \vec{\xi} = \begin{vmatrix} \vec{i}_2 & \vec{j}_2 & \vec{k}_2 \\ -i_{12}\omega^{(2)} \sin\phi_2 & -i_{12}\omega^{(2)} \cos\phi_2 & 0 \\ A_0 \cos\phi_2 & -A_0 \sin\phi_2 & 0 \end{vmatrix} = i_{12} A_0 \omega^{(2)} (\sin^2\phi_2 + \cos^2\phi_2)\vec{k}_2$$

$$= i_{12} A_0 \omega^{(2)} \vec{k}_2$$

$$\therefore \vec{\omega}^{(12)} \times \vec{R}_{ref} = \begin{vmatrix} \vec{i}_2 & \vec{j}_2 & \vec{k}_2 \\ -\omega^{(2)} i_{12} \sin\phi_2 & -\omega^{(2)} i_{12} \cos\phi_2 & -\omega^{(2)} \\ r_{1x} & r_{1y} & r_{1z} \end{vmatrix}$$

To simplify the derivation, it is assumed that $\omega^{(2)} = 1, \phi_2 = 0$. However, this does not affect the final result. Thus, the relative velocity is derived as,

$$\begin{aligned} \vec{v}_{ref} &= \vec{\omega}^{(12)} \times \vec{R}_{ref} - \vec{\omega}^{(1)} \times \vec{\xi} \\ &= (r_{1y} - r_{1z} i_{12})\vec{i}_2 - r_{1x}\vec{j}_2 + i_{12}(r_{1x} - A_0)\vec{k}_2 \end{aligned} \qquad (3.11)$$

The reference point satisfies the meshing equation

$$\vec{n}_1^{(2)} \cdot \vec{v}_{ref} = 0 \qquad (3.12)$$

By introducing equation 3.5 into the above meshing equation, the equation is derived as,

$$\vec{n}_1^{(2)} \cdot \vec{v}_{ref} = n_{1x}^{(2)} \cdot (r_{1y} - r_{1z} i_{12}) - n_{1y}^{(2)} \cdot r_{1x} + n_{1z}^{(2)} \cdot i_{12}(r_{1x} - A_0) = 0$$

Since the coordinate values r_{1x}, r_{1z} are already known, r_{1y} can be obtained from the equation below. Then the reference point on the wheel tooth surface can be determined.

$$\begin{aligned} r_{1y} &= r_{1z} i_{12} + \frac{n_{1y}^{(2)} \cdot r_{1x}}{n_{1x}^{(2)}} - \frac{n_{1z}^{(2)} \cdot i_{12}(r_{1x} - A_0)}{n_{1x}^{(2)}} \\ &= r_{1z} i_{12} - \frac{\cos\delta_1 \cdot r_{1x}}{\sin\delta_1 \cdot \sin\phi_u} + \frac{\cos\phi_u \cdot i_{12}(r_{1x} - A_0)}{\sin\phi_u} \end{aligned} \qquad (3.13)$$

3.3.2 Determine the Meshing Point of the Modified Tooth Surfaces

After the reference point is determined, the next step is to determine the meshing point at the modified tooth surface. Figure 3.6 illustrates the worm wheel manufacturing position, where the hob is mounted with an angle θ_h. The hob used here has the same design parameters as the theoretical worm. Its mounting position is determined by the centre distance A_h and mounting angle θ_h.

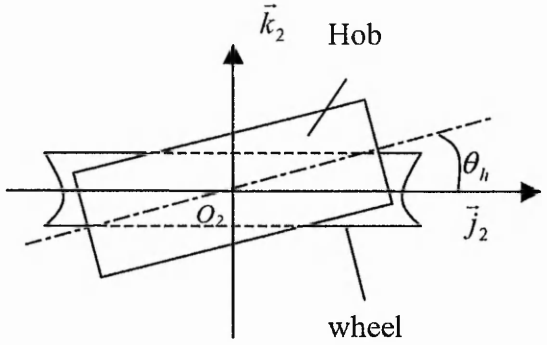

Fig. 3.6 Hob with mounting angle θ_h

Due to the tooth modification, the cutting position of the pre-defined reference point in the wheel tooth surface is different from the meshing position shown in Figure 3.5. There will be a gap between the meshing position and the cutting position. It can be considered that the wheel rotates an angle from the meshing position to reach the cutting position. The vector of the cutting position is represented as $\vec{r}_M^{(2)}$, and the normal vector of the cutting position is represented as $\vec{n}_M^{(2)}$.

The meshing point of the modified tooth surface is described with a new parameter, angle λ. The modified tooth surface of the wheel is different from the original one. As shown in Figure 3.7, to ensure that the reference point is generated at the wheel tooth using the hob, the wheel needs to turn into the right engaging position around the wheel axis with an angle λ. Thus, the hob cuts the wheel to generate the reference point at the position M.

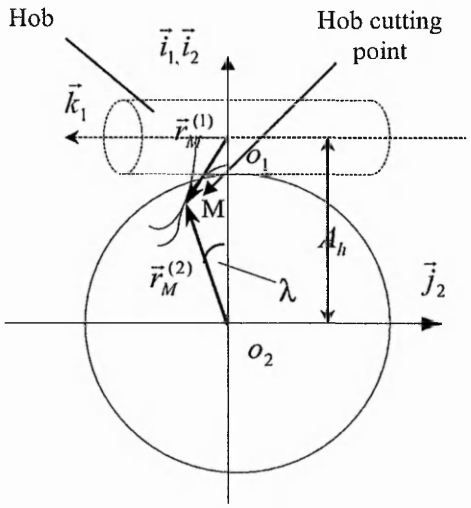

Figure 3.7 Meshing position of the Hob Cutting Process

The normal vector $\vec{n}_M^{(2)}$ should be in coincidence with the normal vector of the reference point. Thus, the normal and the vector at the point M are obtained by rotating the $\vec{n}_{ref}, \vec{R}_{ref}$ around the wheel axis with an angle λ, as shown in below

$$\vec{n}_M^{(2)} = n(\vec{n}_1^{(2)}, \lambda) = \begin{pmatrix} n_{Mx}^{(2)} \\ n_{My}^{(2)} \\ n_{Mz}^{(2)} \end{pmatrix} = \begin{pmatrix} \cos\lambda & -\sin\lambda & 0 \\ \sin\lambda & \cos\lambda & 0 \\ 0 & 0 & 1 \end{pmatrix} \cdot \begin{pmatrix} n_{1x}^{(2)} \\ n_{1y}^{(2)} \\ n_{1z}^{(2)} \end{pmatrix} = \begin{pmatrix} n_{1x}^{(2)} \cos\lambda - n_{1y}^{(2)} \sin\lambda \\ n_{1y}^{(2)} \cos\lambda + n_{1x}^{(2)} \sin\lambda \\ n_{1z}^{(2)} \end{pmatrix} \tag{3.14}$$

$$\vec{r}_M^{(2)} = r(\vec{r}_1^{(2)}, \lambda) = \begin{pmatrix} r_{Mx}^{(2)} \\ r_{My}^{(2)} \\ r_{Mz}^{(2)} \end{pmatrix} = \begin{pmatrix} \cos\lambda & -\sin\lambda & 0 \\ \sin\lambda & \cos\lambda & 0 \\ 0 & 0 & 1 \end{pmatrix} \cdot \begin{pmatrix} r_{1x} \\ r_{1y} \\ r_{1z} \end{pmatrix} = \begin{pmatrix} r_{1x} \cos\lambda - r_{1y} \sin\lambda \\ r_{1y} \cos\lambda + r_{1x} \sin\lambda \\ r_{1z} \end{pmatrix} \tag{3.15}$$

The movement of the hob can be simplified as moving along its axis. This assumption does not affect conjugation of the tooth surfaces (Wang et. al, 1988), thus, the relative velocity of the meshing point is presented as

$$\vec{v}_M^{(21)} = \vec{v}^{(2)} - \vec{v}^{(1)} = \vec{\omega}^{(2)} \times \vec{r}_M^{(2)} - \vec{\omega}^{(1)} \cdot p$$

$$
\begin{aligned}
&= \vec{k}_2 \times (r_{Mx}^{(2)}\vec{i}_2 + r_{My}^{(2)}\vec{j}_2 + r_{Mz}^{(2)}\vec{k}_2) + i_{12}\cdot p\cdot\cos\theta_h\vec{j}_2 + i_{12}\cdot p\cdot\sin\theta_h\vec{k}_2 \\
&= r_{Mx}^{(2)}\vec{j}_2 - r_{My}^{(2)}\vec{i}_2 + i_{12}\cdot p\cdot\cos\theta_h\vec{j}_2 + i_{12}\cdot p\cdot\sin\theta_h\vec{k}_2 \qquad (3.16)\\
&= -r_{My}^{(2)}\cdot\vec{i}_2 + (r_{Mx}^{(2)} + i_{12}\cdot p\cdot\cos\theta_h)\cdot\vec{j}_2 + i_{12}\cdot p\cdot\sin\theta_h\vec{k}_2
\end{aligned}
$$

The meshing equation $\vec{n}_M^{(2)}\cdot\vec{v}_M^{(21)} = 0$ at the hob cutting point M is written as

$$n_{Mx}^{(2)}v_{Mx}^{(21)} + n_{My}^{(2)}v_{My}^{(21)} + n_{Mz}^{(2)}v_{Mz}^{(21)} = 0$$

by introducing the equations (3.12) and (3.13) into the meshing equation

$$
\begin{aligned}
&-(n_{1x}^{(2)}\cos\lambda - n_{1y}^{(2)}\sin\lambda)(r_{1y}\cos\lambda + r_{1x}\sin\lambda) \\
&+(n_{1y}^{(2)}\cos\lambda + n_{1x}^{(2)}\sin\lambda)(r_{1x}\cos\lambda - r_{1y}\sin\lambda + i_{12}\cdot p_w\cdot\cos\theta_h) + n_{1z}^{(2)}\cdot i_{12}\cdot p\cdot\sin\theta_h = 0
\end{aligned}
$$

it is further derived as below

$$
\begin{aligned}
&r_{1x}\cdot n_{1y}^{(2)} - n_{1x}^{(2)}\cdot r_{1y} + i_{12}\cdot p\cdot n_{1y}^{(2)}\cdot\cos\theta_h\cdot\cos\lambda + i_{12}\cdot p\cdot n_{1x}^{(2)}\cdot\cos\theta_h\cdot\sin\lambda \\
&+ n_{1z}^{(2)}\cdot i_{12}\cdot p\cdot\sin\theta_h = 0
\end{aligned}
$$

$$
\begin{aligned}
&i_{12}\cdot p\cdot n_{1x}^{(2)}\cdot\cos\theta_h\cdot\sin\lambda + i_{12}\cdot p\cdot n_{1y}^{(2)}\cdot\cos\theta_h\cdot\cos\lambda \\
&= n_{1x}^{(2)}\cdot r_{1y} - r_{1x}\cdot n_{1y}^{(2)} - n_{1z}^{(2)}\cdot i_{12}\cdot p\cdot\sin\theta_h
\end{aligned} \qquad (3.17)
$$

where, p is the pitch of the hob. Re-write the equation in the style below

$$\alpha\cdot\sin\lambda + \beta\cdot\cos\lambda = \gamma \qquad (3.18)$$

by solving the equation above, λ is determined

$$\lambda = tg^{-1}\frac{\gamma}{\sqrt{\alpha^2+\beta^2-\gamma^2}} - tg^{-1}\frac{\beta}{\alpha} \qquad (3.19)$$

where,

$$\alpha = i_{12}\cdot p\cdot n_{1x}^{(2)}\cdot\cos\theta_h$$

$$\beta = i_{12}\cdot p\cdot n_{1y}^{(2)}\cdot\cos\theta_h$$

$$\gamma = n_{1x}^{(2)}\cdot r_{1y} - r_{1x}\cdot n_{1y}^{(2)} - n_{1z}^{(2)}\cdot i_{12}\cdot p\cdot\sin\theta_h$$

3.3.3 Determine the Hob Mounting Parameters

During modification, a normal hob is used to manufacture the wheel with a specific mounting angle θ_h and centre distance A_h. The hob itself performs a screw motion in the manufacturing process. The velocity of a cutting point on its tooth surface is perpendicular to its normal. This condition is expressed as $\vec{n}_M^{(2)} \cdot \vec{v}_M = 0$. The normal at the point M of the modified tooth surface $\vec{n}_M^{(2)}$ is given in the above (3.14). From Figure 3.7, $\vec{r}_M^{(1)} = \vec{r}_M^{(2)} - A\ \vec{i}_2$, hence, the velocity at point M is derived as below.

$$\begin{aligned}\vec{v}_M &= \vec{\omega}^{(1)} \times \vec{r}_M^{(1)} + p \cdot \vec{\omega}^{(1)} = \vec{\omega}^{(1)} \times (\vec{r}_M^{(2)} - A_h \cdot \vec{i}_2) + p \cdot \vec{\omega}^{(1)} \\ &= -\omega^{(1)} \vec{j}_2 \times (r_{Mx}^{(2)} \vec{i}_2 + r_{My}^{(2)} \vec{j}_2 + r_{Mz}^{(2)} \vec{k}_2 - A_h \vec{i}_2) - p\omega^{(1)} \vec{j}_2 \\ &= \omega^{(1)} [-r_{Mz}^{(2)} \vec{i}_2 - p\vec{j}_2 + (r_{Mx}^{(2)} - A_h)\vec{k}_2]\end{aligned} \tag{3.20}$$

where, A_h is the centre distance of mounting the modified wheel, p is the pitch of the hob. The equation $\vec{n}_M^{(2)} \cdot \vec{v}_M = 0$ is further derived as

$$n_{Mx}^{(2)} v_{Mx} + n_{My}^{(2)} v_{My} + n_{Mz}^{(2)} v_{Mz} = 0$$

$$n_{Mx}^{(2)} (-r_{Mz}^{(2)}) + n_{My}^{(2)} (-p) + n_{Mz}^{(2)} (r_{Mx}^{(2)} - A_h) = 0$$

hence, the mounting centre distance of the hob can be obtained as below

$$A_h = r_{Mx}^{(2)} - r_{Mz}^{(2)} \cdot \frac{n_{Mx}^{(2)}}{n_{Mz}^{(2)}} - p \cdot \frac{n_{My}^{(2)}}{n_{Mz}^{(2)}} \tag{3.21}$$

When the hob mounting angle θ_h is given by the designer, the angle λ is obtained by equation 3.19, $\vec{n}_M^{(2)}$ can be calculated using equation 3.14, and the centre distance for hob mounting is determined by equation 3.21. Thus, the parameters of hob mounting are now determined.

3.3.4 Determination of the Worm Modification Parameters

After the wheel is manufactured using the hob with the above mounting position, the worm has to be modified in order to ensure that the worm and wheel mesh at the reference point of the modified wheel tooth surface. Again the meshing position of the modified worm and wheel is different from the meshing position shown in Figure 3.5, there is a gap between them. As illustrated in Figure 3.8, when the modified worm and wheel mesh in the reference point, the modified meshing position M_1 can be described with another angular parameter λ_1. Its position vector and normal vector are expressed as below

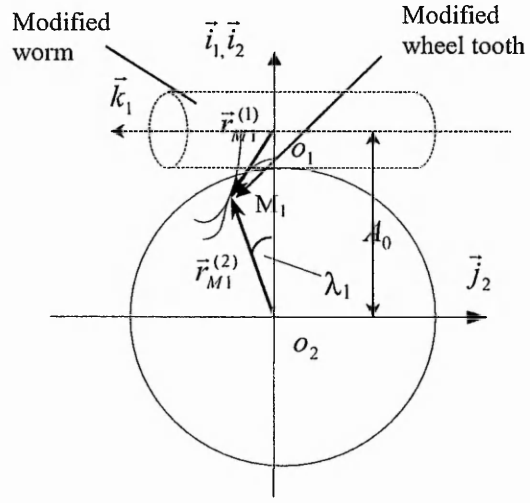

Figure 3.8 Meshing position of the Modified Tooth Surface

$$\vec{n}_{M1}^{(2)} = n(\vec{n}_1^{(2)}, \lambda_1) = \begin{pmatrix} n_{M1x}^{(2)} \\ n_{M1y}^{(2)} \\ n_{M1z}^{(2)} \end{pmatrix} = \begin{pmatrix} n_{1x}^{(2)} \cos\lambda_1 - n_{1y}^{(2)} \sin\lambda_1 \\ n_{1y}^{(2)} \cos\lambda_1 + n_{1x}^{(2)} \sin\lambda_1 \\ n_{1z}^{(2)} \end{pmatrix} \tag{3.22}$$

$$\vec{r}_{M1}^{(2)} = r(\vec{r}_1^{(2)}, \lambda_1) = \begin{pmatrix} r_{M1x}^{(2)} \\ r_{M1y}^{(2)} \\ r_{M1z}^{(2)} \end{pmatrix} = \begin{pmatrix} r_{1x} \cos\lambda_1 - r_{1y} \sin\lambda_1 \\ r_{1y} \cos\lambda_1 + r_{1x} \sin\lambda_1 \\ r_{1z} \end{pmatrix} \tag{3.23}$$

Because the worm is supposed to be installed in the normal position, the mounting angle of the worm is zero. According to the equation 3.19, λ_1 is obtained as below,

$$\lambda_1 = tg^{-1}\frac{\gamma_1}{\sqrt{\alpha_1^{\,2}+\beta_1^{\,2}-\gamma_1^{\,2}}} - tg^{-1}\frac{\beta_1}{\alpha_1} \tag{3.24}$$

where,

$\alpha_1 = i_{12}\cdot p_w \cdot n_{1x}^{(2)}$

$\beta_1 = i_{12}\cdot p_w \cdot n_{1y}^{(2)}$

$\gamma_1 = n_{1x}^{(2)}\cdot r_{1y} - r_{1x}\cdot n_{1y}^{(2)}$

When λ_1 is obtained, the meshing point after modification is determined using equations 3.22 and 3.23. The worm radius at the meshing point is considered as the reference radius of the modified worm, which is expressed as,

$$r_{wf} = \left|\vec{k}_1 \times \vec{r}_{M1}^{(1)}\right| = \left|\vec{k}_1 \times (r_{M1x}^{(1)}\cdot\vec{i}_1 + r_{M1y}^{(1)}\cdot\vec{j}_1 + r_{M1z}^{(1)}\cdot\vec{k}_1)\right| = \left|r_{M1x}^{(1)}\cdot\vec{j}_1 - r_{M1y}^{(1)}\vec{i}_1\right| \tag{3.25}$$

$r_{M1x}^{(1)} = r_{M1x}^{(2)} - A_0$

$r_{M1y}^{(1)} = r_{M1z}^{(2)}$

$$\therefore r_{wf} = \sqrt{(r_{M1x}^{(1)})^2 + (r_{M1y}^{(1)})^2} = \sqrt{(r_{M1x}^{(2)} - A_0)^2 + (r_{M1z}^{(2)})^2} \tag{3.26}$$

When the pitch of the worm p_w is given by the designer, its reference radius r_{wf} is determined by equation (3.26). To secure smooth transmission of the modified worm gear drive, the equation (3.27) is introduced here, which enables continuous tooth contact during the tooth engagement.

$$p_{nh} = p_{nw} \tag{3.27}$$

where, p_{nh} and p_{nw} are the normal pitch of the hob and the modified worm respectively.

Thus, by solving the set of equations (3.21), (3.26) and (3.27), the design parameters of the modified drive can be obtained, including the radius r_{01}^* and lead angle δ_1^* of the modified worm. However, the hob mounting angle and the pitch of the modified

worm need to be given by the designer first, and may be modified later according to the simulation results.

3.3.5 An Example of Tooth Modification

The numerical model has been applied to an involute worm gear drive (ZI) with the following specifications: number of worm threads Z_1=3, number of wheel teeth Z_2=44, module m=9.8, worm reference radius r_w=39.2, worm base radius r_b is 27.22mm, worm lead angle at the reference circle $\delta_f = 20.56°$, worm lead angle at the base circle $\delta_b = 28.37°$, centre distance $A_0 = 255.00$mm, normal pressure angle 20°.

Using the methods developed above, the modification parameters are determined as follows: worm pitch radius r=39.196 mm, worm base radius 27.214mm, worm lead angle at the reference circle $\delta_f' = 20.58°$, worm lead angle at the base circle $\delta_b' = 28.41°$, hob mounting angle =0.5°, the hob mounting centre distance is 254.96 mm. pitch of the modified worm = 14.71 mm.

Chapter 4. Determination of the Modified Tooth Surfaces

4.1 Procedure of Tooth Surface Generation

A mathematical model for generating the modified tooth surfaces has been developed based on differential geometry. It allows calculation of the modified tooth surface of both the worm and the wheel. The general meshing equation derived in this chapter is capable of generating the tooth surfaces produced by the hob with an arbitrary mounting angle θ_h.

The procedure for generating the modified tooth surfaces is shown in Figure 4.1. It starts with the input of the modified parameters. The modified worm surfaces are calculated with the parameters obtained from the analytical method given in Chapter 3, while the modified tooth surface of the wheel is generated using the general meshing equation derived later. The programme is developed within the software package MATLAB.

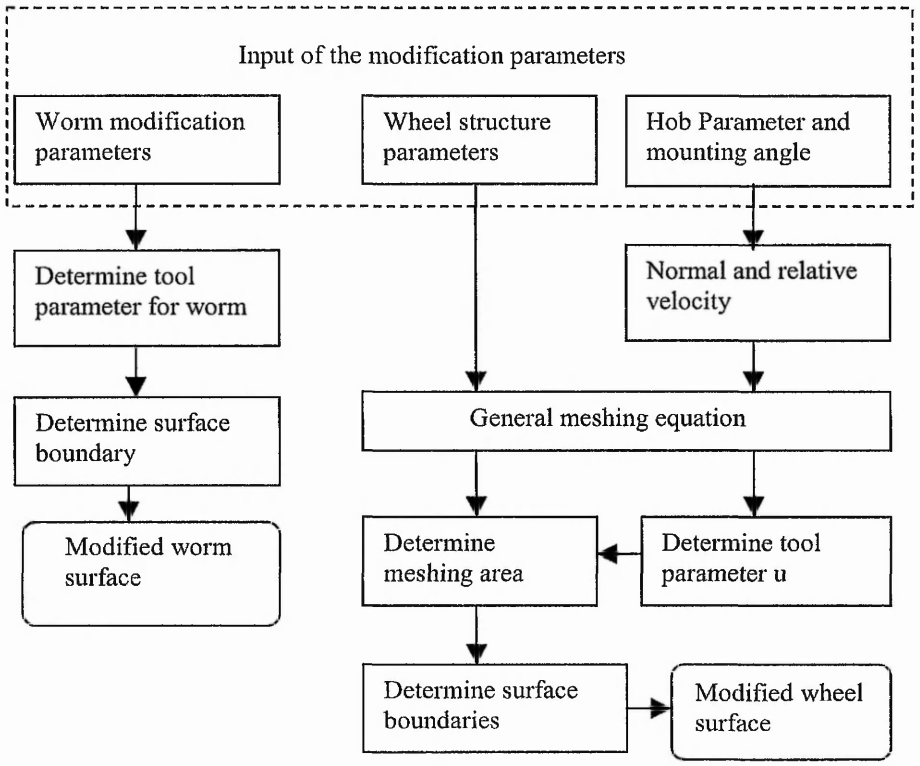

Fig 4.1 Flowchart of determination of the tooth surfaces

4.2 Generation of the Modified Worm Tooth

With the modification parameters obtained from Chapter 3 and referring to equation (2.1), the vector of the modified worm surface can be obtained:

$$\vec{r}_1^{\,A} = \begin{pmatrix} x_1^A \\ y_1^A \\ z_1^A \end{pmatrix} = \begin{pmatrix} r_{01}^* \cdot \cos\phi_u + u \cdot \cos\delta_1^* \cdot \sin\phi_u \\ r_{01}^* \cdot \sin\phi_u - u \cdot \cos\delta_1^* \cdot \cos\phi_u \\ -u \cdot \sin\delta_1^* + p^*\phi_u \end{pmatrix} \tag{4.1}$$

The normal to the modified worm surface is expressed as:

$$N_1^A = \frac{\partial r_1^A}{\partial \phi_u} \times \frac{\partial r_1^A}{\partial u}$$

Thus, the unit normal is represented as:

$$\vec{n}_1^{\,A} = \frac{N_1^A}{\left|N_1^A\right|} = -\sin\phi_u \sin\delta_1 \vec{i}_1 + \cos\phi_u \sin\delta_1 \vec{j}_1 - \cos\delta_1 \vec{k}_1 \tag{4.2}$$

In the above equations (4.1) and (4.2), r_{01}^*, the radius of the base cylinder of the worm, is smaller than the original radius r_{01}; δ_1^*, the lead angle of the worm, is larger than the original angle δ_1; and p^*, the pitch of the worm, is also larger than the original pitch. It is still an involute worm gear, but a little smaller than the original one.

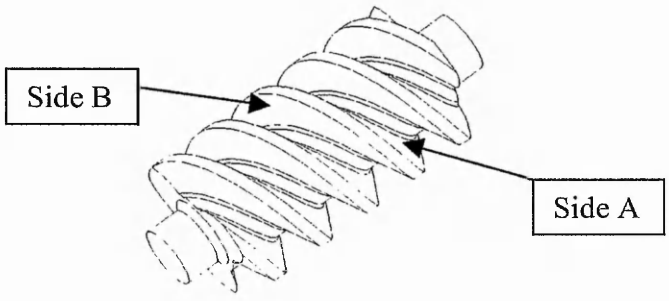

Figure 4.2 Two side surfaces of the worm teeth

However, this is only one side of the tooth surface (side A, see Figure 4.2); to build a three dimensional model, the other side of the tooth must be generated. The surface of side B is generated by the tool as shown in Figure 4.3.

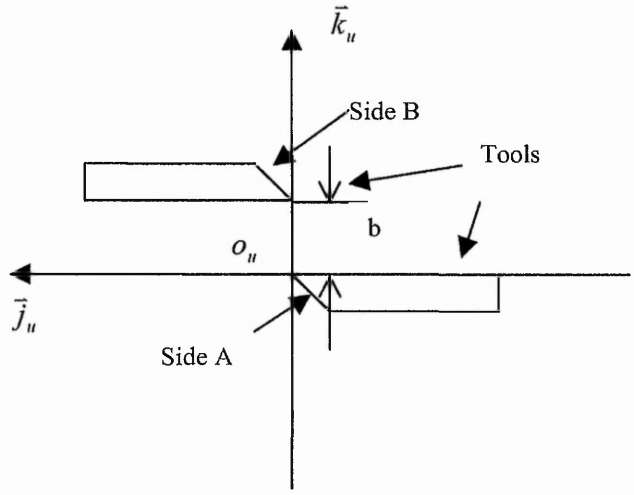

Fig.4.3 The tool positions for generating two sides of the worm tooth thread

The vector of the tool cutting edge for side B is represented in Σ_u as:

$$\vec{r}_u' = x_u'\vec{i}_u + y_u'\vec{j}_u + z_u'\vec{k}_u = \begin{pmatrix} x_u' \\ y_u' \\ z_u' \end{pmatrix} = \begin{pmatrix} r_{01} \\ u\cos\delta_1 \\ u\sin\delta_1 \end{pmatrix} \tag{4.3}$$

Hence, using the transform matrix M_{1u}, the tooth surface vector in Σ_1 is given by

$$\vec{r}_1^{\,B} = \vec{r}_1'(u,\phi_u) = M_{1u}\cdot\vec{r}_u' = \begin{pmatrix} x_1' \\ y_1' \\ z_1' \end{pmatrix} = \begin{pmatrix} r_{01}^*\cdot\cos\phi_u + u\cdot\cos\delta_1^*\cdot\sin\phi_u \\ -r_{01}^*\cdot\sin\phi_u + u\cdot\cos\delta_1^*\cdot\cos\phi_u \\ u\cdot\sin\delta_1^* + b - p^*\phi_u \end{pmatrix} \tag{4.4}$$

$$M_{1u} = \begin{bmatrix} \cos\phi_u & \sin\phi_u & 0 & 0 \\ -\sin\phi_u & \cos\phi_u & 0 & 0 \\ 0 & 0 & 1 & b - p^*\phi_u \\ 0 & 0 & 0 & 1 \end{bmatrix}$$

where, b is the distance between the two positions of the tool as shown in Figure 4.3, and ϕ_u is the tool rotation angle with respect to the worm. The rotation direction of ϕ_u is counter-clockwise, which is opposite to the direction generating side A. The normal vector to the tooth surface is

$$N_1^B = \frac{\partial r_1^B}{\partial \phi_u} \times \frac{\partial r_1^B}{\partial u} \quad , \quad \vec{n}_1^B = \frac{N_1^B}{\left| N_1^B \right|}$$

where, $\frac{\partial r_1^B}{\partial \phi_u} = (-r_{01} \sin\phi_u + u \cos\delta_1^* \cos\phi_u)\vec{i}_1 + (-r_{01} \cos\phi_u - u \cos\delta_1^* \sin\phi_u)\vec{j}_1 - p^* \vec{k}_1$

$$\frac{\partial r_1^B}{\partial u} = \cos\delta_1^* \sin\phi_u \vec{i}_1 + \cos\delta_1^* \cos\phi_u \vec{j}_1 + \sin\delta_1^* \vec{k}_1$$

$$N_1^B = \frac{\partial r_1^B}{\partial \phi_u} \times \frac{\partial r_1^B}{\partial u} = \begin{vmatrix} \vec{i}_1 & \vec{j}_1 & \vec{k}_1 \\ -r_{01} \sin\phi_u + u \cos\delta_1^* \cos\phi_u & -r_{01} \cos\phi_u - u \cos\delta_1^* \sin\phi_u & -p^* \\ \cos\delta_1^* \sin\phi_u & \cos\delta_1^* \cos\phi_u & \sin\delta_1^* \end{vmatrix}$$

$$= -u \cos\delta_1^* \sin\phi_u \sin\delta_1^* \vec{i}_1 - u \cos\delta_1^* \cos\phi_u \sin\delta_1^* \vec{j}_1 + u \cos^2 \delta_1^* \vec{k}_1$$

Hence, the unit normal to side B is represented as:

$$\vec{n}_1^B = \frac{N_1^B}{\left| N_1^B \right|} = -\sin\phi_u \sin\delta_1^* \vec{i}_1 - \cos\phi_u \sin\delta_1^* \vec{j}_1 + \cos\delta_1^* \vec{k}_1 \qquad (4.5)$$

Using the outside diameter and root diameter of the worm as the boundary, the worm tooth surface is determined by the equations (4.1) and (4.4).

4.3 Generation of the Tooth Surfaces of the Modified Wheel

4.3.1 Principle of wheel modification

The modification of the wheel tooth surface is based on altering the mounting angle θ_h of the hob. In other words, the parameters of the hob remain unchanged while the mounting angle is altered to achieve the designed tooth surfaces. The modification enables the wheel tooth surface to be in tangency meshing with the modified worm, as well as locating the local contact area at an appropriate position. Figure 4.4 shows the position of the hob.

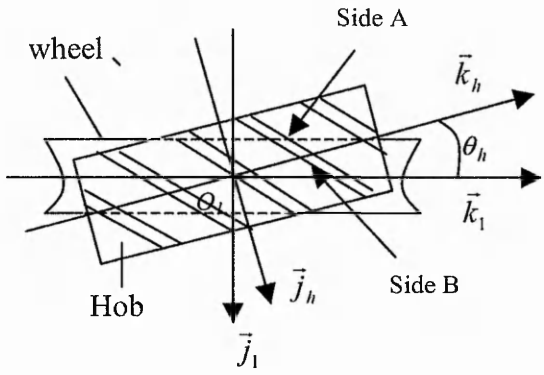

Figure 4.4 Hob mounting position

4.3.2 Equations for hob tooth surfaces

According to the gear theory (Litvin, 1994), the hob is recognised as a worm but provided with slots and relief teeth for cutting. Therefore, the tooth surfaces of the hob are represented as below:

Side A:

$$\vec{r}_1^{\,A} = \begin{pmatrix} x_1^A \\ y_1^A \\ z_1^A \end{pmatrix} = \begin{pmatrix} r_{01} \cdot \cos\phi_u + u \cdot \cos\delta_1 \cdot \sin\phi_u \\ r_{01} \cdot \sin\phi_u - u \cdot \cos\delta_1 \cdot \cos\phi_u \\ -u \cdot \sin\delta_1 + p\phi_u \end{pmatrix} \tag{4.6}$$

$$\vec{n}_1^{\,A} = -\sin\phi_u \sin\delta_1 \vec{i}_1 + \cos\phi_u \sin\delta_1 \vec{j}_1 - \cos\delta_1 \vec{k}_1$$

Side B:

$$\vec{r}_1^{\,B} = \begin{pmatrix} x_1^B \\ y_1^B \\ z_1^B \end{pmatrix} = \begin{pmatrix} r_{01} \cdot \cos\phi_u + u \cdot \cos\delta_1 \cdot \sin\phi_u \\ -r_{01} \cdot \sin\phi_u + u \cdot \cos\delta_1 \cdot \cos\phi_u \\ u \cdot \sin\delta_1 + b - p\phi_u \end{pmatrix} \tag{4.7}$$

$$\vec{n}_1^{\,B} = -\sin\phi_u \sin\delta_1 \vec{i}_1 - \cos\phi_u \sin\delta_1 \vec{j}_1 + \cos\delta_1 \vec{k}_1$$

where, r_{01} is the radius of the base cylinder of the hob, δ_1 is the lead angle of the hob, p is the pitch of the hob and b is the tool distance. All these parameters are equal to those of the original worm. The variables ϕ_u and u are the tool parameters with respect to the hob.

4.3.3 Meshing equation with hob mounting angle

The wheel tooth surface is generated by the meshing of the hob with the wheel. However, with the hob mounting angle θ_h, the meshing equation developed for normal orthogonal worm gear drives is not applicable. A general meshing equation to fulfil the hob with arbitrary mounting angle θ_h has to be derived. The meshing equation of side A is expressed as:

$$\vec{n}_1^{\,A} \cdot \vec{v}_A^{(12)} = 0$$

The vectors for the relative velocity and the normal of the wheel tooth surface are represented by the variables $u, \phi_u, \phi_1, \theta_h$, as shown below,

$$\vec{v}_A^{(12)} = \vec{v}(\vec{r}_1^{\,A}, \theta_h) = \vec{\omega}^{(12)} \times \vec{r}_1^{\,A} - \vec{\omega}^{(2)} \times \vec{\xi} \qquad (4.8)$$

where,

$$\vec{\omega}^{(1)} = \omega^{(1)} \vec{k}_1$$

$$\vec{\omega}^{(2)} = \omega^{(2)} (\sin\phi_1 \cos\theta_h \vec{i}_1 + \cos\phi_1 \cos\theta_h \vec{j}_1 + \sin\theta_h \vec{k}_1)$$

$$\vec{\xi} = A_0 \cos\phi_1 \vec{i}_1 - A_0 \sin\phi_1 \vec{j}_1$$

$$\vec{\omega}^{(12)} = \vec{\omega}^{(1)} - \vec{\omega}^{(2)} = -\omega^{(2)} \cos\theta_h \sin\phi_1 \vec{i}_1 - \omega^{(2)} \cos\theta_h \cos\phi_1 \vec{j}_1 + (\omega^{(1)} - \omega^{(2)} \sin\theta_h) \vec{k}_2$$

Hence,

$$\vec{v}_A^{(12)} = \vec{\omega}^{(12)} \times \vec{r}_1^{\,A} - \vec{\omega}^{(2)} \times \vec{\xi} = \begin{vmatrix} \vec{i}_1 & \vec{j}_1 & \vec{k}_1 \\ -\omega^{(2)} \cos\theta_h \sin\phi_1 & -\omega^{(2)} \cos\theta_h \cos\phi_1 & \omega^{(1)} - \omega^{(2)} \sin\theta_h \\ x_1^A & y_1^A & z_1^A \end{vmatrix}$$

$$- \begin{vmatrix} \vec{i}_1 & \vec{j}_1 & \vec{k}_1 \\ \omega^{(2)} \sin\phi_1 \cos\theta_h & \omega^{(2)} \cos\phi_1 \cos\theta_h & \omega^{(2)} \sin\theta_h \\ A_0 \cos\phi_1 & -A_0 \sin\phi_1 & 0 \end{vmatrix}$$

$$= [-\omega^{(2)} \cos\phi_1 \cos\theta_h \cdot z_1^A - y_1^A \cdot (\omega^{(1)} - \omega^{(2)} \sin\theta_h) - A_0 \omega^{(2)} \sin\phi_1 \sin\theta_h] \vec{i}_1$$

$$+ [(\omega^{(1)} - \omega^{(2)} \sin\theta_h) \cdot x_1^A + \omega^{(2)} \sin\phi_1 \cos\theta_h \cdot z_1^A - A_0 \omega^{(2)} \sin\theta_h \cos\phi_1] \vec{j}_1$$

$$+ [\omega^{(2)} \cos\phi_1 \cos\theta_h \cdot x_1^A - \omega^{(2)} \sin\phi_1 \cos\theta_h \cdot y_1^A + A_0 \omega^{(2)} \cos\theta_h] \vec{k}_1$$

The meshing equation is written as

$$\vec{n}_1^A \cdot \vec{v}_A^{(12)} = n_{1x} v_x^{(12)} + n_{1y} v_y^{(12)} + n_{1z} v_z^{(12)} = 0$$

where,

$$n_{1x} v_x^{(12)} = -\sin\delta_1 \sin\phi_u [-\omega^{(2)} \cos\phi_1 \cos\theta_h \cdot z_1^A - y_1^A \cdot (\omega^{(1)} - \omega^{(2)} \sin\theta_h) - A_0 \omega^{(2)} \sin\phi_1 \sin\theta_h];$$

$$n_{1y} v_y^{(12)} = \sin\delta_1 \cos\phi_u [(\omega^{(1)} - \omega^{(2)} \sin\theta_h) \cdot x_1^A + \omega^{(2)} \sin\phi_1 \cos\theta_h \cdot z_1^A - A_0 \omega^{(2)} \sin\theta_h \cos\phi_1];$$

$$n_{1z} v_z^{(12)} = -\cos\delta_1 [\omega^{(2)} \cos\phi_1 \cos\theta_h \cdot x_1^A - \omega^{(2)} \sin\phi_1 \cos\theta_h \cdot y_1^A + A_0 \omega^{(2)} \cos\theta_h];$$

By introducing x_1^A, y_1^A, z_1^A into the meshing equation of the worm and wheel, the meshing equation can be further derived as:

$$\omega^{(2)} \cos\theta_h \sin(\phi_1 + \phi_u)(u - p\phi_u \sin\delta_1) + \omega^{(2)} r_{01} \cos\theta_h \cos\delta_1 \cos(\phi_1 + \phi_u)$$
$$-(\omega^{(1)} - \omega^{(2)} \sin\theta_h) r_{01} \sin\delta_1 + A_0 \omega^{(2)} \sin\theta_h \sin\delta_1 \cos(\phi_1 + \phi_u) + A_0 \omega^{(2)} \cos\theta_h \cos\delta_1 = 0$$

$$\omega^{(2)} \cos\theta_h \sin(\phi_1 + \phi_u) u = \omega^{(2)} \cos\theta_h \sin(\phi_1 + \phi_u) \cdot p\phi_u \sin\delta_1 - \omega^{(2)} r_{01} \cos\theta_h \cos\delta_1 \cos(\phi_1 + \phi_u)$$
$$+(\omega^{(1)} - \omega^{(2)} \sin\theta_h) r_{01} \sin\delta_1 - A_0 \omega^{(2)} \sin\theta_h \sin\delta_1 \cos(\phi_1 + \phi_u) - A_0 \omega^{(2)} \cos\theta_h \cos\delta_1$$

Therefore, the tool parameter u of side A can be determined from the general meshing equation and is represented as:

$$u = p\phi_u \cdot \sin\delta_1 - r_{01} \cdot \cos\delta_1 \cdot ctg(\phi_1 + \phi_u) + \frac{(i_{12} - \sin\theta_h) \cdot r_{01} \cdot \sin\delta_1}{\cos\theta_h \cdot \sin(\phi_1 + \phi_u)}$$
$$- A_0 \cdot \sin\delta_1 \cdot ctg(\phi_1 + \phi_u) \cdot tg\theta_h - A_0 \frac{\cos\delta_1}{\sin(\phi_1 + \phi_u)} \qquad (4.9)$$

For the side B of the hob, the relative velocity is represented as:

$$\vec{v}_B^{(12)} = \vec{v}'(\vec{r}_1^B, \theta_h) = \vec{\omega}^{(12)} \times \vec{r}_1^B - \vec{\omega}^{(2)} \times \vec{\xi}$$

where,

$$\vec{\omega}^{(1)} = \omega^{(1)} \vec{k}_1$$

$$\vec{\omega}^{(2)} = \omega^{(2)} (\sin\phi_1 \cos\theta_h \vec{i}_1 + \cos\phi_1 \cos\theta_h \vec{j}_1 + \sin\theta_h \vec{k}_1)$$

$$\vec{\xi} = A_0 \cos\phi_1 \vec{i}_1 - A_0 \sin\phi_1 \vec{j}_1$$

$$\vec{\omega}^{(12)} = \vec{\omega}^{(1)} - \vec{\omega}^{(2)} = -\omega^{(2)} \cos\theta_h \sin\phi_1 \vec{i}_1 - \omega^{(2)} \cos\theta_h \cos\phi_1 \vec{j}_1 + (\omega^{(1)} - \omega^{(2)} \sin\theta_h)\vec{k}_2$$

$$\vec{v}_B^{(12)} = \vec{\omega}^{(12)} \times \vec{r}_1^{\,B} - \vec{\omega}^{(2)} \times \vec{\xi} = \begin{vmatrix} \vec{i}_1 & \vec{j}_1 & \vec{k}_1 \\ -\omega^{(2)} \cos\theta_h \sin\phi_1 & -\omega^{(2)} \cos\theta_h \cos\phi_1 & \omega^{(1)} - \omega^{(2)} \sin\theta_h \\ x_1^B & y_1^B & z_1^B \end{vmatrix}$$

$$- \begin{vmatrix} \vec{i}_1 & \vec{j}_1 & \vec{k}_1 \\ \omega^{(2)} \sin\phi_1 \cos\theta_h & \omega^{(2)} \cos\phi_1 \cos\theta_h & \omega^{(2)} \sin\theta_h \\ A_0 \cos\phi_1 & -A_0 \sin\phi_1 & 0 \end{vmatrix}$$

$$= [-\omega^{(2)} \cos\phi_1 \cos\theta_h \cdot z_1^B - y_1^B \cdot (\omega^{(1)} - \omega^{(2)} \sin\theta_h) - A_0 \omega^{(2)} \sin\phi_1 \sin\theta_h]\vec{i}_1$$
$$+ [(\omega^{(1)} - \omega^{(2)} \sin\theta_h) \cdot x_1^B + \omega^{(2)} \sin\phi_1 \cos\theta_h \cdot z_1^B - A_0 \omega^{(2)} \sin\theta_h \cos\phi_1]\vec{j}_1$$
$$+ [\omega^{(2)} \cos\phi_1 \cos\theta_h \cdot x_1^B - \omega^{(2)} \sin\phi_1 \cos\theta_h \cdot y_1^B + A_0 \omega^{(2)} \cos\theta_h]\vec{k}_1$$

The meshing equation is written as

$$\vec{n}_1^{\,B} \cdot \vec{v}_B^{(12)} = n_{1x}^B v_x^{(12)} + n_{1y}^B v_y^{(12)} + n_{1z}^B v_z^{(12)} = 0$$

where

$$n_{1x}^B v_x^{(12)} = -\sin\delta_1 \sin\phi_u [-\omega^{(2)} \cos\phi_1 \cos\theta_h \cdot z_1^B - y_1^B \cdot (\omega^{(1)} - \omega^{(2)} \sin\theta_h) - A_0 \omega^{(2)} \sin\phi_1 \sin\theta_h];$$
$$n_{1y}^B v_y^{(12)} = -\sin\delta_1 \cos\phi_u [(\omega^{(1)} - \omega^{(2)} \sin\theta_h) \cdot x_1^B + \omega^{(2)} \sin\phi_1 \cos\theta_h \cdot z_1^B - A_0 \omega^{(2)} \sin\theta_h \cos\phi_1];$$
$$n_{1z}^B v_z^{(12)} = \cos\delta_1 [\omega^{(2)} \cos\phi_1 \cos\theta_h \cdot x_1^B - \omega^{(2)} \sin\phi_1 \cos\theta_h \cdot y_1^B + A_0 \omega^{(2)} \cos\theta_h];$$

By introducing x_1^B, y_1^B, z_1^B, the meshing equation is derived as

$$\omega^{(2)} \cos\theta_h \sin(\phi_u - \phi_1)(u + b\sin\delta_1 - p\phi_u \sin\delta_1) + \omega^{(2)} r_{01} \cos\theta_h \cos\delta_1 \cos(\phi_u - \phi_1)$$
$$-(\omega^{(1)} - \omega^{(2)} \sin\theta_h) r_{01} \sin\delta_1 + A_0 \omega^{(2)} \sin\theta_h \sin\delta_1 \cos(\phi_u - \phi_1) + A_0 \omega^{(2)} \cos\theta_h \cos\delta_1 = 0$$

$$\omega^{(2)} \cos\theta_h \sin(\phi_u - \phi_1) u = \omega^{(2)} \cos\theta_h \sin(\phi_u - \phi_1) \cdot (p\phi_u - b)\sin\delta_1$$
$$-\omega^{(2)} r_{01} \cos\theta_h \cos\delta_1 \cos(\phi_u - \phi_1) + (\omega^{(1)} - \omega^{(2)} \sin\theta_h) r_{01} \sin\delta_1$$
$$- A_0 \omega^{(2)} \sin\theta_h \sin\delta_1 \cos(\phi_u - \phi_1) - A_0 \omega^{(2)} \cos\theta_h \cos\delta_1$$

Thus, the tool parameter u for the side B is determined by the meshing equation and is represented as below:

$$u = (p\phi_u - b)\cdot\sin\delta_1 - r_{01}\cdot\cos\delta_1\cdot ctg(\phi_u - \phi_1) + \frac{(i_{12} - \sin\theta_h)\cdot r_{01}\cdot\sin\delta}{\cos\theta_h\cdot\sin(\phi_u - \phi_1)}$$
$$- A_0\cdot\sin\delta_1\cdot ctg(\phi_u - \phi_1)\cdot tg\theta_h - A_0\frac{\cos\delta_1}{\sin(\phi_u - \phi_1)} \tag{4.10}$$

4.3.4 Equation of contact lines between hob and the wheel

The contact lines are the instantaneous contact paths between the conjugating surfaces of the hob and wheel. With respect to any instant value of the hob rotating angle ϕ_u, a contact line on the wheel tooth surface is generated by the hob. The wheel tooth surface consists of the assembly of the contact lines. Determination of the contact line is based on the requirement that at any point on the line the meshing equation must hold. Thus, the contact lines on the wheel tooth surface are represented as the following equations.

Equations for the contact lines in respect to the side A:

$$\begin{cases} u = p\phi_u\cdot\sin\delta_1 - r_{01}\cdot\cos\delta_1\cdot ctg(\phi_1 + \phi_u) + \dfrac{(i_{12} - \sin\theta_h)\cdot r_{01}\cdot\sin\delta_1}{\cos\theta_h\cdot\sin(\phi_1 + \phi_u)} \\ -A_0\cdot\sin\delta_1\cdot ctg(\phi_1 + \phi_u)\cdot tg\theta_h - A_0\dfrac{\cos\delta_1}{\sin(\phi_1 + \phi_u)} \\ \vec{r}_2 = \vec{r}_2(u, \phi_u, \phi_1, \theta_h) = M_{20}(\phi_2)\cdot M_{0\theta}(\theta_h)\cdot M_{\theta 1}(\phi_1)\cdot \vec{r}_1^{\,A}(u, \phi_u) \end{cases} \tag{4.11}$$

Equations for the contact lines in respect to the side B:

$$\begin{cases} u = (p\phi_u - b)\cdot\sin\delta_1 - r_{01}\cdot\cos\delta_1\cdot ctg(\phi_u - \phi_1) + \dfrac{(i_{12} - \sin\theta_h)\cdot r_{01}\cdot\sin\delta_1}{\cos\theta_h\cdot\sin(\phi_u - \phi_1)} \\ -A_0\cdot\sin\delta_1\cdot ctg(\phi_u - \phi_1)\cdot tg\theta_h - A_0\dfrac{\cos\delta_1}{\sin(\phi_u - \phi_1)} \\ \vec{r}_2 = \vec{r}_2(u, \phi_u, \phi_1, \theta_h) = M_{20}(\phi_2)\cdot M_{0\theta}(\theta_h)\cdot M_{\theta 1}(\phi_1)\cdot \vec{r}_1^{\,B}(u, \phi_u) \end{cases} \tag{4.12}$$

Where, θ_h is the modified hob mounting angle; $M_{20}, M_{0\theta}$ and $M_{\theta 1}$ are the transfer matrices from the fixed coordinate system Σ_0 to the wheel coordinate system Σ_2, from the reference coordinate system Σ_θ to Σ_0, and from the hob coordinate system Σ_1 to the reference system Σ_θ respectively. The reference coordinate system Σ_θ has a mounting angle θ_h with the fixed coordinate system Σ_0.

$$M_{\theta 1} = \begin{bmatrix} \cos\phi_1 & -\sin\phi_1 & 0 & 0 \\ \sin\phi_1 & \cos\phi_1 & 0 & 0 \\ 0 & 0 & 1 & 0 \\ 0 & 0 & 0 & 1 \end{bmatrix}$$

$$M_{0\theta} = \begin{bmatrix} 1 & 0 & 0 & 0 \\ 0 & \cos\theta_h & -\sin\theta_h & 0 \\ 0 & \sin\theta_h & \cos\theta_h & 0 \\ 0 & 0 & 0 & 1 \end{bmatrix} \tag{4.13}$$

$$M_{20} = \begin{bmatrix} \cos\phi_2 & 0 & -\sin\phi_2 & A_0\cos\phi_2 \\ -\sin\phi_2 & 0 & -\cos\phi_2 & -A_0\sin\phi_2 \\ 0 & 1 & 0 & 0 \\ 0 & 0 & 0 & 1 \end{bmatrix} \tag{4.14}$$

Figure 4.5 shows the contact lines on the tooth, i.e. the modified wheel tooth surface generated by the hob.

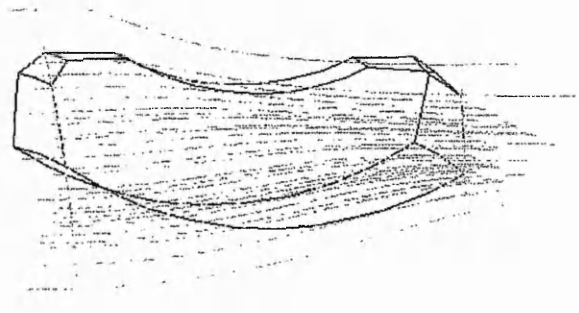

Figure 4.5 Contact lines on the wheel surface

4.4 Numerical Analysis of the Localised Tooth Contact

The meshing of tooth surfaces of conventional worm gear drives is theoretically in line contact. However, after the modification, the meshing of the worm gear drive is substituted by the local contact , i.e. 'point' or zone contact, and the original meshing principle is not applicable any more.

Tooth contact analysis (TCA) programmes are developed for the computerised analysis of tangency of tooth surfaces in meshing. It is applied to predict the contact pattern for the modified worm gear drives.

To ensure the continuous tangency contact between the tooth surfaces, the contact point vectors of the tooth surfaces must be equal and the normals should be collinear at every instant (Litvin, 1994). This condition of continuous tangency of the meshing surfaces can be represented by the equations

$$\begin{aligned} r_f^{(1)}(u_1,\phi_{u1},\phi_1) &= r_f^{(2)}(u_2,\phi_{u2},\phi_2) \\ n_f^{(1)}(u_1,\phi_{u1},\phi_1) &= n_f^{(2)}(u_2,\phi_{u2},\phi_2) \end{aligned} \qquad (4.15)$$

where, u_i,ϕ_{ui} are the surface parameters, ϕ_i are the angles of rotation; $n_f^{(1)},n_f^{(2)}$ are the unit normal vectors of the surfaces of the worm and wheel respectively, while $r_f^{(1)},r_f^{(2)}$ are the position vectors of the surfaces of the worm and wheel respectively. The equations consist of six scalar equations, but only five are independent because of $\left|n_f^{(1)}\right|=\left|n_f^{(2)}\right|=1$. Therefore, the mathematical model of the tooth contact is a system of five non-linear equations with six unknowns. By introduction of the equations (4.1) (4.2), (4.6) and (4.9), the equations (4.15) can be represented as:

$$f_i(u_1,\phi_{u1},\phi_1,u_2,\phi_{u2},\phi_2)=0 \qquad (i=1,2,...,5) \qquad (4.16)$$

Solution of the equation system is by an iterative process using the Levenberg-Marquardt method (MathSoft Inc, 1995). The co-ordinate values and the normal of the reference point can be used as first guess values for calculation. Choose one unknown as the input variable, the rest of the unknowns can be obtained by numerical computation. The computation results represent the contact path of the tooth surfaces.

4.5 Determine the Contact Path Using TCA Method

As introduced in section 4.4, the condition of continuous tangency of the meshing surfaces can be represented by the equations (4.15). For the worm gear drives, the equation can be expressed as

$$\begin{aligned} r_f^{(wm)}(u_1,\phi_{u1},\phi_1) &= r_f^{(wl)}(u_1',\phi_{u1}',\phi_1') \\ n_f^{(wm)}(u_1,\phi_{u1},\phi_1) &= n_f^{(wl)}(u_1',\phi_{u1}',\phi_1') \end{aligned} \tag{4.17}$$

Where, *wl* and *wm* refers to the tooth surfaces of wheel and worm respectively. The equations are considered in the fixed coordinate system $\Sigma_0 = [o;\vec{i},\vec{j},\vec{k}]$. During the meshing process, the tooth contact occurs on the tooth surface of side B. So, according to Chapter 3, the tooth surface vector and normal of the side B of the worm are expressed as:

$$\begin{aligned} r_f^{(wm)}(u_1,\phi_{u1},\phi_1) &= M_{f1}\cdot\vec{r}_1^{\,B} \\ n_f^{(wm)}(u_1,\phi_{u1},\phi_1) &= M_{f1}\cdot\vec{n}_1^{\,B} \end{aligned} \tag{4.18}$$

Where: $M_{f1} = \begin{pmatrix} \cos\phi_1 & -\sin\phi_1 & 0 \\ \sin\phi_1 & \cos\phi_1 & 0 \\ 0 & 0 & 1 \end{pmatrix}$

Therefore, the vector of the worm tooth surface is represented as:

$$\vec{r}_f^{(wm)}(u_1,\phi_{u1},\phi_1) = \begin{pmatrix} r_{fx}^{(wm)} \\ r_{fy}^{(wm)} \\ r_{fz}^{(wm)} \end{pmatrix} = \begin{pmatrix} \cos\phi_1 & -\sin\phi_1 & 0 \\ \sin\phi_1 & \cos\phi_1 & 0 \\ 0 & 0 & 1 \end{pmatrix} \begin{pmatrix} r_{01}\cdot\cos\phi_{u1} + u\cdot\cos\delta_1\cdot\sin\phi_{u1} \\ -r_{01}\cdot\sin\phi_{u1} + u\cdot\cos\delta_1\cdot\cos\phi_{u1} \\ u\cdot\sin\delta_1 + b - p\phi_{u1} \end{pmatrix}$$

$$= \begin{pmatrix} r_{01}\cdot\cos(\phi_{u1}-\phi_1) + u\cdot\cos\delta_1\cdot\sin(\phi_{u1}-\phi_1) \\ -r_{01}\cdot\sin(\phi_{u1}-\phi_1) + u\cdot\cos\delta_1\cdot\cos(\phi_{u1}-\phi_1) \\ u\cdot\sin\delta_1 + b - p\phi_{u1} \end{pmatrix} \tag{4.19}$$

and the normal is represented as:

$$\vec{n}_f^{wm} = \begin{pmatrix} n_{fx}^{wm} \\ n_{fy}^{wm} \\ n_{fz}^{wm} \end{pmatrix} = \begin{pmatrix} \cos\phi_1 & -\sin\phi_1 & 0 \\ \sin\phi_1 & \cos\phi_1 & 0 \\ 0 & 0 & 1 \end{pmatrix} \begin{pmatrix} -\sin\phi_{u1}\sin\delta_1 \\ -\cos\phi_{u1}\sin\delta_1 \\ \cos\delta_1 \end{pmatrix} = \begin{pmatrix} -\sin(\phi_{u1}-\phi_1)\sin\delta_1 \\ -\cos(\phi_{u1}-\phi_1)\sin\delta_1 \\ \cos\delta_1 \end{pmatrix} \tag{4.20}$$

If there is misalignment Δβ regarding the worm mounting angle, as shown in Figure 4.6, and the clockwise direction is defined as positive while the counterclockwise is defined as negative for the worm mounting angle, then the vector and normal for the worm tooth surface are represented as:

$$\vec{r}_f^{(wm)}(u_1,\phi_{u1},\phi_1) = M_{\beta 1}\cdot\begin{pmatrix} r_{fx}^{(wm)} \\ r_{fy}^{(wm)} \\ r_{fz}^{(wm)} \end{pmatrix} = \begin{pmatrix} r_{fx}^{(wm)} \\ r_{fy}^{(wm)}\cdot\cos\Delta\beta - r_{fz}^{(wm)}\cdot\sin\Delta\beta \\ r_{fy}^{(wm)}\cdot\sin\Delta\beta + r_{fz}^{(wm)}\cdot\cos\Delta\beta \end{pmatrix}$$

$$\vec{n}_f^{wm}(\phi_{u1},\phi_1) = M_{\beta 1}\cdot\begin{pmatrix} n_{fx}^{wm} \\ n_{fy}^{wm} \\ n_{fz}^{wm} \end{pmatrix} = \begin{pmatrix} n_{fx}^{wm} \\ n_{fy}^{wm}\cdot\cos\Delta\beta - n_{fz}^{wm}\cdot\sin\Delta\beta \\ n_{fy}^{wm}\cdot\sin\Delta\beta + n_{fz}^{wm}\cdot\cos\Delta\beta \end{pmatrix} \tag{4.21}$$

where, $M_{\beta 1}$ is the transform matrix from the misaligned worm to the fixed coodinate system and is written as,

$$M_{\beta 1} = \begin{pmatrix} 1 & 0 & 0 \\ 0 & \cos\Delta\beta & -\sin\Delta\beta \\ 0 & \sin\Delta\beta & \cos\Delta\beta \end{pmatrix}$$

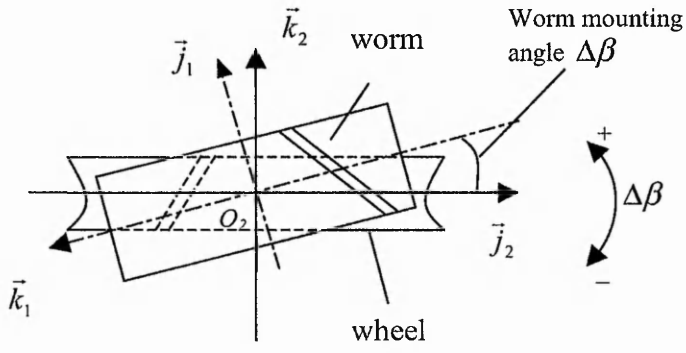

Figure 4.6 Worm gear drive with misalignment in worm mounting angle

According to Section 4.3.3, the tooth surface vectors of side B of the wheel tooth in the fixed coordinate system Σ_0 are represented as

$$\begin{cases} r_f^{(wl)}(u_1', \phi_{u1}', \phi_1') = M_{0\theta} \cdot M_{\theta 1} \cdot \vec{r}_1^{\,B'} \\ \vec{n}_1^{\,B'} \cdot \vec{v}_B^{(12)'} = 0 \end{cases} \tag{4.22}$$

and the normal of the wheel tooth in the fixed coordinate system Σ_0 is written as:

$$n_f^{(wl)}(u_1', \phi_{u1}', \phi_1') = M_{0\theta} \cdot M_{\theta 1} \cdot \vec{n}_1^{\,B'} \tag{4.23}$$

Therefore, the equations can be evolved as:

$$\begin{cases} \vec{r}_f^{(wl)}(u_1', \phi_{u1}', \phi_1') = \begin{pmatrix} \vec{r}_{fx}^{(wl)}(u_1', \phi_{u1}', \phi_1') \\ \vec{r}_{fy}^{(wl)}(u_1', \phi_{u1}', \phi_1') \\ \vec{r}_{fz}^{(wl)}(u_1', \phi_{u1}', \phi_1') \end{pmatrix} \\ = \begin{pmatrix} 1 & 0 & 0 \\ 0 & \cos\theta_h & -\sin\theta_h \\ 0 & \sin\theta_h & \cos\theta_h \end{pmatrix} \cdot \begin{pmatrix} \cos\phi_1' & -\sin\phi_1' & 0 \\ \sin\phi_1' & \cos\phi_1' & 0 \\ 0 & 0 & 1 \end{pmatrix} \cdot \begin{pmatrix} r_{01} \cdot \cos\phi_{u1}' + u_1' \cdot \cos\delta_1' \cdot \sin\phi_{u1}' \\ -r_{01} \cdot \sin\phi_{u1}' + u_1' \cdot \cos\delta_1' \cdot \cos\phi_{u1}' \\ u_1' \cdot \sin\delta_1' + b - p\phi_{u1}' \end{pmatrix} \\ u_1' = (p\phi_{u1}' - b) \cdot \sin\delta_1' - r_{01}' \cdot \cos\delta_1' \cdot ctg(\phi_{u1}' - \phi_1') + \dfrac{(i_{12} - \sin\theta_h) \cdot r_{01}' \cdot \sin\delta_1'}{\cos\theta_h \cdot \sin(\phi_{u1}' - \phi_1')} \\ - A_0 \cdot \sin\delta_1' \cdot ctg(\phi_{u1}' - \phi_1') \cdot tg\theta_h - A_0 \dfrac{\cos\delta_1'}{\sin(\phi_{u1}' - \phi_1')} \end{cases} \tag{4.24}$$

The normal of the wheel is represented as

$$\vec{n}_f^{\,wl}(\phi_{u1}', \phi_1') = \begin{pmatrix} \vec{n}_{fx}^{\,wl}(u_1', \phi_{u1}', \phi_1') \\ \vec{n}_{fy}^{\,wl}(u_1', \phi_{u1}', \phi_1') \\ \vec{n}_{fz}^{\,wl}(u_1', \phi_{u1}', \phi_1') \end{pmatrix}$$

$$= \begin{pmatrix} 1 & 0 & 0 \\ 0 & \cos\theta_h & -\sin\theta_h \\ 0 & \sin\theta_h & \cos\theta_h \end{pmatrix} \cdot \begin{pmatrix} \cos\phi_1' & -\sin\phi_1' & 0 \\ \sin\phi_1' & \cos\phi_1' & 0 \\ 0 & 0 & 1 \end{pmatrix} \cdot \begin{pmatrix} -\sin\phi_{u1}'\sin\delta_1' \\ -\cos\phi_{u1}'\sin\delta_1' \\ \cos\delta_1' \end{pmatrix}$$

$$= \begin{pmatrix} 1 & 0 & 0 \\ 0 & \cos\theta_h & -\sin\theta_h \\ 0 & \sin\theta_h & \cos\theta_h \end{pmatrix} \cdot \begin{pmatrix} -\sin(\phi_{u1}' - \phi_1')\sin\delta_1' \\ -\cos(\phi_{u1}' - \phi_1')\sin\delta_1' \\ \cos\delta_1' \end{pmatrix} \quad (4.25)$$

For the worm gear drive without misalignment in the worm mounting angle, by introducing (4.19), (4.20), (4.23) and (4.24) into the equation (4.17), the condition for continuous localized tooth contact can be expressed by using the equation system below:

$$\begin{cases} \vec{r}_{fx}^{(wl)}(u_1', \phi_{u1}', \phi_1') = \vec{r}_{fx}^{(wm)}(u_1, \phi_{u1}, \phi_1) \\ \vec{r}_{fy}^{(wl)}(u_1', \phi_{u1}', \phi_1') = \vec{r}_{fy}^{(wm)}(u_1, \phi_{u1}, \phi_1) \\ \vec{r}_{fz}^{(wl)}(u_1', \phi_{u1}', \phi_1') = \vec{r}_{fz}^{(wm)}(u_1, \phi_{u1}, \phi_1) \\ \vec{n}_{fx}^{wl}(\phi_{u1}', \phi_1') = \vec{n}_{fx}^{wm}(\phi_{u1}, \phi_1) \\ \vec{n}_{fy}^{wl}(\phi_{u1}', \phi_1') = \vec{n}_{fy}^{wm}(\phi_{u1}, \phi_1) \\ u_1' = (p\phi_{u1}' - b)\cdot\sin\delta_1' - r_{01}'\cdot\cos\delta_1'\cdot ctg(\phi_{u1}' - \phi_1') + \dfrac{(i_{12} - \sin\theta_h)\cdot r_{01}'\cdot\sin\delta_1'}{\cos\theta_h\cdot\sin(\phi_{u1}' - \phi_1')} \\ -A_0\cdot\sin\delta_1'\cdot ctg(\phi_{u1}' - \phi_1')\cdot tg\theta_h - A_0\dfrac{\cos\delta_1'}{\sin(\phi_{u1}' - \phi_1')} \end{cases} \quad (4.26)$$

Because of $\left|\vec{n}_f^{wm}(\phi_{u1}, \phi_1)\right| = \left|\vec{n}_f^{wl}(\phi_{u1}', \phi_1')\right| = 1$, the equation $\vec{n}_f^{wm}(\phi_{u1}, \phi_1) = \vec{n}_f^{wl}(\phi_{u1}', \phi_1')$ generates only two independent scalar equations as shown in (4.26).

For the worm gear drive with misalignment $\Delta\beta$ in the worm mounting angle, by introducing (4.19), (4.21), (4.23) and (4.24) into the equation (4.17), the condition for continuous localized tooth contact can be expressed by using the equation system (4.27).

$$\begin{cases} \vec{r}_{fx}^{(wl)}(u_1^{'},\phi_{u1}^{'},\phi_1^{'}) = r_{fx}^{(wm)}(u_1,\phi_{u1},\phi_1) \\ \vec{r}_{fy}^{(wl)}(u_1^{'},\phi_{u1}^{'},\phi_1^{'}) = r_{fy}^{(wm)}(u_1,\phi_{u1},\phi_1)\cdot\cos\Delta\beta - r_{fz}^{(wm)}(u_1,\phi_{u1},\phi_1)\cdot\sin\Delta\beta \\ \vec{r}_{fz}^{(wl)}(u_1^{'},\phi_{u1}^{'},\phi_1^{'}) = r_{fy}^{(wm)}(u_1,\phi_{u1},\phi_1)\cdot\cos\Delta\beta + r_{fz}^{(wm)}(u_1,\phi_{u1},\phi_1)\cdot\sin\Delta\beta \\ \vec{n}_{fx}^{wl}(\phi_{u1}^{'},\phi_1^{'}) = n_{fx}^{wm}(\phi_{u1},\phi_1) \\ \vec{n}_{fy}^{wl}(\phi_{u1}^{'},\phi_1^{'}) = n_{fy}^{wm}(\phi_{u1},\phi_1)\cdot\cos\Delta\beta - n_{fz}^{wm}(\phi_{u1},\phi_1)\cdot\sin\Delta\beta \\ u_1^{'} = (p\phi_{u1}^{'} - b)\cdot\sin\delta_1^{'} - r_{01}^{'}\cdot\cos\delta_1^{'}\cdot ctg(\phi_{u1}^{'} - \phi_1^{'}) + \dfrac{(i_{12} - \sin\theta_h)\cdot r_{01}^{'}\cdot\sin\delta_1^{'}}{\cos\theta_h\cdot\sin(\phi_{u1}^{'} - \phi_1^{'})} \\ -A_0\cdot\sin\delta_1^{'}\cdot ctg(\phi_{u1}^{'} - \phi_1^{'})\cdot tg\theta_h - A_0\dfrac{\cos\delta_1^{'}}{\sin(\phi_{u1}^{'} - \phi_1^{'})} \end{cases} \tag{4.27}$$

Actually, in the equation (4.21), (4.24) and (4.25), the transform matrix $M_{\beta 1}$ $M_{0\theta}$ has similar elements. If $\theta_h = \Delta\beta$, then $M_{0\theta} = M_{\beta 1}$; then, the equation (4.27) can be simplified as (4.28):

$$\begin{cases} \begin{pmatrix} \cos\phi_1^{'} & -\sin\phi_1^{'} & 0 \\ \sin\phi_1^{'} & \cos\phi_1^{'} & 0 \\ 0 & 0 & 1 \end{pmatrix}\cdot\begin{pmatrix} r_{01}\cdot\cos\phi_{u1}^{'} + u_1^{'}\cdot\cos\delta_1^{'}\cdot\sin\phi_{u1}^{'} \\ -r_{01}\cdot\sin\phi_{u1}^{'} + u_1^{'}\cdot\cos\delta_1^{'}\cdot\cos\phi_{u1}^{'} \\ u_1^{'}\cdot\sin\delta_1^{'} + b - p\phi_{u1}^{'} \end{pmatrix} = \begin{pmatrix} r_{fx}^{(wm)} \\ r_{fy}^{(wm)} \\ r_{fz}^{(wm)} \end{pmatrix} \\ \begin{pmatrix} \cos\phi_1^{'} & -\sin\phi_1^{'} & 0 \\ \sin\phi_1^{'} & \cos\phi_1^{'} & 0 \\ 0 & 0 & 1 \end{pmatrix}\cdot\begin{pmatrix} -\sin\phi_{u1}^{'}\sin\delta_1^{'} \\ -\cos\phi_{u1}^{'}\sin\delta_1^{'} \\ \cos\delta_1^{'} \end{pmatrix} = \begin{pmatrix} n_{fx}^{wm} \\ n_{fy}^{wm} \\ n_{fz}^{wm} \end{pmatrix} \\ u_1^{'} = (p\phi_{u1}^{'} - b)\cdot\sin\delta_1^{'} - r_{01}^{'}\cdot\cos\delta_1^{'}\cdot ctg(\phi_{u1}^{'} - \phi_1^{'}) + \dfrac{(i_{12} - \sin\theta_h)\cdot r_{01}^{'}\cdot\sin\delta_1^{'}}{\cos\theta_h\cdot\sin(\phi_{u1}^{'} - \phi_1^{'})} \\ -A_0\cdot\sin\delta_1^{'}\cdot ctg(\phi_{u1}^{'} - \phi_1^{'})\cdot tg\theta_h - A_0\dfrac{\cos\delta_1^{'}}{\sin(\phi_{u1}^{'} - \phi_1^{'})} \end{cases} \tag{4.28}$$

The equations above are applicable to the involute worm gear drives.

4.6 An example of worm gear drive with localised tooth contact

To investigate the effect of manufacturing errors on the tooth contact path, a ZI worm gear drive has been chosen by the author to present the various tooth contact paths under different errors. The sample worm gear drive has the following specifications: number of worm threads Z_1=3, number of wheel teeth Z_2=56, module m=8.5, worm reference radius r_w=45.0, worm base radius r_b=24.992, worm lead angle = 26.986°,

pitch of the modified worm = 79.898 mm, centre distance A_0 = 283.0 mm, normal pressure angle 22.5^0.

Using the methods developed in Chapter 3, the modification parameters are determined as follows: worm base radius r_b=24.799 mm, worm lead angle = 27.158°, hob mounting angle =-0.233°, pitch of the modified worm = 79.979 mm. The tooth contact path is investigated under the circumstance that both the diameter and lead angle of the worm have been modified and errors of the worm mounting angle exist in assembly. The tooth contact paths under the different worm mounting angle errors are shown in Figure 4.9 to Figure 4.14 with the error ranging from $\Delta\beta$= -0.30° to $\Delta\beta$= 0.20°.

From the result of tooth contact analysis, it is clear that the mounting angle of the worm will affect the contact path. When the $\Delta\beta$ changes from 0 to 0.20°, with a positive error of the mounting angle, the contact path shifts to the left half of the tooth surface (positive direction of the K_2 axis), while a negative error of the worm mounting angle ($\Delta\beta$ from 0 to -0.30°) causes the contact path to move towards the right side of the tooth surface (negative direction of the K_2 axis). The results of numerical analysis clearly show the contact position and its moving direction, which helps to investigate the contact situation. Comparing Figure 4.9 to Figure 4.14, the contact paths stay within the middle part of the tooth surface. It proves that the modified worm gear drive is insensitive to errors. The calculation results of the numerical analysis are given in the appendix A.

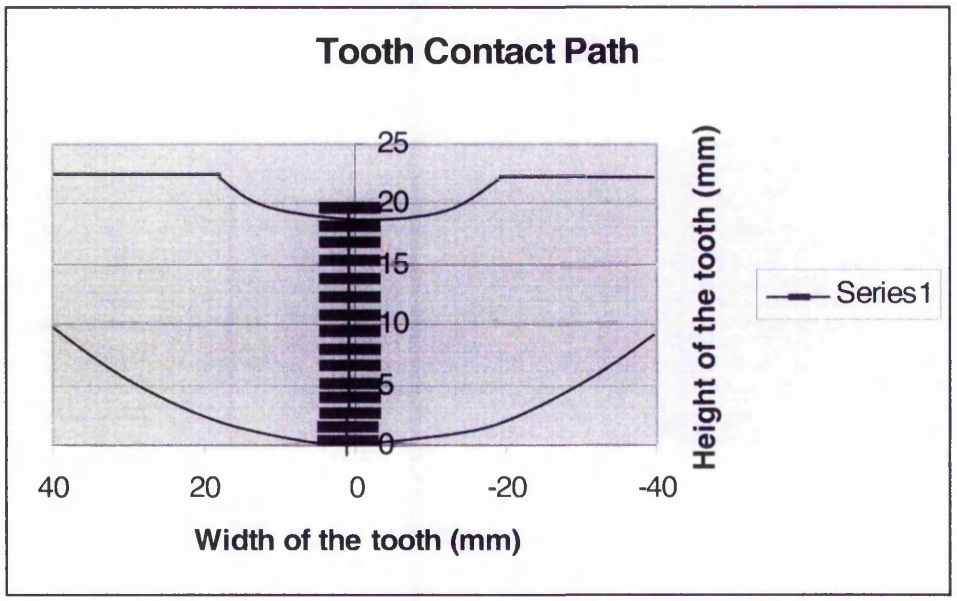

Figure 4.9 Tooth contact path of the worm gear drive with $\Delta\beta=0^0$

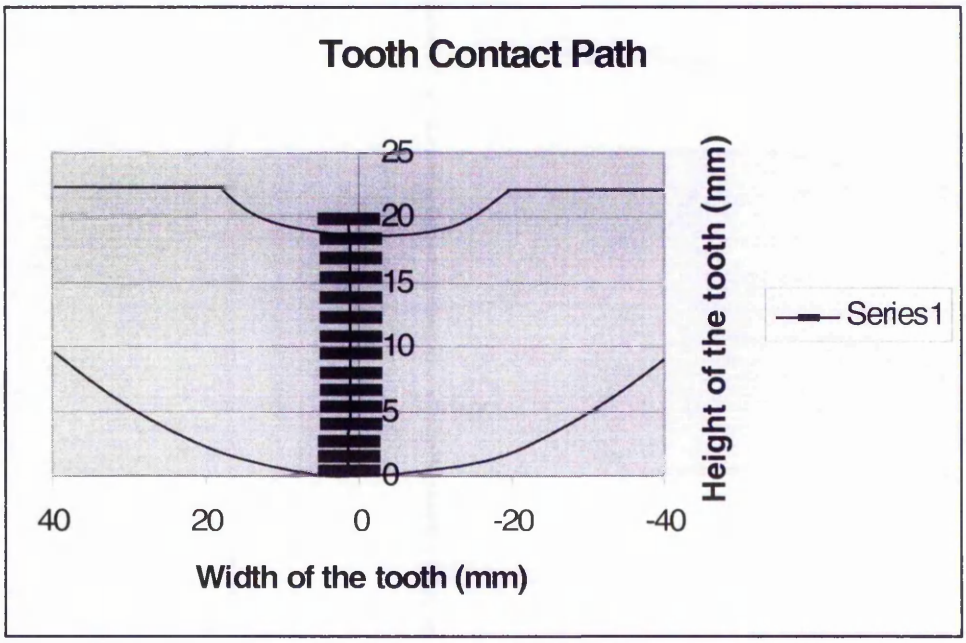

Figure 4.10 Tooth contact path of the worm gear drive $\Delta\beta= 0.10^{\circ}$

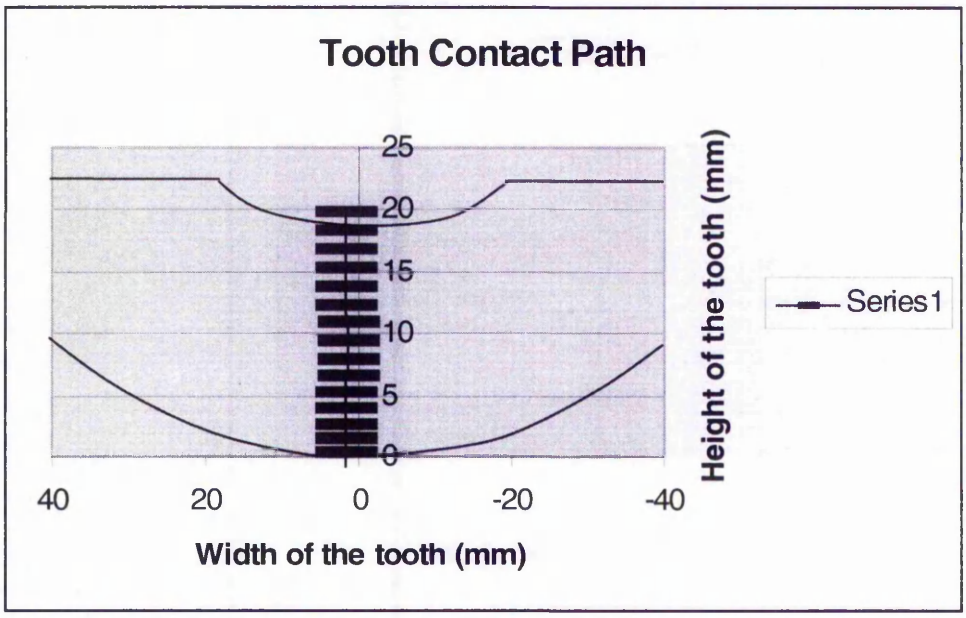

Figure 4.11 Tooth contact path of the worm gear drive $\Delta\beta = 0.20^{\circ}$

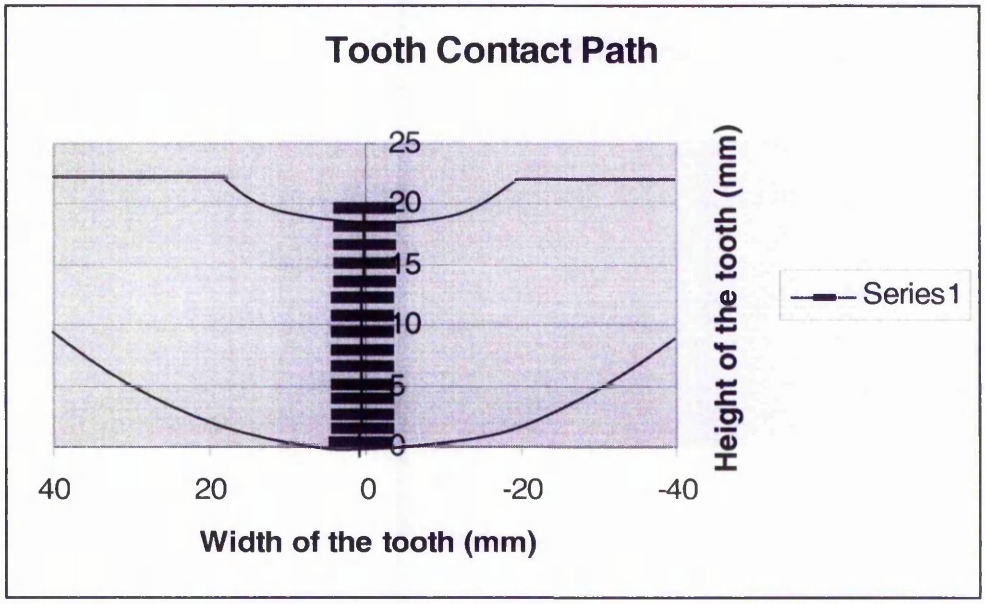

Figure 4.12 Tooth contact path of the worm gear drive $\Delta\beta = -0.10^{\circ}$

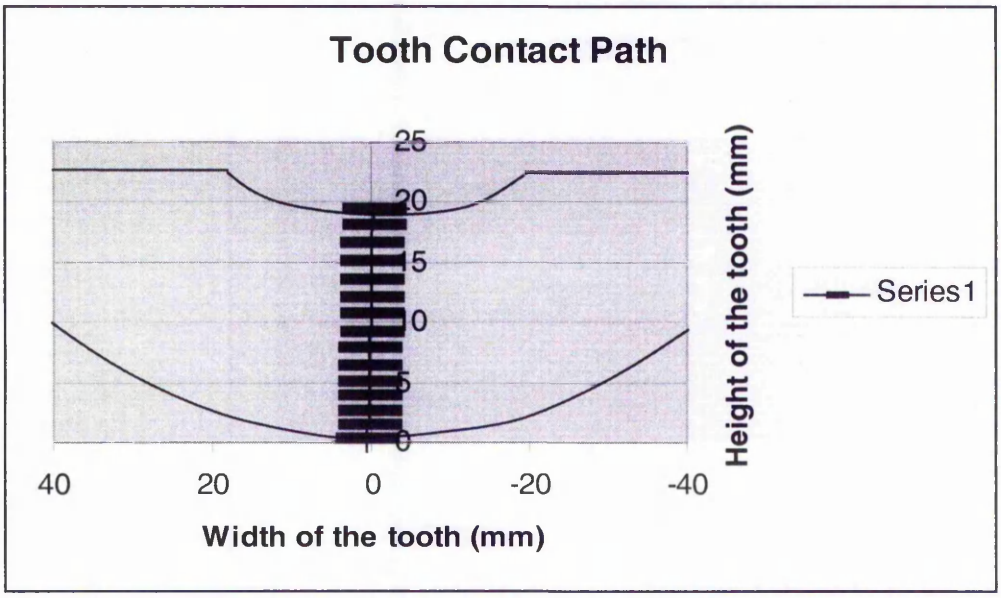

Figure 4.13 Tooth contact path of the worm gear drive $\Delta\beta$= -0.20°

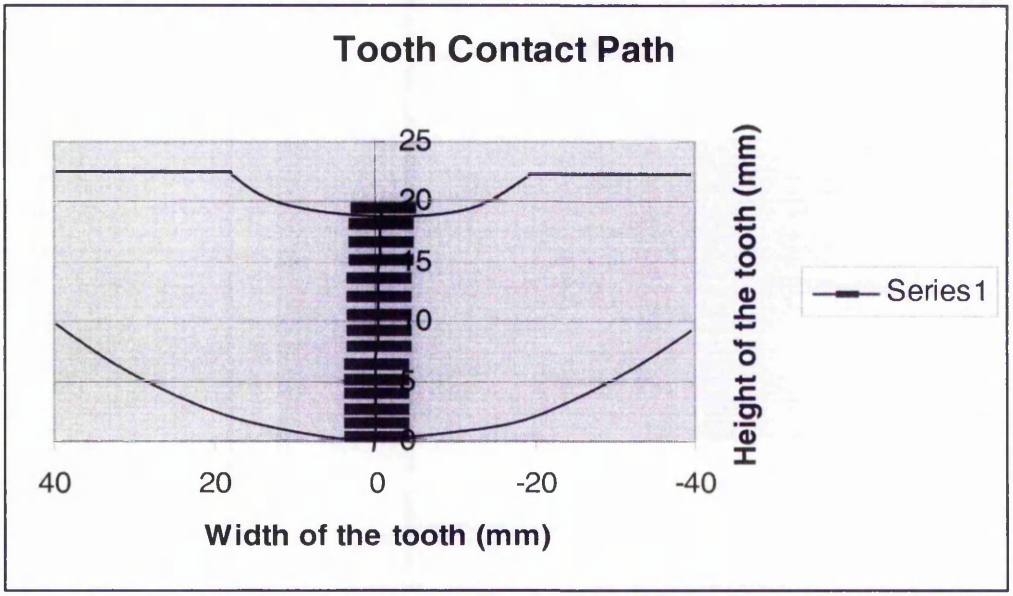

Figure 4.14 Tooth contact path of the worm gear drive $\Delta\beta$= -0.30°

Chapter 5 Three-Dimensional Simulation for Worm Gear Drives

Due to the complexity of the worm gear tooth profiles, three-dimensional simulation of worm gear drives is a complicated and challenging task. There has been no relevant work found in this area. The literature review given in Chapter 2 reveals that the three dimensional modelling has been restricted by the software techniques and packages available, and those currently applied in worm gear research are now out of date. A complete 3D model for worm gear drives has not been reported before this research.

The investigation presented in this chapter includes the following:
(1) the modelling methods for helical surfaces,
(2) the modelling methods for conjugate surfaces,
(3) the methods for assembling the worm gear models, and
(4) simulation of the motion and tooth contact of worm gear drives.

In this research, three-dimensional modelling and simulation are conducted within the environment of an advanced CAE package Pro-Engineer. Within the modelling process three models are involved: worm model, wheel model and assembly model. Using the assembly model, the localised contact can be simulated.

5.1 The Modelling Process of Worm

The analytical expression for the surface of the involute worm is represented in the equation (3.2), with which the tooth surface of the worm can be calculated. However, in three dimensional modelling, it is much more convenient to generate the worm by using the geometric approach as shown in Figure 3.2.

It is known that the transverse section of the involute worm surface is an involute curve with the radius of the base circle r_{01}. Based on the geometric approach shown in Figure 3.2, when the involute curve rotates along the spiral trajectory around the worm axis, its envelope forms a surface. This surface is actually the profile of the

worm tooth. The procedure adopted in this research for worm modeling is based on this eveloping process. Figure 5.1 shows the flow chart of the procedure.

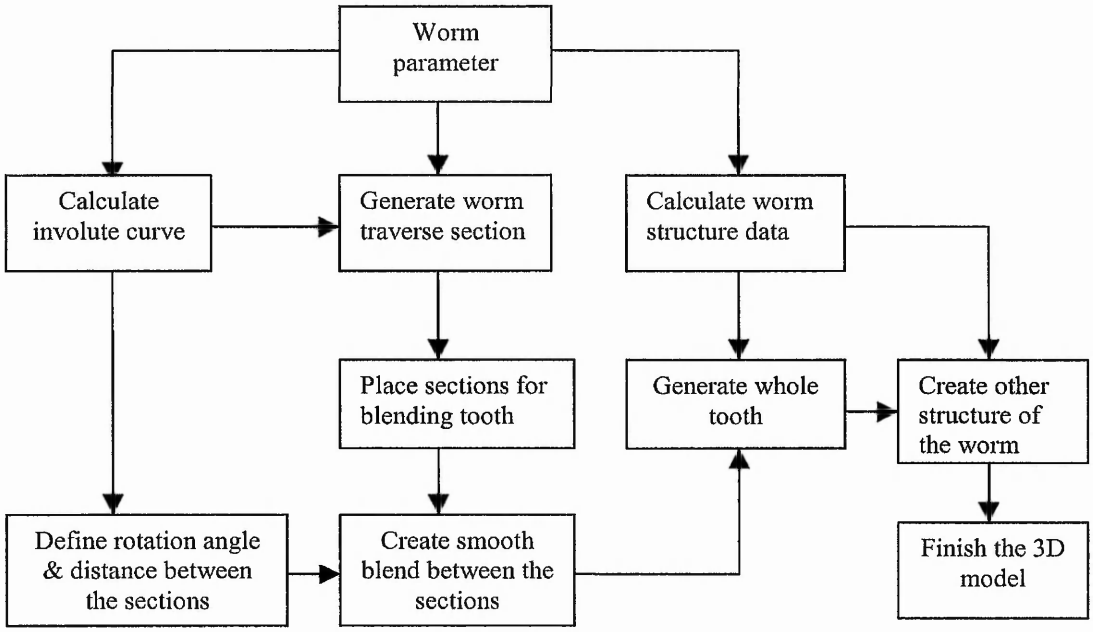

Figure 5.1 Procedure of worm modelling process

The worm model is built based on the numerical data obtained from the analytical model. First of all, an involute curve data file is calculated using the following equations (5.1)

$$inv\alpha = \tan\alpha - \alpha$$

$$\begin{pmatrix} x \\ y \end{pmatrix} = \begin{pmatrix} \frac{r_{01}}{\cos\alpha} \cdot \sin(inv\alpha) \\ \frac{r_{01}}{\cos\alpha} \cdot \cos(inv\alpha) \end{pmatrix} \qquad (5.1)$$

where, α is an angle variable parameter and r_{01} is the radius of base circle.
The calculation results of the equation (5.1) are stored in the data files. The first step of the worm modelling is to use the sketcher in Pro Engineer to create a sketch of the transverse section. Starting with coordinate system definition, the author imported

involute curve from the data file. The curve must be connected with the coordinate system. An involute curve is created in the transverse section, shown in Figure 5.2.

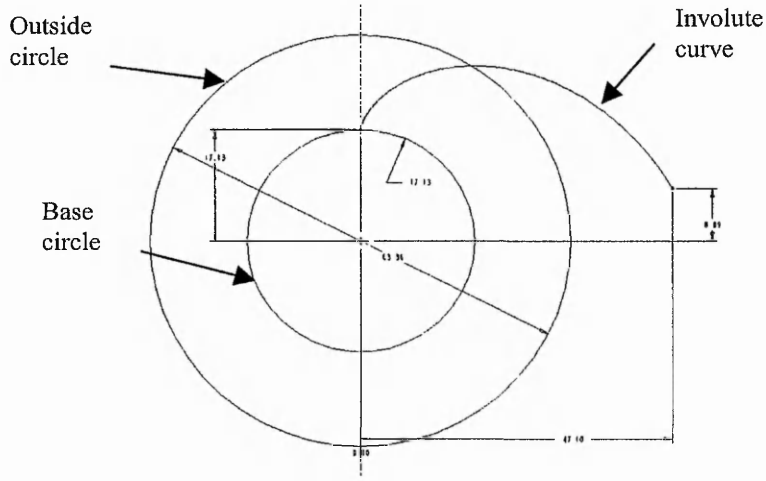

Figure 5.2 Involute curve in transverse section

After all the involute curves of the tooth are created, the next step is to combine the involute curves with the root circle and the outside circle of the worm. Thus, the transverse section of the modified worm is obtained as shown in Figure 5.3, where the diameter of the base circle, the pitch circle and the tooth number are determined by the worm design parameters.

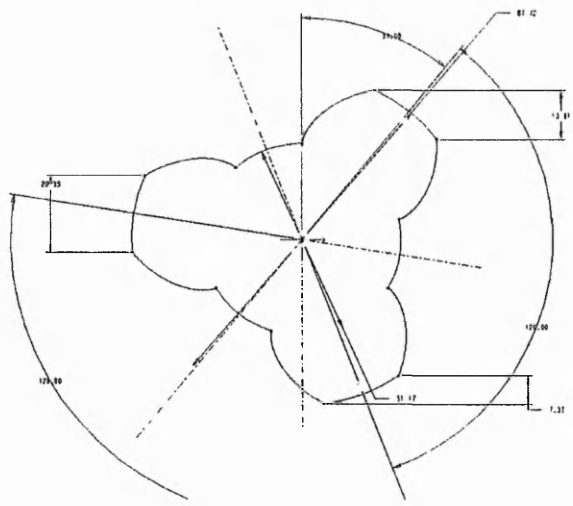

Fig. 5.3 The transverse section of worm

After rotating and moving the transverse section along the worm axis with the constraint of the axial pitch of the worm, a three-dimensional model can be created (Figure 5.4). The blend function of Pro-Engineering is used to complete this step. In order to have the correct tooth geometry, it is important to calculate the distance and rotation angle between the blend sections, which are determined by the thread number and the lead. The shaft is created according to the diameter and length of the worm mounting shaft.

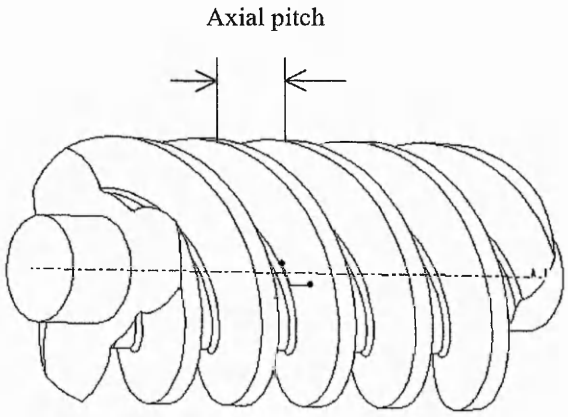

Figure 5.4 3D model of the worm

5.2 The Modelling Process of the Wheel

A novel method for modelling the wheel has been developed in this chapter. Figure 5.5 shows the procedure for the modelling process. The key part of the modelling of the wheel is the creation of the wheel tooth surface, which is more complicated than the modelling of the worm tooth. The wheel tooth surface is manufactured by a hob that has the same tooth profile as the worm. Actually the tooth surface consists of the contact lines between the hob and the wheel under the designed manufacturing motion. General geometric modelling methods in CAD packages are not able to generate such a tooth surface.

5.2.1 Creation of the tooth surface

Because the wheel tooth surface consists of the instantaneous contact lines, the first step in building the wheel model is to obtain all the contact lines of the wheel

surfaces. As mentioned in Chapter 4, the contact lines are determined by the meshing equation. It can be calculated from the equations below.

$$\begin{cases} u = p\phi_u \cdot \sin\delta_1 - r_{01} \cdot \cos\delta_1 \cdot ctg(\phi_1 + \phi_u) + \dfrac{(i_{12} - \sin\theta_h) \cdot r_{01} \cdot \sin\delta}{\cos\theta_h \cdot \sin(\phi_1 + \phi_u)} \\ -A_0 \cdot \sin\delta_1 \cdot ctg(\phi_1 + \phi_u) \cdot tg\theta_h - A_0 \dfrac{\cos\delta_1}{\sin(\phi_1 + \phi_u)} \\ \vec{r}_2 = \vec{r}_2(u, \phi_u, \phi_1, \theta_h) = M_{2\theta}(\phi_2, \theta_h) \cdot M_{\theta 1}(\phi_1, \theta_h) \cdot \vec{r}_1(u, \phi_u) \end{cases}$$

With respect to a value of worm rotating angle ϕ_1, one contact line can be obtained with a set of the tool rotating angles ϕ_u. So, a group of points of the contact line is gained. The points are calculated using the equation above and saved into a data file. Importing the data file, the points are created as the DATUM-POINTS in Pro-engineer, which is offset to the coordinate system Σ_2. By connecting the points, the contact line is created as a DATUM_CURVE, as shown in Figure 5.6.

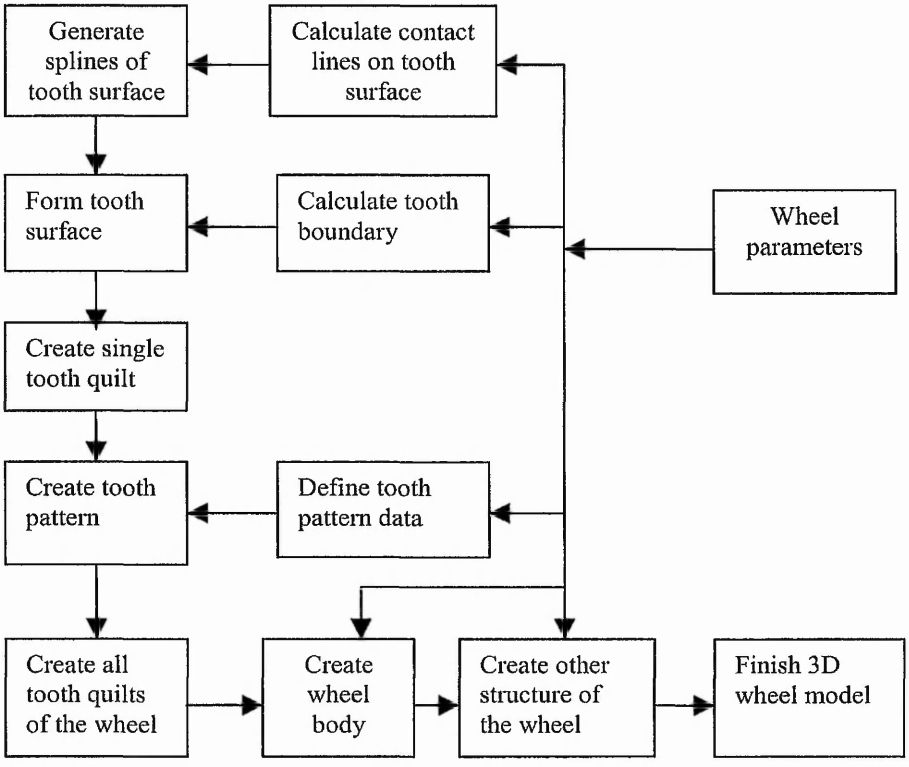

Figure 5.5 Procedure of Wheel Modelling

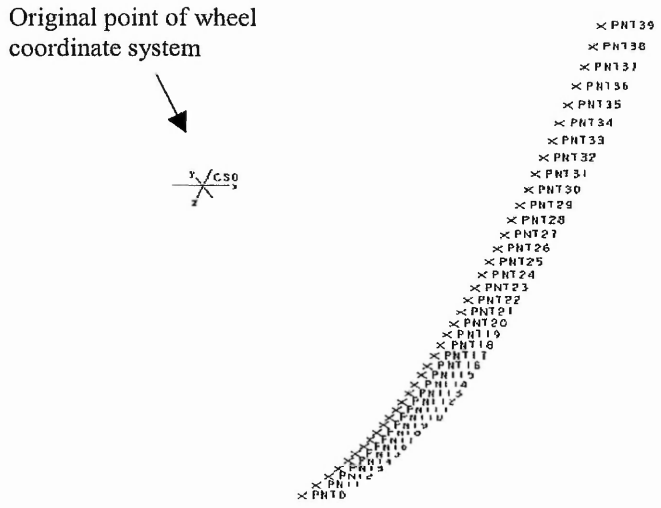

Figure. 5.6 A group of points in one contact line

After the creation of all the contact lines on the wheel tooth, the boundaries for the tooth surface must be defined in order to generate the surface. The generation of the tooth surface is completed by the function "blended surface". The contact lines are associated curve by curve, the "blend" function ensures a smooth transition between the curves. Then the tooth surface is created within the boundaries. (See Fig. 5.7)

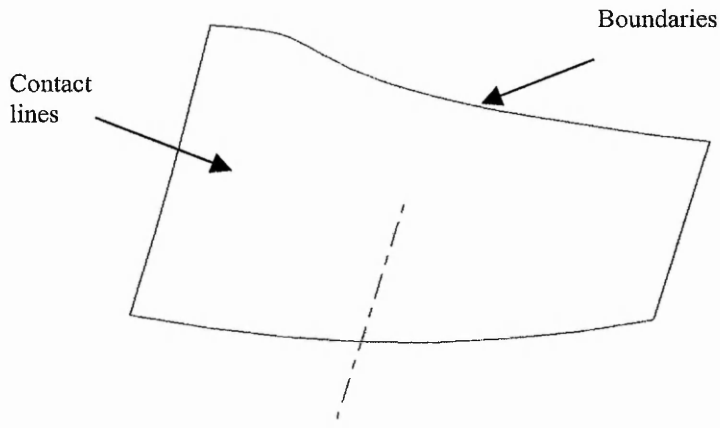

Fig 5.7 Contact lines and boundaries for wheel tooth surface

5.2.2. Creation of tooth body

Similarly, the other side tooth surface can be obtained (see Fig.5.8). The next step is to create a close tooth quilt. The top and bottom surfaces of the tooth are generated using the SWEEP function in Pro-engineer. To sweep a surface, the sweeping trajectory must be defined in the reference plane. Then a cross-section follows along the trajectory to form the surface. For the tooth top and bottom surfaces, their sections and trajectories for sweeping are drawn based on the design parameters of worm gear drives, such as outside diameters and root diameters of worm and wheel. The sweep surfaces are shown in Figure 5.9 and Figure 5.10.

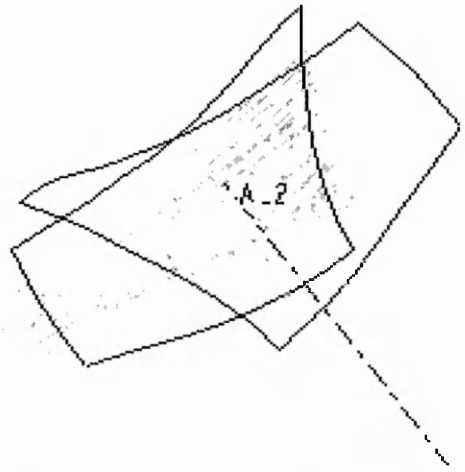

Figure 5.8 Two sides of tooth surface

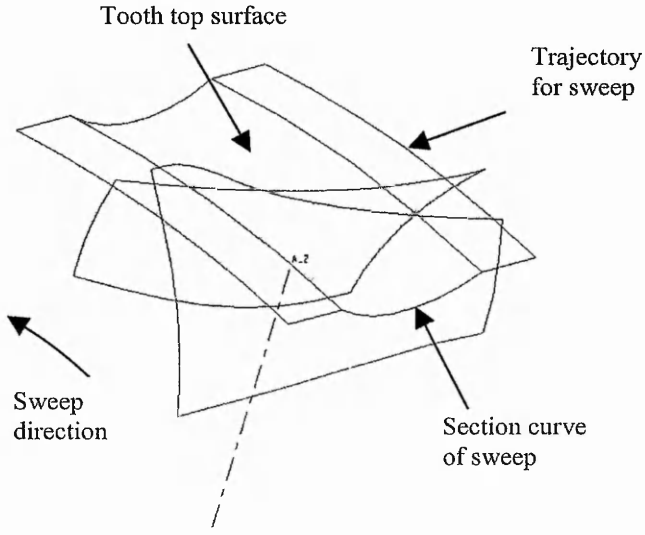

Fig.5.9 Sweeping the top surface

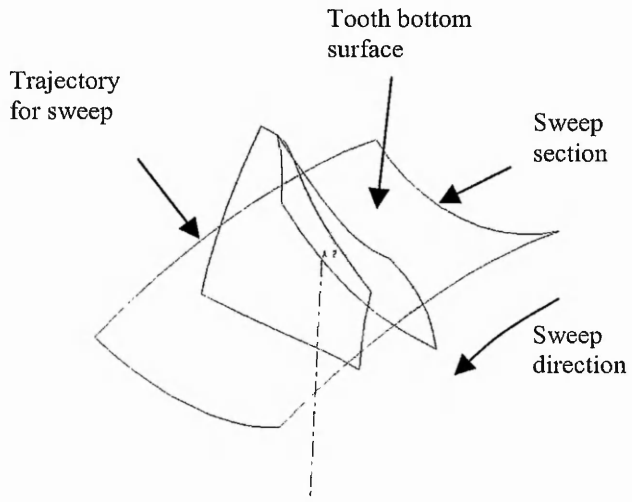

Fig. 5.10 Sweeping the bottom surface

The two side faces of the tooth body, which are planes, have been created as figure 5.11. When all the surfaces of the tooth body are completed, a close volume is achieved. Merging all the surfaces of the close volume, the quilt of the whole tooth is formed as shown in figure 5.11. In some cases, additional structures like chamfer are added to the body.

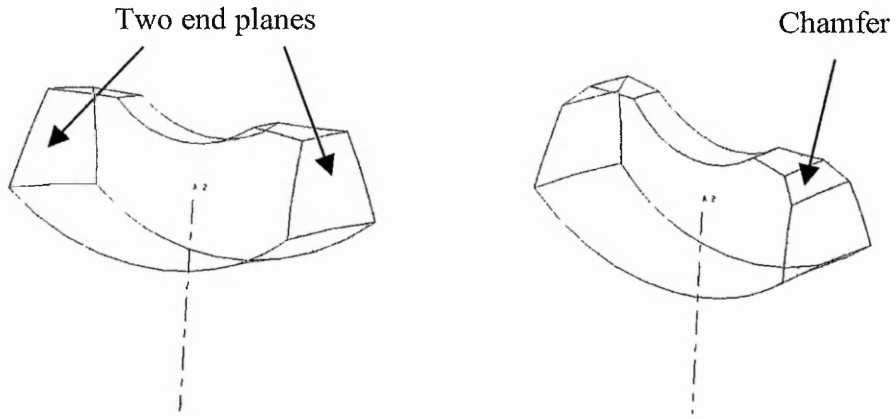

Fig. 5.11 Quilt of tooth body

5.2.3 Creation of the wheel

After the first tooth quilt has been formed, a tooth pattern of two teeth is made with the tooth interval angle between them. The interval angle is determined by the design parameters (360°/tooth number), and the tooth quilt is copied by rotating the interval angle around the z axis. Then duplicate all the tooth quilts using the tooth pattern created, and the rest of the teeth of the wheel are completed as shown in Figure 5.13.

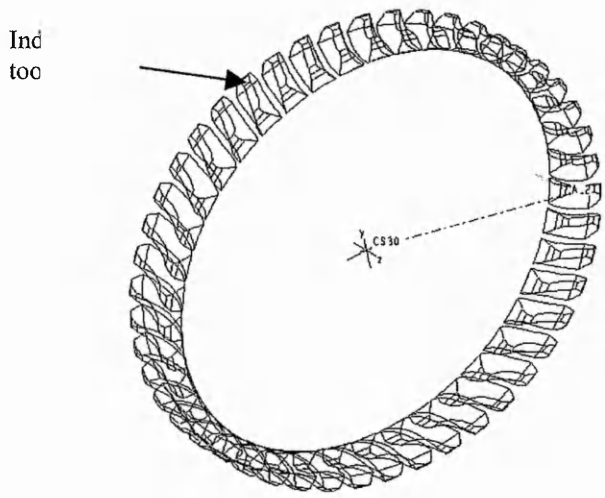

Fig. 5.13 Tooth quilts of whole wheel

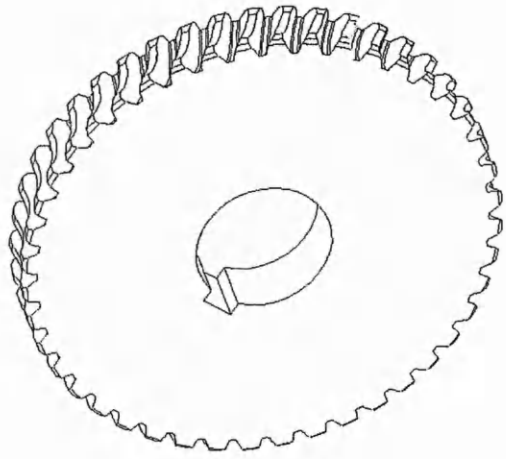

Figure 5.14 3D solid model of the wheel

However, the tooth quilts still need to be transformed into solid tooth bodies in order to create a wheel part. The wheel body is created below the tooth quilts. After merging the tooth bodies with the wheel body, a three-dimensional wheel model is finished as Figure 5.14.

5.3 The Assembly Model

The assembly model provides the possibility to conduct the virtual movement of worm gear drives as well as to simulate the instantaneous tooth contact. It combines the worm model and wheel model with accurate geometric relationship. The process for assembly modelling and three-dimensional simulation is outlined in Figure 5.15.

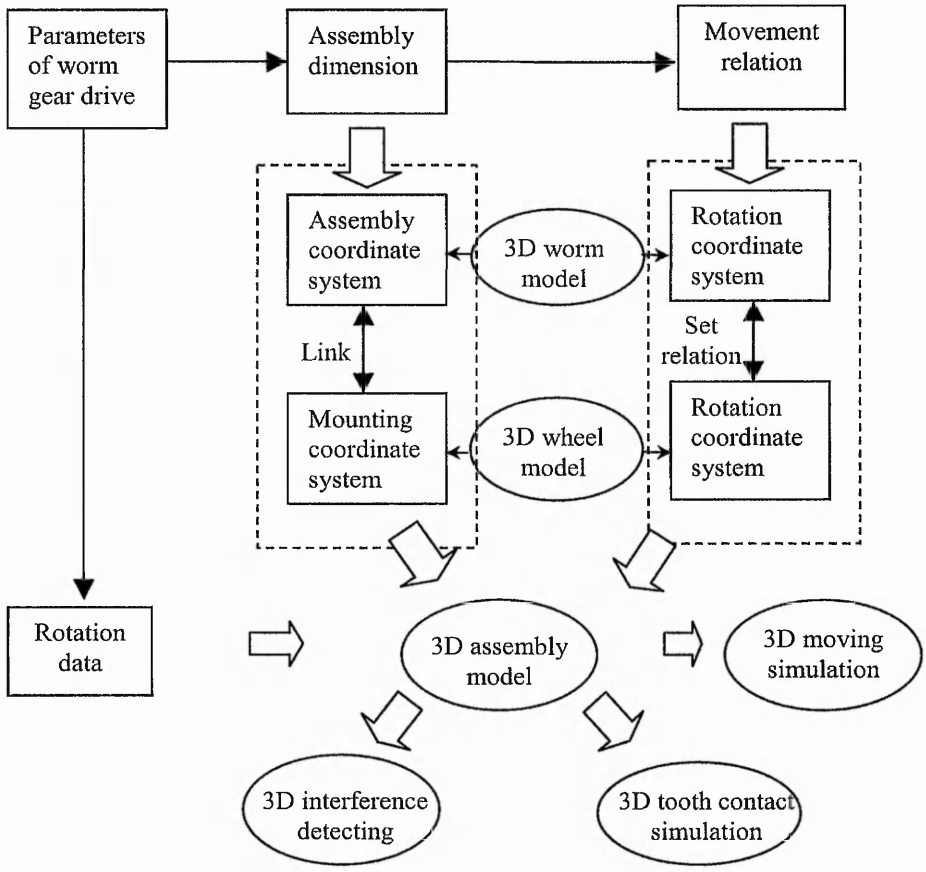

Fig. 5.15 Process for assembly modelling and 3D simulation

In order to establish the relationship between the worm and the wheel, some local coordinate systems are set up on the models. For the wheel model, besides the global

coordinate system of the wheel, two additional local coordinate systems are added. One local coordinate system is the wheel rotation system, located at the centre of the wheel and rotating with the wheel. It is used to measure the rotation angle of the wheel. When this local system rotates with respect to the global system, the wheel model rotates as well. Another local coordinate system is the worm assembly system, which is placed at a position offsetting the wheel centre with the designed centre distance. It is used as the reference for mounting the worm shown in Figure 5.16.

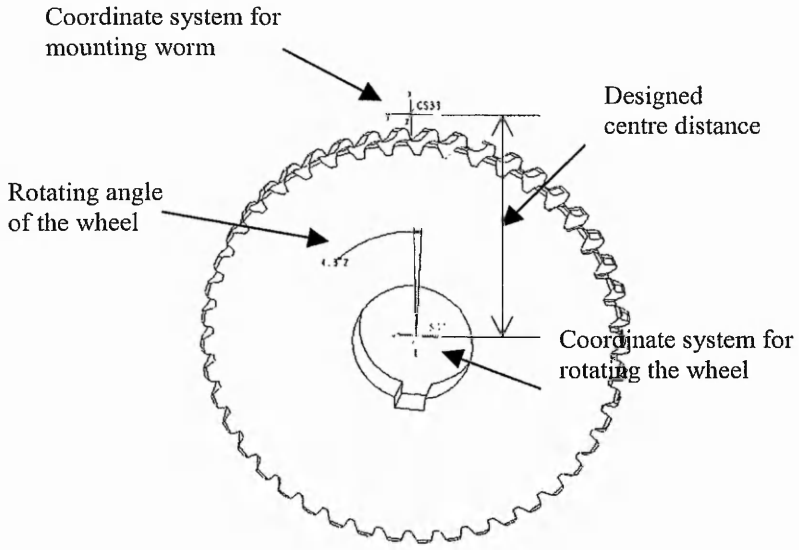

Figure 5.16 Wheel model with local coordinate system

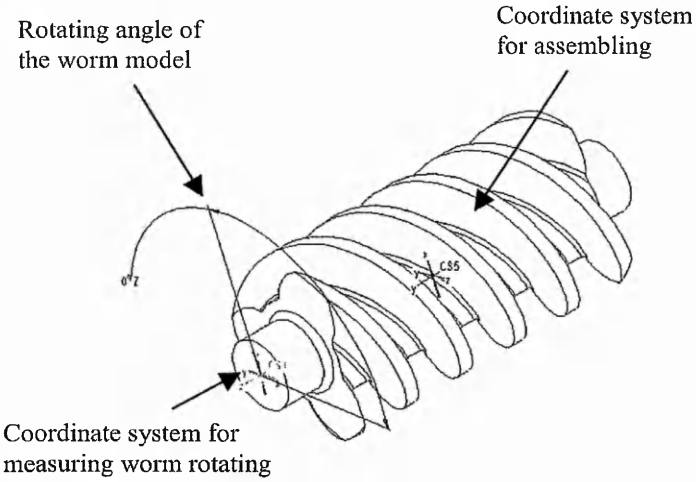

Figure5.17 Worm model with local coordinate system

For the worm model, two local coordinate systems are created as well. One is located at the centre position of the worm, which is used as the reference for assembling. The other is put at the same position of the worm's global coordinate system but with an angle (worm rotating angle) from the original system. By changing the value of the worm rotating angle, the worm model spins. Therefore, it is used to measure the model's angle displacement from the start position. (Figure 5.17)

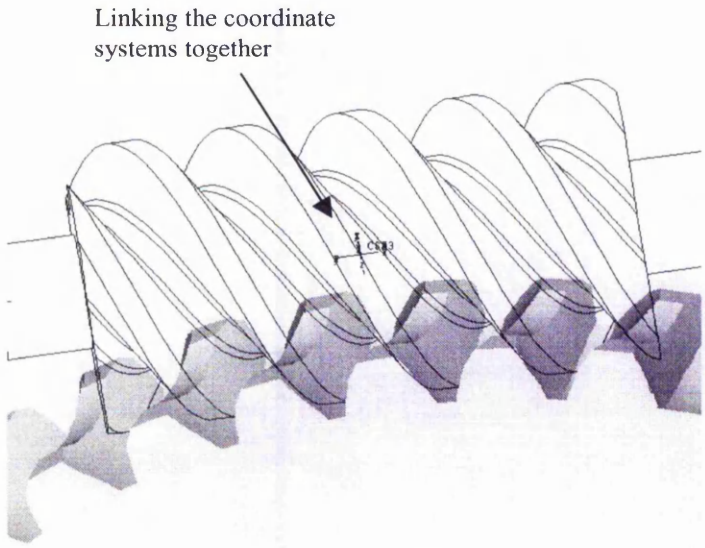

Figure 5.18 Linking the worm and wheel coordinate systems

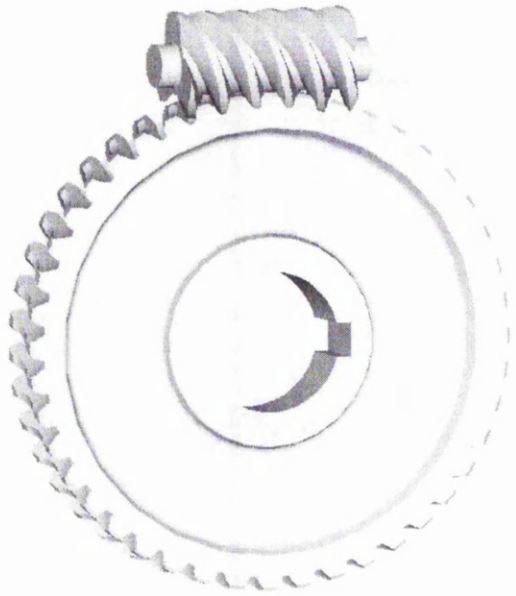

Figure 5.19 Assembly model for involute worm gear

In order to install the worm model together with the wheel model, the mounting coordinate system in the wheel is connected to the assembling coordinate systems in the worm (shown in Fig. 5.18) by placing the origins of the two coordinate systems at the same point. A full assembly model of involute worm gear drive is shown in Figure 5.19.

5.4 Movement relation and three dimensional simulation

It is important to establish an accurate movement relationship within the assembly model, so that the model can calculate the accurate position of every instant of tooth meshing. The RELATIONS function in Pro-Engineer enables the designer to set up such relationships. Using Pro-programme, a relation with the designed transmission ratio is created between the worm and wheel. Hence, when the worm rotates, the wheel turns following the relation automatically. So the motion simulation for worm gear drives can be conducted.

An example of Pro-programming for relation of an assembly model is shown in Figure 5.20. The relation is created for the tooth contact simulation, and the rotation angle of the worm is defined as a variable in the relation. From the assembly model, the dimension labels of the rotation angles such as $D646:2 and $D5710:0 can be detected, which represent the position angles of the worm and wheel respectively. In the Pro-programme, the two dimensions can be expressed as the functions of the defined variable (worm rotation angle). By changing the worm rotation angle, every moment of the worm gear driving process can be simulated.

At this stage, using the interference detection calculation in Pro/Engineer, the tooth contact pattern of the worm gear drive can be roughly estimated. When the interference between the contact teeth become very small, the interference detected is recognised as just a touch between the tooth surfaces. Therefore, the detected interference area can be roughly considered as the tooth contact pattern. However, a large interference and tooth edge interference detected in the calculation are not acceptable for simulation of tooth contact pattern. The procedure of the tooth contact simulation is shown in Figure 5.21.

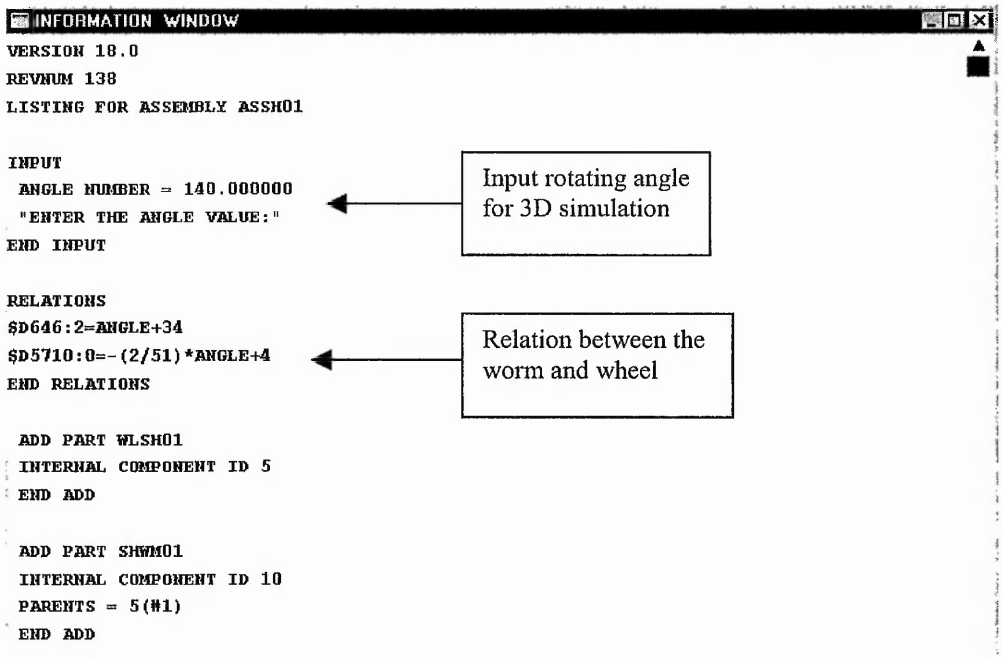

Figure 5.20 Relation within the assembly model

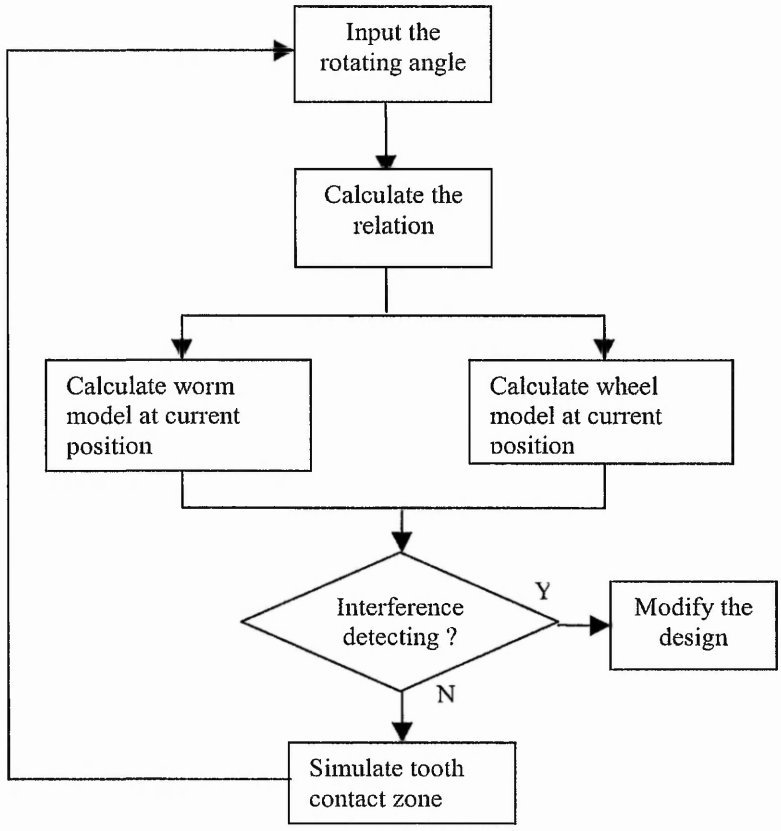

Figure5.21 Procedure of tooth contact simulation

To simulate the tooth contact area of worm gear drives, it is necessary to adjust the worm rotation angles to a proper start position where the worm and wheel are just touching. Thus, the contact zone between the worm and wheel can be estimated. Using the assembly model, it is also very convenient to modify the parameters to simulate various misalignments that often occur in assembling worm gear drives. Figure 5.22 shows the simulation of the contact zone between the worm and wheel.

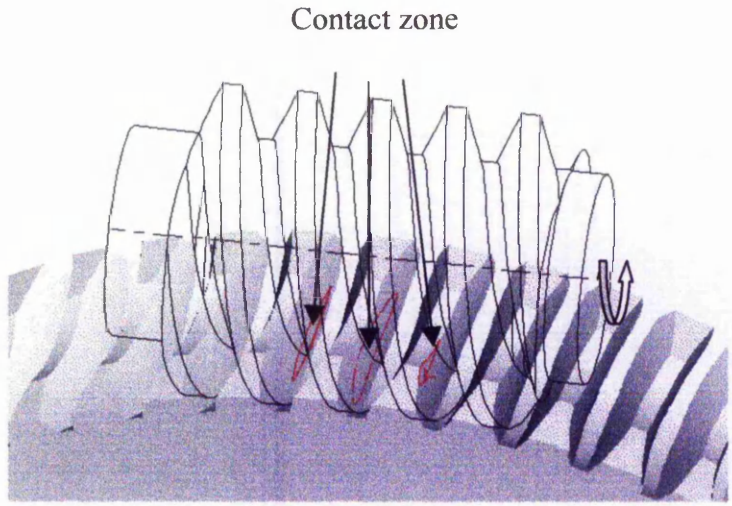

Figure 5.22 Contact zone between worm and wheel

5.5 Tooth Contact Simulation

The three dimensional simulation has been applied to an involute worm gear drive with the following specifications:

- number of worm threads Z_1=2,
- number of wheel teeth Z_2=51,
- module m=7,
- worm reference radius r_w=42,
- centre distance E = 220.5mm,
- normal pressure angle 20^0.

Using the methods developed in chapter 3, the modification parameters are determined as follows:

- worm pitch radius r = 40 mm,
- worm lead angle = 9.683°,
- hob mounting angle = 0.225°,
- pitch of the modified worm = 6.84mm.

Based on the modelling process shown in Figure 5.15, the assembly model is created and the three-dimensional simulation has been conducted for three cases:

- *case 1*, mesh without errors;
- *case 2*, mesh with centre distance error (see Figure 5.23) $\Delta E = \pm 0.25mm$; and
- *case 3*, mesh with shaft alignment error (see Figure 5.24) $\Delta\beta = \pm 0.2°$.

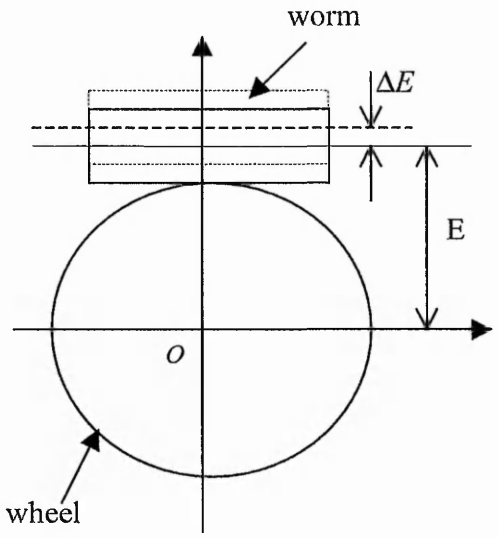

Figure 5.23. The worm gear drive with the centre distance error ΔE

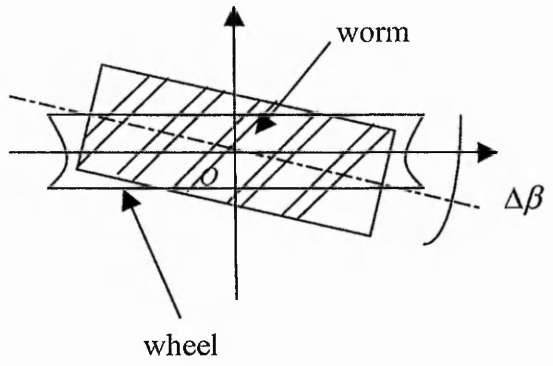

Figure 5.24.The worm gear drive with the shaft alignment error $\Delta\beta$

The simulation results obtained are shown in Figures 5.25, 5.26 and 5.27 respectively for the three cases. The mesh situations were recorded at four particular moments of the meshing process for all three cases:

- *moment 1*: teeth1, 2 and 3 are in mesh;
- *moment 2*: tooth 1 is almost out of the mesh, while the contact areas of teeth 2 and 3 increase;
- *moment 3*: tooth 1 is completely out of the mesh, and teeth 2 and 3 are in mesh with further increasing of their contact areas;
- *moment 4*: tooth 4 gets into the mesh with teeth 2 and 3 remaining in mesh.

According to the simulation results, the following can be concluded:

(1) The simulation can clearly show the contact pattern and its direction of motion, which provides a useful visual aid for the designer to investigate the contact.

(2) Comparing Figures 5.25, 5.26 and 5.27, the contact areas stay almost at the same places and the size of the contact area almost remains the same as well. It is clear that the modified worm gear drive is insensitive to errors.

(3) Any interference between the modified tooth surfaces can be detected by the three-dimensional model and, therefore, it can be avoided at the design stage. This is an important achievement in the analysis of localised contact of worm gears, because previous methods often caused interference and could not detect its position.

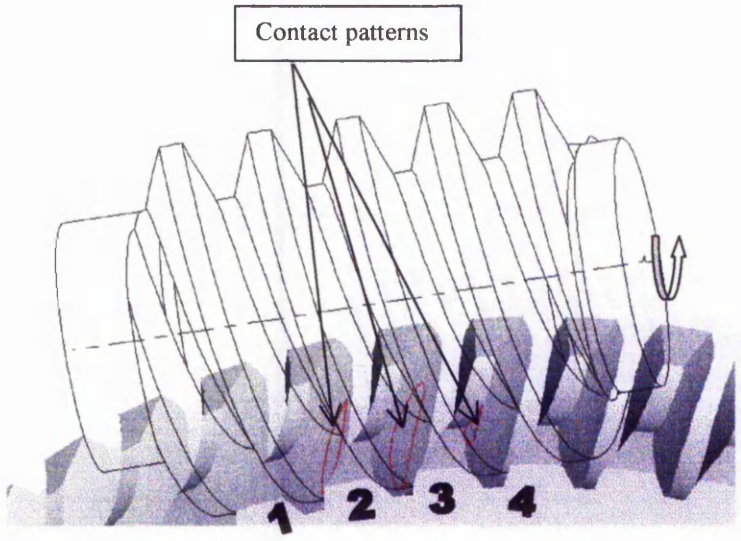

(a) Mesh at moment 1

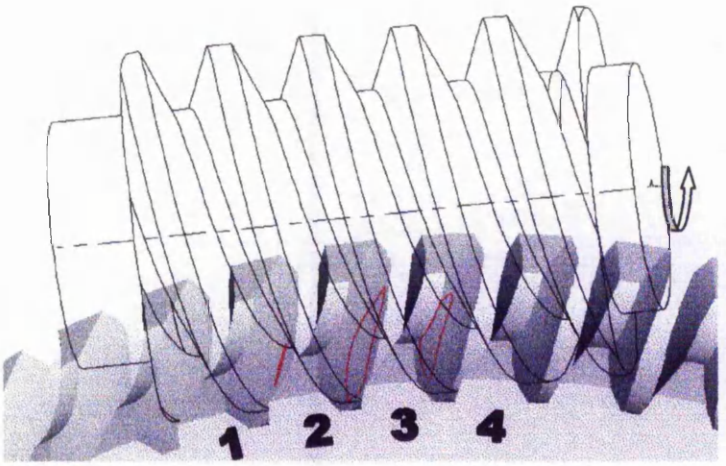

(b) Mesh at moment 2

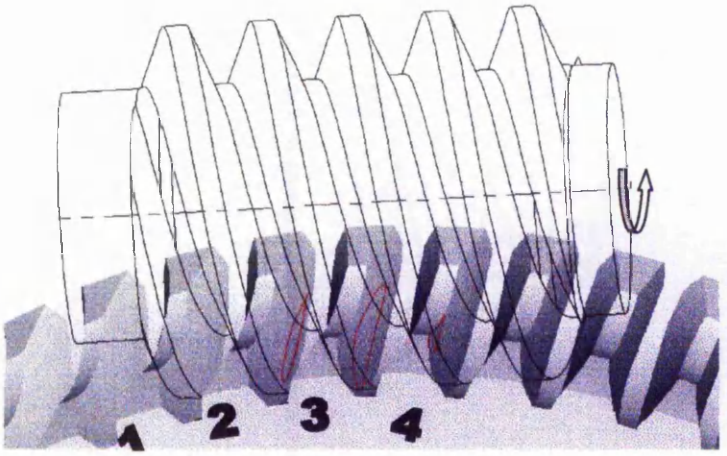

(c) Mesh at moment 3

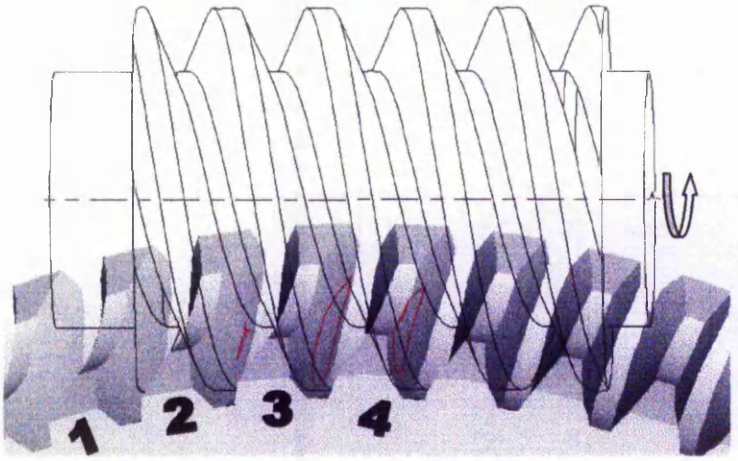

(d) Mesh at moment 4

Figure 5.25. Contact Simulation of the worm gearing without errors

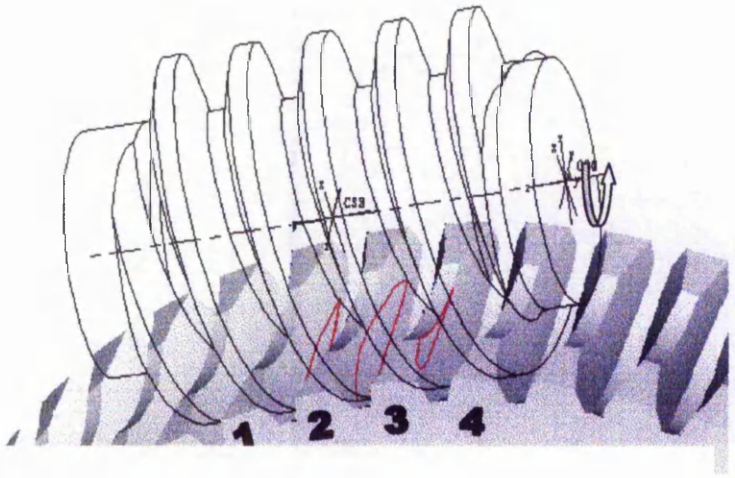

(a) Mesh at moment 1

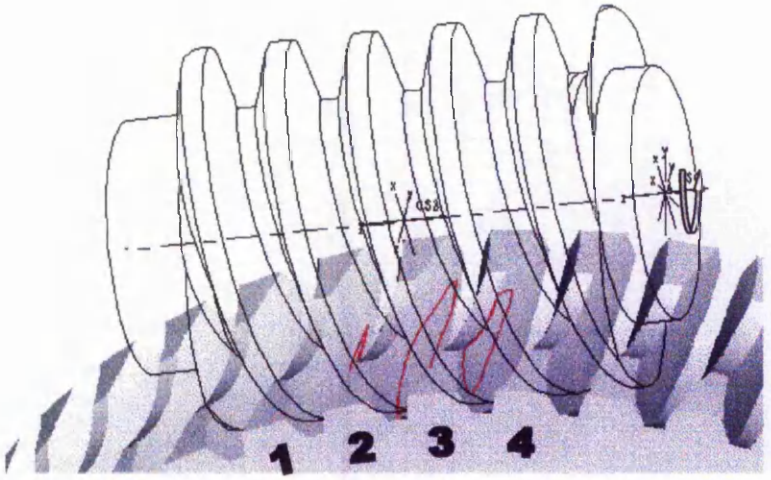

(b) Mesh at moment 2

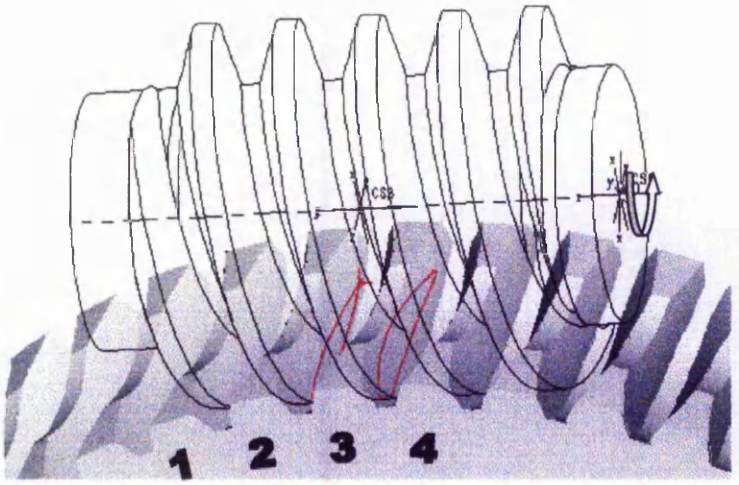

(c) Mesh at moment 3

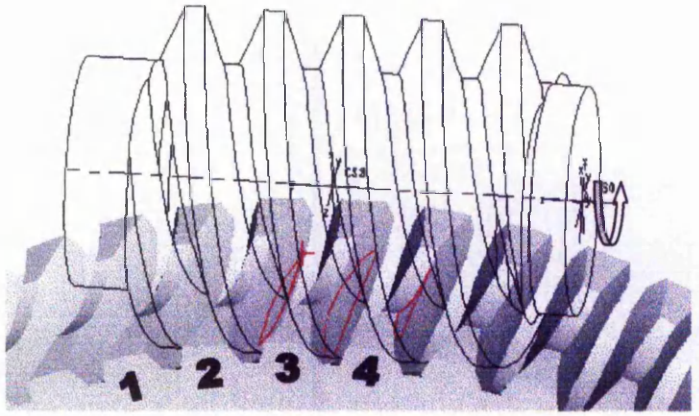

(d) Mesh at moment 4

Figure 5.26 Contact Simulation of the worm gearing with assembly error ΔE

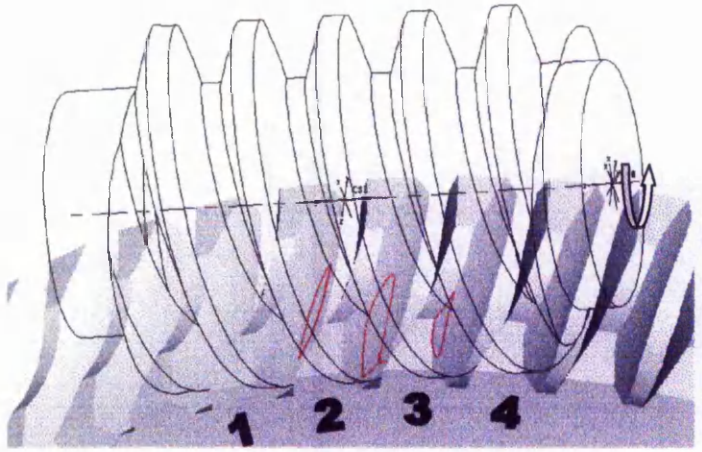

(a) Mesh at moment 1

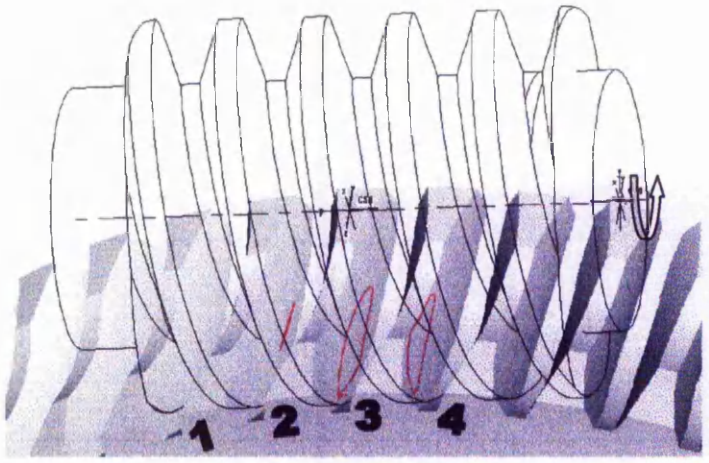

(b) Mesh at moment 2

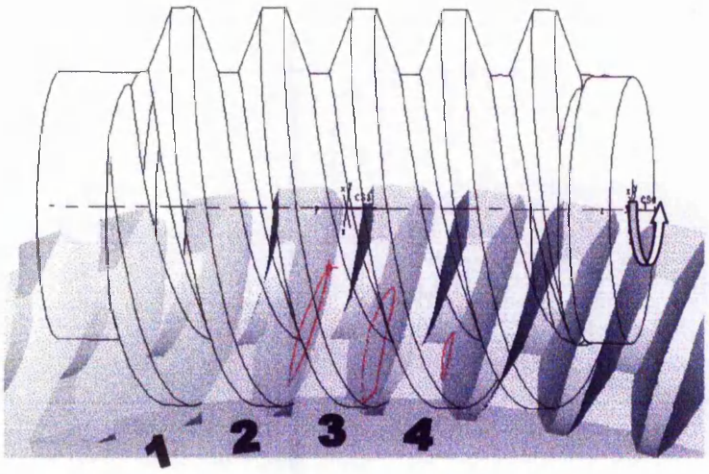

(c) Mesh at moment 3

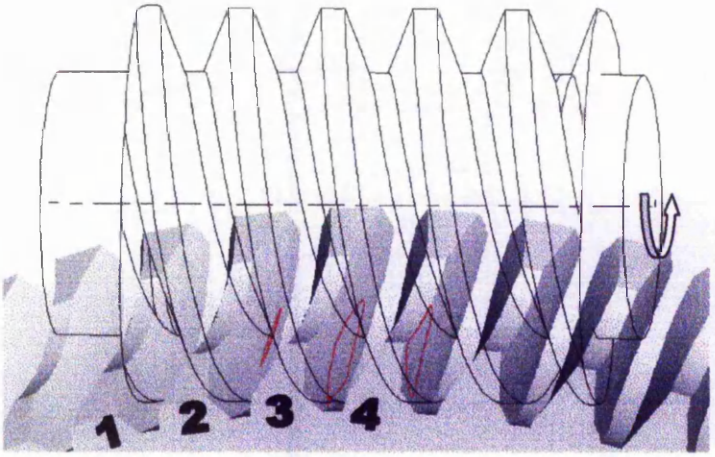

(d) Mesh at moment 4

Figure 5.27. Contact simulation of the worm gearing with shaft misalignment

Chapter 6 Finite Element Model Generation

Due to the complexity of the tooth geometry of worm gear drives, the current standards for calculating the strength and stress of worm gear drives are expressed using the method for estimating the permissible load which is limited by the tooth surface stress and bending stress. However, the tooth stress itself and the stress distribution of the worm gear tooth cannot be calculated directly.

The current advance in gear design is to pursue high loading capacity and low weight for gear drives; gear models with high accuracy and reliability are demanded. The finite element method has emerged as a very active tool of research. It provides the possibility to achieve an accurate and reliable worm gear model.

In recent gear research (Li JF, 1998, Lu J and Litvin, 1995) the finite element method has been applied to evaluate gear tooth stress and load distribution between the simultaneously contacting tooth pairs. However any application in worm gear drives has not been reported yet. The latest draft international standard (ISO, 1999) proposed that the finite element method should be recognised as a precise method to calculate the tooth stress and load capacity. Although the latest draft standard provided a formula to calculate the tooth root stress, the finite element method is considered as more precise than the formula provided.

The finite element modelling process of worm gear drives is investigated in this chapter. Geometric models of worm gear drives can be either imported from the 3D solid models developed in Pro/Engineer or created within the environment of the FEA software package. To generate a proper mesh for 3D worm and wheel models, the geometric models need to be converted into a combination of several simple shapes, so that the meshing process can be performed. The details of the geometric operation for meshing worm gear drives are described in this chapter. The material properties and the boundary constraints of the models are briefly described as well.

6.1 The Coordinate System

To create the FE model, the worm gear is located in a global cylindrical co-ordinate system, shown as Figure 6.1:

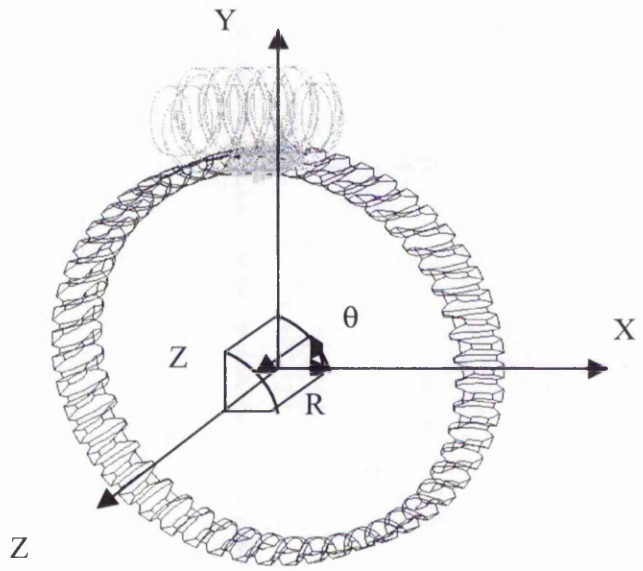

Figure 6.1 Global cylindrical coordinate system

Since the cylindrical coordinate system (R,θ, Z) is able to represent the wheel rotating motion exactly (Z axis is the wheel rotating axis), it is chosen as the global system for finite element modelling, which makes it more convenient to build geometric models and to interpret FEA results.

6.2 Generation of Wheel FE Model

Finite element modelling of the worm wheel involves several steps. The first step is to create an accurate geometry for the 3D tooth profile and export the model as an IGES file that is a standard file format for graphic exchange. The completion of this step has been described in chapter 5. Then, the IGES file created in pro-Engineer is imported into the software ANSYS 5.3. When the IGES file is retrieved in ANSYS, it is usually only a geometric model with the surface information. Within the pre-processor of ANSYS, it is necessary to merge the surfaces to create proper volumes. After that, the proper element type and material property need to be chosen and the mesh of models will be performed.

6.2.1 The FE mesh for the wheel

It has proved to be difficult to apply mapped meshing to the gear wheel body, due to the complexity of the tooth surface geometry. In order to resolve this problem, it is necessary to divide the body into some individual units of 6-sided volumes so that the software can implement the mapped mesh. For this particular project, the IGES file is imported into ANSYS 5.3 and a part of the wheel body containing six teeth is created using the surface geometry obtained from the IGES file. Figure 6.2 shows the tooth volume. The whole volume is further divided into 57 sub-volumes which are suitable for mapped meshing. The gear wheel body with 57 individual volumes and areas is shown in Figure 6.3.

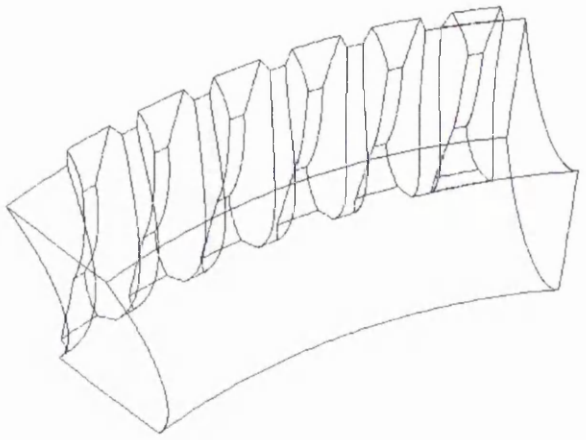

Figure 6.2 The tooth geometry from IGES file

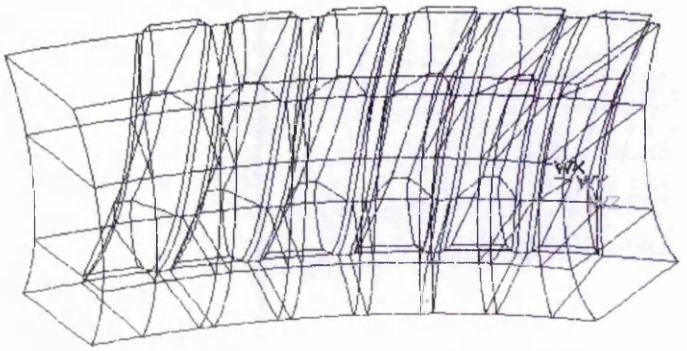

Figure.6.3 Individual Volumes for mapped mesh

The fillet creation is one of the most important details for the volume generation. To get the tooth body with the fillet, firstly the fillet area is created in the ANSYS pre-processor. Then, the intersection lines between fillet and tooth surface are treated as the borders for dividing the whole tooth volume into the sub-volumes, shown as Figure 6.4. Thus, the fillet-areas will be the side surfaces of the sub-volumes. By doing so, the meshing process will be much easier to perform.

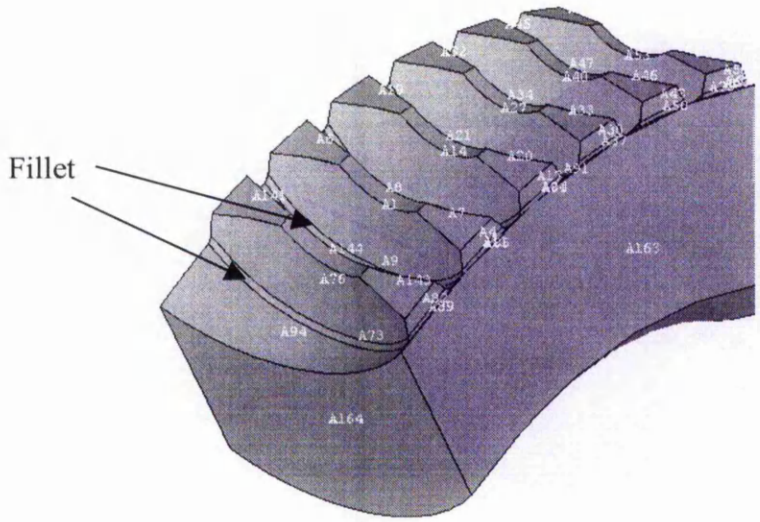

Figure 6.4 Fillets of the wheel tooth body

The number of element divisions on the boundary lines of the individual volumes was controlled manually to define the mesh density. e.g. the division of the fillet edge is given as three so that the fillet edge will be meshed by three elements.
The wheel model created is an involute cylindrical gear-wheel with 56-teeth and speed ratio 3/56. The throat radius of the wheel is 37.160 mm and the outside diameter is 500 mm. Gear face width is 78.0mm. Initially the six-tooth model of the gear wheel is meshed in order to estimate the influence of the load on the neighbouring teeth of the loaded tooth. The 20-noded element (solid-95) is used to mesh the model, Figure 6.5 shows the element. The mesh result of the whole model can be seen in Figure 6.6.

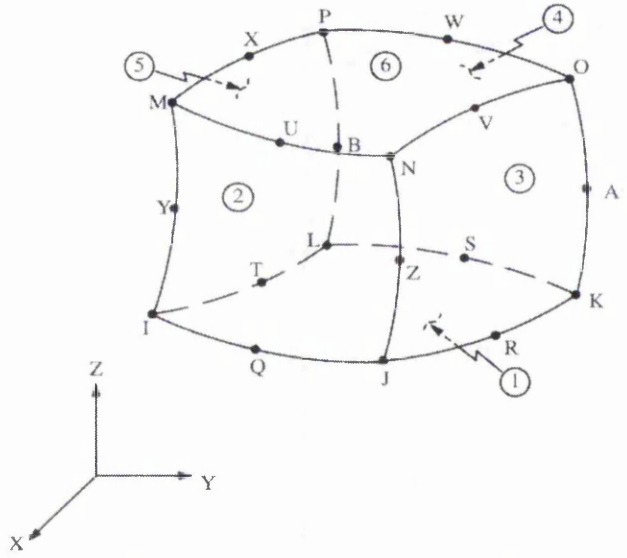

Figure 6.5 Solid 95 element with 20 nodes

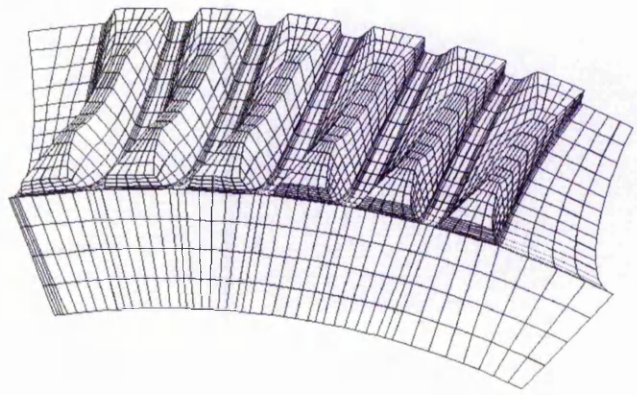

Figure 6.6 The meshed worm wheel model

6.3 Generation of Worm FE Model

The worm model is composed of helical surfaces so that the meshing process becomes much more complicated. Two approaches have been applied to generate two types of worm FE models: portion model and whole worm model. The worm model created is an involute cylindrical worm with three heads and the lead angle of the

worm is 13.5 degree. The outside tooth diameter is 107mm and the root diameter of the worm tooth is 71mm. The pressure angle is 22.5 degree.

6.3.1 FE mesh of the worm portion

Using mapped meshing is the first approach. For the mapped meshing, the volume of the model must be able to be simplified into six-side individual volumes. One portion of the worm was built to generate the mesh (Figure 6.7). The worm portion is further divided into individual volumes in order to fit mapped meshing. Again, a fillet creation process similar to that mentioned in section 6.2.1 was applied here. The mesh of the worm portion also consisted of 20-noded elements (Solid-95), as shown in Figure 6.8.

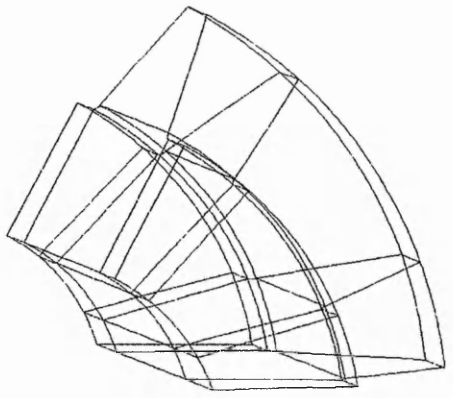

Figure 6.7 Part volume of the Worm

However, it is very difficult, if not impossible, to build a whole worm FE model using mapped meshing, because the mapped meshing function cannot be applied to a helical shape.

The portion model of the worm developed above is applicable to a general purpose engineering analysis. However, sometimes, it is necessary to have a complete model of the worm to investigate the continuous tooth contact process. A different approach is developed to achieve a complete finite element model for the worm.

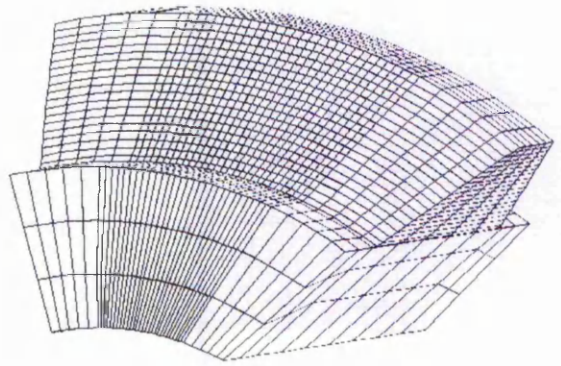

Figure 6.8 FE Mesh of the worm portion

6.3.2 FE mesh of whole worm

To create a whole model of the worm, the author investigated a useful approach for finite element modelling of helical geometry. The idea to develop a complete worm FE mesh is based on the fact that mesh extrusion of shell elements can generate 3D elements and this function can produce elements to fit helical shapes such as the worm profile. A function command called **VEXT** operation in ANSYS5.3 is applied to perform the mesh extrusion. Because a rotation of the shell elements around an axis is allowed during the **VEXT** operation, the extrusion process is able to produce a helical shape mesh.

The mesh extrusion can only be performed successfully if the following requirements are met:

1. The given area is meshed with 2D elements and appropriate meshing density (for the worm model, the area is the transverse section of the worm).
2. Appropriate type of 3D element is specified and activated. As the 3D element is extruded from the 2D element, the selected 3D element of the model must have the same nodes and lateral as the 2D element. For the worm model, Solid 45 element is selected. (Figure 6.9)
3. The desired number of element divisions must be specified (using NDIV on the ESIZE command). The extrusion command will use the number of divisions for the element density of the drag path.

4. The appropriate rotation angle around the extrusion axis must be chosen carefully in order to generate a proper mesh. Otherwise either over-distorted elements will be generated or mesh extrusion will fail.

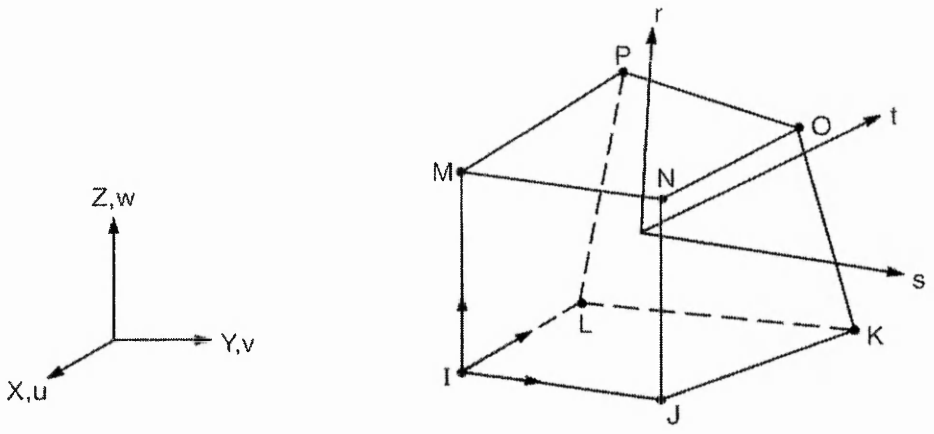

Figure 6.9 Solid element 45 with 8 nodes

Using a programme language called *ANSYS Parameter Language*, a modelling programme is developed to conduct the process of extruding the worm FE model. Figure 6.10 shows the flow chart of the modelling programme. The programme consists of the following five major steps:

a. generate the transverse section of the worm with the design parameters, and place the axis of the worm as the axis for mesh extrusion, shown as Figure 6.11
b. choose the proper meshing density, mesh the transverse section with quadrilateral shell element. (Element shell 63 is selected)
c. choose the proper type of solid element for creating the 3D worm model. (Element solid 45 is selected)
d. define the element density of the drag path, extrude the meshed section to form one layer of the model, shown as Figure 6.13
e. Repeat the mesh extrusion to generate the whole worm model, then delete all the existing shell elements, because after extrusion all the shell elements are not needed for the 3D worm model. The completed worm model is shown in Figure 6.14.

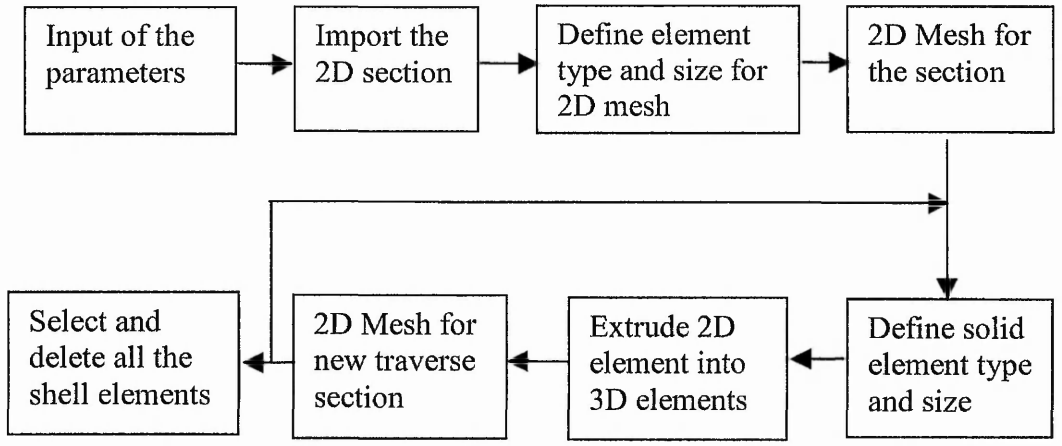

Figure 6.10 Flow chart of the meshing process

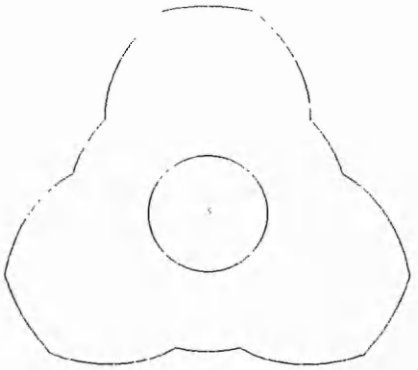

Figure 6.11 The traversal section of the worm

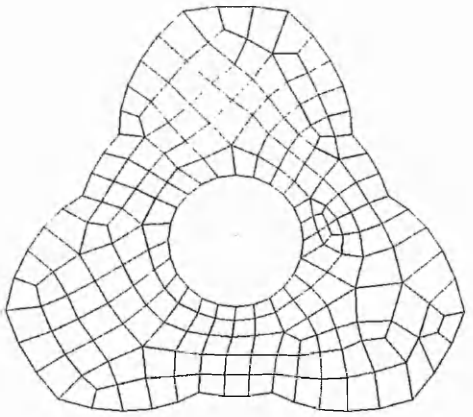

Figure 6.12. 2D mesh of the transverse section of the worm

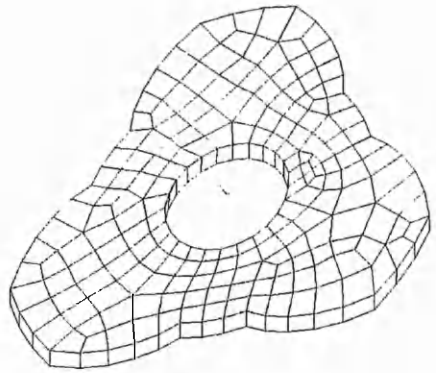

Figure 6.13 One layer meshed worm piece formed by extrusion

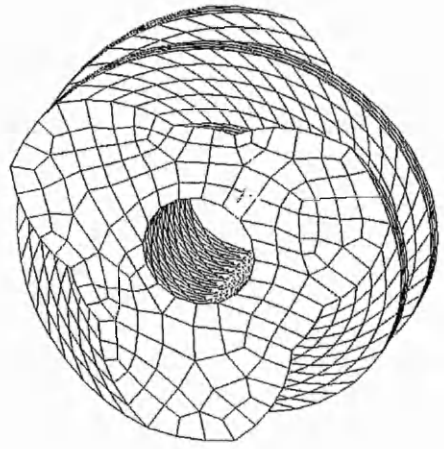

Figure 6.14.The final extruded worm model

Below is the programme:

Command	**Notification**
zval=0	define the starting position
anginc=- 3.75	define the rotation angle
zstep=-.8345	define the drag distance
ntime=30	define the extrusion times
/prep7	start command
asel,,loc,z,zval-0.01,zval+0.01	select the travese section
et,1,63	select the shell element
amesh,all	mesh the area

et,2,45	select the solid element
esize,,1	define the density of the drag path
*do,i,1,ntime	start the circulation process
/gopr	
type,2	make solid element active
vext,all,,,0,anginc,zstep	extrude shell elements into solid element
zval=zval+zstep	
*if,i,lt,ntime,then	
asel,,loc,z,zval-0.01,zval+0.01	select new traverse section
type,1	
amesh,all	mesh the section
*endif	
*enddo	Check the extrusion times
asel,,type,,1	select all area with the shell element
aclear,all	delete the shell element

This approach can successfully generate a whole worm mesh, but the problem of element exaggerated distortion (Figure 6.15a) may arise if the worm helical geometry is over-twisted. The degenerated element produced in the extrusion (Figure 6.15b) also could cause a problem for bending calculation because it is too hard to bend. The small rotation angle and drag distance of extrusion can help to avoid the problems.

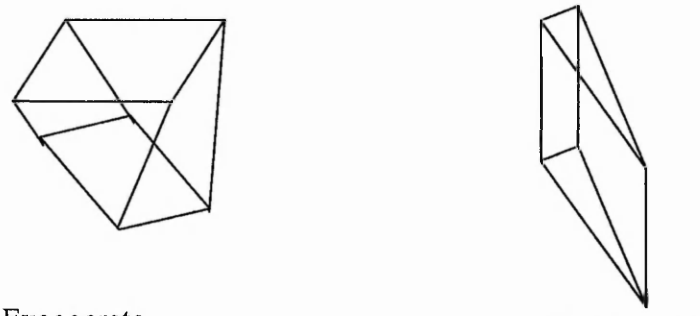

Figure 6.15 Undesired elements caused by the mesh extrusion

6.4 Empirical Analysis of the Worm Gear Drive

In order to evaluate the fidelity of the worm and wheel models, it is necessary to compare the FEA results with existing experimental work. It was decided that the experimental work conducted in Nagoya Research & Development Center, Mitsubishi Heavy Industries Ltd.(1996) would be used to evaluate the computer simulation.

The experimental work applied an optical interferometer for measuring the deflection of the tooth, as shown in Figure 6.16. The JIS 3 type worm and wheel were selected for the experiment, of which the tooth profile is similar to the involute type worm and wheel.

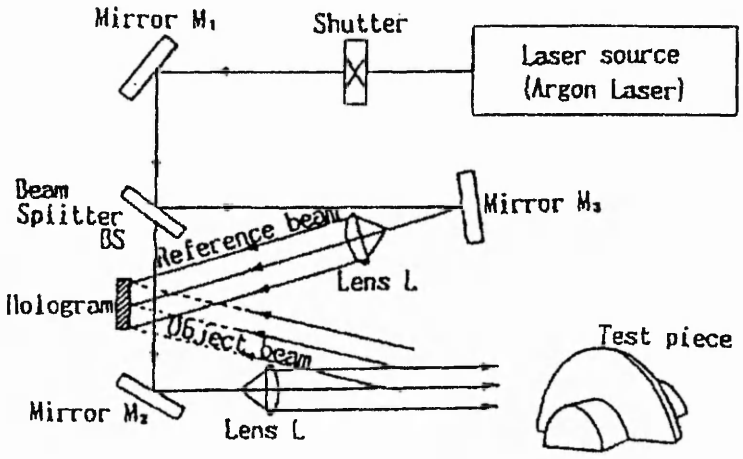

Figure 6.16 Experimental work for measuring the deflection of the tooth

6.4.1 Empirical results of the tooth deflection analysis

The static loads were applied to different position of the tooth surface. From the empirical results, the following empirical equation of tooth deflection for worm gearing was derived by SUDOH et. al. (1996) as:

$$W = V(\bar{r})\frac{\sqrt{F(\theta)F(\theta_p)}\sqrt{G(\bar{y})G(\bar{y}_p)}}{\sqrt{F(\hat{\theta})G(\hat{y})}} \cdot UP/m \qquad (6.4.1)$$

where, $\bar{y} = 1 - \frac{y}{h}$; $\bar{y}_p = 1 - \frac{y_p}{h}$; $\hat{y} = |\bar{y} - \bar{y}_p|$; $\bar{\theta} = |\theta - \theta_p|$; W is the tooth deflection; h is whole tooth height and m is the module. P refers to the concentrate force; U is the absolute tooth deflection; $V(\bar{r}), G(y), F(\theta)$ are characteristic functions of tooth deflection (Appendix B), y and y_p are the coordinates of measuring and loading points (tooth bottom is the origin). Using this formula, the tooth deflection can be calculated.

6.4.2 Empirical approximate equation of the tooth root stress

The empirical equation for tooth root stresses was also constructed according to the experimental work. The equation was the only tooth stress formula for a worm gear found through the literature survey. It is presented as follows.

$$\sigma = \sigma_0 \cdot K_v \cdot K_s \cdot K_\alpha \cdot K_\theta \qquad (6.4.2)$$

Where, σ_0 is the fundamental nominal stress; K_v is the influence coefficient of tooth height, K_s is the influence coefficient of the tooth width; K_α is the stress concentration coefficient; and K_θ is the influence coefficient which accounts for the increase in root stress at the edge of tooth width of worm wheel. For further details, see appendix B.

.

6.5 FE Analysis of the Tooth Deflection

The computational simulation of the tooth deflection is conducted using the developed models. The boundary conditions and the material properties of the models are defined according to the general design of worm gear drives.

6.5.1 Material property and boundary conditions for FE models

In order to keep accordance with the experimental work, the model material of both the worm and the wheel is defined as steel. However, in the experimental report of the Mitsubishi Heavy Industries Ltd.(1996), the detailed material data was not explicitly given. Based on general engineering data, the Young's Modulus and the Poisson's ratio are considered as 206000 N/mm^2 and 0.3 respectively.

The boundary conditions are the exterior influences on the FE model, such as force, pressure and restraints, etc. For the investigation of the worm gear drives, the main boundary conditions are the transmitted load and its constraints. According to the assembly method of worm gear drives, the wheel is fixed on the shaft. Two side surfaces of the wheel tooth are free surfaces. Therefore, the constraints of the model are applied to the bottom area and the two dividing areas of tooth portion, all the nodal displacements along the constraint areas were fully constrained, as shown in Figure 6.17. According to the calculation, the load mainly affects the tooth to which it is applied, the effect of the load on the neighbouring teeth can be neglected. To reduce the calculation time the FE model with one tooth is used to investigate the deflection and the stress of the tooth. The concentrated load or distributed load is applied to the loading position on the tooth surface, which can be determined from the TCA calculation mentioned in Chapter 4.

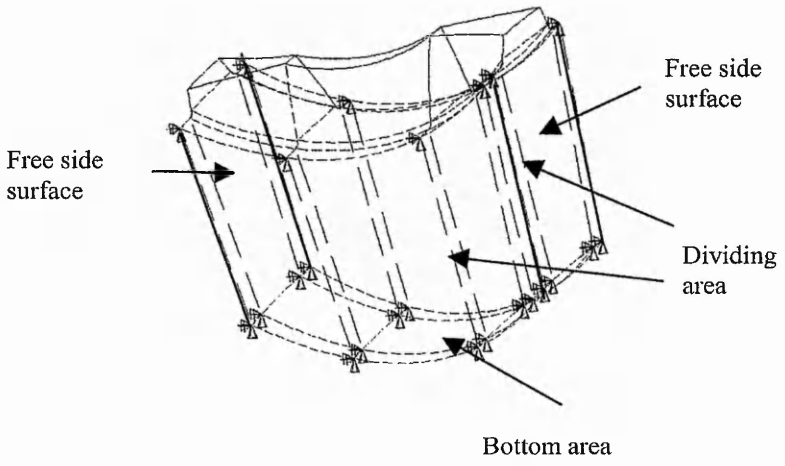

Figure 6.17 Boundary constraints for the tooth model

6.5.2 FEA results of the tooth deflection analysis

To investigate the wheel tooth deflection, the load is applied to the FE model at the same position as the experimental work (X=4mm, Y=14mm), as shown in Figure 6.18.

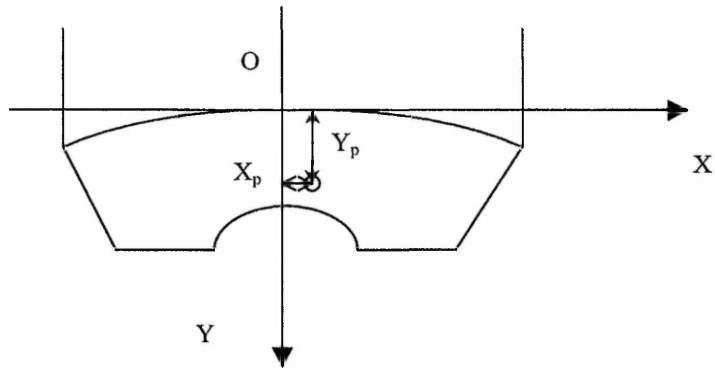

Figure 6.18. Loading position of tooth surface

The results of the tooth deflection along the x and y direction are presented in Figure 6.19 and Figure 6.20 respectively. For positions apart from the loading point, there is a close agreement of tooth deflections between results obtained by the empirical equation (6.4.1) and the FE simulation for both X and Y directions. But for the tooth deflection near the loading position, divergence to some extent exists between the empirical equation and the FE simulation. However, if the concentrated load is properly distributed in the loading position, the divergence will decrease significantly.

The existing divergence between the results of FEA and empirical equation could be explained as follows:

(1) Although the load in the experimental work was considered as a 'concentrated' load, it still would spread into an area when it was applied to the tooth.

(2) The difference of material property between the assumed FE model and the real experiment may cause the divergence.

(3) The FEA calculation itself will bring approximation into the results.

Nevertheless, regarding the whole trend of the tooth deflection, the result of FE simulation has a reasonable coincidence with that of the experimental equation. The closely related qualitative and quantitative tooth deflection between the FE simulation and the experiment shows the validity of the presented model.

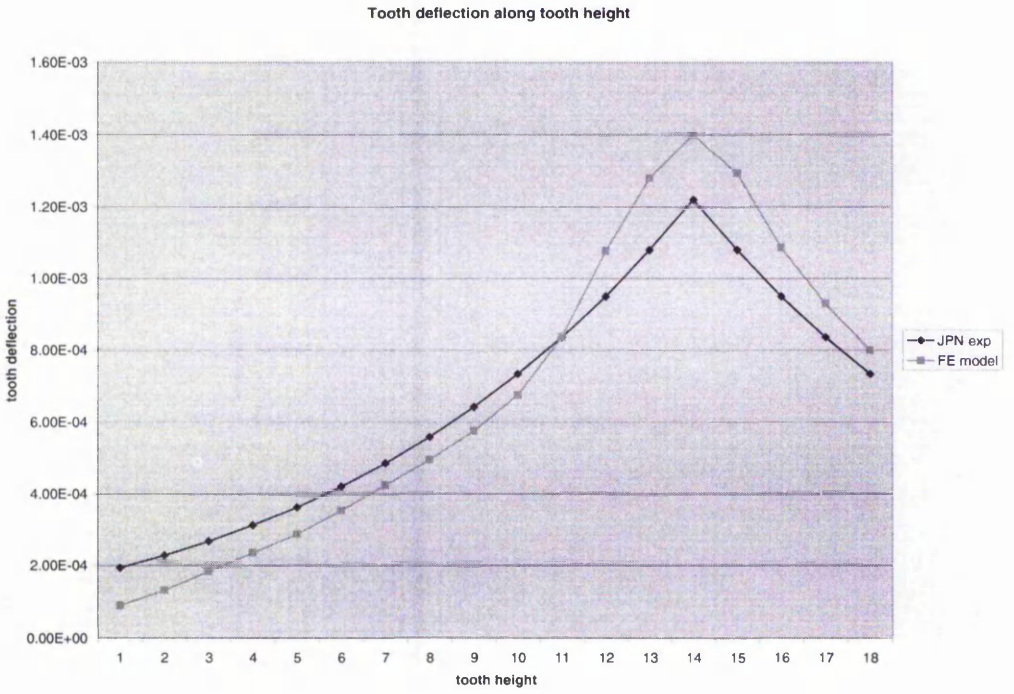

Figure 6.19 Tooth deflection along the tooth height

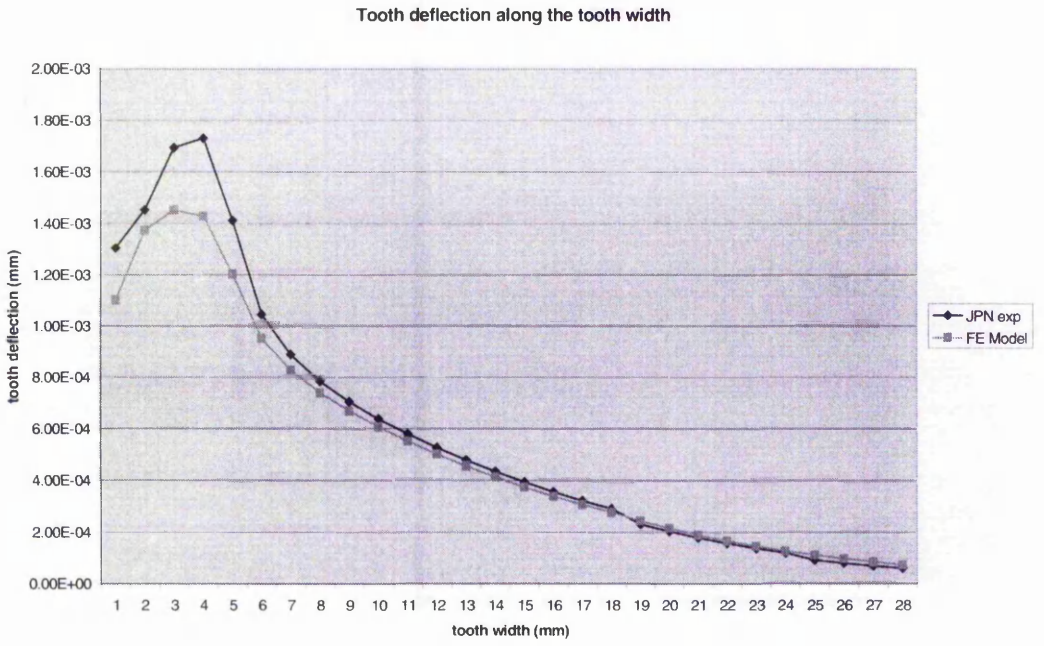

Figure 6.20 Tooth deflection along the tooth width

6.6 Stress Analysis of the Worm Gear Drives

The current formulae available to the designer for calculation of the tooth stress are conducted for parallel-type gears (Dudley,1984, Handbook of practical gear design, McGraw-Hill, Inc). With respect to worm gears, the widely accepted method is to calculate the permissible load capacity. The permissible load capability of worm gear drives is limited either by the surface stress in the gear teeth or the bending stress. This refers to both the worm threads and the worm wheel teeth. Therefore the determination of the load capacity involves four calculations, i.e. both the surface stress and bending stress for the worm threads and the worm wheel teeth, and the permissible load capacity is considered as the lowest of the four values (Stokes, 1992). However, this calculation method cannot be used to calculate the tooth stress.

With the increasing requirement of large loading capacity and small size for worm gear drives, it is important for the designer to know the real tooth stresses. The finite element method provides a possibility to calculate the tooth stress of the worm gear drives. In the next section, the tooth root stress is analysed based on the finite element model and the results are compared with the empirical equation (6.4.2).

6.6.1 Tooth root stress analysis for worm wheel

To investigate the tooth stresses different loads are applied to the finite element model. For the worm wheel, the following alternatives for the load position are investigated (Figure 6.21):

(a) Load is acting near the tip of the tooth (position A, Z=0, X=17mm);
(b) Load is acting at the middle part of the tooth surface(position B, Z=0, X=14mm)
(c) Load is acting near the tooth root (position C, Z=0, X=9mm)

The loads are applied as evenly distributed in an area of 2 square millimeters around the position.

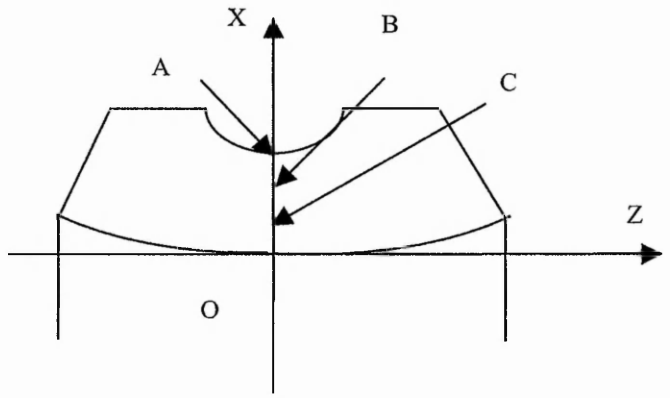

Figure 6.21 Loading position for stress investigation

The full investigation of the stress distribution in worm gear teeth is a highly complex problem. The analysis here only refers to the stress concentrations associated with the fillet at the tooth root. In the analysis, the load is applied to the specific positions of the tooth surface. For each case, the tooth root stress has been calculated. Figure 6.22, 6.23 and 6.24 show the contour plots of the results of the finite element analysis. The principal stress values of the tooth root are listed in the Table 6.1. The FEA results are compared with those obtained from the empirical equation.

From the calculation results of the bending stress and its contour plots, the following can be found:

(1) The stress concentration occurs in the area of the tooth root and the occurrence of the biggest bending stress is located near the root.

(2) The value of local contact stress around the loading position is quite high. The values are often higher than the bending stress. However, the experimental data of contact stress is not available now.

(3) The FEA results of tooth root stress are comparable to the empirical results (Table 6.1).

From the results of FEA, it is also noticed that maximum tension stress occurs close to the loading position when the load is applied near the tooth tip (position A). Actually it is the stress of local contact area that is influenced by the specific geometry of the wheel tooth. However, the discussion here is only focused on the principal stresses at the tooth root, which are presented in Table 6.1.

Table 6.1 Bending stress at the tooth root

Loading position	**A**	**B**	**C**
FEA results (1^{st} principal stress)	**1.349×10^7 Pa**	**1.245×10^7 Pa**	**$1.072.\times10^7$ Pa**
Empirical equations	**1.734×10^7 Pa**	**1.481×10^7 Pa**	**1.123×10^7 Pa**

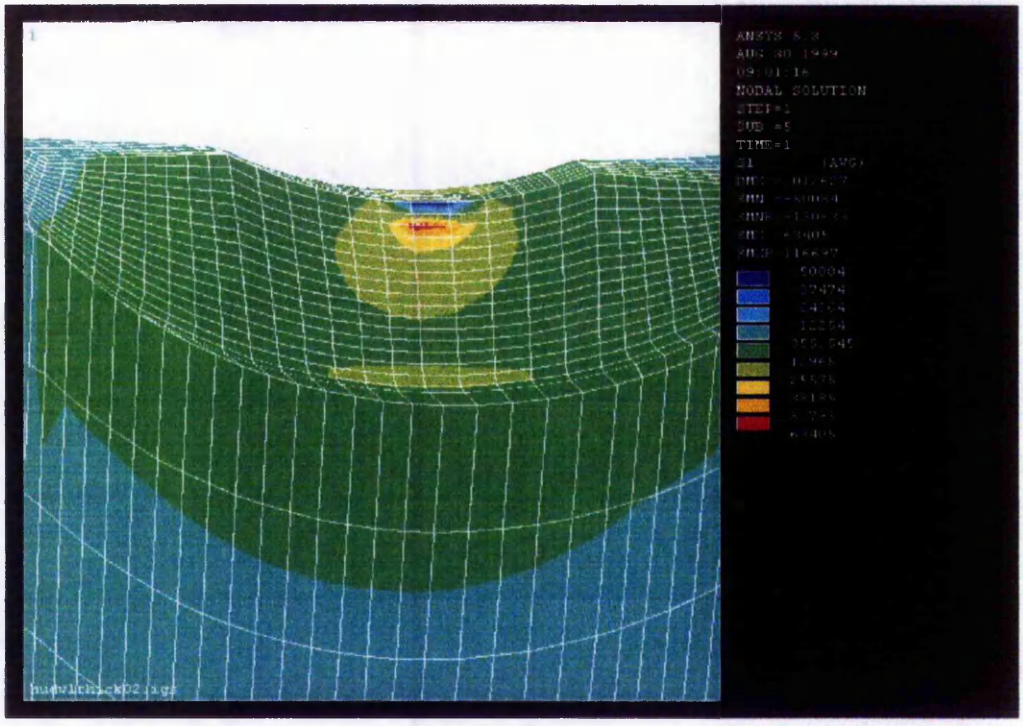

Figure 6.22 Stress contour of the wheel tooth (position A)

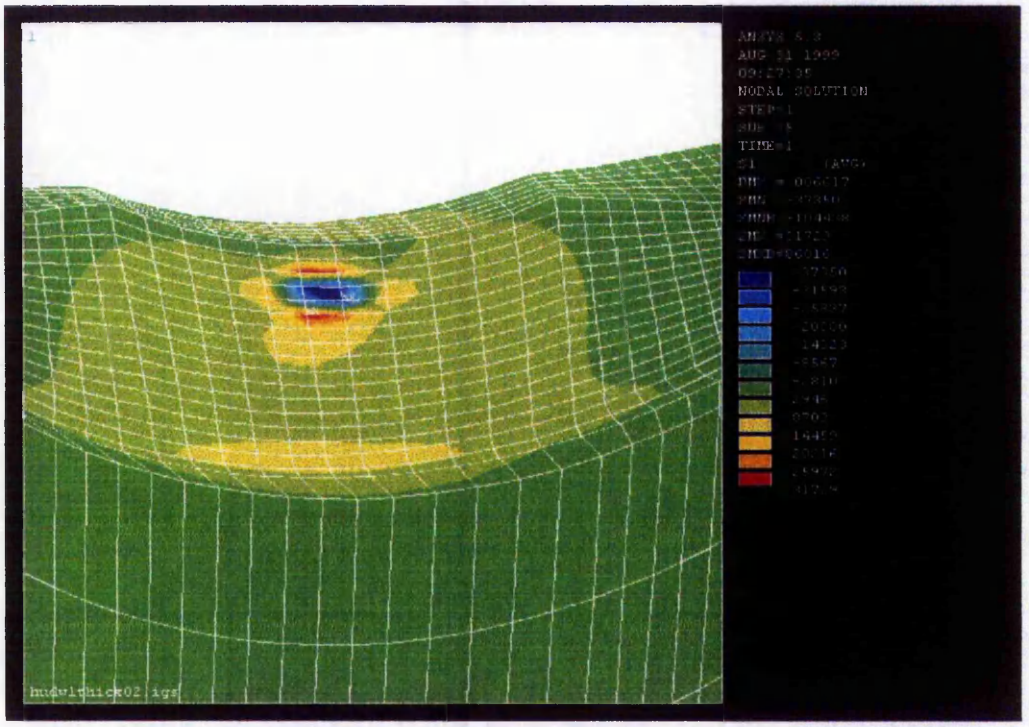

Figure6.23 Stress contour of the worm wheel tooth (position B)

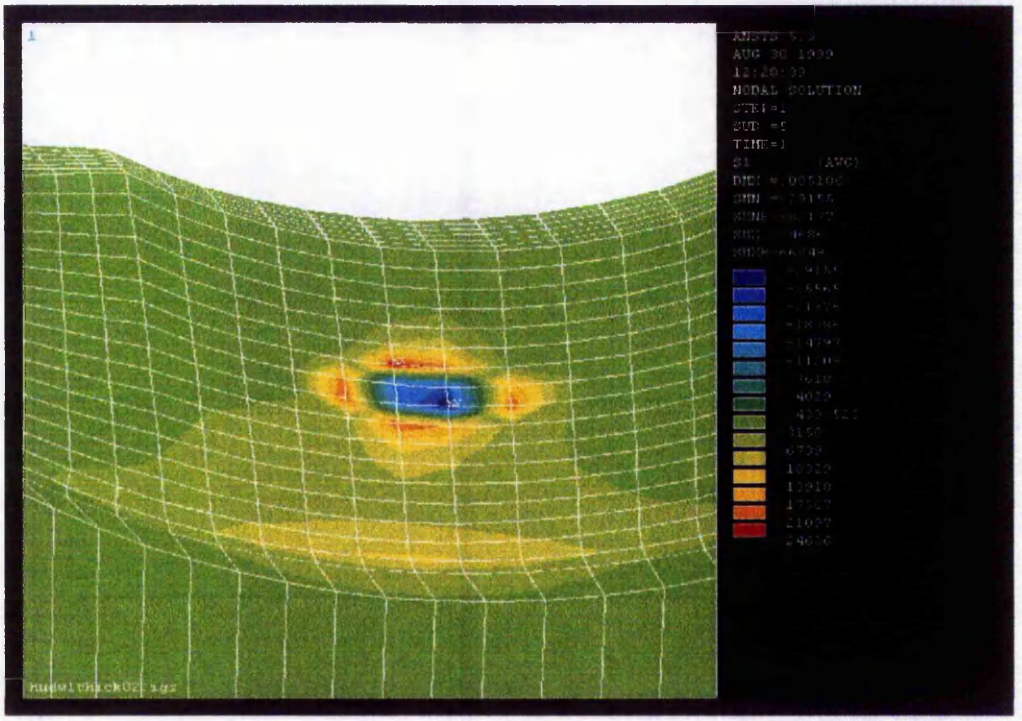

Figure 6.24 Stress contour of the worm wheel tooth (position C)

6.6.2 Stress analysis for worm

To investigate the tooth stresses of the worm, different loads were applied to its finite element model. The following loading positions of the worm tooth are investigated (Figure 6.25):

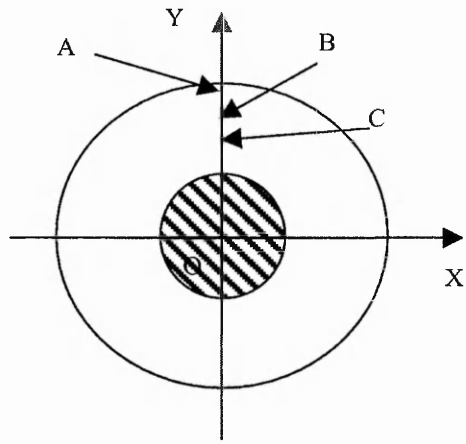

Figure 6.25 Loading position for worm stress investigation

(a) Load is acting near the tip of the worm tooth (position A, X=0, Y=17mm);
(b) Load is acting at the middle part of tooth surface(position B, X=0, Y=14mm)
(c) Load is acting near the tooth root (position C, X=0, Y=10mm)
The loads are again applied as concentrated load at the positions.

Similar to the stress analysis of worm wheel, the investigation here is only referred to the stress concentration associated with the fillet at the worm tooth root. In the analysis, the tooth bending stresses under concentrated load are investigated. Figure 6.26, 6.27 and 6.28 show the contour plots of the results of the finite element analysis. The bending stress values of the tooth root are listed in the Table 6.2, where the FEA results are compared with the empirical results.

From the calculation results of the bending stress and its contour plots, the following can be derived:

(1) The bending stress concentration has been observed in the area of the tooth root. The biggest bending stress value occurs near the root.

(2) The local contact stress around the loading position also is high, its values are often higher than the bending stress.

(3) The FEA results of tooth root stress are comparable to the empirical results. However, the empirical equation is likely to give a larger calculation result of tooth stress, which provides some safety factor in engineering application.

Table 6.2 principal stress at the tooth root

Loading position	**A**	**B**	**C**
FEA results (1^{st} principal stress)	**1.2589×10^7 Pa**	**0.9915×10^7 Pa**	**0.8025×10^7 Pa**
Empirical results	**1.576×10^7 Pa**	**1.335×10^7 Pa**	**0.9595×10^7 Pa**

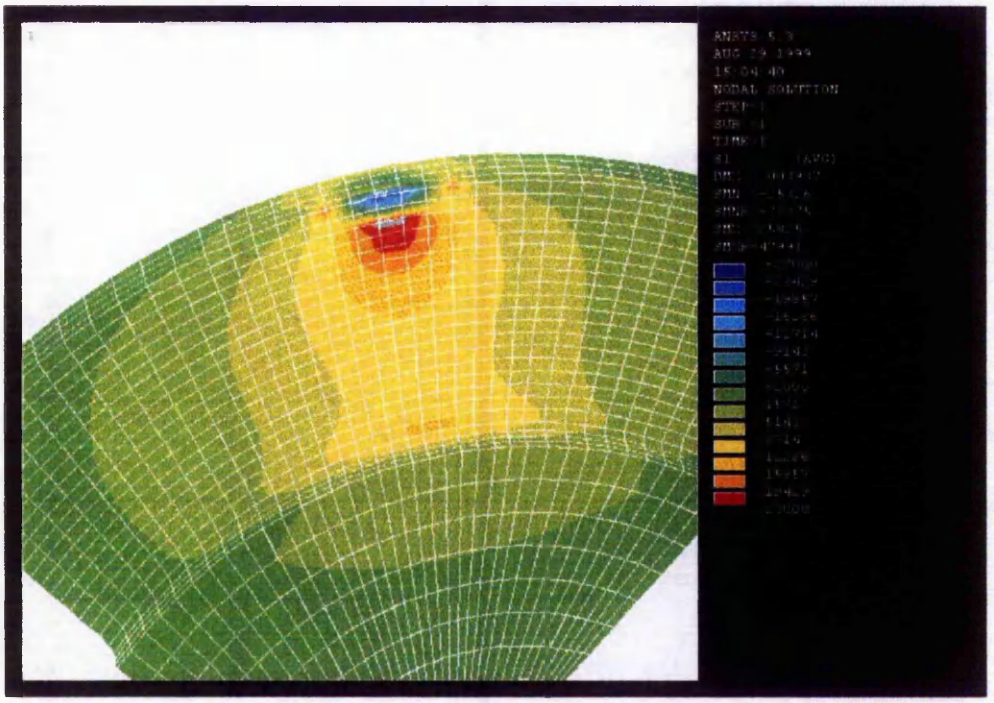

Figure 6.26 Stress contour of the worm tooth (position A)

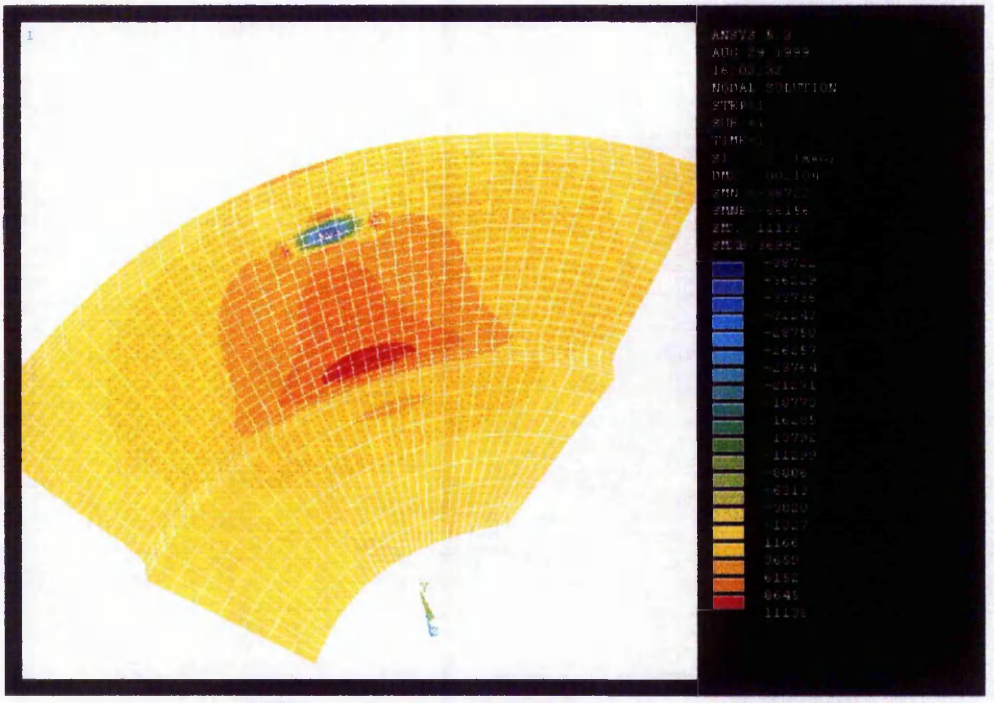

Figure 6.27 Stress contour of the worm tooth (position B)

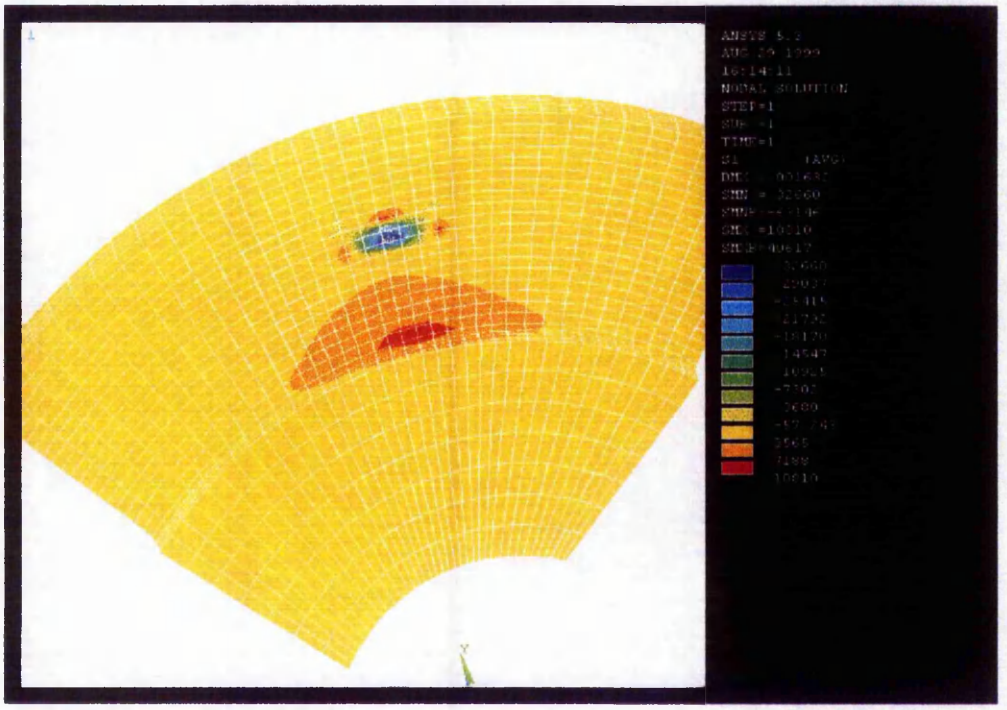

Figure 6.28 Stress contour of the worm tooth (position C)

6.7 Evaluation of the Maximum Shearing Stress of Tooth Root

At the last stage of this research, the latest private circulation version of British Standard (ISO/CD 14521) for rating the loading capacity of worm gear drives is available for evaluation. The draft standard has provided a method to calculate the actual tooth root stress. The calculation is based on a nominal shear stress assumption. The shear stress at the tooth root is represented as:

$$\tau_F = \frac{F_{tm2}}{b_{2H} \cdot m_{x1}} \cdot Y_{eps} \cdot Y_F \cdot Y_\gamma \cdot Y_K$$

Where, F_{tm2} is the tangential force to the worm wheel, b_{2H} is the effective wheel facewidth and m_{x1} is the axial module. According to this equation the load is considered as an even distribution along the wheel tooth surface.

The contact factor Y_{eps} takes into account the load distribution to all simultaneously meshed teeth.

The lead factor Y_γ takes into account the influence of the lead angle:

$$Y_\gamma = 1/\cos\gamma_{m1}$$

The rim thickness factor Y_K takes into account the influence of the rim thickness S_k.

$$Y_K = 1.0 \quad \text{when } S_K \geq 1.5 \cdot m_{x1}$$

The tooth form factor Y_F takes into account the bending stress component and is calculated by the equation below.

$$Y_F = 2.9 \cdot m_{x1} / S_{fn2}$$

$$S_{fn2} = 1.06 \cdot S_{f2}$$

with: $S_{f2} = S_{m2} - \Delta S + (d_{m2} - d_{f2}) \cdot \tan\alpha_0 / \cos\gamma_{m1}$

with: $S_{m2} \approx p_{x1} \cdot (1 - S^*_{mx1})$

p_{x1}: axial pitch, S^*_{mx1}: Tooth thickness coefficient, d_{m2}: worm wheel reference diameter, d_{f2}: worm wheel root diameter, γ_{m1}: reference lead angle of worm, α_0: pressure angle.

ΔS is the tooth thickness loss through wear during the required life expectancy.

The proposed calculation equation was applied to the sample worm gear drive to evaluate its feasibility. For the sample worm wheel tooth model, $p_{x1} = 26.7mm$, $S^*_{mx1} = 0.5$, $b_{2H} = 74mm$, $d_{m2} = 476.0mm$, $d_{f2} = 455.0mm$, $\gamma_{m1} = 15.8°$, $\alpha_0 = 22.5°$. Assuming that the tangential force F_{tm2} equals 1000N and ΔS is 1mm, the following factors can be calculated:

$$S_{m2} \approx p_{x1} \cdot (1 - S^*_{mx1}) = 26.7 \cdot (1 - 0.5) = 13.35$$

$$S_{f2} = S_{m2} - \Delta S + (d_{m2} - d_{f2}) \cdot \tan\alpha_0 / \cos\gamma_{m1} = 13.35 + 21 \cdot \tan 22.5° / \cos 15.8° = 21.4mm$$

$$Y_F = 2.9 \cdot m_{x1} / S_{fn2} = 2.9 \times 8.5 / 21.4 = 1.152$$

$$Y_\gamma = 1 / \cos\gamma_{m1} = 1.039$$

$$Y_{eps} = 1.0$$

Finally, the nominal shear stress at the tooth root is obtained as below,

$$\therefore \tau_F = \frac{F_{tm2}}{b_{2H} \cdot m_{x1}} \cdot Y_{eps} \cdot Y_F \cdot Y_\gamma \cdot Y_K = 1.9035 \times 10^6 (Pa)$$

The calculation of the tooth root stress is also performed using the finite element model. The same tangential force is evenly distributed along the tooth face width and the result is shown as Figure 6.29. and Table 6.3.

According to the theory of complex stress calculation, shear stress can be solved using Mohr's method (Hearn, E. J, 1997). The maximum shear stress is represented as:

$$\tau_{\max} = \frac{1}{2}(\sigma_1 - \sigma_3)$$

Introducing the results of FEA in Table 6.3 into the formula above, the shear stress at the tooth root is $\tau_{\max} = 1.889 \times 10^6 (Pa)$. The result of finite element analysis shows a good agreement with the equation of draft standard (ISO/CD 14521).

It is clear that the finite element model can provide a reasonable accuracy for tooth stress analysis. For the localised tooth contact (point contact), the load is not evenly distributed along the tooth face width, so the calculation equation available in draft standard is not applicable. Under such circumstances, the finite element method has to be used to calculate the tooth stress.

From the results of both stress and deflection analysis, it is obvious that the finite element models have a good accuracy for mechanical calculation and analysis of worm gears.

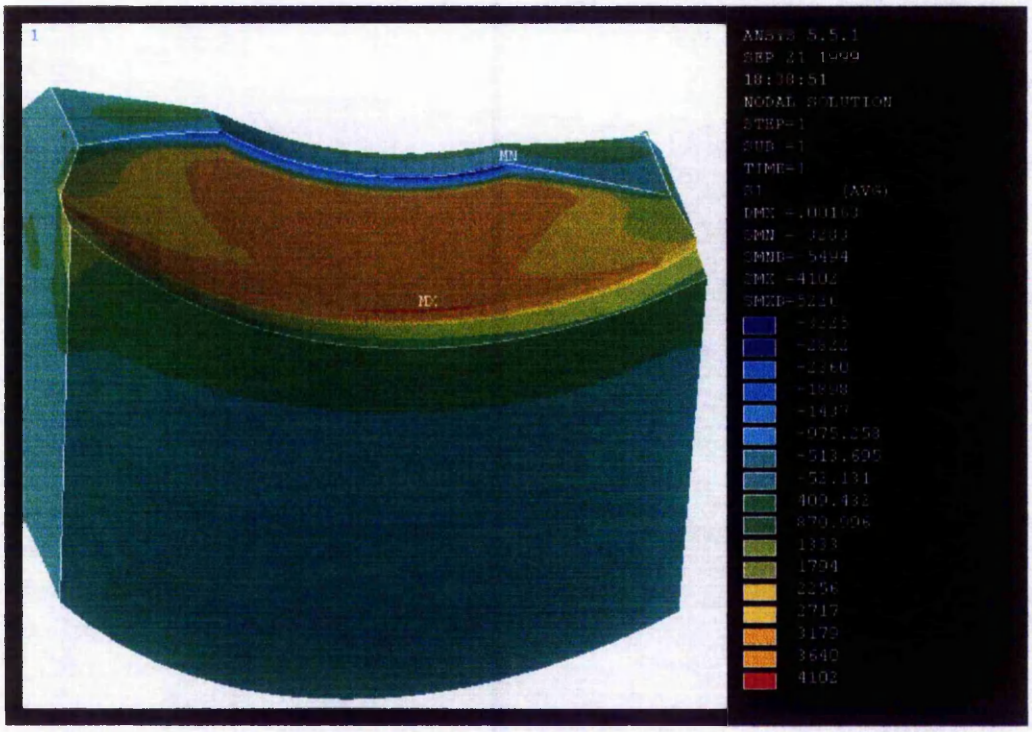

Figure 6.29 Tooth root stress under the evenly distributed tangential force

Table 6.3 Maximum Nodal Stress of the FEA Results

Node number	1st Principal stress (σ_1)	2nd Principal stress (σ_2)	3rd Principal stress (σ_3)
2475	4.102e6 (Pa)	0.991e6 (Pa)	0.324e6 (Pa)

Chapter 7 A General Approach to Calculate Load Share of Worm Gear Drives

The conventional design method for gear drives usually leads to the over estimation of the required tooth strength. Moreover, the different design standards produce distinctly different results with up to 30 percent difference in the stress estimation (Von Eiff et. al. 1990). On the other hand, for worm gear drives working under heavy load, such as those used for opening the cover of a high pressure vessel or used in machine tools, the tooth failure is often caused by the accelerated wear and there has not been a proper rating method for it.

It is desired to increase the loading capacity of a worm gear without increasing its size. A worm gear drive with high contact ratio is a feasible way to achieve the above purpose. With two or more tooth pairs in simultaneous contact, the load share carried by each tooth pair can be significantly reduced. However, the design for such a high contact ratio worm gear drive requires an accurate evaluation of the load share among the meshing teeth. So, a more accurate method for rating the loading capacity of worm gear drives is required.

A general approach has been developed and is reported in this chapter for evaluation of the load share between contacting tooth pairs of a worm and its mating gear. There are many factors that influence the load distribution. Generally speaking, the tooth elastic deformation, the meshing transmission error, and the manufacturing and assembly error will substantially affect the load share values.

7.1 General Assumptions

In order to simplify the analysis and calculation, the following assumptions are adopted.

- The contact path of the worm gear is determined using the TCA method. Under the load, the tooth contact path of the worm gearing keeps the same route as the theoretical path calculated from the TCA programme.

- Friction force is not considered in the tooth contact zone, and the distribution of contact pressure is not affected by the presence of lubricant.
- The tooth surface normal at the contact point stays the same as the theoretical one before the tooth deflection, and shearing or contact deformation is sufficiently small and their effects can be neglected.
- The gear box does not deform, and the shaft and bearing of the worm gear drive do not displace under load.

7.2 The Condition of Deformation Compatibility for Worm Gear Drives

The determination of load share between the simultaneous contact tooth pairs depends on the deformation compatibility condition of the worm gear drives. In order to investigate the compatibility condition, it is necessary to recall the condition of continuous transmission of worm gears.

7.2.1 The condition of continuous transmission of worm gears

In conventional design methods the teeth of both the worm and the wheel are considered as rigid bodies. Since the tooth is a rigid body, no elastic deformation exists in the meshing process. To ensure smooth continuous transmission, the tooth pitch of the worm and wheel are required to be equal at any meshing instant (Figure 7.1).

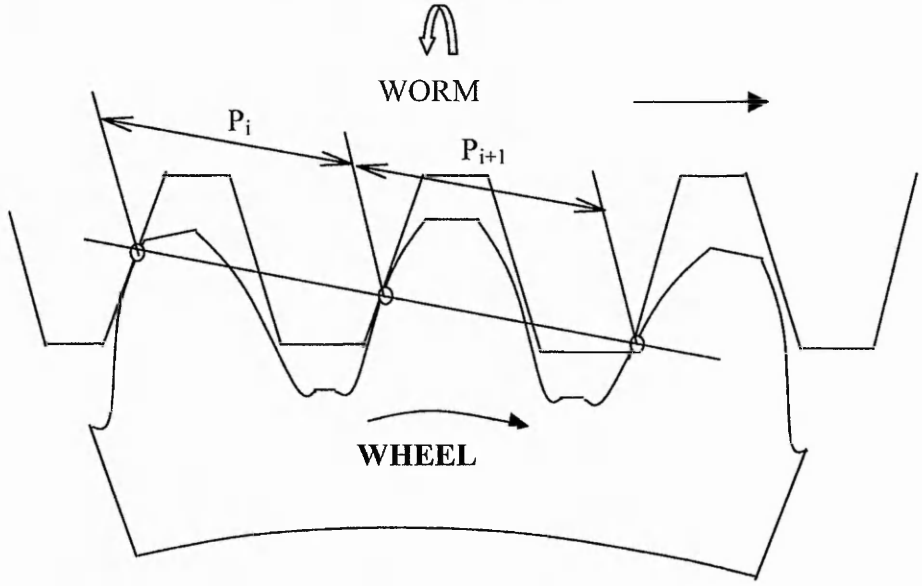

Figure 7.1 The continuous transmission condition for rigid worm gears

If there are no manufacturing and assembly errors, the condition of equal pitch can assure ideal continuous transmission for worm gear drives. However in reality, ideal continuous transmission cannot occur due to the errors.

7.2.2 The condition of deformation compatibility

In reality, two factors may significantly affect the continuous transmission. One is the tooth profile error caused by manufacturing and assembly errors. The other is the tooth elastic deformation for both the worm and the wheel, which is determined by the load acting on the contacting teeth. If the total displacement of the *i*th tooth pair in contact is represented as Δ_i (Figure 7.2), the corresponding rotation increment is written as Δ_i/R_i, i.e. the extra rotation caused by the total displacement. Therefore, to assure the continuous transmission, it is necessary that every tooth pair in contact has the same rotation increment under the load. It can be written as:

$$\Delta_{i-1}/R_{i-1} = \Delta_i/R_i = \Delta_{i+1}/R_{i+1} \qquad (7.1)$$

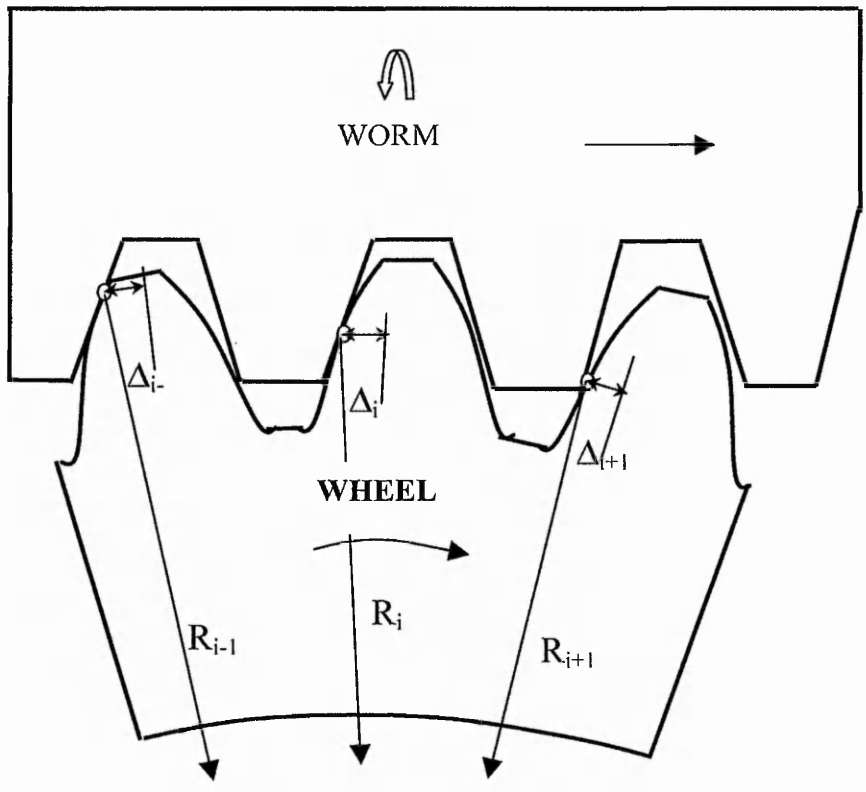

Figurte7.2 Condition of deformation compatibility

The total displacement comprises the elastic deformation and the geometric mismatch of the tooth surfaces caused by manufacturing and assembly errors. Equation 7.1 is widely recognised as the compatible condition for tooth deformation. (Gosselin,1995, Litvin,1996)

7.3 Determining the Contact Area using Hertzian Formula

Theoretically, tooth pairs of conventional worm gear drives are in line contact. However, for worm gear drives with localised tooth contact, the worm and gear teeth contact each other at a point according to the result of the tooth contact analysis in chapter 4. Due to the tooth elastic deformation, under load, the contact zone is spread over an elliptical area whose centre is the theoretical contact point. In this research, the Hertzian assumption is applied to determine the contact zone.

7.3.1 Hertzian assumption

For elastic and isotropic material, Hertz proposed an assumption for a general contact loading case. He showed that the intensity of pressure between the contacting surfaces could be represented by the semi-ellipsoid construction shown in Figure. 7.3

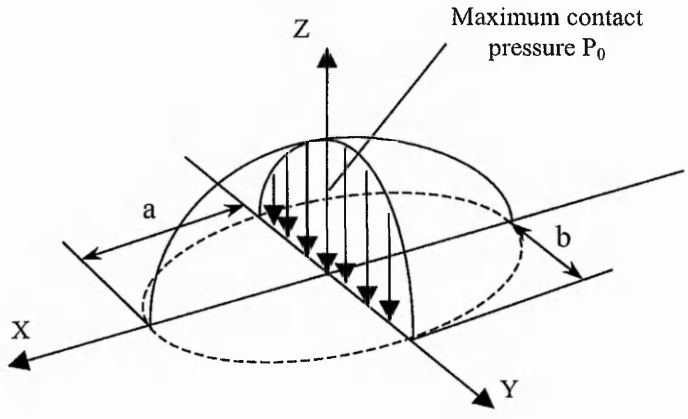

Figure 7.3 Hertzian representation of pressure distribution between contact surfaces

The contact pressure at any point within the contact area was represented by the equation

$$p_{x,y} = p_0\sqrt{1-\frac{x^2}{a^2}-\frac{y^2}{b^2}} \qquad (7.3.1)$$

Where p_0 is the maximum pressure at the centre of the contact area, a and b are the major and minor semi-axes, respectively.

The total load is then given by the volume of the semi-ellipsoid, i.e.

$$P = \frac{2}{3}\pi \cdot a \cdot b \cdot p_0 \qquad (7.3.2)$$

Therefore, the maximum pressure p_0 is given in terms of the applied load as

$$p_0 = \frac{3P}{2\pi ab} \qquad (7.3.3)$$

7.3.2 Determination of the contact ellipse

For any given contact load P it is necessary to determine the value of major and minor axes before the maximum contact stress can be evaluated. The following procedure can be applied to determine the axes of the contact ellipse.

7.3.2.1 Calculation of the deflection of the contact bodies

The method of deflection evaluation is proposed below, and consists of three steps: the computation of the auxiliary parameters, the selection of the deflection coefficients and the determination of the elastic deflection.

- The equations of elastic deflection and contact ellipse

From the theory of contact mechanics (Boresi P., 1984), the expression of the elastic deflection δ is given as:

$$\delta = c_\delta \frac{P}{\pi}\left(\frac{A+B}{b/\Delta}\right) \tag{7.3.4}$$

$$b = c_b \sqrt[3]{P\Delta} \tag{7.3.5}$$

$$a = \sqrt{\left|\frac{\delta}{A}\right|} \tag{7.3.6}$$

Actually, the deflection δ expresses the sum of the "deflections" of the two contact bodies as they approach each other. In the equation (7.3.4), A, B, Δ are auxiliary parameters that are used for calculating the deflection of bodies in point contact. The c_δ and c_b are the coefficients, a and b are the semi-axes of the contact ellipse.

- Computation of auxiliary parameters

Δ is a function of the elastic constants E (Young's modulus) and ν (Poisson's ratio) of the contact bodies, it is given as:

$$\Delta = \frac{1}{A+B}\left(\frac{\left[1-\nu_1^2\right]}{E_1} + \frac{\left[1-\nu_2^2\right]}{E_2}\right) \tag{7.3.7}$$

A and B are related to the surface curvature of the contact bodies, they can be expressed as (Boresi, 1984):

$$\begin{aligned} A = {} & \frac{1}{4}(k_I^{(1)} + k_{II}^{(1)} + k_I^{(2)} + k_{II}^{(2)}) \\ & -\frac{1}{4}\sqrt{[(k_I^{(1)} - k_{II}^{(1)}) + (k_I^{(2)} - k_{II}^{(2)})]^2 - 4(k_I^{(1)} - k_{II}^{(1)})(k_I^{(2)} - k_{II}^{(2)})\sin^2\sigma^{(12)}} \end{aligned} \tag{7.3.8}$$

$$B=\frac{1}{4}(k_I^{(1)}+k_{II}^{(1)}+k_I^{(2)}+k_{II}^{(2)})$$
$$+\frac{1}{4}\sqrt{[(k_I^{(1)}-k_{II}^{(1)})+(k_I^{(2)}-k_{II}^{(2)})]^2-4(k_I^{(1)}-k_{II}^{(1)})(k_I^{(2)}-k_{II}^{(2)})\sin^2\sigma^{(12)}} \quad (7.3.9)$$

Where, $k_I^{(i)}, k_{II}^{(i)}$ $(i=1,2)$ are the principal curvatures of the contact surfaces. $\sigma^{(12)}$ is the angle formed by the unit vectors of principal directions. Since the equations of the worm gear drive are known, the principal curvatures of the tooth surfaces can be obtained. The calculation procedure of surface curvature refers to the approach developed by Wang (1982) that is presented in Appendix C. The approach can determine the principal curvatures and the directions of the tooth surface.

The selection of the deflection coefficients c_δ and c_b can be determined using Figures 7.4 and 7.5, which are provided by Boresi (1984).

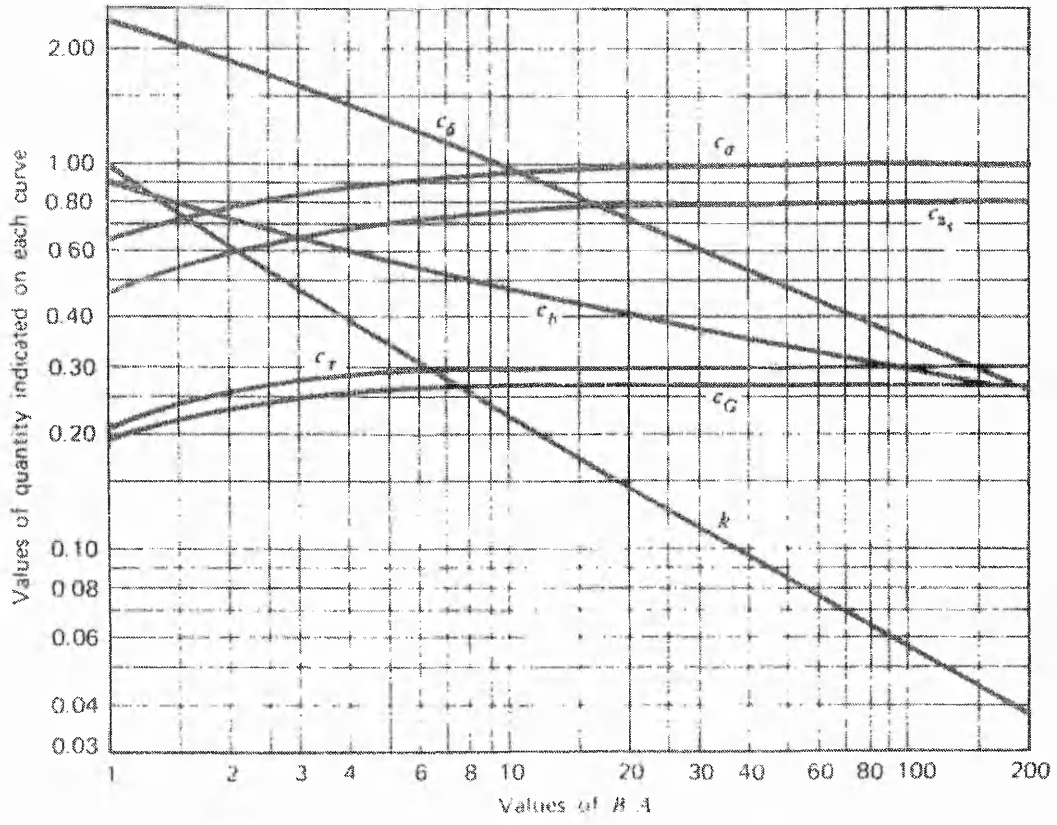

Figure 7.4 Stress and deflection coefficients for two bodies in contact at a point

620 / CONTACT STRESSES

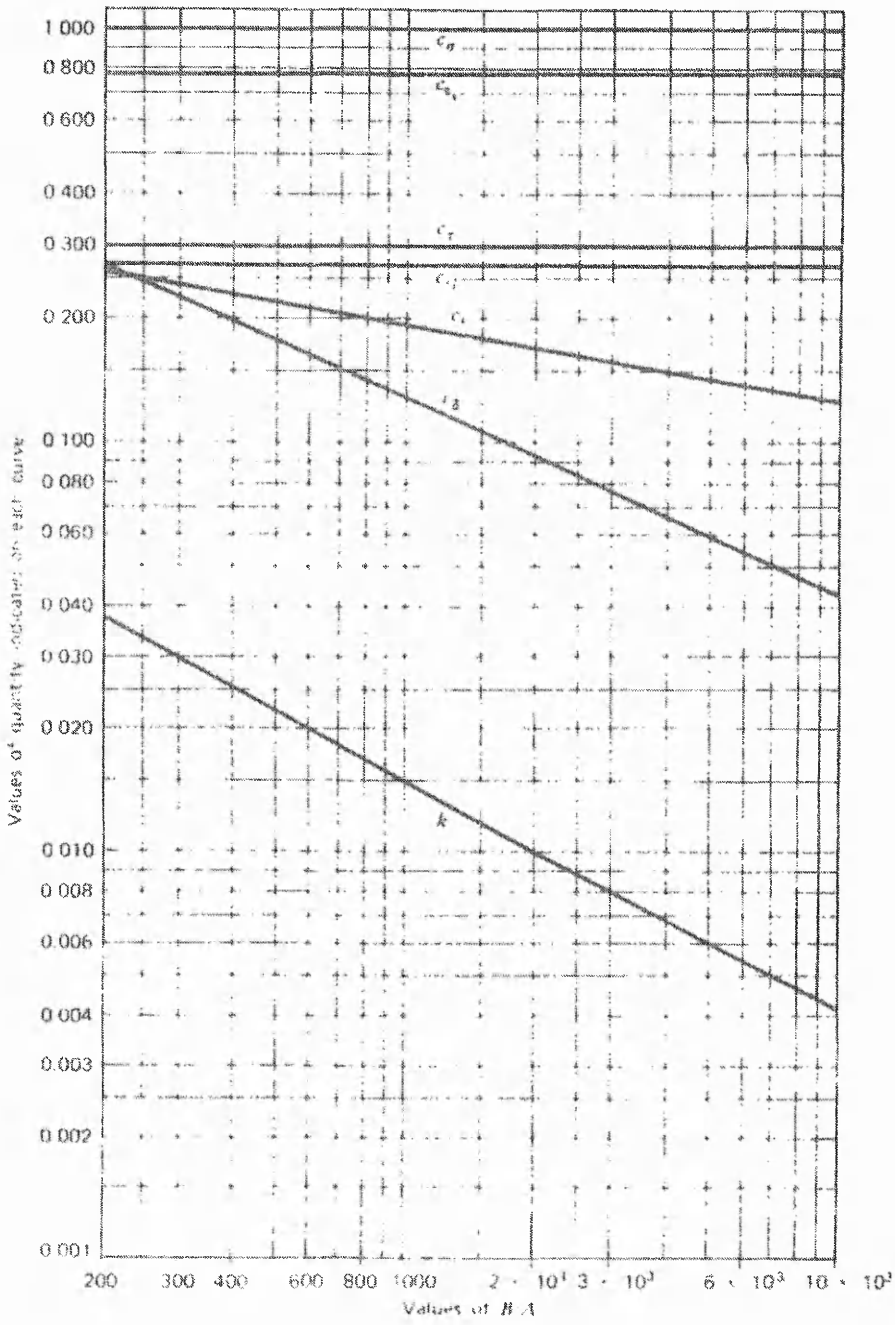

Figure 7.5 Stress and deflection coefficients for two bodies in contact at a point

The parameters of an example of multi-start involute worm gear drive have been listed in the Table 7.1.

Table 7.1 Parameters of an example of Involute worm gear drive

Worm thread number	3	Pressure angle	22.5^0
Diameter quotient	10.590	Centre distance	283.00
Tooth module	8.5	Worm base diameter	49.477
Wheel tooth number	56	Worm root diameter	71.029
Wheel outside diameter	499.999	Worm pitch diameter	90.018
Wheel throat radius	37.16	Worm outside diameter	106.995
Wheel tooth face width	78.003	Worm lead	80.112

The calculation results of the contact ellipse for the above worm gear drive are listed in Table 7.2.

Table 7.2 Calculation results of the contact ellipse (Load =1000 N)

ϕ_u (degree)	18.0	61.14	104.1	146.7	189.0	231.1	272.9
u (mm)	32.31	36.32	40.49	44.76	49.08	53.42	57.77
ϕ_1 (degree)	148.1	188.1	228.2	268.2	308.2	348.2	388.2
semi-axis b (mm)	1.062	1.031	1.045	1.125	1.27	1.32	1.351
semi-axis a (mm)	4.797	5.014	4.82	4.272	3.77	3.578	3.605

7.3.3 Determination of the distribution of contact pressure

With equation (7.3.3), the pressure at the centre of the contact ellipse is determined when the semi-axes are known. Then, the pressure at any position of the contact ellipse is represented as equation (7.3.1). To simplify the finite element calculation process, the contact ellipse is divided into a number of elements, the pressure on each element of the contact ellipse is assumed as an average pressure, shown as Figure 7.6.

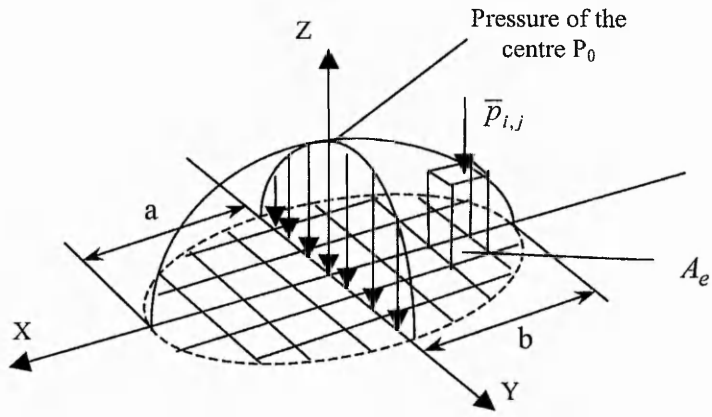

Figure 7.6 Finite element representation of Hertizan contact pressure

The average pressure can be calculated as

$$\overline{p}_{i,j} = \frac{1}{A_e} \int_{y_{j-1}}^{y_j} \int_{x_{i-1}}^{x_i} p_0 \sqrt{1 - \frac{x^2}{a^2} - \frac{y^2}{b^2}} dxdy \qquad (7.3.11)$$

Where, the subscripts i and j represent the position of any element of the contact ellipse, A_e is the area of the element. There is no doubt that the more the elements of the contact ellipse are divided, the more accurate the calculation result will be.

7.4 Mesh Stiffness

Mesh stiffness is defined as the combined stiffness at the contact position of the engaging tooth pairs. It is a key factor in determination of the load share among the simultaneously engaging tooth pairs.

During the engaging process, the force is transmitted at the contact point determined by the theoretical contact position of the worm and the wheel. The mesh is shown in Figure 7.7. Both worm tooth and wheel tooth have a deformation under the load. The sum of

elastic deformation comprises the deformations of worm tooth U_1 and wheel tooth U_2, i.e. $U=U_1+U_2$.

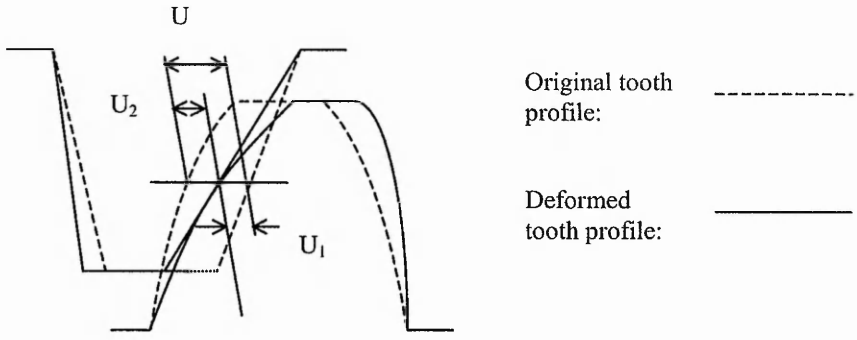

Figure 7.7 Tooth deformation under the load

With respect to an individual tooth, its elastic deformation is composed of two components: bending deformation and contact deformation. The tooth bending compliance is defined as the displacement along the normal to the tooth profile where a unit load is applied, while the tooth contact compliance is defined based on Hertzian assumptions (Zhang J., et. al., 1998). Because the contact position always shifts during the engagement, the bending and contact compliance, and hence the meshing stiffness, vary over the engaging process.

When one pair of teeth is in the mesh position δ, the following assumptions are considered: (1) tooth deformation is elastic; (2) the centre of contact ellipses will not shift after the elastic deformation. Therefore, the magnitude of the deformation $U_i(\delta)$ at the centre of the contact ellipses for the worm U_1 or the gear wheel U_2 is recognised as the instantaneous nominal deformation for the meshing position.

Using the finite element model developed in Chapter 6, the solution for meshing stiffness can be obtained from the FEA calculation. Based on the results from section (7.3), the total load distributed on the contact ellipse is: $F_\delta = \iint p(x,y)dxdy$. Applying the load on the FE models of the worm and wheel, the deformation magnitude $U_i(\delta)$ at the centre of the

contact ellipse, which includes both bending and contact deformation, can be calculated. So the instantaneous stiffness for an individual tooth is defined as:

$$K_i(\delta) = \frac{F_\delta}{U_i(\delta)} \qquad (7.4.1)$$

So, the instantaneous meshing stiffness at the contact point of the engaging tooth pairs is:

$$K_\delta = \frac{K_1(\delta) \cdot K_2(\delta)}{K_1(\delta) + K_2(\delta)} \qquad (7.4.2)$$

During the engaging process, the contact point moves on the tooth surface forming a contact path, which can be determined using the TCA calculation in chapter 4. Therefore, the instantaneous meshing stiffness depends on the contact path of the worm gear drive. With a different manufacturing error, the contact path of the worm gear drive changes accordingly. The change affects the meshing stiffness significantly. The meshing stiffness for a worm gear drive is actually a function of contact position which is defined as a meshing stiffness function along contact path (MSFACP) in this research.

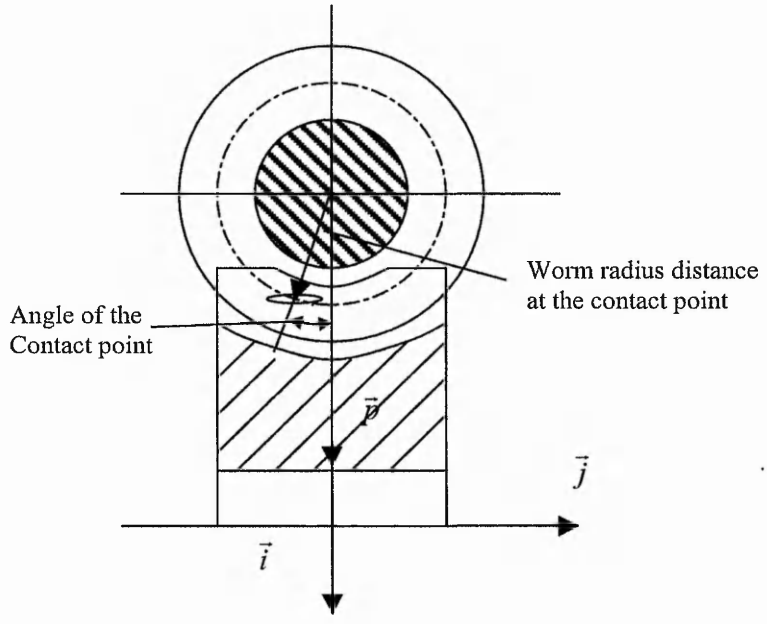

Figure 7.8 The description of the contact point

To calculate the MSFACP, a polar coordinate system has been set to locate the contact position. The position of the contact point is defined using the radius and the angle, as shown in Figure 7.8. Since the contact path has been obtained using the TCA calculation, while the contact positions can also be represented by the intersection points between the contact path and the coaxial circles surrounding the worm axis. Thus the MSFACP is a function of the radius of contact point.

The computation of MSFACP is based on the finite element models. The load has been assigned to the worm model and the wheel model at respective contact points with Hertzian distribution. The deformation of the contact point is calculated and the stiffness of both worm and worm wheel are obtained.

- Computation of the worm tooth stiffness

The worm tooth has an identical geometry at any of its axial sections. With respect to the radius of the contact point, its stiffness can be represented by an identical function of the radius. So, this stiffness function can be applied to the tooth contact path under any circumstances.

The meshing stiffness of the sample worm gear drive shown in Table 7.1 has been evaluated by the author. Based on the finite element model of the sample worm gears, the stiffness function of the worm has been calculated and the results are shown in Table 7.3, where, R_c is the radius of the contact position, Δ is the deformation of the contact point and K_w is the stiffness of the contact position of the worm tooth. In the calculation, a load of 1000 N is applied to the worm model.

Analysing the stiffness data with a regression method, the MSFACP is obtained. The curve of worm instantaneous stiffness along the contact path is shown in Figure 7.9, where the curve describes the stiffness of the contact path from the tooth root to the tip, with reference to the radius distance of the contact point.

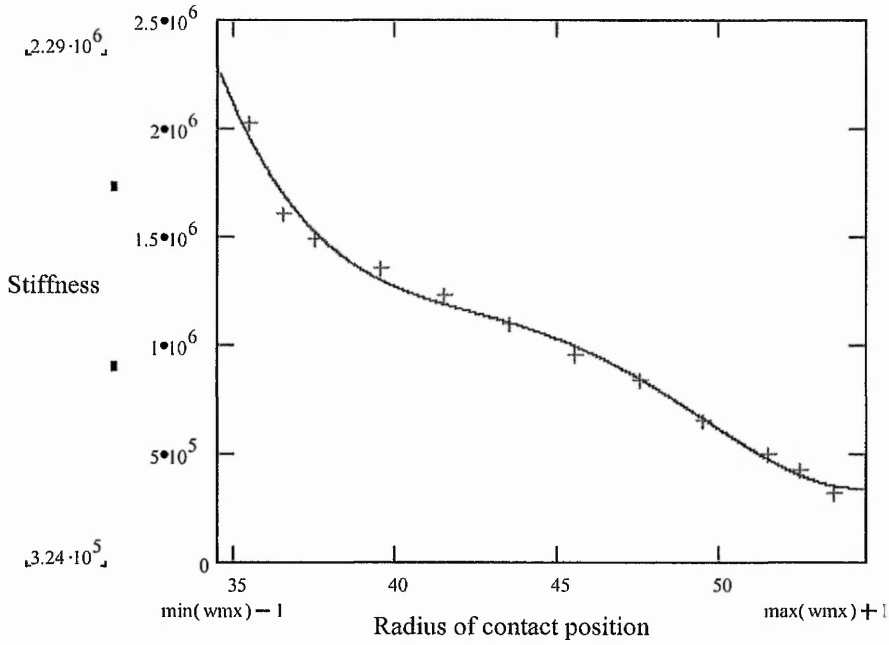

Figure 7.9 The contact path stiffness of worm tooth

Table 7.3 Stiffness Data of the worm tooth based on FEA results

R_c (mm)	Δ (mm)	K_w (N/mm)
53.5	0.003084	3.24e5
52.5	0.002334	4.28e5
51.5	0.001984	5.04e5
50.05	0.001789	5.59e5
49.5	0.001528	6.545e5
48.5	0.001369	7.30e5
47.5	0.00119	8.40e5
46.5	0.001133	8.83e5
45.5	0.001046	9.56e3
44.5	0.000973	1.028e6
43.5	0.000911	1.098e6
42.5	0.000859	1.164e6

41.5	0.000814	1.229e6
40.5	0.000774	1.292e6
39.5	0.000739	1.353e6
38.5	0.000705	1.418e6
37.5	0.000670	1.493e6
36.5	0.000622	1.608e6
35.5	0.000494	2.024e6

- Computation of stiffness of the wheel tooth

For the worm wheel tooth, the representation of its stiffness is more complex than for the worm tooth due to the facts that the contact path on the worm wheel tooth varies regarding the different manufacturing and assembly errors and the geometry of the worm wheel tooth is a non-uniform shape. There is no doubt that the stiffness is different when the contact occurs along the different contact path on the wheel tooth. Therefore the stiffness of the wheel tooth must be evaluated individually with respect to each contact path.

Using the finite element model on the wheel, tooth stiffness has been calculated for the different contact paths. The stiffness is represented as a function of radius of the contact point. With different assembly errors, the worm wheel has different stiffness functions. Several calculation examples are given below.

(1) worm gear set with worm mounting angle misalignment 0^0

According to the TCA calculation in chapter 4, the contact path for the specific assembly can be determined. The tooth contact point moves from the top of the wheel tooth towards the root in the process of engagement. With the finite element model, the wheel tooth stiffness regarding the contact path is calculated, and shown in Table7.4 and Figure 7.10. The curve shown in Figure 7.10 describes the stiffness of the wheel tooth along the contact path from the tooth top to the root, with reference to the radius distance of the contact point. As can be seen, the stiffness increases from tooth top to tooth root.

Table 7.4 Wheel Tooth Stiffness Data from FEA results

R_c (mm)	Δ (mm)	K_w (N/m)
53.37	0.00137	7.30e5
51.57	0.001736	5.76e5
48.46	0.002173	4.60e5
45.42	0.002491	4.014e5
43.93	0.002655	3.77e5
41.02	0.003441	2.91e5
38.24	0.004682	2.14e5
35.59	0.007559	1.32e5

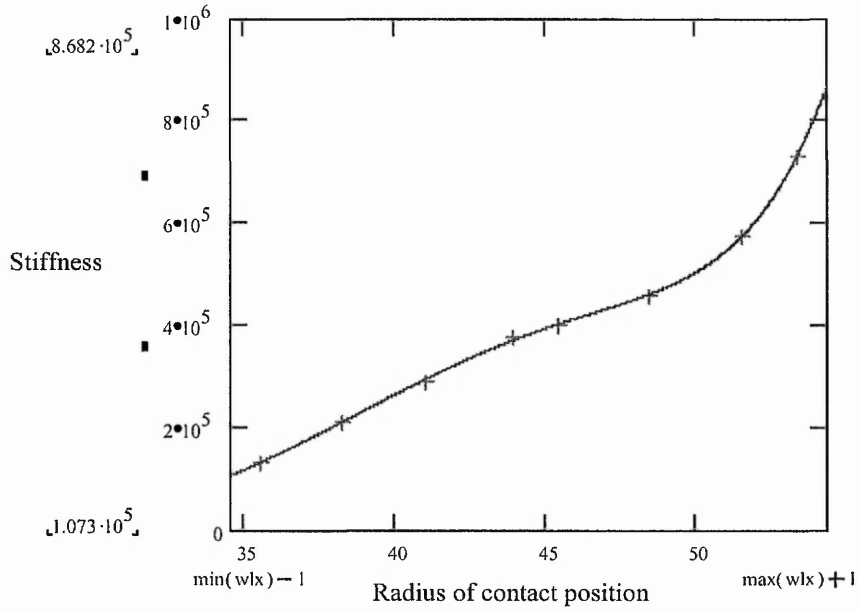

Figure 7.10 The Stiffness Curve of the wheel tooth

(2) worm gear set with worm mounting angle misalignment 0.05^0

Similarly, the contact path of the above worm gear set assembly can be determined according to the TCA calculation. Because of the difference in the assembly error, the contact path of the worm gear is changed. Applying the contact path obtained with the

finite element model, the stiffness data of the contact path is obtained and shown in Table7.5 and Figure 7.11. The stiffness curve describes the stiffness of the contact path from the wheel tooth top to the root, with reference to the radius distance of the contact point.

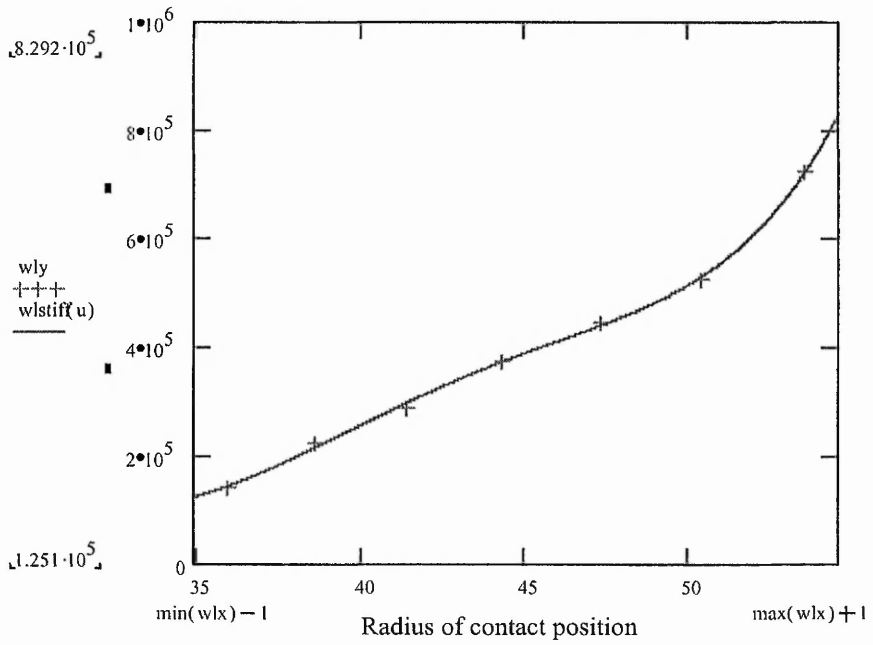

Figure 7.11 The Stiffness Curve of the wheel tooth

Table 7.5 Worm Wheel Tooth Stiffness Data from FEA results

R_c (mm)	Δ (mm)	K_w (N/m)
53.55	0.001378	7.252e5
50.4	0.001904	5.252e5
47.31	0.002237	4.47e5
44.3	0.002665	3.752e5
41.38	0.00347	2.88e5
38.58	0.004471	2.24e5
35.92	0.007046	1.42e5

(3) worm gear set with worm mounting angle misalignment:0.15^0

Based on the results of TCA calculation and finite element analysis, the stiffness data of the contact path on the wheel tooth are shown in Table7.6. Figure 7.12 shows the curve of the worm wheel tooth stiffness with the misalignment worm mounting angle 0.15 degree. The stiffness curve describes the stiffness of the contact path from the tooth top to the root, with reference to the radius distance of the contact point. Comparing Figure 7.10, 7.11 and 7.12, it can be seen that the stiffness of the wheel tooth, regarding the different misalignment of 0^0, 0.05^0 and 0.15^0, has the same increasing trend from tooth top to tooth root. However, the actual stiffness value is determined by the tooth geometry at the contact position.

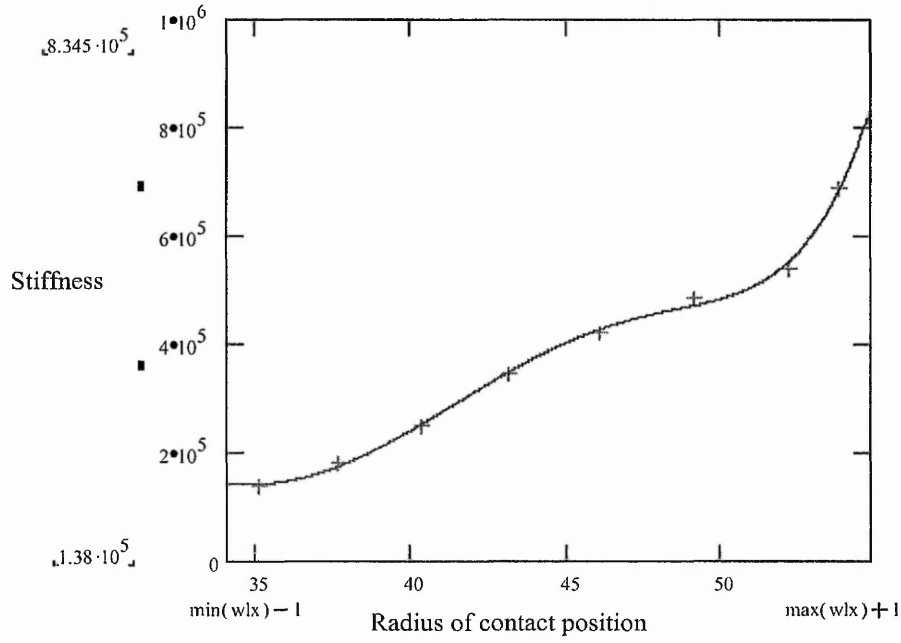

Figure 7.12 The Stiffness Curve of the wheel tooth

Table 7.6 Worm Wheel Tooth Stiffness Data based on FEA results

R_c (mm)	Δ (mm)	K_w (N/m)
53.77	0.001448	6.91e5
52.19	0.001852	5.40e5
49.1	0.002057	4.861e5
46.09	0.00237	4.22e5
43.16	0.002902	3.45e5
40.34	0.003983	2.51e5
37.65	0.005455	1.833e5
35.11	0.007262	1.38e5

- Computation of the instantaneous meshing stiffness

After the calculation of the tooth stiffness of worm and wheel, the instantaneous meshing stiffness of the worm gear drive can be obtained using equation (7.4.2).

The meshing stiffness can be represented as a function, of which the variable is still the position of the contact point, related to the radius of the contact point. With the instantaneous meshing stiffness, the elastic deformation of the contact position under different loads can be estimated. The meshing stiffness is an important parameter to describe the mechanical characteristics of worm gear meshing process, and its value varies along the contact path. From Figure 7.13 to Figure 7.15, the curves show the meshing stiffness of the worm gear drives with different errors in the worm mounting angle.

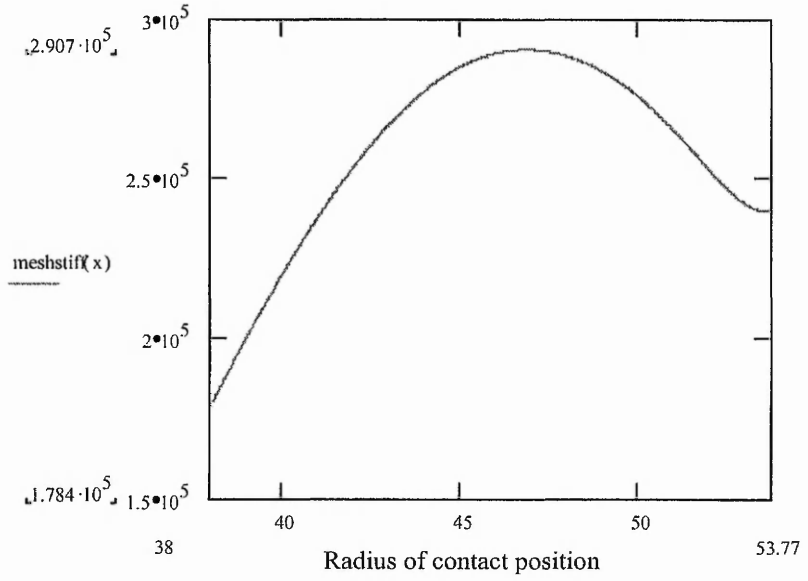

Figure 7.13 Meshing stiffness without worm mounting angle misalignment

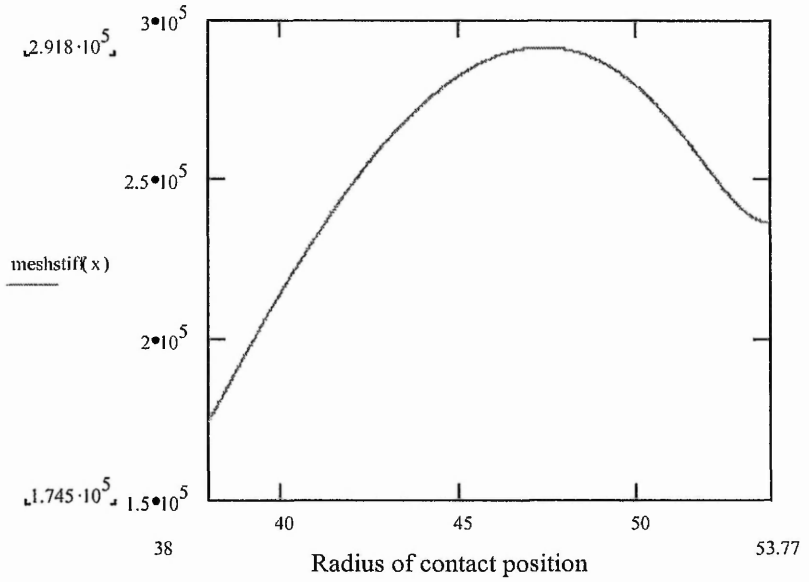

Figure 7.14 Meshing stiffness with worm mounting angle misalignment of 0.05 degree

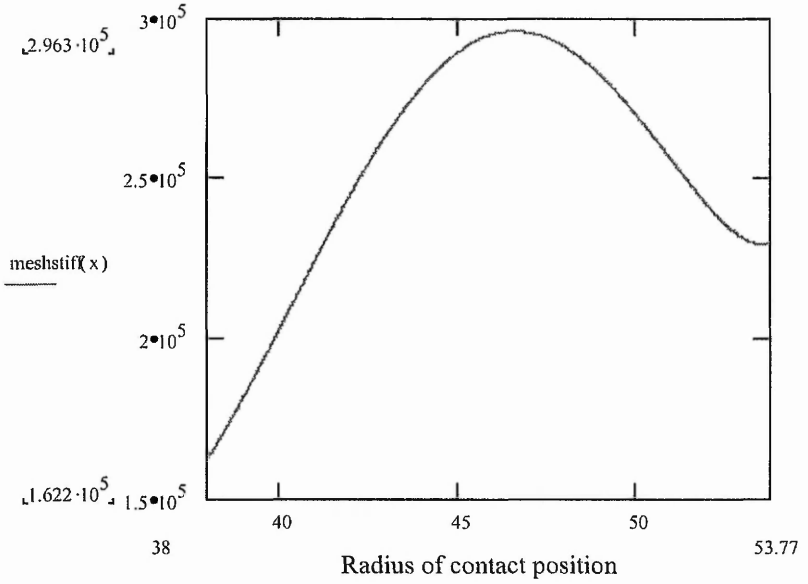

Figure 7.15 Meshing stiffness with worm mounting angle misalignment of 0.15 degree

Although the calculation results show that meshing stiffness varies with the different contact paths, the general tendency of the meshing stiffness of worm gear drives is similar regardless of the difference in contact path. In the process of tooth engagement, the meshing stiffness starts from the minimum value, when the wheel tooth tip and worm tooth root are in contact. Then the meshing stiffness increases gradually to reach the maximum value, when the worm and wheel teeth are in contact in the middle part of the tooth. After that, the meshing stiffness decreases slowly until the worm and wheel teeth exit the engagement. However, at the last moment of the tooth contact, the meshing stiffness value is still at a high value that is approximately the mean of the maximum and minimum values. So the meshing stiffness in the exit-engaging position is much bigger than in the enter-engaging position. This conclusion is quite different from the existing results for spur gears, which show the meshing stiffness is similar at entry and exit positions of the engagement. This is because the stiffness at the wheel tooth tip is much lower than the stiffness at the worm tooth tip, while the stiffness difference between the tooth tip and tooth root for the worm is bigger than that for the wheel.

7.5 Determine the Theoretical Transmission Error from TCA

The theoretical transmission error is caused by the misalignment of the worm gear drives. The transmission function for an ideal worm gear drive is a linear one, and is represented as

$$\phi_2(\phi_1) = \frac{Z_1}{Z_2} \cdot \phi_1$$

where Z_1 and Z_2 are the gear tooth numbers.

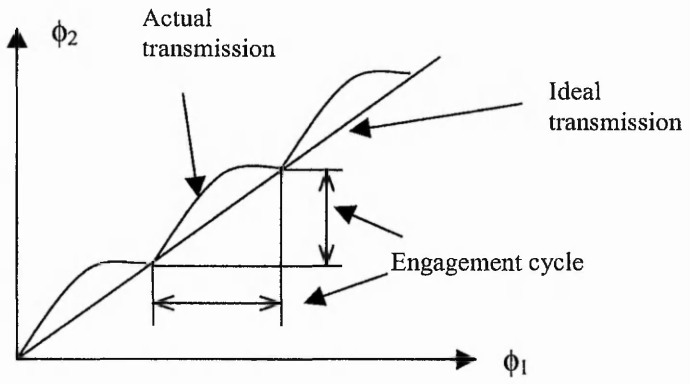

Figure 7.16 transmission error function

However, ideal gear drives do not exist in reality, the errors of alignment will induce the ϕ_2 diverging from the original position, so that there is error in the transmission process. Figure 7.16 shows the transmission function $\phi_2'(\phi_1)$ for a misaligned gear drive. For worm gear drives, the cycle of engagement is determined with the rotation angles of worm and gear wheel obtained as $\phi_1 = 2\pi / Z_1$ and $\phi_2 = 2\pi / Z_2$. In each cycle of the engagement, the transmission error is represented as

$$\Delta\phi_2(\varphi_1) = \phi_2'(\phi_1) - \phi_2(\phi_1) = \phi_2'(\phi_1) - \frac{Z_1}{Z_2} \cdot \phi_1,$$

where $\phi_2'(\phi_1)$ can be found using the TCA method described in Chapter 4. However, the transmission error obtained above does not take account of the tooth elastic deformation. More discussion about the transmission error under load can be found in section 7.9.

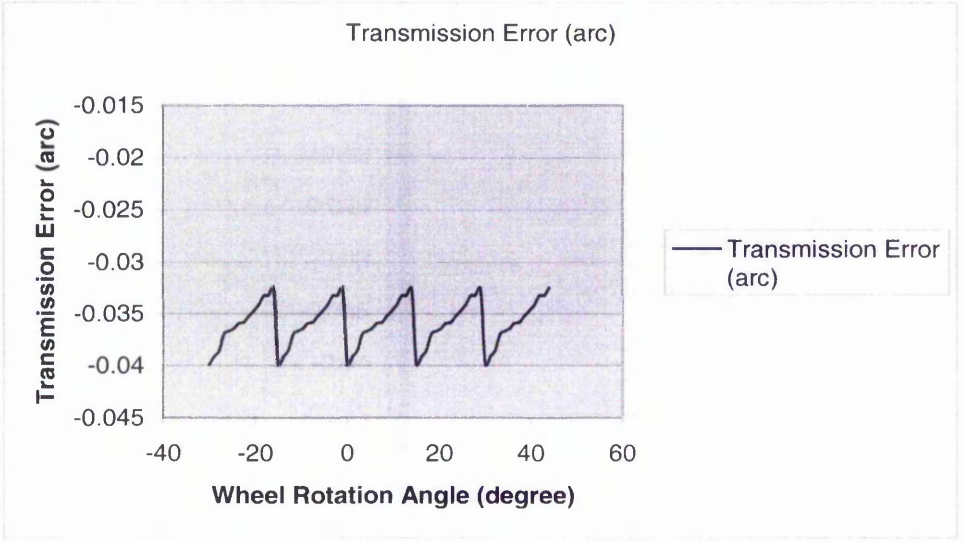

Figure 7.17 Transmission error for the worm gear drive

A typical example of transmission error is shown in Figure 7.17, which is obtained from the TCA results completed by the author. The transmission errors obtained from TCA are based on the assumption that the gear teeth are rigid bodies, i.e., no elastic deformation is considered.

7.6 Mathematical Model of Load Share of Worm Gear Drives

Usually, a worm gear has more than one pair of teeth engaged during the meshing process, and the number of simultaneous contact teeth and the load sharing percentage among the teeth always vary in the process. The contacting tooth pairs have different displacement under the load. According to the compatibility condition for smooth tooth rotation, the following conditions must be met in order to maintain the smooth motion transmission.

(i) The extra tooth rotation angle caused by the displacement under the load must be the same for all the simultaneously engaged teeth pairs. Otherwise, the continuous smooth transmission is not possible.

(ii) The sum of the torque contributions of each engaging tooth pair must be equal to the total applied torque.

If there are n tooth pairs in contact simultaneously (Figure 7.2), the vectors to describe the total displacement and the rotation increment at each contact point can be expressed as $\vec{\Delta}$ and $\Delta\vec{\theta}$, respectively.

$$\vec{\Delta} = \begin{bmatrix} \Delta_1 \\ \Delta_2 \\ : \\ \Delta_n \end{bmatrix} \tag{7.6.1}$$

$$\Delta\vec{\theta} = \begin{bmatrix} \Delta\theta_1 \\ \Delta\theta_2 \\ : \\ \Delta\theta_n \end{bmatrix} \tag{7.6.2}$$

Where, $\Delta_1, \Delta_2, .., \Delta_n$ and $\Delta\theta_1, \Delta\theta_2, .., \Delta\theta_n$ refer to the displacement and rotation increment at the contact point of each meshing tooth pair. The radius matrix for the worm gear drives is written as:

$$[R] = \begin{bmatrix} R_1 & & & 0 \\ & R_2 & & \\ & & .. & \\ 0 & & & R_n \end{bmatrix} \tag{7.6.3}$$

Where, $R_1, R_2, .., R_n$ represent the radius of each contact point of the respective tooth pair. The vector for torque distribution is written as:

$$\vec{d} = \begin{bmatrix} d_1 \\ d_2 \\ : \\ d_n \end{bmatrix} \tag{7.6.4}$$

Where, $d_1, d_2, .., d_n$ are the torque share coefficients of the respective contact tooth pair. Therefore, the load vector is expressed as:

$$\vec{T} = T \cdot \vec{d} \qquad (7.6.5)$$

It is obvious that the sum of the coefficients is equal to one, so, we have:

$$\sum_{i=1}^{n} d_i = 1 \qquad (7.6.6)$$

The contact force at the theoretical contact position is defined as

$$\vec{P} = [R]^{-1} \cdot \vec{T} = T \cdot [R]^{-1} \cdot \vec{d} \qquad (7.6.7)$$

For each pair of contact teeth, there are bending elastic deformation and contact elastic deformation in the contact area. It is assumed that the load is applied at the contact point and the contact is spread over an elliptical area whose centre remains the theoretical contact point. The vector to depict the elastic deformation is written as:

$$\vec{\delta} = \begin{bmatrix} \delta_1 \\ \delta_2 \\ \vdots \\ \delta_n \end{bmatrix} \qquad (7.6.8)$$

where, $\delta_1, \delta_2, .., \delta_n$ refer to the elastic deformations at each contact point of the respective tooth pair. The matrix of meshing stiffness represents the local meshing stiffness at each contact point. It is written as

$$[K] = \begin{bmatrix} K_{\delta 11} & & & 0 \\ & K_{\delta 22} & & \\ & & .. & \\ 0 & & & K_{\delta nn} \end{bmatrix} \qquad (7.6.9)$$

Therefore, the sum of elastic deformation can be represented as:

$$\vec{P} = T \cdot [R]^{-1} \cdot \vec{d} = [K] \cdot \vec{\delta}$$

$$\vec{\delta} = T \cdot [K]^{-1} \cdot [R]^{-1} \cdot \vec{d} \qquad (7.6.10)$$

According to the motion relation of worm gear drives, the relation between the displacement increment and rotation increment can be written as:

$$\vec{\Delta} = [R] \cdot \Delta\vec{\theta} \qquad (7.6.11)$$

The transmission error at the contact point of every simultaneously meshing tooth pair can be represented as:

$$\Delta\vec{\varphi} = \begin{bmatrix} \Delta\varphi_1 \\ \Delta\varphi_2 \\ \vdots \\ \Delta\varphi_n \end{bmatrix} \qquad (7.6.12)$$

So, the displacement caused by the transmission error is written as:

$$\vec{\tau} = [R] \cdot \Delta\vec{\varphi} \qquad (7.6.13)$$

The total displacement of the contact tooth pairs under load can be described as the sum of elastic deformation (both bending and contacting deformation) and transmission error (the tooth profile separation caused by manufacturing error or misalignment).

$$\vec{\Delta} = \vec{\delta} + \vec{\tau} \qquad (7.6.14)$$

Introducing the equation (7.6.10), (7.6.11) and (7.6.13) into equation (7.6.14):

$$[R] \cdot \Delta\vec{\theta} = T \cdot [K]^{-1} \cdot [R]^{-1} \cdot \vec{d} + [R] \cdot \Delta\vec{\varphi} \qquad (7.6.15)$$

From the condition of deformation compatibility, to assure the continuous transmission, it is necessary that every tooth pair in contact has the same rotation increment under the load, eg. $\Delta\theta_1 = \Delta\theta_2 = \cdot\cdot = \Delta\theta_n = \Delta\theta$. Therefore, $\Delta\vec{\theta}$ can be expressed as:

$$\Delta\vec{\theta} = \Delta\theta \cdot \begin{bmatrix} 1 \\ 1 \\ \vdots \\ 1 \end{bmatrix} = \Delta\theta \cdot [1] \qquad (7.6.16)$$

Therefore, the equation (7.6.15) can be transformed into:

$$\vec{d} = \frac{1}{T} \cdot [R] \cdot [K] \{ [R] \cdot \Delta\vec{\theta} - [R] \cdot \Delta\vec{\varphi} \} = \frac{1}{T} [R] \cdot [K] \cdot [R] \cdot \{ \Delta\theta - \Delta\vec{\varphi} \} \qquad (7.6.17)$$

$\Delta\theta$ can be determined as follows,

$$\because \sum_{i=1}^{n} d_i = 1$$

$$\therefore \sum_{i=1}^{n} \left(\frac{1}{T} [R] \cdot [K] \cdot [R] \cdot \{ \Delta\vec{\theta} - \Delta\vec{\varphi} \} \right) = 1 \qquad (7.6.18)$$

$$\therefore \Delta\theta = \frac{T + \sum_{i=1}^{n} [R] \cdot [K] \cdot [R] \cdot \Delta\vec{\varphi}}{\sum_{i=1}^{n} [R] \cdot [K] \cdot [R] \cdot [1]} \qquad (7.6.19)$$

If no transmission error exists, e.g. $\Delta\vec{\varphi} = 0$

$$\therefore \Delta\theta = \frac{T}{\sum_{i=1}^{n} [R] \cdot [K] \cdot [R] \cdot [1]} \qquad (7.6.20)$$

Where, T is the total torque. θ is the nominal increment of rotation angle, which is determined by material, tooth geometry, load and errors caused by misalignment. Then, $\vec{d}$ can be calculated using equation (7.6.17). Therefore, the load distribution has been achieved.

7.7 Contact Ratio

The contact ratio m_c of worm gear drives is defined by the formula below,

$$m_c = \frac{\Delta\phi_1}{\frac{360^\circ}{Z_1}}$$

Where $\Delta\phi_1$ is the total rotation angle of the worm while one pair of teeth of the worm gear drive is in mesh. Angle $\Delta\phi_1$ can be determined using the output data from the TCA computation. It is the difference between the values of the worm rotation angle at the mesh-in position ($\phi_1^{'}$) and the mesh-out position ($\phi_1^{''}$), expressed as $\Delta\phi_1 = \phi_1^{'} - \phi_1^{''}$. Figure 7.18 shows the tooth contact path of the worm gear drive with localised tooth contact, and the start and end position of the mesh process, where, $\phi_1^{'}$ and $\phi_1^{''}$ are determined by the TCA method.

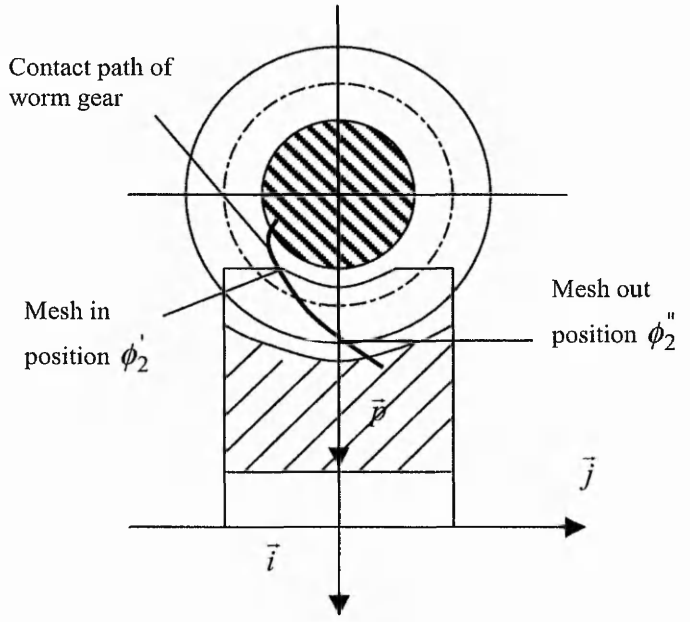

Figure 7.18 Tooth contact path with start and end positions of the mesh process

For the worm gear drive with the design parameters listed in Table 7.1, the numerical analysis (TCA) shows that the contact ratio is 2.17.

7.8 The Calculation Procedure for the Load Distribution

A computer programme has been developed to calculate the load share amongst multiple tooth pairs in contact. The calculation procedure is shown in Figure 7.19. It starts with input of an instantaneous rotation angle corresponding to the contact position, followed by the computation of the tooth contact path using TCA. With the results of TCA, the relation between the rotation angle and the theoretical contact point is determined.

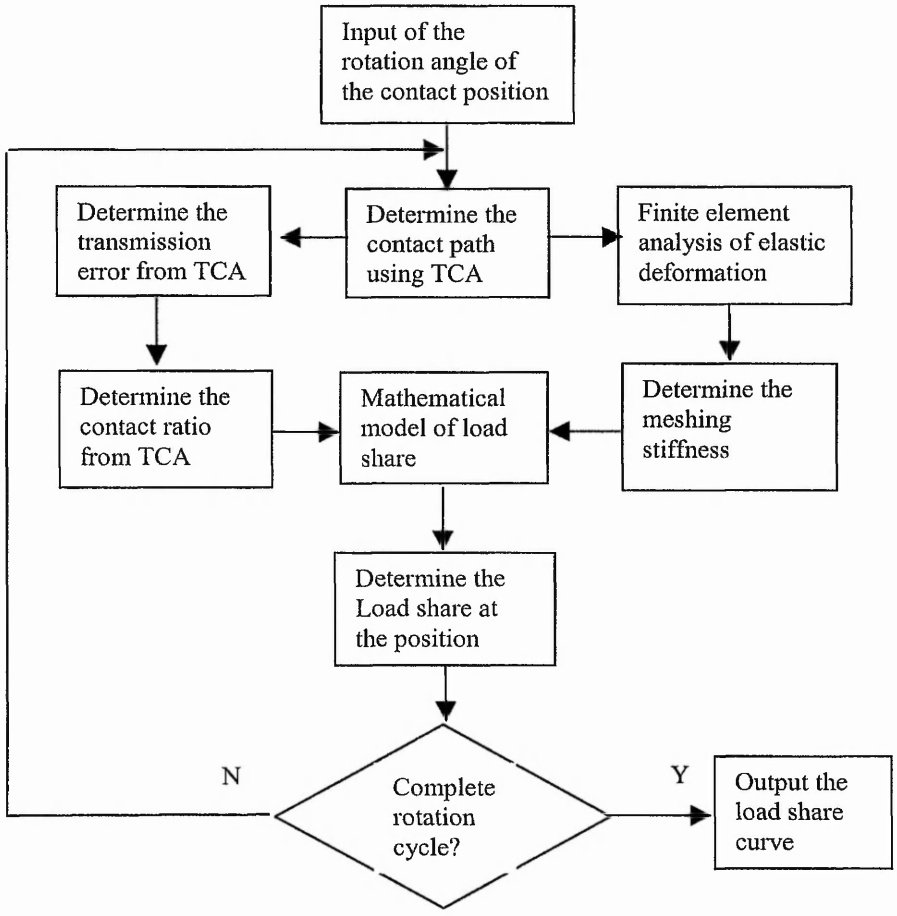

Figure 7.19 The load share calculation procedure for worm gear drives

In the next step, meshing stiffness along the contact path is calculated based on the results of finite element analysis. Meanwhile, the transmission error of the contact path and contact ratio are obtained using the TCA method. The transmission error is influenced by

various factors, amongst which the modification of tooth profile, the manufacturing errors and the assembly error have major contributions. After that, the results of meshing stiffness and transmission error are applied into the matrix $[K]$ and vector $\Delta\vec{\varphi}$, which are defined in chapter 7.6. Using the equations (7.6.20) and (7.6.17), the load distribution can be determined.

7.8.1 An example of load share calculation

As an example, the load share calculation for the worm gear drive shown in Table 7.1 has been conducted. The torque applied to the worm gear drive is 5000 Nm. The meshing stiffness and the transmission error along the tooth contact path are determined using the methods described in sections 7.3 and 7.4. The contact ratio is also obtained from the TCA output.

Based on the results obtained, analysis of the load share of the worm gear drive shows the following:

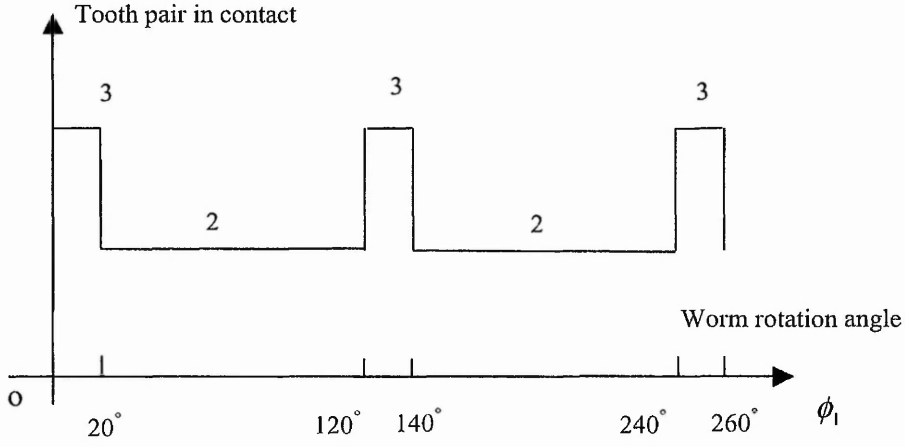

Figure 7.20 Engagement cycle

The contact ratio of the sample worm gear is 2.17. It means that when the worm rotation angle ϕ_1 increases from 0 ~ 20 degree, there are three pairs of teeth in contact simultaneously. During this period, the first pair of teeth of the worm gear drive is just

involved into the engagement, while the third pair of teeth is at the last stage of its engagement. After ϕ_1 turning 20°, the third pair teeth is out of engagement. Then there are only two pairs of teeth remaining in contact. This situation continues with the increase of angle ϕ_1 until ϕ_1=100 degree, when another pair of teeth joins the engagement. The engagement cycle is shown in Figure 7.20.

- **Load share with three pairs of teeth in contact**

(1) Considering the situation with three pairs of teeth in contact and solving the equations (7.6.20) and (7.6.17), the result of load share in the range ϕ_1=0~20 degrees is obtained. For the first pair of teeth, the contact position starts from the tooth tip, where the meshing stiffness is the lowest. The load share is shown in Figure 7.21.

(2) For the second pair of teeth, when ϕ_1 is from 0~20 degrees, the contact point is at the middle part of the tooth surface. The load share is shown in Figure 7.22. After the worm has turned 120 degrees, the first pair of teeth is in the original position of the second pair of teeth and has the same load share.

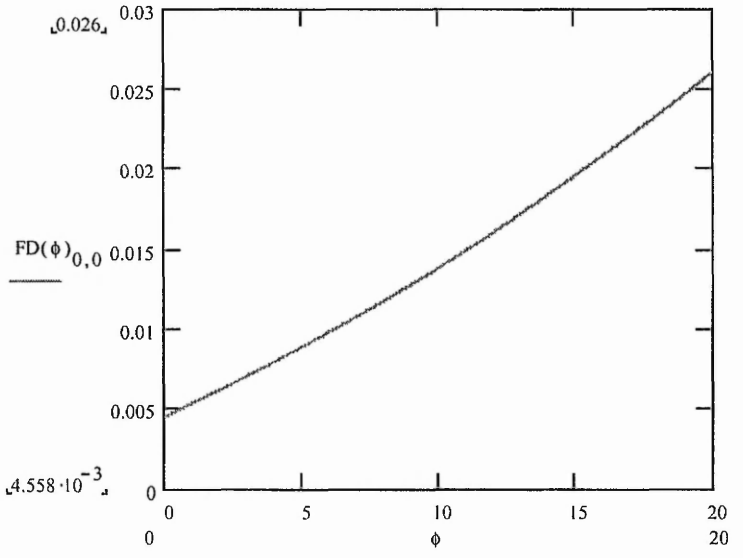

Figure 7.21 The load share of the first pair of teeth (ϕ_1 from 1~20 degree)

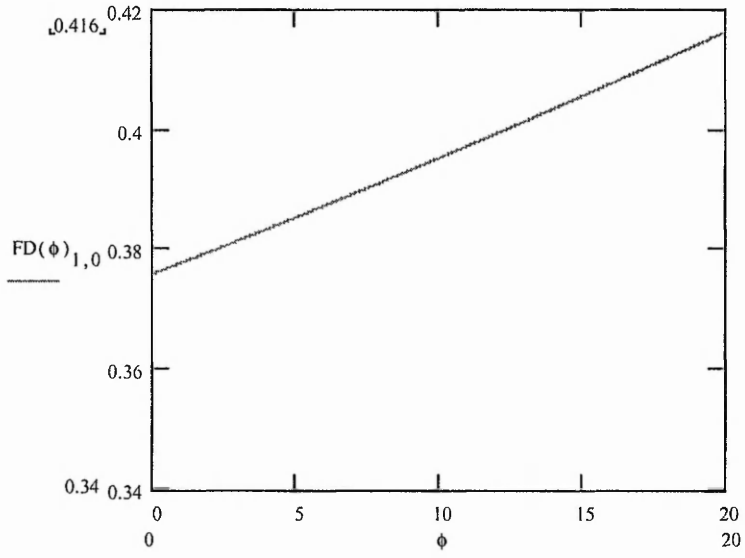

Figure 7.22 The load share of the second pair of teeth (ϕ_1 from 1~20 degree)

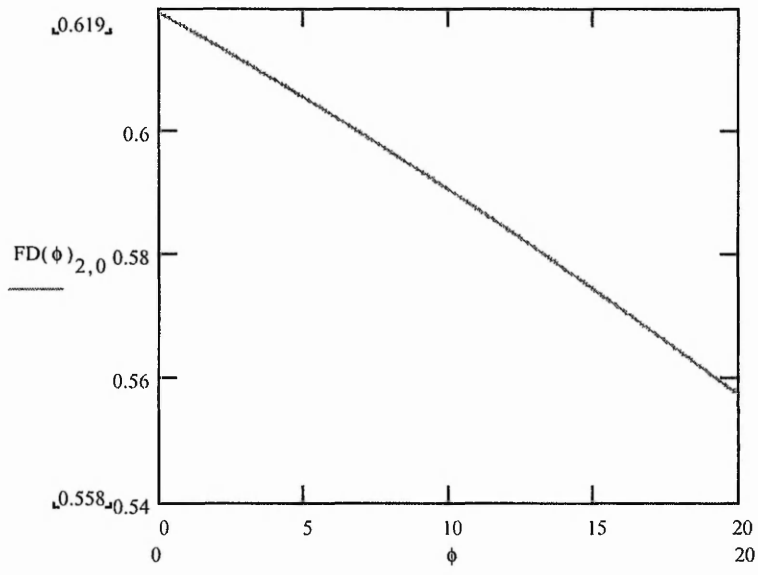

Figure 7.23 The load share of the third pair of teeth (ϕ_1 from 1~20 degree)

(3) For the third pair of teeth, the load share is shown in Figure 7.23. When ϕ_1 is in the region of 1~20 degrees, the contact point approaches the tooth root of the worm wheel where the meshing stiffness is higher than at the tooth tip, and hence, the load

share is higher than that of the wheel tooth tip (as shown in Figure 7.10). After that, the tooth pair exits the contact and does not bear any load. Similarly, after ϕ_1 turning 240 degree the first pair of teeth will be in the same contact position and have the same load share as the third pair of teeth.

- **Load share with two pairs of teeth in contact**

1. Considering the situation with only two pairs of teeth in contact and solving the equations (7.6.17) and (7.6.20), the result of load share in the range ϕ_1=20~120 is achieved. When the worm gear's contact point arrives at a critical position (ϕ_1=20 degree), the third pair of teeth is out of engagement. Therefore, the other two tooth pairs bear a sudden increase in load share. At that moment, the maximum load share occurs to the second pair of teeth. Then the load share of the first pair tooth increases gradually and the load share by the second pair decreases. The total load is shared by the two pairs until ϕ_1=120 degree, when a new pair of teeth is engaged. The load shares of the first pair and second pair are shown in Figure 7.24 and Figure 7.25 respectively. It is obvious that the first pair of teeth will be in the same position as the second pair after turning 140 degrees.

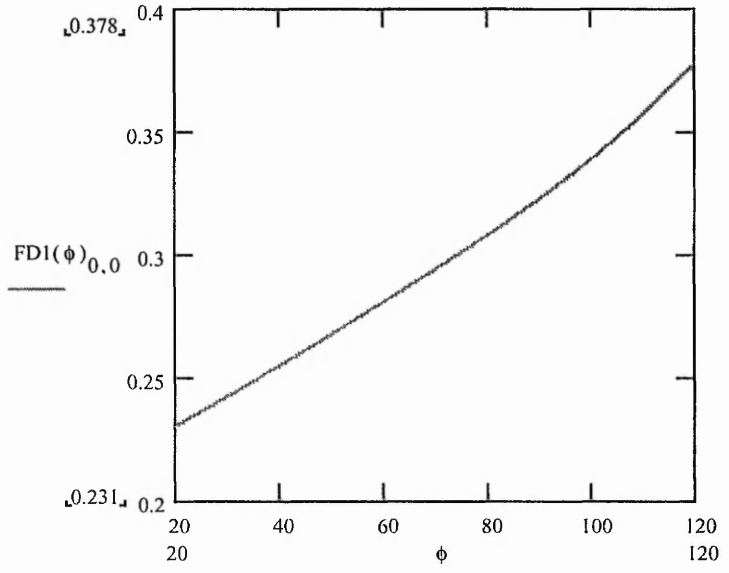

Figure 7.24 The load share of the first pair tooth (ϕ_1 from 20~120 degree)

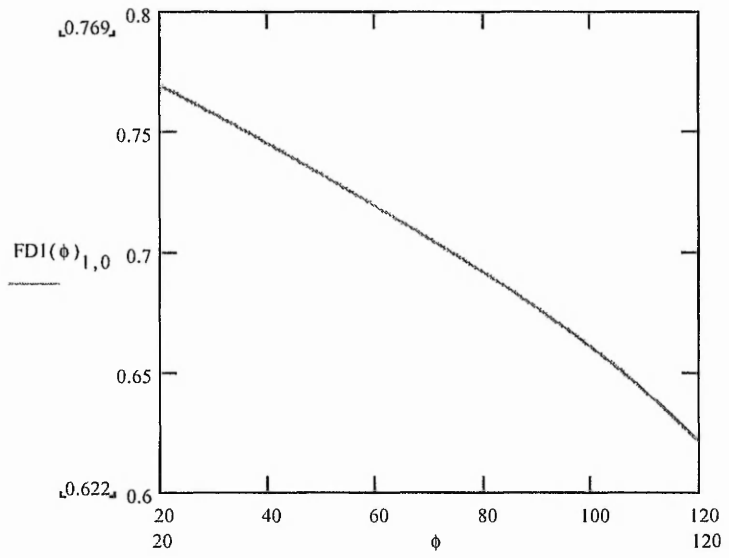

Figure 7.25 The load share of the second pair of teeth (ϕ_1 from 20~120 degree)

- **Percentage of Load share of a tooth pair in the engaging cycle**

Combining the load share results of all the stages of the tooth engaging cycle, the complete load share description for a pair of teeth in the engaging process, i.e. from the moment of starting contact until finishing contact, is shown in Figure 7.26.

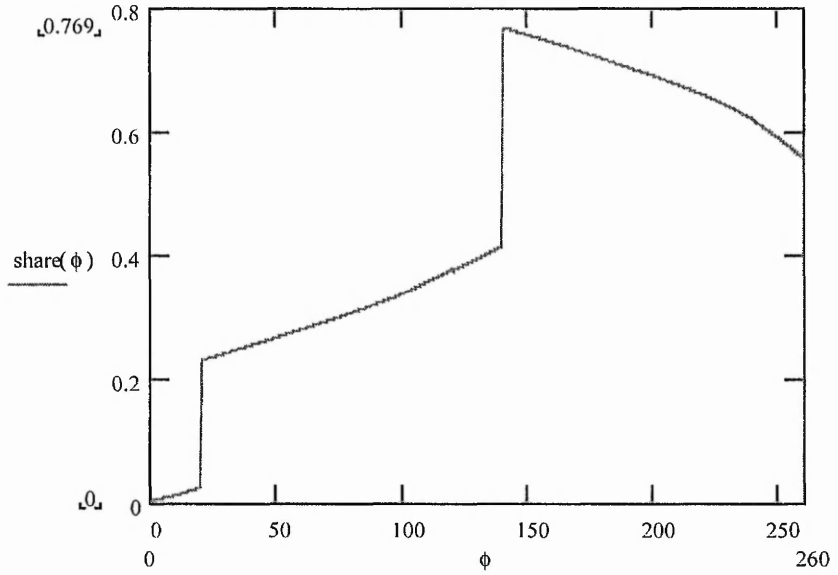

Figure 7.26 The load share by a pair of teeth (ϕ_1 from 0~260 degree)

Figure 7.26 has indicated the following conclusions on the load share of the tooth pairs:
(1) At the starting contact position, where the tip of the wheel tooth and the root of the worm tooth are in contact, the load share of the engaged tooth pair is quite small. Because of the low stiffness of the wheel tooth tip, the meshing stiffness of the starting position is lower as well (see Figure7.13). So the tooth pair only share a lower percentage of the load.
(2) At the ending contact position, where the root of the wheel tooth and the tip of the worm tooth are in contact, the load share of the engaged tooth pair remains about at 50 percent of the load. This means the tooth pair of the worm gear still bears a higher load before quitting the engagement. Because the worm tooth tip and the wheel tooth root both have a higher stiffness, the meshing stiffness of the ending position is much higher than that of the starting position (see Figure7.13). So the tooth pair shares a higher percentage of the load.
(3) When the worm rotation angle equals about 140 degrees, the tooth pair bears the highest percentage of the load (76.9%).
(4) When the other tooth pair is getting into or out of the engagement, there are abrupt changes of the load share of the tooth pair at that moment. The abrupt change is the main cause of impact vibration in worm gear drives.

7.8.2 Further analysis of load share for worm gears under different assembly errors

With different assembly errors, the tooth contact path of the worm gear varies. The meshing stiffness and the transmission error of these contact paths are different, therefore the load shares of the worm gear drives are different. Figure 7.27 and Figure 7.28 show the load share of the worm gear drive under different assembly errors.

- Misalignment of the worm mounting angle by 0.05°

With the above misalignment, the meshing stiffness and theoretical transmission error are obtained from the TCA calculation. The TCA also shows that the contact ratio of the worm gear drive is about 2.04 because of the effect of the misalignment. Using the same approach, the load share of the worm gear drive is shown as below.

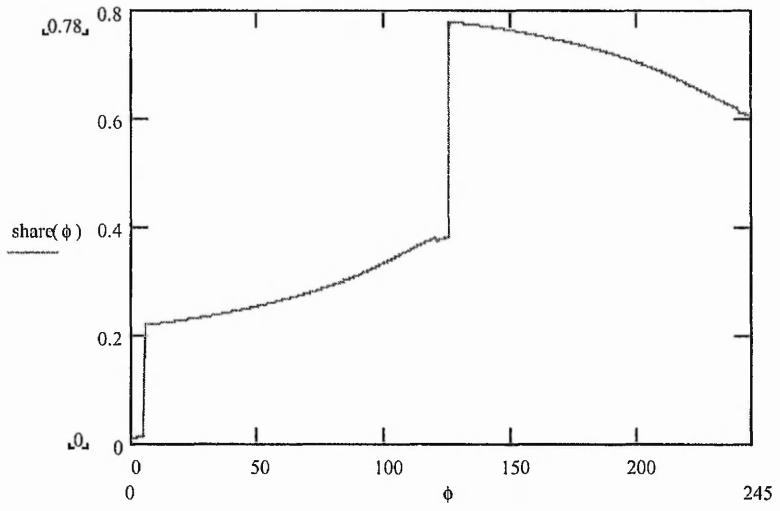

Figure 7.27 The load share by a pair of teeth ($\Delta\beta$=0.05)

- Misalignment of the worm mounting angle by 0.15°

With a misalignment of worm mounting angle equal to 0.15 degree, the TCA result found that the contact ratio of the worm gear drive is about 2.08 because of the effect of the misalignment. Using the same approach, the load share of the worm gear drive is shown in Figure 7.28.

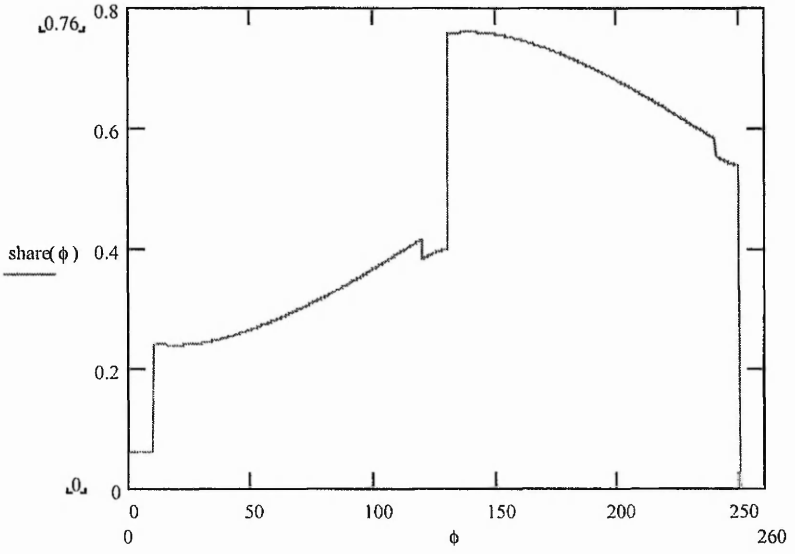

Figure 7.28 The load share by a pair of teeth (ϕ_1 from 0~260 degree, $\Delta\beta$=0.15)

7.9 The Transmission Error and Contact Ratio under Load

Under load, elastic deflection of the tooth body will occur, and the real transmission error is determined by the actual total displacement of the contact tooth pairs. As described in section 7.6, the total displacement can be represented as the sum of the elastic deformation and the theoretical transmission error (the tooth profile separation caused by manufacturing error or misalignment), shown as below,

$$\vec{\Delta} = \vec{\delta} + \vec{\tau}$$

Since the load share of the worm gear has been solved in the above paragraph, the elastic deformation at every instant of the engagement is expressed as

$$\delta_i = \frac{P \cdot d_i}{K_i}$$

Where, P is the total load, d_i is the percentage load share at the contact position and K_i is the meshing stiffness at the same position.

Then, the total displacement at the contact position is written as $\Delta_i = \delta_i + R_i \cdot \Delta\varphi_i$

The real transmission error under load can be described as

$$TE_i = \frac{\Delta_i}{R_i} = \frac{\delta_i}{R_i} + \Delta\varphi_i$$

Because the theoretical transmission error $\Delta\varphi_i$ has been obtained from TCA, the transmission error under the load P can be achieved. It is obvious that under load the transmission error is different from the theoretical one. A computer program has been developed to calculate the transmission error under load, shown as Figure 7.29. The program combines the TCA process, estimation of tooth meshing stiffness from the finite element model and determination of load share of the engaging tooth. The method is applied for a pair of worm gear drives with the design parameters listed in Table 7.1. The real transmission error of the worm gear drive is evaluated under different assembly errors and loads.

According to the calculation results, under the normal load the tooth elastic deformation of the worm gear is comparable to the displacement caused by the theoretical transmission error (tooth gap caused by the manufacturing error). Therefore, the real transmission error of worm gear drives is recognised as a load-dependent function:

- Without load or with very light load, the tooth elastic deformation can be neglected. The transmission error of the worm gear drive can be represented by the conventional method. i.e. the transmission error results from TCA are applicable.
- With increasing load, the amount of tooth elastic deformation is close to the displacement caused by the transmission error. Then the elastic deformation will significantly compensate for the tooth gap caused by the manufacturing error and the transmission error will be reduced substantially.

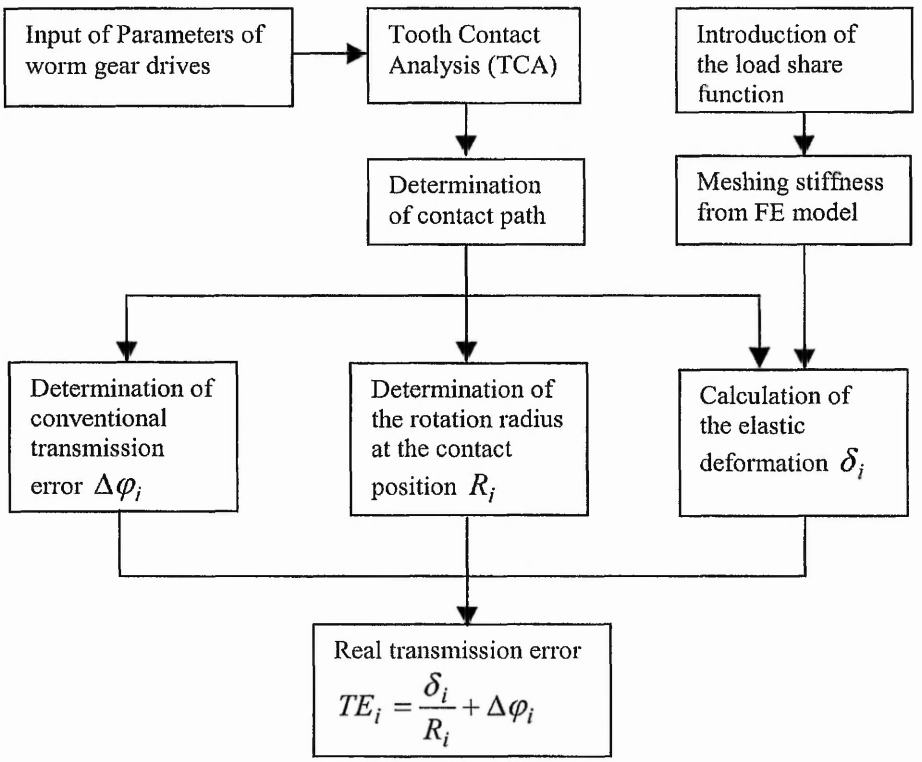

Figure 7.29 The calculation flowchart of the real transmission error

- Under heavy loads, when the tooth elastic deformation is considerably larger than the tooth gap caused by the manufacturing error, the real transmission error is dominated by the elastic deformation. However, in such situations the original transmission error still contributes to reducing the real transmission error.

It is clear that the conventional method to evaluate the transmission error is not applicable to the worm gear under load. The approach developed here enables the real transmission error under load to be evaluated. It is especially valuable for high speed transmissions.

Even if the original transmission error (obtained from TCA) for the worm gear drive does not exist, i.e. a perfect worm gear drive is manufactured, the tooth elastic deformation still occurs under load. Figure 7.30 illustrates an example of transmission error caused by pure tooth elastic deformation under the load. The tooth elastic deformation is determined by the load share and meshing stiffness. The figure proves that even a perfectly-made worm gear drive will have a transmission error when the load is applied.

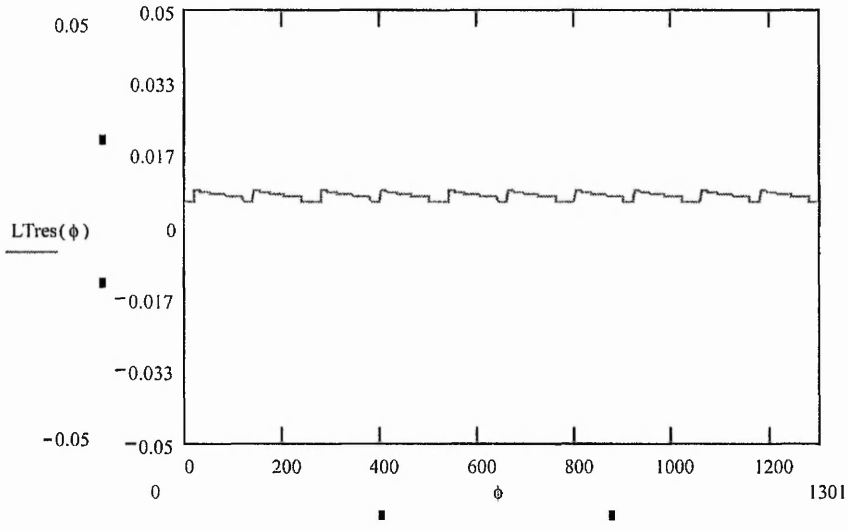

Figure 7.30 Transmission error caused by tooth elastic deformation (T=4000Nm)

Figure 7.31 and Figure 7.32 show the loaded transmission error of the worm gear drive with different assembly errors. The transmission error under load is compared with the

transmission error without load in each case. It can be seen from the figures that under load the transmission error has been significantly reduced. This can be interpreted as showing that the elastic deformation under the load can compensate the tooth gap caused by the manufacturing error.

Following the above conclusion, it is clear that transmission error will substantially change under load. The conventional method for evaluating transmission error cannot describe it correctly. A method to calculate loaded transmission error has been developed and can effectively find the solution.

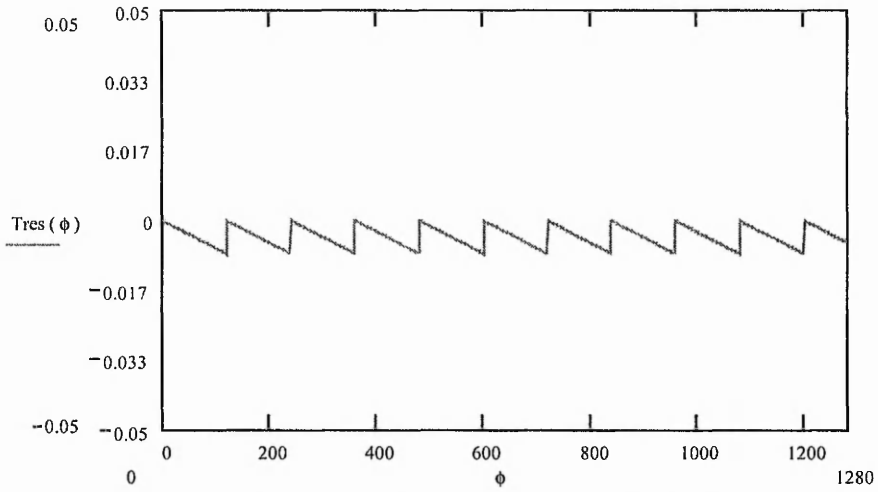

(a) Theoretical transmission error (without load)

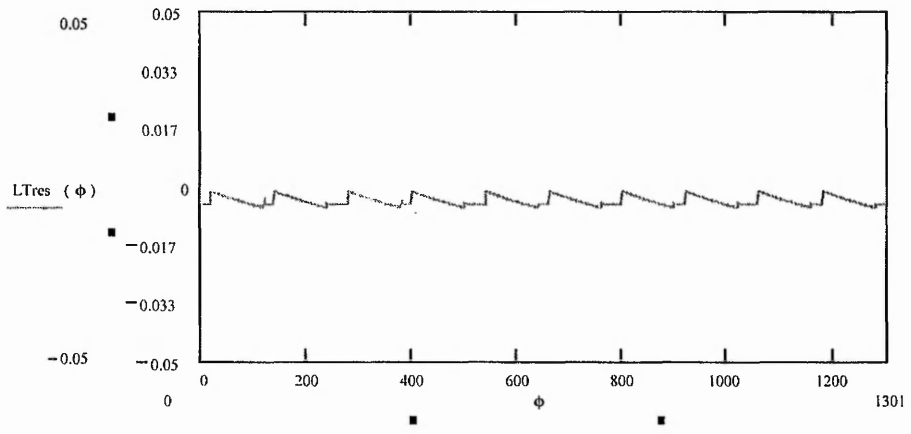

(b) Transmission error under load (T=2000 Nm)

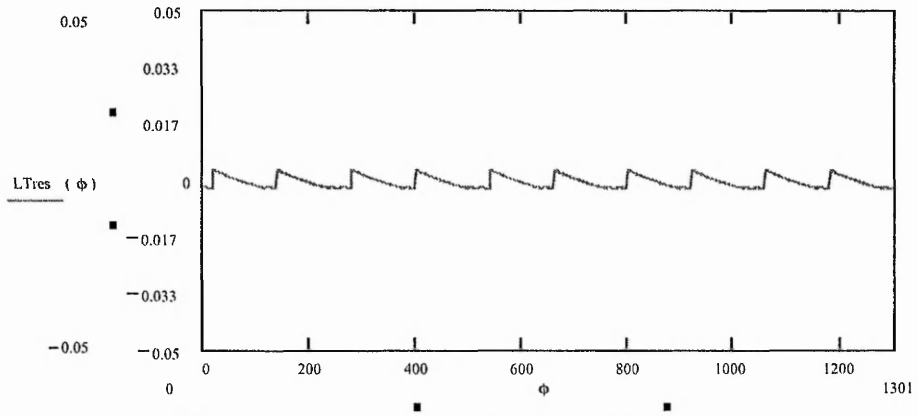

(c) Transmission error under load (T=4000 Nm)

Figure 7.30 Transmission errors of the worm gear drive (worm mounting angle error =0)

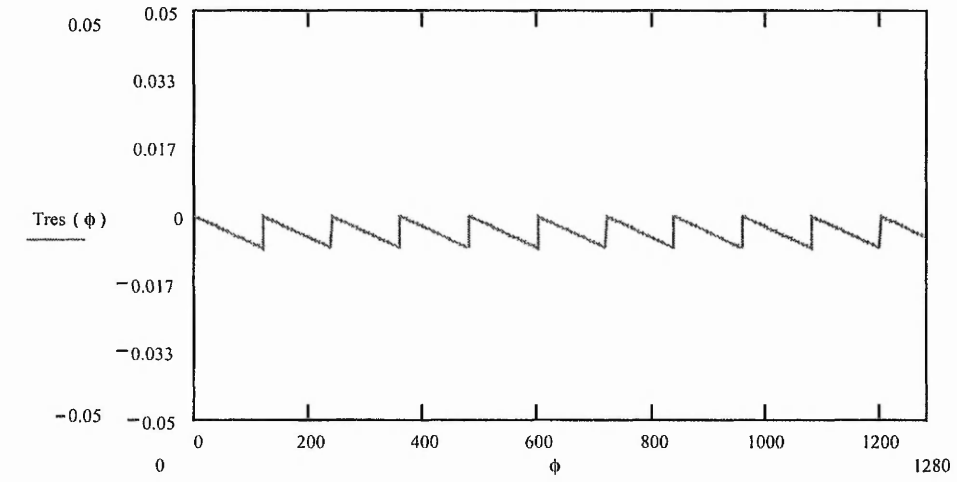

(a) Theoretical transmission error (without load)

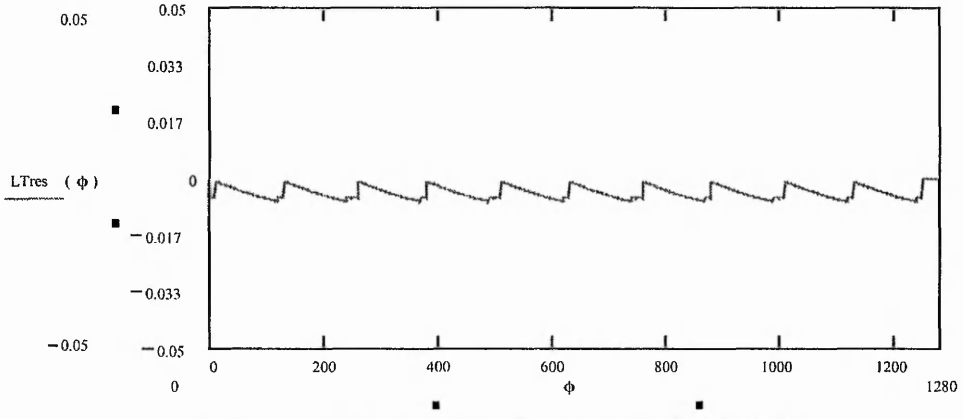

(b) Transmission error under load (T=2000 Nm)

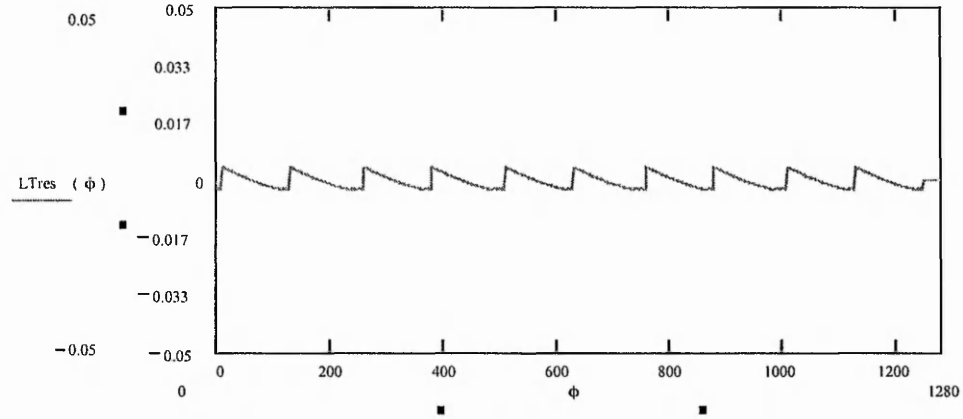

(c) Transmission error under load (T=4000 Nm)

Figure 7.31 Transmission errors of the worm gear drive (worm mounting angle error $=0.15^0$)

Chapter 8 Discussion and Conclusion

In spite of previous intensive research into worm gear drives, many problems still remain in worm gear design. The conventional design method generates worm gear tooth pairs in line tooth contact, which is very sensitive to manufacturing errors. Current load rating methods for worm gears, such as BS721-2:1983, are not precise enough. Moreover, the tooth root stress of worm gears, which is important in evaluating service life, cannot be calculated using the existing design standard. Because of the complex tooth geometry, it is difficult to use the traditional analytical formula to solve these problems.

In this project, a novel approach has been developed that covers parametric design, three dimensional simulation and finite element analysis for worm gear drives with localised tooth contact. The approach proposed a new method to design worm gear drive with localised tooth contact. The modification parameters are determined by the method proposed in Chapter 3 to achieve preferable localised tooth contact. A tooth contact analysis computation program also has been developed to investigate the tooth contact path and contact pattern. The improved worm gear drive has better tooth contact and is insensitive to manufacturing errors.

The implementation of three dimensional modelling and simulation for worm gear drives has established the knowledge and expertise to evaluate and improve their design using advanced CAD technology. The modelling methods developed enable the creation of different curves, tooth conjugate surfaces and helical surfaces, making the methods applicable to various gear drives. The resultant three dimensional models and simulations can provide visualisation for a proposed design, and the tooth contact position can be estimated during the simulation. It is valuable for both academic research and industrial application.

During the process of finite element modelling and analysis, FE models of worm gear drives have been created and validated. The mesh generation of worm gear models has been investigated as well. The meshing procedures suitable for tooth geometry with helical surface are provided. Depending on the FE models, the calculations of

tooth deflection and tooth root stress are performed. Then, an approach for evaluation of the load share of worm gear drives has been developed using the finite element method. Within the approach, an elastic model considering tooth deflection and geometric error of the tooth profile is used to predict the load share. The finite element method is applied to calculate the elastic deflection. The concept of meshing stiffness is defined for worm gear drives and the instantaneous meshing stiffness is represented as a function of the tooth contact path. Calculation of meshing stiffness has been done based on the finite element model. The transmission error caused by tooth profile geometry is obtained from Tooth Contact Analysis. Taking into account various factors, the load share of worm gear drives can be determined. The results of FEA are compared with published experimental work.

8.1 Development of the Localised Tooth Contact for Worm Gear Drive

The sensitivity to manufacturing errors and deflection is an important measurement of worm gearing performance. Due to the errors and deflections, the theoretical contact lines of conventional worm gear drives shift to the boundary of the tooth surfaces, resulting in edge contact. Therefore, reduction of the sensitivity is an important research topic of worm gearing.

The literature survey conducted by this research revealed the major existing approaches to achieve localised tooth contact: (1) Trial and error method to obtain localised tooth contact, (2) Modifying tooth profiles to get localised tooth contact, and (3) tooth contact analysis (TCA) method for localised tooth contact. However, current methods for worm gear drive with localised tooth contact depend on the designer's expertise. They cannot ensure optimum transmission quality and may cause tooth surface interference during the tooth modification.

A numerical method has been established to obtain a preferable localised tooth contact (PLTC) for worm gear drives. The design parameters of worm gear drives are modified in order to control the tooth contact pattern. The completed mathematical model offers a solution to determine an ideal position for a local contact zone and achieve optimum contact properties for worm gearing. It consists of four major steps:

- Modify the tooth geometry parameters to locate the contact area around a reference point chosen by the designer;
- Create the worm and wheel tooth surfaces with the modified parameters;
- Derive the mathematical model of localised contact;
- Analyse the tooth contact using a numerical approach.

The tooth contact analysis for worm gear drives has been conducted and a calculation programme is provided to find the tooth contact path. Taking account of worm gear drives with various design parameters, the programme can predict their tooth contact path and unloaded transmission error.

The numerical analysis of the contact path of the modified worm-gear drives proves the tooth contact of the new type worm gearing is stable both in contact pattern and size. Compared with traditional line contact, the PLTC is much less sensitive to errors and can achieve high transmission quality and cut down the time and effort spent in production and assembly. Therefore, this project has contributed a novel method to develop a new type worm gearing with preferable localised tooth contact.

8.2 Three Dimensional Modelling and Simulation

Three dimensional modelling as well as simulation of worm gear drive is necessary for design evaluation and further finite element analysis. But it has not been reported yet. With a combination of advanced CAD/CAE techniques, an approach to three dimensional modelling and simulation has been developed for the optimum design of worm gearing. The following have been completed:

- The establishment of three dimensional models for worm, wheel and assembly. According to the results obtained from the proposed design, the 3D models of worm and wheel have been built within the environment of the CAD software package Pro/Engineer. The 3D assembly model is created by combining the worm model and wheel model with the designed geometric relationship.

- A method has been developed for three dimensional simulation of the worm gearing, which includes virtual engagement of worm and wheel and 3D tooth contact simulation. The former simulates the kinematic relationship established

between the worm and wheel models and the latter enables imitation of the contact pattern at every instant of tooth engagement. The 3D simulation provides a great visual aid for investigating the tooth contact. With the 3D simulation, the contact pattern of the worm gearing and its moving direction can be predicted, and interference between the modified tooth surfaces can be detected and hence avoided at the design stage. This is a significant achievement in the analysis of localised contact of worm gears, because the previous methods often cause interference and can not detect its position. The 3D simulation also lays a solid foundation for the finite element analysis in the future work.

The three dimensional modelling and simulation enable the visualisation of the design of a worm gear drive. This will benefit the development process of the product and help designers to improve their work, and reduce the product cycle time and the costs.

8.3 Finite Element Modelling and Analysis of Worm Gear Drive

Conventional tooth contact analysis is usually based on the assumption of rigid teeth. On the other hand, a uniform load along an ideal contact line is always assumed for tooth stresses analysis. Both of them are far from the real situation. The finite element method has emerged recently as a very active tool for engineering analysis and is able to provide a feasible solution for existing problems.

The process of finite element modelling has been developed for the worm gear drive with modified tooth geometry. Finite element analyses were performed within the environment of the software ANSYS. The results have been compared with published empirical results; the comparison shows a good agreement between the finite element analysis and empirical work. Throughout the process of finite element analysis, several topics have been explored.

- A three dimensional elastic FEA model has been developed using the ANSYS software package, and appropriate elements have been chosen to mesh the model. The material property and boundary conditions of the models have been investigated as well.

- The tooth stress distribution and deformation have been investigated using finite element models. Particularly the tooth root stress has been analysed and the results are compared to the empirical results.
- Loaded tooth contact pattern has been investigated and Hertzian theory has been applied to explain the elastic deformation between two contacting teeth. A general approach to solve the contact area and deformation has been presented.
- The tooth meshing stiffness has been investigated using the three dimensional elastic model. Represented as a function of the tooth contact path, the tooth meshing stiffness is calculated based on the finite element model. The meshing stiffness is an important concept for loading analysis of worm gear drives.
- The load share between the contacting tooth pair has been determined. The concept of a deformation compatibility condition for worm gear drives has been proposed, providing the fundamental for determination of the load share percentage of the tooth pairs in contact. A mathematical model has been derived and an explicit expression of load share in worm gear drives has been given. Considering all the factors such as meshing stiffness, unloaded transmission error and contact ratio, the mathematical model is able to calculate the load share percentage of the tooth pair in contact.
- The concept of loaded transmission error (transmission error under load) is introduced considering the real load share of the tooth pair. The analysis shows that real transmission error under load is influenced by tooth elastic deformation and original unloaded transmission error. The real transmission error is substantially changed under load.

Although the above approach has been developed with respect to involute worm gears, the proposed method is quite general and can be applied to predict the deformation, stress and loaded transmission error for other gears.

8.4 Conclusions

In this project, a general approach has been developed successfully for design, modelling and analysis of worm gear drive with localised tooth contact. By applying the theory of differential geometry, CAD and FEA technology, this approach has provided the methodologies to solve the remaining problems in existing design methods.

The following conclusions have been drawn from the project:

1. The concept of localised tooth contact has been applied to worm gear drives, It ensures that a worm gear has a stable tooth contact property and insensitivity to manufacturing errors. The design method to implement localised tooth contact has been established and tested by the application of the design of involute worm gear drive. It has been proved that the proposed method contributes a valuable approach for worm gear design.

2. Three dimensional Modelling and Simulation for worm gear drives has been conducted. The completed models have displayed motion, tooth contact and interference checking for worm gear drives based upon design and assembly information. The visualisation will help designers improve their design, and reduce the cycle time and costs of the product.

3. The finite element method offers a solution to the unsolved problems in current worm gear design. The calculation of tooth stress and evaluation of load share are important in worm gear design but remain unknown in the existing design standard. The FEA of the worm gear models has developed a general method to obtain the solutions of load share and tooth stress and the results have been validated by the published experimental work. The results obtained are the fundamentals of the design of worm gear drive with high contact ratio and compact size.

8.5 Suggestion for Future Work

The approach developed in this research enables design, modelling and analysis for worm gear drives with localised tooth contact. The main areas of further work are refinement of the details of the approach. It would make the approach more complete if the following are considered.

Optimum design of the worm gear drives with localised tooth contact

Within current research, the localised tooth contact position is determined by the designer and can be adjusted according to the results of contact simulation. To achieve an ideal design of worm gear drive with localised tooth contact, optimum

calculation of the worm gear design parameters should be added into the approach. The mathematical model for optimum calculation should be developed aiming at obtaining optimum loading and contact characteristics.

Improving the three dimensional modelling method

In this research, the three dimensional modelling method of the wheel is based on the results of differential geometric calculation described in Chapter 4. The modelling process involved creation of datum points and lines, creation of tooth surface and body, and creation of the whole structure of the wheel. Both calculation and geometric modelling techniques are applied to build the three dimensional model, which made the process complicated. Therefore, a parameter modelling method, i.e. building the wheel model using its design parameters directly, would be more efficient for worm gear modelling. Thus, the calculation process and multi-step geometric modelling will be avoided and the wheel model can be created using some simple commands with the design parameters. The following factors should be considered while developing the new modelling method:

- enough precision of the tooth geometry
- reasonable speed of the modelling process
- small data volume of the geometric models

Enhancing the transfer from 3D model to FE model

At present in this research, the worm and wheel models are saved as IGES files and imported into the FEA software package to generate FE models. During this process, sometimes the models lost information, then extra modelling manipulations are needed to repair the models. Moreover, due to the geometry complexity of the worm and wheel, the meshing of the models (element generation) cannot be completed automatically. It is always necessary to introduce much hand-manoeuvring to divide the models into some simple geometry, so that the software can mesh them. To enable automatic meshing for worm gear models, a meshing calculation programme needs to be developed.

The meshing methods described in Chapter 6 have already provided an approach to obtain meshing of both the worm and the wheel models successfully. It can be programmed as an additional meshing function within the FEA software package. Since the method has already been developed, this is not difficult but just needs time.

Investigating other affecting factors

The research work conducted in this project is based on certain assumptions (chapter 7.2). Some factors such as lubrication and elastic deformations of the shaft, bearing and gear-box are not counted in the calculation. Another limitation is that all calculations are based upon static analysis; dynamic response of the worm gear drive is not considered in this project even though the static load share will be different from that under rotation. Therefore, further research into the dynamic behaviour of the worm gear drive has to be initiated in order to improve the fidelity of the approach.

Nevertheless, this project has developed a general approach for design, modelling and analysis of worm gear drive with localised tooth contact, which has solved the remaining problems in existing design methods. By applying the theory of differential geometry, CAD and FEA technology, this project has also provided a method to evaluate the load sharing of worm gear drives. The achievement from this project has laid a basis for design of worm gear drives with high loading capacity and compact size.

References

Arai, N., Harada, S., and Aida, T., 1981, "Research on bending strength properties of spur gears with a thin rim," Bulletin of the Japanese Society of Mechanical Engineers, Vol. 24, No. 195, pp. 1642~1650.

Bair_BW, Tsay_CB ,1998, "ZK-type dual-lead worm and worm gear drives: Contact teeth, contact ratios and kinematic errors", JOURNAL OF MECHANICAL DESIGN, Vol.120, No.3, pp.422-428.

Bar G., 1990, "CAD of Worms and Their Machining Tools", Computer & Graphics, Vol. 14, No3/4, pp405-411.

Bercsey T. and Horak P.,1996, " A New Tribological Model of Worm Gear Teeth Contact", Proceedings, ASME Power Transmission and Gearing Conference, DE-Vol. 88, October 6-9, San Diego, California.

Bibel G.D., Kumar A., Reddy S. and Handschuh R., 1995 " Contact stress analysis of spiral bevel gears using finite element analysis", ASME Journal of Mechanical Design, June 1995, vol. 117 pp235~240.

Bibel G.D., Reddy S. K., Savage M. and Handschuh R.F., 1994, "Effect of rim thickness on spur gear bending stress", ASME Journal of Mechanical Design, Dec. Vol. 116, pp. 1157~1162.

Boresi A. P. and Sidebottom O.M., 1985, "Advanced Mechanics of Materials", John Wiley & Sons, Chichester, England.

Chang, S. H., Huston, R.L., and Coy, J.J., 1983, "A finite element stress analysis of spur gears including fillet radii and rim thickness effects", ASME Journal of Mechanisms, Tramsmissions, and Automation in Design, Vol. 105, No. 3 pp. 327-330, Sept.

Chang, S. L., Tsay C. B. and Nagata S., 1997, "A General Mathematical Model for

Gears Cut by CNC Hobbing Machines", ASME Journal of Mechanical Design, Vol. 119, pp. 108-113.

Chong, T.H., and Kubo, A., 1985,"Simple stress formula for a thin-rimmed spur gear", ASME Journal of Mechanisms, Transmissions, and Automation in Design, Vol. 107, No.3, pp. 406-423, Sept.

Colbourne, J.R., 1989, "The Use of Oversized Hobs to Cut Worm-Gears," ***AGMA Technical Paper 89FTM8***, American Gear Manufacturers Association, Alexandria, VA.

Dabnichki P. and Crocombe A., 1999, "Finite element Modelling of local contact conditions in gear teeth", Journal of Strain Analysis, Vol. 34, No 2, pp129-142.

Du S., Randall R.B. and Kelly D.W., 1998, "Modelling of spur gear mesh stiffness and static transmission error", Proceedings of Instn.Mech. Engrs Vol. 212 PartC, pp287-297.

Donno M. D. and Litvin F.L., 1998, "Computerised Design, Generation and Simulation of Meshing of A Spiroid Worm-Gear Drive with Double-Crowned Worm", Proceedings of DECT'98, ASME Design and Technical Conferences, Sep. 13-16 Atlanta, Georgia, USA.

Dudas I., Banyal K. and Varga G., 1996, "Simulation of Meshing of Worm Gearing", Proceedings of 7th ASME International Power Transmission and Gearing Conference, Oct. 6-9, San Diego, California.

Dudley D. W., 1984, "Handbook of practical gear design" McGraw-Hill, Inc, London.

Elkholy_AH, Elsharkawy_AA, 1997, "Load distribution and tooth fillet stress of straight bevel gears using a stiffness variation technique" INTERNATIONAL JOURNAL OF MATERIALS & PRODUCT TECHNOLOGY, Vol.12, No.4-6, pp.396-415.

Elkholy_AH, Elsharkawy_AA, Yigit_AS, 1998, "Effect of meshing tooth stiffness and manufacturing error on the analysis of straight bevel gears", MECHANICS OF STRUCTURES AND MACHINES, Vol.26, No.1, pp.41-61.

Feng P.H. and Litvin F. L., 1998, "Determination of Principal Curvatures and Contact Ellipse for Profile Crowned Helical Gears", Proceedings, ASM Design Engineering Technical Conferences, Sept. 13-16, Atlanta, Georgia, USA.

Filiz I. Huseyin and Eyercioglu O., 1995, "Evaluation of Gear Tooth Stresses by Finite Element Method", ASME Journal of Engineering for Industry, Vol. 117, May, pp. 232-239.

Gao Y., Xu X. and Liu G., 1993, "The controllable curvature modification theory for point contact niemann's worm gear drive"

Gosselin C., Cloutier L. and Nguyen Q. D., 1995, " A General Formulation for the Calculation of the Load Sharing and Transmission Error Under Load of Spiral Bevel and Hypoid Gears", Mechanism and Machine Theory, Vol. 30, No. 3, pp. 433-450.

Hearn, E. J, 1997, "Mechanics of materials : an introduction to the mechanics of elastic and plastic deformation of solids and structural materials. vol 1", Butterworth-Heinemann, Oxford, England.

Huseyin Filiz I. and Eyercioglu O., 1995, " Evaluation of gear tooth stresses by finite element method", Transactions of ASME, Journal of Engineering for Industry, vol. 117, May, pp232 ~239.

International Standard (Committee Draft ISO/CD for Circulation), 1999, "Load capacity calculation of worm gears", ISO/TC 60/SC 1/GT 7N 171/CD 14521, British Standard Institution.

J.C. Leming, High Contact Ratio Spur Gears, Gear Design Manufacturing and Inspection Manual, SAE AE_15 (1990)].

Janninck, W. L., 1988, "Contact Surface Topology of Worm Gear Teeth", *Gear Technology*, Vol. 5, No. 2, pp. 31-47.

Korn, G.A. and Korn, T.M., 1968, Mathematics Handbook for Scientists and Engineers, McGraw-Hill, NY.

Li_JF, Wang_JX, Zhang_G, Wang_SY, 1998a, "Static analysis of bevel gears using finite element method", COMMUNICATIONS IN NUMERICAL METHODS IN ENGINEERING, Vol.14, No.4, pp.367-380

Li_JF, Zhang_Z, Ji_L, Wang_SY, 1998b, "Finite element analysis of cylindrical gears", COMMUNICATIONS IN NUMERICAL METHODS IN ENGINEERING, Vol.14, No.10, pp.963-975.

Litvin F. L.,1994, "Gear Geometry and Applied Theory", Prentice-Hall Inc., New Jersey 07631, USA.

Litvin F. L., Chen J. s., Lu J. and Handschuh R. F., 1996, "Application of Finite Element Analysis for Determination of Load Share, Real Contact Ratio, Precision of Motion, and Stress Analysis" ASME Journal of Mechanical Design, vol. 118, pp 561~567

Litvin F.L. and Kin V., 1992, "Computerised simulation of meshing and bearing contact for single-enveloping worm gear drives", ASME Journal of Mechanical Design, Vol. 114, pp. 313~316.

Litvin F.L., 1995, "Applied Theory of Gearing: State of the Art", Transactions of the ASME, Special 50th Anniversary Design Issue, Vol. 117, pp129~134.

Litvin F.L., Chen J.S., Sep T.M. and Wang J.C., 1995, "Computerised simulation of transmission errors and shift of bearing contact for face-milled hypoid gear drive", ASME Journal of Mechanical Design, Vol.117, No. 2, pp.262-268

Litvin F.L., Chen N.X., Lu J. and Handschuh R.F., 1995, "Computerised design and generation of low-noise helical gears with modified surface topology", ASME Journal of

Mechanical Design, Vol.117, No.2, pp.254 ~ 261.

Litvin F.L., Seol I.H., Kim D., Lu J. and Wang A.G., etc. 1996, "Kinematic and geometric models of gear drives" ASME Journal of Mechanical Design, Vol. 118, No.4, pp. 544~550.

Litvin F.L., Wang A.G. and Handschuh R.F., 1996, "Computerised design and analysis of face-milled, uniform tooth height spiral bevel gear drives" ASME Journal of Mechanical Design, Vol. 118, No. 4, pp.573 ~ 579.

Litvin_FL, Chen_JS, Lu_J, Handschuh_RF 1996, "Application of finite element analysis for determination of load share, real contact ratio, precision of motion, and stress analysis." JOURNAL OF MECHANICAL DESIGN, , Vol.118, No.4, pp.561-567.

Lu J., Litvin F. L. and Chen J.S., 1995, "Load Share and Finite Element Stress Analysis for Double Circular-Arc Helical Gears", Mathematical and Computer Modelling, Vol 21, No. 10, pp. 13-30.

MathSoft Inc., 1995, "Mathcad 6.0, User's Guide", 101 Main Street, Cambridge Massachusetts, 02142 USA

Moriwaki I., Fukuda T., Watabe Y. and Saito K., 1993, "Global local finite element method (GLFEM) in gear tooth stress analysis" Transaction of the ASME, Journal of Mechanical Design, Dec. 1993, Vol. 115, pp1008 ~ 1012.

Oda, S., Nagamura, K., and Aoki, k., 1981, "Stress analysis of thin rim spur gears by finite element method", Bulletin of the Japanese Society of Mechanical Engineers, Vol. 24, No. 193, pp. 1273~1280.

Park Y.B. and Yang D.Y., 1998, "Finite Element Analysis for Precision Cold Forging of Helical Gear using Recurrent Boundary Conditions", Proceedings of Instn Mech Engrs, Vol. 212 PartB, pp.231-240

Qin D. and Kato M., 1995, " The hourglass worm gearing with local conjugate contact", Proceedings of International Congress-Gear Transmissions'95, 26th-28th, Sept. Sofia, Bulgaria. pp99~103.

Rao C.R.M. and Muthuveerappan G., 1993, " Finite Element Modelling and Stress Analysis of Helical Gear Teeth", Journal of Computers & Structures, Vol. 49, No 6, pp. 1095-1106.

Ramamuri V., Nayak H., Vijayendra H. and Sujatha C., 1998, "Static and Dynamic Analysis of Spur and Bevel Gears Using FEM", Mechanic and Machine Theory, Vol. 33 No.8, pp. 1177-1193.

Seol I. H. and Litvin F. L., 1996a, "Computerised Design, Generation and Simulation of Meshing and Contact of Modified Involute, Klingelnberg and Flender Type Worm-gear Drives" ASME Journal of Mechanical Design., Vol. 118, pp 551 ~555

Seol I.H. and Litvin F.L., 1996b,"Computerized design, generation and simulation of meshing and contact of worm-gear drives with improved geometry", Computer methods in applied mechanics and engineering, Vol.138, No.1-4, pp. 73~103.

Shen Q., Zhou C. and Wu X., 1989, "The principle about using conventional gear hob to make point contact worm gearing", Machine Design NO.5 (in Chinese)

Simon V., 1993a, "Load Distribution in Double Enveloping Worm Gears" ASME Journal of Mechanical Design, Vol. 115, pp496 ~500

Simon V., 1993b, "Stress Analysis in Double Enveloping Worm Gears By Finite Element Method. Journal" ASME Journal of Mechanical Design., Vol. 115, pp 179 ~185.

Simon V., 1990. "EHD Lubrication of Double Enveloping worm Gears. "Proceeding of the Japan International Tribology Conference.

Simon V., 1996a, "Stress analysis in worm gears with ground concave worm profile"

MECHANISM AND MACHINE THEORY, Vol.31, No.8, pp.1121-1130

Simon V., 1996b, "Displacements in worm gears with ground concave worm profile" MECHANISM AND MACHINE THEORY, Vol.31, No.8, pp.1131-1140

Stokes A., 1992, "Gear Handbook: Design and Calculations", Butterworth-Heinemann Ltd, London, Great Britain.

Sudoh K., Tanaka Y., Matsumoto S., and Tozaki Y., 1996, "Load Distribution Analysis Method for Cylindrical Worm Gear Teeth", JSME International Series C-Dynamics Control Robotics Design and Manufacturing, Vol. 39, No. 3, pp. 606-613.

Tasi M. H. and Tsai Y.C., 1997, " A Method for Calculating Static Transmission Errors of Plastic Spur Gears Using FEM Evaluation", Journal of Finite Elements in Analysis and Design, Vol. 27, pp 345-357.

Tsay C. B. and Chang S. L., 1994, "Design of pencil-type milling cutters for worm surface generation", Journal of Materials Processing Technology, vol 42, pp 361-376.

Vinula H., Miloiu G., Visa F., Tiscann C., "Numerical Research Regarding Contact Localisation at Cylindrical Worm Gears"

Von Eiff, H., Hirschmann K.H., and Lechner, G., 1990, "Influence of gear tooth geometry of teeth stress of external and internal gears", ASME Journal of Mechanical Design, Vol. 112, No.4, pp. 575-583.

Wang, S and Liu P., 1982, "Meshing Principle of Cylindrical Worm Gear Drives", Tianjin Science and Technology Publication Ltd., China.

Wang, X, Wu X and Shen Q, 1988, "A Study on the Design of the Hob for the Worm Gearing with Controllable Second-Order Contact Characteristics," Journal of Xi'an Jiaotong University, Vol. 22, No 2, pp 1~12.

Wang S. and Zhang H., 1991, "Research on the Controllable Modification of ZC_1 Worm

Drive", 8th World Congress on the Theory of Machines and Mechanisms, Prague, Czechoslovakia, August 26~31.

Wilcox L. and Coleman W., 1973, "Application of finite elements to the analysis of gear tooth stresses ", Transactions of ASME, Journal of Engineering for Industry, Nov. pp1139 ~1149.

Winter H. and Wilkesmann, 1981, "Calculation of Cylinderical Worm Gear Drives of Different Tooth Profiles", ASME Journal of Mechanical Design, Vol. 103, No1, pp. 73-82.

Wu H.,1979, "Meshing Principle of Gears", Harbin University of Technology, China.

Yoshino H. and Muta Y., 1997, "Tooth surface modification method applicable to various types of worm gears." Proceedings of International Conference on Mechanical Transmissions and Mechanisms. July 1st-4th, Tianjin, China. pp598~602.

Zhang XK, 1986, "Calculation for modification of worm gear drives using conventional gear hob" Gears (in Chinese), pp4~9.

Zhang Y., Litvin F.L. and Handschuh R.F., 1995, "Computerised design of low-noise face-milled spiral bevel gears", Mechanism and Machine theory, Vol. 30 No. 8, pp. 1171~1178.

Zhang Y., Litvin F.L., Maruyama N., Takeda R. and Sugimoto M., 1994, "Computerised analysis of meshing and contact of gear real tooth surfaces", ASME Journal of Mechanical Design, Vol. 116, No. 3, pp. 677 ~ 682.

Zhang J.J., Esat I.I., Shi Y.H., 1999, "Load analysis with varying mesh stiffness", COMPUTERS & STRUCTURES, Vol.70, No.3, pp.273-280.

Zhang Y., Fang Z., 1999, "Analysis of Tooth Contact and Load Distribution of Helical Gears with Crossed Axes", Mechanism and Machine Theory, Vol. 34, pp41-57.

Zheng C. Q. and Lei J., 1989, "A General Method for Computing Worm Gear Conjugate Mesh Property: Part2-The Mathematic Model of Worm Gear Manufacturing and Working Processes", ASME Journal of Mechanism, Transmissions, and Automation in Design, Vol. 111, pp148-152.

Zheng C. Q., Lei J. and Savage M., 1989, "A General Method for Computing Worm Gear Conjugate Mesh Property: Part1-The Generating Surface", ASME Journal of Mechanism, Transmissions, and Automation in Design, Vol. 111, pp143-147.

Appendix A The Numerical Analysis Results of Localised Tooth Contact

The numerical analysis is applied to an worm gear drive (ZI) with the following specifications:

number of worm threads Z_1=3,

number of wheel teeth Z_2=56,

module m=8.5,

worm reference radius r_w=45.0,

worm base radius r_b=24.992,

worm lead angle = 26.986°,

pitch of the modified worm = 79.898 mm,

centre distance A_0 = 283.0 mm,

normal pressure angle 22.5^0.

Using the methods developed in Chapter 3, the modification parameters are determined as follows:

worm base radius r_b=24.799 mm,

worm lead angle = 27.158°,

hob mounting angle =-0.233°,

pitch of the modified worm = 79.979 mm.

The results of the numerical analysis are shown as below:

Table A.1 Results of TCA for worm gear drive with $\Delta\beta=0^0$

X_2	Y_2	Z_2	ϕ_1	ϕ_2	ϕ_{u1}	ϕ_{u2}
243.3	-43.85	0.8001	128	129.1	-3.892	-3.109
241.7	-44.32	0.7964	148.1	149.1	17.85	18.6
240.1	-44.77	0.7983	168.1	169.1	39.53	40.24
238.5	-45.2	0.8052	188.1	189.1	61.14	61.82
236.9	-45.61	0.8163	208.2	209.1	82.66	83.32
235.3	-46	0.831	228.2	229.1	104.1	104.7
233.8	-46.36	0.8489	248.2	249.1	125.5	126.1

232.2	-46.7	0.8694	268.2	269.1	146.7	147.3
230.7	-47.01	0.8922	288.2	289.1	167.9	168.5
229.3	-47.3	0.917	308.2	309.1	189	189.6
227.8	-47.55	0.9436	328.2	329.1	210.1	210.7
226.5	-47.78	0.9717	348.2	349.1	231.1	231.6
225.1	-47.99	1.001	368.2	369.1	252	252.6
223.9	-48.17	1.032	388.2	389.1	272.9	273.4
222.6	-48.32	1.064	408.2	409.1	293.7	294.2
221.5	-48.45	1.096	428.2	429.1	314.4	315

Table A.2 Results of TCA for worm gear drive with $\Delta\beta=0.10^0$

X_2	Y_2	Z_2	ϕ_1	ϕ_2	ϕ_{u1}	ϕ_{u2}
243.4	-43.66	1.306	127.4	129.1	-4.184	-3.031
241.8	-44.15	1.269	147.5	149.1	17.58	18.66
240.2	-44.62	1.244	167.5	169.1	39.27	40.29
238.6	-45.06	1.228	187.6	189.1	60.88	61.85
237	-45.49	1.219	207.6	209.1	82.41	83.33
235.4	-45.89	1.217	227.7	229.1	103.9	104.7
233.8	-46.26	1.22	247.7	249.1	125.2	126.1
232.3	-46.61	1.228	267.8	269.1	146.5	147.3
230.8	-46.93	1.24	287.8	289.1	167.7	168.5
229.3	-47.22	1.255	307.8	309.1	188.8	189.6
227.9	-47.48	1.273	327.8	329.1	209.9	210.6
226.5	-47.71	1.294	347.8	349.1	230.8	231.6
225.2	-47.92	1.317	367.9	369.1	251.8	252.5
223.9	-48.1	1.342	387.9	389.1	272.6	273.3
222.7	-48.26	1.368	407.9	409.1	293.4	294.1

Table A.3 Results of TCA for worm gear drive with $\Delta\beta=0.20^0$

X_2	Y_2	Z_2	ϕ_1	ϕ_2	ϕ_{u1}	ϕ_{u2}
243.5	-43.48	1.799	126.8	129.1	-4.466	-2.954
241.9	-43.98	1.733	146.9	149.1	17.31	18.72
240.3	-44.47	1.681	167	169.1	39.01	40.33
238.7	-44.93	1.643	187.1	189.1	60.63	61.88
237	-45.37	1.615	207.2	209.1	82.17	83.34

235.4	-45.78	1.597	227.2	229.1	103.6	104.7
233.9	-46.16	1.587	247.3	249.1	125	126
232.3	-46.51	1.583	267.3	269.1	146.3	147.3
230.8	-46.84	1.584	287.4	289.1	167.5	168.4
229.3	-47.14	1.59	307.4	309.1	188.6	189.5
227.9	-47.4	1.6	327.4	329.1	209.6	210.6
226.5	-47.64	1.614	347.4	349.1	230.6	231.5
225.2	-47.86	1.63	367.5	369.1	251.5	252.4
223.9	-48.04	1.65	387.5	389.1	272.4	273.3
222.7	-48.2	1.671	407.5	409.1	293.2	294.1
221.5	-48.34	1.694	427.5	429.1	314	314.8

Table A.4 Results of TCA for worm gear drive with $\Delta\beta$=-0.10^0

X_2	Y_2	Z_2	ϕ_1	ϕ_2	ϕ_{u1}	ϕ_{u2}
243.2	-44.05	0.2822	128.7	129.1	-3.589	-3.186
241.6	-44.49	0.3131	148.7	149.1	18.14	18.54
240	-44.92	0.3443	168.7	169.1	39.81	40.2
238.4	-45.34	0.3758	188.7	189.1	61.4	61.79
236.9	-45.74	0.4078	208.7	209.1	82.92	83.3
235.3	-46.12	0.4403	228.7	229.1	104.3	104.7
233.7	-46.47	0.4734	248.7	249.1	125.7	126.1
232.2	-46.8	0.5069	268.7	269.1	147	147.3
230.7	-47.1	0.5411	288.6	289.1	168.2	168.5
229.2	-47.38	0.5757	308.6	309.1	189.3	189.7
227.8	-47.63	0.6109	328.6	329.1	210.3	210.7
226.4	-47.86	0.6466	348.6	349.1	231.3	231.7
225.1	-48.05	0.6828	368.6	369.1	252.2	252.6
223.8	-48.23	0.7194	388.6	389.1	273.1	273.5
222.6	-48.38	0.7566	408.6	409.1	293.9	294.3
221.5	-48.51	0.7942	428.6	429.1	314.7	315.1

Table A.5 Results of TCA for worm gear drive with $\Delta\beta$=-0.20^0

X_2	Y_2	Z_2	ϕ_1	ϕ_2	ϕ_{u1}	ϕ_{u2}
243.1	-44.25	-0.2485	129.3	129.1	-3.275	-3.264
241.5	-44.67	-0.1804	149.3	149.1	18.44	18.48
240	-45.08	-0.1182	169.3	169.1	40.09	40.15
238.4	-45.48	-0.06064	189.2	189.1	61.67	61.76

236.8	-45.87	-0.00669	209.2	209.1	83.18	83.29
235.2	-46.23	0.04442	229.2	229.1	104.6	104.7
233.7	-46.58	0.09332	249.1	249.1	126	126.1
232.1	-46.9	0.1405	269.1	269.1	147.2	147.4
230.6	-47.19	0.1864	289.1	289.1	168.4	168.6
229.2	-47.46	0.2312	309.1	309.1	189.5	189.7
227.8	-47.71	0.2753	329.1	329.1	210.6	210.8
226.4	-47.93	0.3188	349	349.1	231.6	231.7
225.1	-48.12	0.3619	369	369.1	252.5	252.7
223.8	-48.29	0.4048	389	389.1	273.3	273.6
222.6	-48.44	0.4474	409	409.1	294.1	294.4
221.5	-48.57	0.49	429	429.1	314.9	315.1

Table A.6 Results of TCA for worm gear drive with $\Delta\beta$=-0.30^0

X_2	Y_2	Z_2	ϕ_1	ϕ_2	ϕ_{u1}	ϕ_{u2}
243	-44.45	-0.7922	130	129.1	-2.949	-3.342
241.5	-44.85	-0.6846	149.9	149.1	18.74	18.42
239.9	-45.24	-0.5895	169.8	169.1	40.38	40.11
238.3	-45.63	-0.5044	189.8	189.1	61.95	61.73
236.7	-46	-0.4273	209.7	209.1	83.44	83.27
235.2	-46.35	-0.3567	229.7	229.1	104.9	104.7
233.6	-46.68	-0.2913	249.6	249.1	126.2	126.1
232.1	-47	-0.2299	269.6	269.1	147.5	147.4
230.6	-47.29	-0.1719	289.5	289.1	168.7	168.6
229.2	-47.55	-0.1165	309.5	309.1	189.8	189.7
227.7	-47.79	-0.06321	329.5	329.1	210.8	210.8
226.4	-48	-0.01161	349.4	349.1	231.8	231.8
225.1	-48.19	0.03864	369.4	369.1	252.7	252.7
223.8	-48.36	0.08782	389.4	389.1	273.6	273.6
222.6	-48.5	0.1362	409.4	409.1	294.4	294.5
221.4	-48.63	0.1838	429.3	429.1	315.2	315.2

Appendix B Approximate Equation of Tooth Deflection

Sudoh K., et. al.(1996) proposed an empirical equation to calculate tooth deflection. The details of the equation are given below.

1. The coordinate system of tooth surface is shown in Figure B.1.

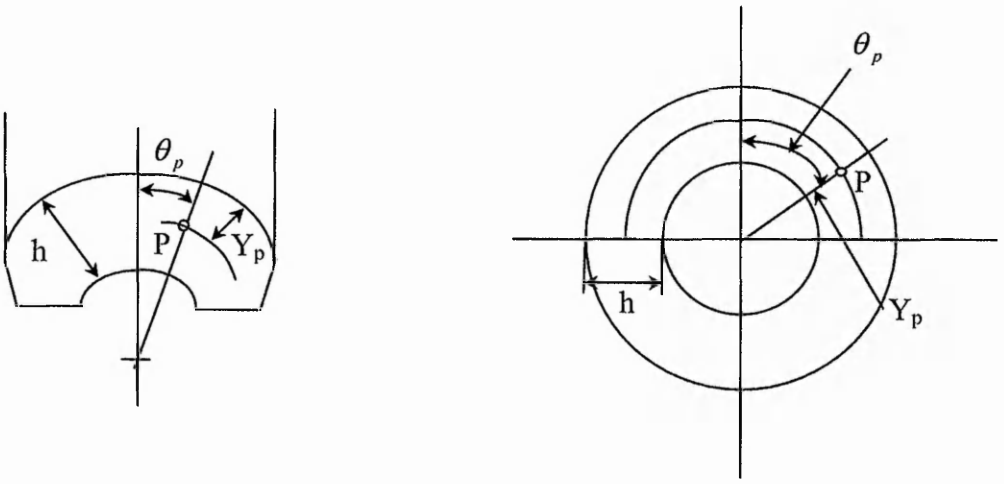

Figure B.1 The coordinate system of tooth surface

2 Absolute tooth deflection $\boldsymbol{U}$

The absolute tooth deflection is defined as the deflection when a unit load is applied to the center of face width and tooth height. The empirical equation of deflection is formulated as shown in Table B.1

Table B.1 absolute tooth deflection

	Worm	Wheel
JIS3 type worm gear	$0.0111e^{3.14\alpha}$	$0.0074e^{3.2\alpha}$

3 Characteristic function of tooth deflection $V(\bar{r})$

$$V(\bar{r}) = 1 - 2.148 \cdot \bar{r} + 1.785 \cdot \bar{r}^2 - 0.584 \cdot \bar{r}^3$$

where, $\bar{r} = \sqrt{\left[(R \pm \frac{y + y_p}{2}) \cdot \lambda \cdot (\theta - \theta_p)\right]^2 + (y - y_p)^2} / h$

The coefficient λ are formulated as shown in Table B.2

Table B.2 Coefficient λ

	Worm	Wheel
JIS3 type worm gear	$0.203e^{2.34\alpha}$	$0.235e^{2.3\alpha}$

4 Characteristic function of tooth deflection in direction of tooth height at the loading point $G(y)$

For both worm and wheel, $G(y)$ is expressed as,

$G(y) = 1 - 4.122 \cdot y + 7.771 \cdot y^2 - 7.108 \cdot y^3 + 2.46 \cdot y^4$

5 Characteristic function of tooth deflection in direction of tooth width at the loading point $F(\theta)$

$F(\theta) = \exp(2.187 \cdot \theta^{1.615})$

Appendix C. Calculation of Surface Curvature for Involute Worm Gear

The conventional approach to calculate the surface curvatures is firstly to define the parametric equations of the surfaces, then differentiate the equations according to the theory of differential geometry. Based on the differentiation, the curvatures of the surfaces can be obtained. However, this method is very complicated and difficult in calculation.

A procedure of surface curvature calculation of worm gear was developed by Wang S.R. (1982). According to his method, the principle curvatures of the worm and wheel can be determined in five steps: (1) determine the principle curvatures of the worm tooth surface $K_I^{(i)}$, (2) determine the normal vector of the contact lines, (3) determine the worm surface curvature along $\vec{a}$ and contact line direction $\vec{t}$, (4) determine the wheel surface curvature along $\vec{a}$ and contact line direction $\vec{t}$ and (5) determine the principle curvature of the wheel tooth surface $K_I^{(i)}$

C.1 Determine the principle curvatures of the worm tooth surface $K_I^{(i)}$

The principle curvature of the worm tooth is represented using the following equation:

$$K_I^{(i)} = K_a \cos^2\varphi + K_u \sin^2\varphi + G_a \sin 2\varphi + (G_u - G_a)\sin^2\varphi \cdot ctg\theta \qquad \text{(C.1)}$$

where, $\vec{\alpha}$ is the unit tangential vector of the cutting edge, θ is the angle between $\vec{\alpha}$ and $\vec{V}^{(u1)}$, φ is the angle from $\vec{\alpha}$ to the direction of the curvature and $\vec{V}^{(u1)}$ is the relative velocity of tool and the worm. K_a, K_u, G_a, G_u are the surface curvature and surface torsion in the direction of $\vec{\alpha}$ and $\vec{V}^{(u1)}$.

For the side B of involute worm gear,

$\vec{\alpha} = \cos\delta_1 \sin\phi_u \vec{i}_1 + \cos\delta_1 \cos\phi_u \vec{j}_1 + \sin\delta_1 \vec{k}_1$

$K_a = 0$

$$G_a = 0$$

$$K_u = \frac{u \cdot \sin\delta_1 \cdot \cos\delta_1}{u^2 \cos^2\delta_1 + r_{01}^2 + p^2}$$

$$G_u = K_u \cdot ctg\theta$$

Using the equation (C.1), the principle curvatures of worm can be obtained as below:

$$K_I^{(1)} = K_u + G_u \cdot ctg\theta = K_u(1 + ctg^2\theta)$$
$$K_{II}^{(1)} = 0 \qquad \text{(C.2)}$$

Their direction is expressed as

$$\begin{cases} \vec{e}_I^{(1)} = \vec{n} \times \vec{e}_{II}^{(1)} \\ \vec{e}_{II}^{(1)} = \dfrac{\vec{\alpha}}{|\vec{\alpha}|} \end{cases} \qquad \text{(C.3)}$$

C.2 Determine the normal vector of the contact lines

The normal vector of the contact line is used as a reference direction for tooth surface curvature calculation, which can be expressed as

$$\vec{a} = \vec{\omega}^{(12)} \times \vec{n} + K_v^{(1)} \cdot \vec{V}^{(12)} + G_v^{(1)} \cdot \left(\vec{n} \times \vec{V}^{(12)}\right) \qquad \text{(C.4)}$$

the above equation can be further expressed as

$$\begin{cases} a_{x1} = (\vec{\omega}^{(12)} \times \vec{n})_{x1} + K_I^{(1)} V_{x1}^{(12)} + G_I^{(1)} (\vec{n} \times \vec{V}^{(12)})_{x1} \\ a_{y1} = (\vec{\omega}^{(12)} \times \vec{n})_{y1} + K_I^{(1)} V_{y1}^{(12)} + G_I^{(1)} (\vec{n} \times \vec{V}^{(12)})_{y1} \\ a_{z1} = (\vec{\omega}^{(12)} \times \vec{n})_{z1} + K_I^{(1)} V_{z1}^{(12)} + G_I^{(1)} (\vec{n} \times \vec{V}^{(12)})_{z1} \end{cases}$$

where,

$$\begin{cases} (\vec{\omega}^{(12)} \times \vec{n})_{x1} = -i_{21} n_{z1} \cos\phi_1 - n_{y1} \\ (\vec{\omega}^{(12)} \times \vec{n})_{y1} = i_{21} n_{z1} \sin\phi_1 + n_{x1} \\ (\vec{\omega}^{(12)} \times \vec{n})_{z1} = -i_{21} (n_{y1} \sin\phi_1 - n_{x1} \cos\phi_1) \end{cases}$$

$$\begin{cases} (\vec{n}\times\vec{V}^{(12)})_{x1} = n_{y1}V_{z1}^{(12)} - n_{z1}V_{y1}^{(12)} \\ (\vec{n}\times\vec{V}^{(12)})_{y1} = n_{z1}V_{x1}^{(12)} - n_{x1}V_{z1}^{(12)} \\ (\vec{n}\times\vec{V}^{(12)})_{z1} = n_{x1}V_{y1}^{(12)} - n_{y1}V_{x1}^{(12)} \end{cases}$$

$$\begin{cases} K_v^{(1)} = K_\alpha \cos^2\varphi + K_u \sin^2\varphi + G_\alpha \sin 2\varphi + (G_u - G_\alpha)\sin^2\varphi \cdot ctg\theta \\ G_v^{(1)} = \dfrac{K_u - K_\alpha}{2}\sin 2\varphi + G_\alpha \cos 2\varphi + \dfrac{G_u - G_\alpha}{2}\sin 2\varphi \cdot ctg\theta \end{cases}$$

Since vectors $\vec{n}, \vec{V}^{(12)}, \vec{\omega}^{(12)}$ have been derived in Chapter 4. By substituting all the known vectors $\vec{n}, \vec{V}^{(12)}, \vec{\omega}^{(12)}$ into the above equation systems, the normal vector of contact lines on tooth surface can be obtained.

C.3 Determine the worm surface curvatures along $\vec{a}$ and contact line direction $\vec{t}$

The worm surface curvatures along $\vec{a}$ and contact line direction $\vec{t}$ are needed in the further calculation of wheel tooth surface curvatures. For the worm tooth surface, assuming that the angle between the principle curvature $\vec{e}_I^{(1)}$ and the normal vector of contact line $\vec{a}$ is γ, as shown in Figure C.1, it can be obtained using the equation below:

$\gamma = \cos^{-1}(\vec{e}_I^{(1)} \cdot \vec{a})$

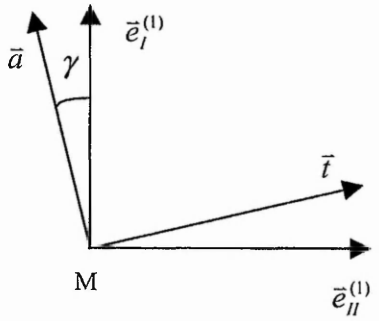

Figure C.1 Directions of contact line and its normal vector

As the principle curvatures of the worm tooth surface are determined in C.1, the surface curvatures along the direction of contact line and its normal vector are obtained using Euler's equation.

$$\begin{cases} K_{\bar{a}}^{(1)} = K_I^{(1)} \cos^2 \gamma + K_{II}^{(1)} \sin^2 \gamma \\ K_{\bar{t}}^{(1)} = K_I^{(1)} \sin^2 \gamma + K_{II}^{(1)} \cos^2 \gamma \end{cases}$$

The surface torsion along the direction of contact line and its normal vector are $G_{\bar{t}}^{(1)}, G_{\bar{a}}^{(1)}$, which can be determined the equation proposed by O. Bonnet (Litvin, 1994), as shown below:

$$G_{\bar{t}}^{(1)} = -G_{\bar{a}}^{(1)} = (K_{II}^{(1)} - K_I^{(1)}) \sin \gamma \cos \gamma$$

C.4 Determine the wheel surface curvatures along $\bar{a}$ and contact line direction $\bar{t}$

To obtain the principle curvature of the wheel tooth, the wheel tooth surface curvatures along $\bar{a}$ and contact line direction $\bar{t}$ need to be determined. In Wang's method, along the direction of $\bar{a}$, the surface curvature difference between the worm and wheel tooth can be expressed as:

$$K_{\bar{a}}^{(1)} - K_{\bar{a}}^{(2)} = \frac{(\bar{a})^2}{\Psi}$$

where, $\Psi = \Phi_t + \bar{a} \cdot \vec{V}^{(12)}$, and

$$\Phi_t = i_{21}[n_{x1} z_1 \sin \phi_1 + n_{y1} z_1 \cos \phi_1 - n_{z1}(x_1 \sin \phi_1 + y_1 \cos \phi_1)]$$

Since $\vec{n}, \vec{V}^{(12)}, i_{21}, \vec{r}$ are all known and $K_{\bar{a}}^{(1)}$ is determined in section C.1, the wheel surface curvature along $\bar{a}$ can be determined as:

$$K_{\bar{a}}^{(2)} = K_{\bar{a}}^{(1)} - \frac{(\bar{a})^2}{\Psi}$$

For the direction $\vec{t}$, because the wheel and worm teeth are in contact, their surface curvature and surface torsion are equal.

$$K_{\vec{t}}^{(1)} = K_{\vec{t}}^{(2)}$$

$$G_{\vec{t}}^{(1)} = G_{\vec{t}}^{(2)}$$

C.5 Determine the principle curvature of the wheel tooth surface $K_I^{(i)}$

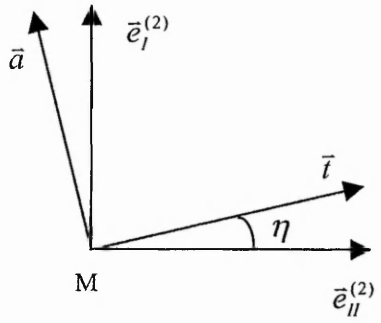

Figure C.2 Principle curvature of wheel tooth surface

For the wheel tooth surface, assuming that the angle between the principle curvature $\vec{e}_{II}^{(2)}$ and direction $\vec{t}$ is η, as shown in Figure C.2, it can be obtained as:

$$\eta = \frac{1}{2} tg^{-1}\left(\frac{2G_{\vec{t}}^{(2)}}{K_{\vec{a}}^{(2)} - K_{\vec{t}}^{(2)}}\right)$$

Since the wheel tooth surface curvatures along $\vec{a}$ and contact line direction $\vec{t}$ are obtained in section C.4, according to general Euler' equation and Bonnet's theory, the principle curvatures of the wheel tooth surface can be determined based on the following equations (Wu, 1979)

$$K_I^{(2)} = \frac{1}{2}(K_{\vec{a}}^{(2)} + K_{\vec{t}}^{(2)}) - \frac{G_{\vec{t}}^{(2)}}{\sin 2\eta}$$

$$K_{II}^{(2)} = \frac{1}{2}(K_{\vec{a}}^{(2)} + K_{\vec{t}}^{(2)}) + \frac{G_{\vec{t}}^{(2)}}{\sin 2\eta}$$

The directions of the principle curvatures can be determined using the equations below.

$$\begin{cases} \vec{e}_I^{(2)} = \vec{a} \cdot \cos\eta - \vec{t} \cdot \sin\eta \\ \vec{e}_{II}^{(2)} = \vec{a} \cdot \sin\eta + \vec{t} \cdot \cos\eta \end{cases}$$